Dissertation

zur Erlangung des Doktorgrades

der Fakultät für Chemie und Pharmazie der

Ludwig-Maximilian-Universität München

Cancer Therapy with Metronomically Scheduled Cyclophosphamide: Experimental Modalities within GDEPT and Tumor Escape Mechanisms

Michael Günther

aus

Buchloe

2006

Erklärung

Diese Dissertation wurde im Sinne von § 13 Abs. 3 bzw. 4 der Promotionsordnung vom 29. Januar 1998 von Dr. Manfred Ogris und Prof. Dr. Ernst Wagner betreut.

Ehrenwörtliche Versicherung

Diese Dissertation wurde selbständig, ohne unerlaubte Hilfe erarbeitet.

München, am 18.12.2006

_____

(Michael Günther)

Dissertation eingereicht am 18.12.2006

1. Gutachter: Prof Dr. Ernst Wagner
2. Gutachter: Priv.-Doz. Dr. Carsten Culmsee

Mündliche Prüfung am 23.01.2007

Wenn du
wieder einmal
zweifelnd vor dir selbst sitzt
und nicht mehr so recht
weiterweißt
nimm deine Träume beim Wort
ehe sie in deinem Zimmer ersticken
ohne ein einziges Mal
geatmet zu haben.

(Heiner Neidig)

Table of contents

1 Introduction

1.1 Novel approaches for cancer treatment

Cancer is a heterogeneous disease which is caused by genetic errors in the cell's genome due to alterations, loss or multiplication of certain genes. The incidence of cancer is still rising and malignant diseases are one of the most prevalent causes of death. Standard treatment for solid cancer is still surgery, followed by radiation and/or chemotherapy. However, these regimes are not always successfully applicable, either due to the tumor being unresectable or already metastasized. Another hindrance for successful treatment of cancer by classical radiation or chemotherapy is the occurrence of resistance towards treatment regimes. Therefore it is important to develop new strategies in tumor therapy, especially for progressed tumors that are withdrawn from classical treatment regimes.

1.1.1 Antiangiogenic therapy

Vasculogenesis and angiogenesis are the fundamental processes by which new blood vessels are formed (1). The growth of new blood vessels, angiogenesis, is a critical step in developing clinical relevant cancer (FIG 2-1).

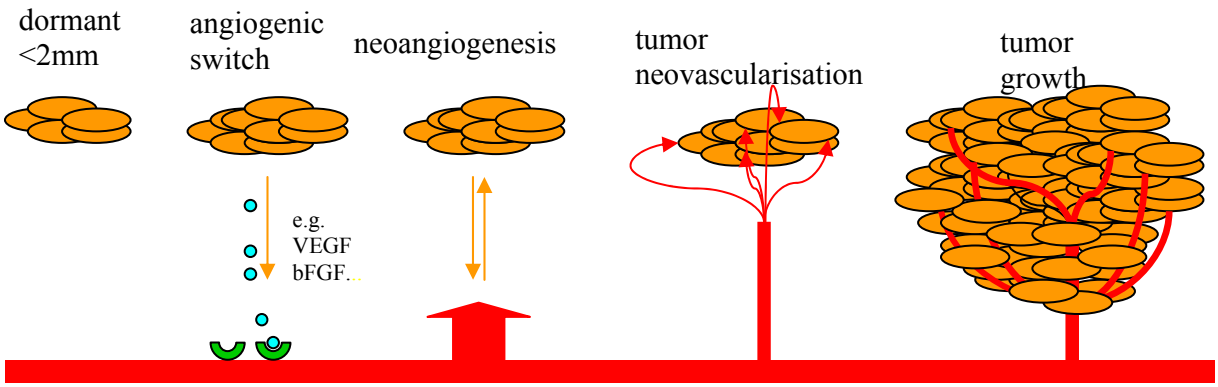

Fig.: 1-1 Stages in tumor development leading to vascularisation: After the angiogenic switch, induced by certain growth factors, initially dormant tumors become angiogenic, blood supply is established and tumors begin to grow.

The hypothesis that tumor growth and also tumor spreading is angiogenesis dependent was first proposed in 1971 (2). Meanwhile this hypothesis has been proven by several experiments and is now widely accepted. In the absence of blood supply, tumor growth is restricted to a microscopic size and the tumor is not able to spread via the vascular system to form haematogenic metastases because tumor

cells are not shed into circulation (3). In these non-angiogenic tumors cell proliferation and apoptosis are balanced (4).

The angiogenic switch could be driven by several factors; e.g. angiogenic oncogenes, upregulation of proangiogenic factors, produced by tumor cells and/or the tumor stroma or down regulation of antiangiogenic factors. With the access to blood supply, oxygen, nutrients and growth factors are not a limiting factor for tumor growth anymore and exponential proliferation of the tumor mass occurs (5). Clinical studies have shown a direct correlation between the density of tumor vessels and an adverse prognosis in patients with various solid tumors regarding tumor growth and metastatic potential (6).

As tumor growth critically depends on a functional blood vessel network and a large number of neoplastic cells depend on the supply of a relatively small number of endothelial cells, tumor vessels are an attractive target in fighting against cancer (7).

1.1.1.1 The angiogenic process and antiangiogenic approaches

The physiological formation of new blood vessels in humans mainly takes place at wound healing and in the course of female menstruation cycle. Angiogenesis exhibits a central role in different pathological processes including malignant diseases (8). Therefore new therapeutic strategies for cancer treatment involve antiangiogenic approaches. The possible starting points are multifaceted and result from the complex process of tumor angiogenesis.

Malignant cells can be present over years in a dormant status (tumor dormancy); oxygen and nutrients are obtained form the established blood vessel network of the healthy tissue and reaches the tumor by diffusion (2). The reason for switching to an angiogenic, active stadium is currently not clarified secludingly. The activation of endothelial cells, however, is the crucial step in switching to an angiogenic tumor stadium (5).

The activated endothelial cells change their gene expression pattern. The secretion of proteolytic enzymes like metalloproteases (MMP-2) aerates the surrounding matrix and enables migration (9). Further on, activated endothelial cells enter the cell cycle and start to proliferate (2). Expression of cell surface aminopeptidases further enhance the process of matrix remodeling (10). Adhesion molecules like integrins enable migration of endothelial cells (11) and modulate survival (12) and cell cycle (13). Immature endothelial cells migrate in the direction of the angiogenic stimulus by forming sprouts. In the course of further differentiation these sprouts form lumen and

a new basal lamina is established (14). This results in the forming of a three dimensional blood vessel network supplying the tumor with oxygen and nutrients.

The complex process of tumor angiogenesis offers multiple options in interfering in terms of antiangiogenic therapy. Current approaches are based on the inhibition of one or more of the crucial steps in the angiogenic process (15). Recently, an antagonist of the angiogenic growth factor VEGF (Avastin^{R}) was approved by the EMEA (European Medicines Agency) for progressed colon carcinoma (16). Several other drugs are in clinical trials.

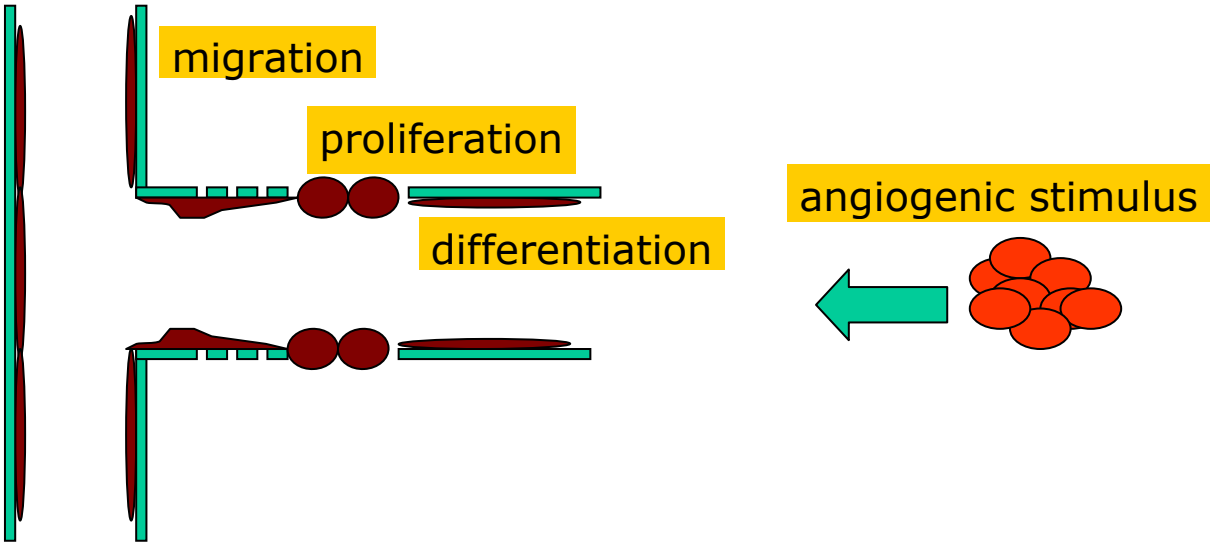

Fig.: 1-2 The complex process of angiogenesis offers several potential points of attacking the tumor driven establishing of a functional blood vessel network. Interference with the angiogenic process can be based on disturbance regarding to cytokine signaling or direct interaction with endothelial cells. The relevant key steps are suitable for analyzing antiangiogenic activity of drugs to evaluate their potential in disrupting the angiogenic process.

1.1.1.2 Metronomically scheduled chemotherapy

Conventional chemotherapeutics affect not only proliferating tumor cells and various types of healthy cells e.g. bone marrow cells, they also interfere with the endothelium of growing tumor vessels (17). This results in an antiangiogenic effect, when conventional chemotherapeutics are optimized in terms of dose and frequency of application. Usually anticancer drugs are scheduled at low doses and continuous application (metronomic schedule) in order to target preferential angiogenic active blood vessels (18), whereas bolus high dose chemotherapy is directed predominately against fast dividing tumor cells.

For example, CPA (cyclophosphamide) was shown to exhibit potent anticancer activity when it was applied in a low dose antiangiogenic schedule. Metronomically scheduled CPA therapy led to decreased angiogenesis in matrigel plug studies (19)

and increased apoptosis of proliferating endothelial cells in the tumor bed. Further in vitro evaluation showed decreased proliferation and migration capability of cultured endothelial cells in the presence of activated CPA (20). Recent studies implied an additional effect beside direct affection of tumor vessel endothelium. Changes in the expression of antiangiogenic cytokines were observed. Thrombospondin-1 was identified as a potential mediator of the effects of metronomic scheduled CPA (21). Low dosed CPA treatment of cultured endothelial cells caused marked increase of thrombospondin-1 mRNA and thrombospondin-1 upregulation was detected in CPA treated experimental tumors (22).

However, despite intensive investigation of metronomic CPA therapy the role of single CPA metabolites, which may mediate antiangiogenic effects, has not been clarified.

Due to the fact that antiangiogenic strategies target preferentially genetically stable endothelial cells, resistance of tumors against treatment should be overcome (23). However, recent studies and our own results indicate the development of mechanisms that revoke tumors from metronomic scheduled chemotherapy (24).

1.1.2 Gene therapy

Gene therapy is part of a growing field of molecular medicine that will gain importance in the treatment of human malignant diseases. Until now, almost two third of all clinical trials performed in gene therapy are directed against cancer (25). As solid tumors exceeding a certain size rely on blood supply, the administration of particulate gene delivery vectors via the bloodstream is a promising concept. For systemic application, these delivery systems have to fulfill certain conditions like adequate circulation time and low immunogenicity (26).

1.1.2.1 Therapeutic concepts for cancer gene therapy

Gene therapeutic approaches for cancer treatment have the advantage of being potentially highly selective. Most approaches combine gene therapy with chemotherapeutic drugs, radiation or other treatments to achieve optimal effects. Several approaches based on gene therapy were investigated in terms of cancer treatment. Replacement and overexpression strategies of proapoptotic or tumor suppressor genes e.g. p53 were the prime fields of gene therapy (27). In the recent years also approaches based on the delivery of genes to modulate host immune response have been investigated (28).

The approach to combine gene delivery with the consecutive application of chosen small molecular drugs was investigated in this thesis. Within the GDEPT (gene directed enzyme prodrug therapy) concept an inactive prodrug is converted into the active, cytotoxic drug by conversion through a specific enzyme, which is overexpressed as a transgene at the tumor site. This concept results in high local concentrations of cytotoxic drugs within the tumor tissue due to selective expression of the relevant enzyme at the tumor site; the systemic burden of toxic metabolites is therefore lower compared to conventional chemotherapy (29). Often, prodrugs are used that are already in clinical use, making it easier for the concept to be approved by regulatory authorities. A major advantage for GDEPT is the bystander effect. Different from strategies to deliver proapoptotic or tumor suppressor genes which affect only the transfected cells, the GDEPT approach aims to affect also non transfected cells in the near vicinity of cells expressing the transgene. Enzymatic activation of anticancer prodrugs by successfully transduced cells also affects the surrounding tissue by diffusion of toxic metabolites. This bystander effect amplifies antitumoral activity (30). It is adequate to deliver the therapeutic gene only to a part of the target cell population which is a more reachable goal with available gene delivery systems. Several therapeutic gene/prodrug combinations were investigated (31). Approaches with encapsulated cells, stably expressing CYP2B1, are already in clinical trials (32). In this thesis, gene transfer of rat CYP2B1 combined with cyclophosphamide (CPA) was evaluated.

1.1.2.2 CYP450/CPA combination

The anticancer drug cyclophosphamide (CPA) is widely used for different forms of cancer. However CPA can be highly toxic due to non specific side effects, and host toxicity is the crucial limiting factor in conventional tumor therapy with CPA (33-35). CPA itself is a prodrug that is transformed by cytochrom P450 enzymes in the liver by hydroxylation. The activated metabolite hydroxycyclophosphamide (4-OH-CPA) undergoes spontaneous β-elimination to generate the compounds phosphoramid mustard and acrolein.

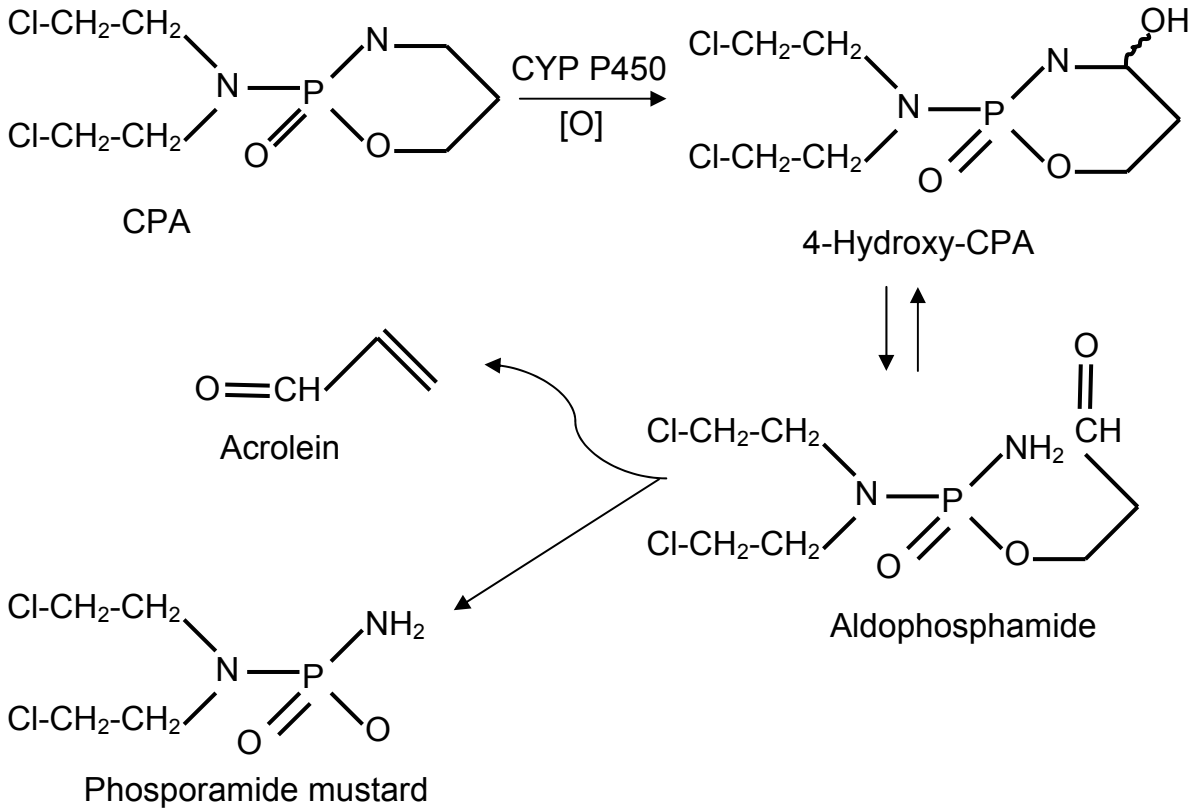

Fig.: 1-3 Simplified diagram of CPA metabolism. CPA is activated by hepatic CYP P450 isoforms (e.g. 2B1 in rat, 2B6 in humans) to form hydroxycyclophosphamide (4-Hydroxy-CPA) which is delivered via the blood stream to the tumor site. 4-Hydroxy-CPA is in equilibrium with its tautomer aldophosphamide. Aldophosphamide can decompose by spontaneous β-elimination and form the alkylating compound phosphoramid mustard and the byproduct acrolein.

These products are highly reactive species that alkylate DNA or proteins. In conventional chemotherapy activated metabolites are distributed systemically via blood stream, affecting cells at the tumor site but also in healthy tissues. Expression of CYP2B1 enzyme within the tumor site should activate CPA locally in order to achieve an adequate cytotoxic concentration range in the tumor area (36). Due to the local activation at the tumor site, applicated CPA doses should be lower at similar antitumoral efficiency, preventing the occurrence of side effects.

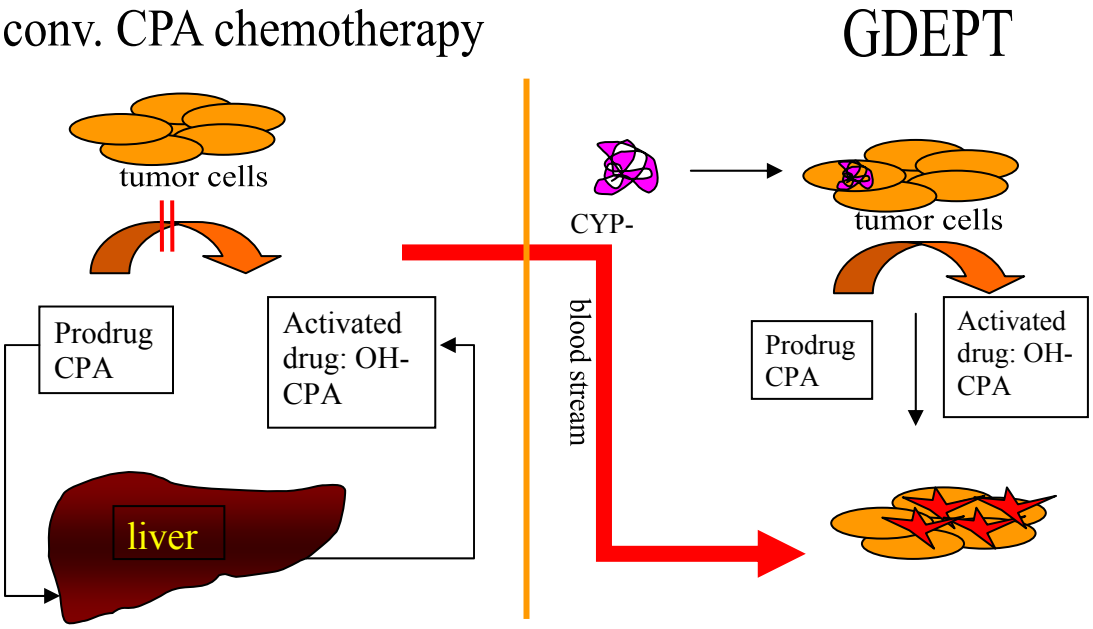

Fig.: 1-4 Comparison of conventional CPA antitumoral therapy and the GDEPT gene therapy approach. To reduce side effects and achieve higher local concentrations of cytotoxic 4-hydroxy-CPA a CPA activating CYP P450 isoform is delivered via gene transfer to the tumor site prior to CPA treatment to enable localized CPA bioactivation.

1.1.2.3 Targeting strategies within the GDEPT concept

Treatment of progressed malignant diseases is only effective if carried out via the systemic route. Systemic application of high dose chemotherapy is limited by side effects and toxicity in healthy tissue. Therapeutic concepts with higher specificity are therefore eligible. Gene therapy of already metastasized tumors is a promising approach to increase specificity and efficiency and may supplement already established treatment regimes. Both tumor cells and tumor vasculature are possible targets for the delivery of genes within the GDEPT concept (37). Approaches for the development of tumor- and tumor vasculature-targeted gene delivery systems are described in the annex.

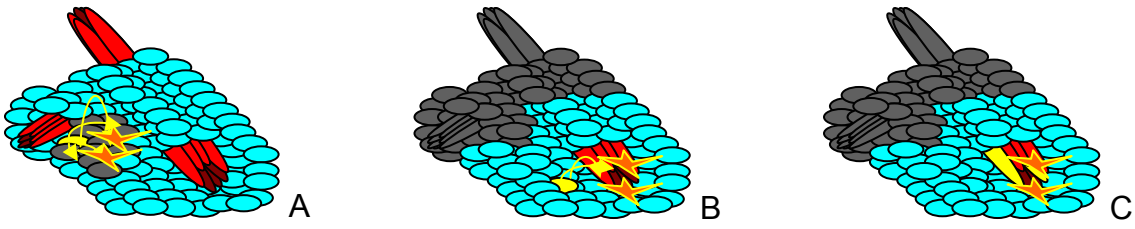

Fig.: 1-5 Different modes of action for the GDEPT bystander effect: A: Gene delivery to tumor cells affects transfected cells and surrounding tumor cells; B: Gene delivery to tumor cells in the vicinity of vessels affects transfected cells and endothelial cells in the near vicinity; C: direct targeting and transfection of endothelial cells can lead to an optimal bystander and antiangiogenic effect. Mode A is not working on chemoresistant tumors, mode B and C also affect angiogenic cells (yellow areas: transfected cells, Arrows: direction of bystander effect; stars: area of cytotoxic effect)

Tumor neoangiogenesis depends on different, complementary pathways and blocking a single pathway with conventional antiangiogenic therapy might be insufficient and compensated by another pathway (38). Further on, the expression pattern of neoangiogenic factors can differ between tumor types and even within the tumor; blocking a distinct factor can lead to the occurrence of compensation mechanisms. The GDEPT concept is not impaired by such compensation mechanisms, as the local activation of cytotoxic drugs mostly leads to DNA and/or protein damage of the affected cells. With the GDEPT approach the cytotoxic effect on the tumor endothelium is rather independent of tumor type and progression stadium and therefore exhibits a universal adaptive approach.

1.1.2.4 PEI-polyplexes

Polyethylenimine (PEI) is a polycation with a high density of positively charged amino groups. Therefore it interacts with negatively charged nucleic acid by electrostatic interaction. In 1995 it was first reported on the ability of PEI to deliver genes and oligonucleotides (39). PEI can be synthesized as a linear (Fig 1-6 A) as well as a branched (Fig 1-6 B) macromolecule in a wide range of molecular weight. The PEIs of different topology and molecular weights exhibit different binding affinities for DNA (40). Recently, difference in in vivo gene expression efficiencies were demonstrated for LPEI (linear PEI) and BPEI (branched PEI), whereas LPEI containing polyplexes resulted in significantly higher transfection efficiency than polyplexes with incorporated BPEI (41).

By complexation with DNA, particles are formed (polyplexes) in which the condensed DNA is protected against physical and biochemical degradation. The particular polyplexes can enter the cells via endocytotic processes. PEI polyplexes mediate efficient gene delivery in vitro; however cellular uptake of plain PEI polyplexes is unspecific due to positive charge on the surface of the particles. Moreover, plain polyplexes tend to aggregate in salt containing biological fluids (42) and exhibit strong cellular and systemic toxicity in vivo (43). PEI can be covalently linked to different functional molecules such as hydrophilic polymers like polyethylene glycol (PEG) or functional peptides, in order to modify the surface of the polyplexes and reduce unspecific interactions, aggregation and induce specificity towards target cells (44).

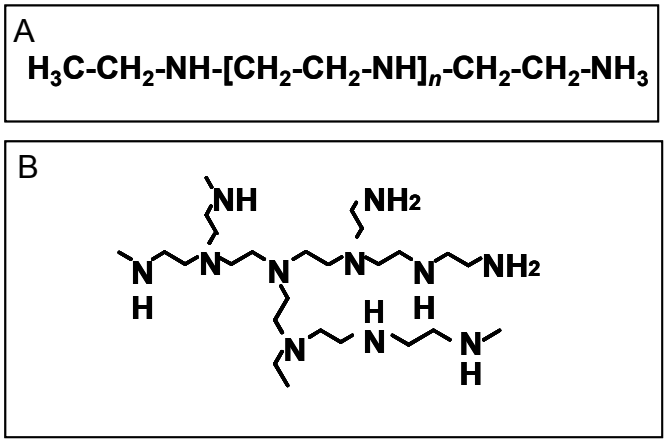

Fig.: 1-6 Different Versions of Polyethylenimine (PEI): A) linear PEI (LPEI) B) branched PEI (BPEI)

1.2 Tumor environment

Solid tumors are characterized by several environmental properties that are different from healthy tissue. Blood vessel networks that are formed by tumor induced angiogenesis are poorly organized and exhibit in a heterogeneous distribution of blood flow. This results in hypoxic areas within the tumor tissue that are not sufficiently supplied with oxygen and nutrients (45;46). The propagation of hypoxic areas depends on tumor type and tumor stadium and can be characterized by measuring blood vessel density, intercapillary distance and the perivascular cuff (FIG 1-7).

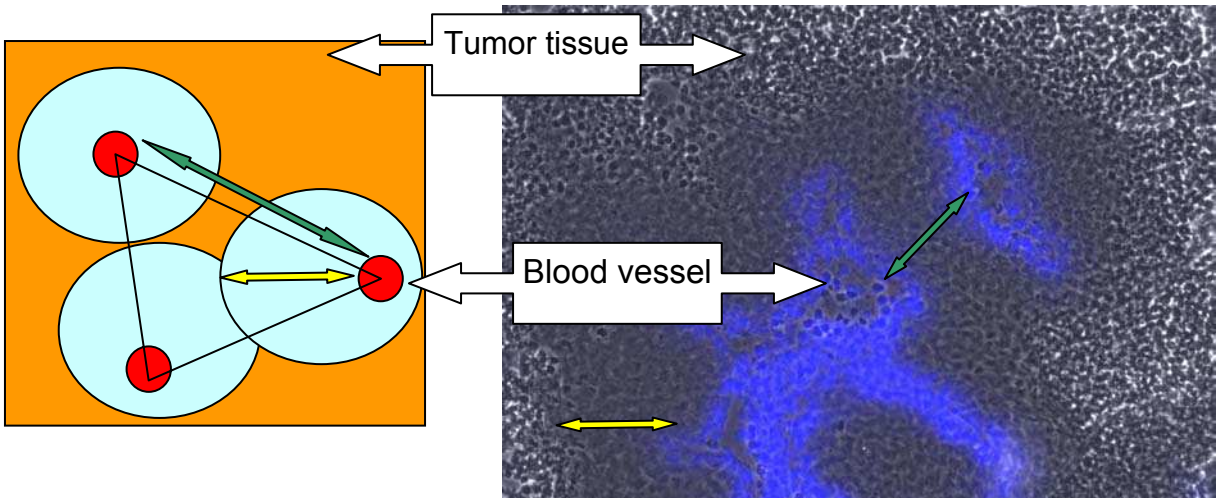

Fig.: 1-7 Vertices of blood supply in tumor tissue. The microscopic picture (right) displays a functional blood vessel (blue staining: systemically applicated Hoechst33258 dye as a tracer; data source: current thesis). The distance between functional blood vessels is described as intercapillary distance (green arrow). The area around the blood vessels that is supplied by oxygen is called perivascular cuff (yellow arrow).

Tumor hypoxia results in several effects in terms of resistance towards chemo- and/or radiotherapy, metastatic potential, angiogenesis and regulation of cell surface molecules (47-49). Moreover, tumor hypoxia may influence therapeutic approaches with delivered and expressed enzymes when the conversion of the prodrug is oxygen dependent. The activity of the CYP P450 2B1 enzyme (cytochrome P450 2B1), that was utilized in this thesis (GDEPT, gene delivered enzyme prodrug therapy) for CPA activation is strongly depending on sufficient oxygen supply (50). Therefore it was required to evaluate this gene therapy approach under tumor specific conditions including hypoxia and limited diffusion.

1.3 Resistance to chemotherapy

Despite advances in the treatment of progressed cancer via chemotherapeutic regimes, outcome is often unsatisfying. One obstacle in chemotherapy such as CPA treatment is the occurrence of resistance against the applied treatment regime (51). Resistance of tumors towards chemotherapeutic treatment are multifaceted (52;53) being primary (intrinsic) or secondary (acquired). In the case of intrinsic resistance, the tumor (and metastasis thereof) is not sensitive towards the treatment regime from the beginning of the treatment. Secondary resistance occurs as a consequence of adoption mechanisms of the tumor under treatment with chemotherapeutic drugs (54). Therefore primary and secondary resistance has to be further investigated and considered for choosing an adequate treatment regime.

Evaluation of primary resistance towards chemotherapeutic treatment is difficult in conventional in vitro monolayer cell cultures because reasons for that kind of resistance are often based on multicellular community effects. Primary resistance can be mediated by interactions through cell-cell-contacts and/or by micro environmental properties. Therefore the phenomena of primary resistance is rather an effect of the collective of tumor cells than of the properties of individual cells (55;56). Therefore, tumor cells have to be cultured as multicellular spheroids to overcome the obstacles for investigation of primary resistance phenomena in vitro. Primary resistance was already described for tumor cells cultured as spheroid and treated with CPA (57).

The reasons for secondary resistance are based either on properties of the individual tumor cells or may result out of changes in the interaction of tumor and tumor stroma cells in vivo. Classic secondary chemoresistance occurs due to adoption processes of individual tumor cells, and can be subdivided into typical multidrug resistance (MDR) and atypical resistance. In contrast to primary resistance phenomena,

classical secondary chemoresistance can be evaluated in standard monolayer cultures. Usually typical multidrug resistance results from effective efflux of the drug by overexpression of transporters of the unspecific ABC (ATP-binding cassette) transporter family (53). On the other hand, atypical secondary resistance of the individual tumor cells can be mediated by the expression of alternative ABC-transporters, intracellular detoxication mechanisms, increased DNA repair, modification of drug target molecules or modulation of apoptotic and survival pathways (e.g. NF-κB modulation) (54;58-60). More recently, a form of acquired drug resistance based on changes in the interplay of tumor and tumor stroma cells is discussed (61;62). Tumor therapy approaches that do not target tumor cells directly but modulate cytokine expression and/or are antiangiogenic strategies should be, in theory, independent of drug resistance, due to the genetic stability of the targeted cells. Interestingly, acquired resistance occurs towards treatment approaches that do not directly target tumor cells. Failure of antiangiogenic treatment regimes may be due to the forming of so called mosaic vessels. In this situation tumor cells take over the function of endothelial cells to ensure tumor blood supply despite ongoing antiangiogenic treatment (63;64). For investigation of the complex process leading to failure of antiangiogenic treatment in vivo studies have to be carried out.

1.3.1.1 Multicellular tumor spheroids

Conventional monolayer culture of tumor cells is not suitable to evaluate phenomena of primary drug resistance due to the fact that these are strongly connected with interactions of tumor cells via cell-cell contacts and micro environmental properties. Therefore, cell culture systems are required that allow three dimensional growth of tumor cells. Multicellular tumor spheroid cultures represent such a cell culture system that is closer to the situation of in vivo tumors regarding cell contacts and environment (65). Multicellular spheroids of tumor cells can be generated by distribution of a single cell suspension in a matrix forming preparation containing the cell culture medium. In this thesis a modified chondrocyte cell culture system was used in order to establish three dimensional tumor spheroids (66;67).

1.3.1.2 NF-κB

NF-κB is a crucial factor in angiogenesis of tumors and in mediating resistance towards chemotherapeutic treatment (68-71). Antitumoral effects of cytotoxic anticancer drugs are often mediated by apoptotic processes initialized through

damage of DNA or proteins in cancer cells. Chemotherapy resistance evoking changes in apoptotic pathways can occur upstream of caspase activation and may be regulated by stress response mechanisms. NF-κB is one crucial stress responsive transcription factor controlling multiple pathways that are connected with apoptosis, cell survival and cytokine expression. Moreover, NF-κB is involved in several pathways regarding to the expression of proangiogenic cytokines (72;73). In order to evaluate a potential role of NF-κB in chemoresistance to CPA therapy, cancer cells were reisolated from in vivo tumors and monitored for NF-κB activity levels.

1.4 Objectives of this thesis

To overcome current obstacles of tumor therapy, new anticancer strategies regarding efficiency, reduced side effects and resistance have to be investigated. Therefore, low dose CPA therapy was combined with a gene therapy approach (GDEPT concept). In this context studies were performed to provide i) a suitable in vitro tumor mimicking cell culture model and evaluation of the GDEPT approach in vitro and in vivo, ii) to evaluate effects of the CPA metabolite acrolein on antiangiogenic activity and iii) to elucidate limitations regarding primary and secondary resistance.

1. Evaluation of the GDEPT concept with P450 CYP2B1 as the therapeutic gene in combination with low dose CPA treatment. A starting point was to establish an appropriate cell culture model mimicking tumor environment. In situ activation of CPA, enzymatic activity of the expressed transgene and influences regarding limited diffusion were to be studied and compared with experiments performed with conventional cell culture technique. Further on, bystander activity that is one of the basic principals of GDEPT had to be investigated in the new cell culture system. In the context of bystander activity an additional focus was on antiangiogenic strategies. Moreover, targeting and therapeutic gene delivery was investigated on primary endothelial cells (compare Annex to the thesis).
2. Metronomic scheduled CPA was shown in several studies to affect tumor induced angiogenesis. It was already shown that activated CPA inhibits proangiogenic properties of cultured endothelial cells. A potential antiangiogenic role of the metabolite acrolein in a metronomic scheduled CPA therapy was investigated in this thesis. One additional aim was the development of a reliable method for measuring antiangiogenic effects in experimental tumors.
3. Elucidation and classification of primary and secondary resistance of tumors in vivo. Resistance phenomena that occurred during CPA therapy were evaluated with special attention to changes in tumor vessel markers.

2 Materials and methods

2.1 Chemicals and reagents

2.1.1 Polyethylenimine (PEI)

Branched PEI with an average molecular weight of 25kDa (BPEI) and linear PEI with an average molecular weight of 22kDa (LPEI) were obtained from Sigma-Aldrich (Munich, Germany) and Euromedex (Exgen 500, Euromedex, Souffelweyersheim, France), respectively.

Both were dissolved in water, neutralized with HCl and gel filtrated on a Sephadex G-25 superfine column using 20mM HEPES, 0.25M NaCl, pH 7.4. For polyplex preparation, LPEI and BPEI were used as a 1mg/ml working solution.

2.1.2 Plasmid DNA

Plasmid pCMV-LUC (Photinus pyralis luciferase under control of the CMV promoter/enhancer) described in (74) was produced endotoxin-free by Elim Biopharmaceuticals (San Francisco, CA, USA) or Aldevron (Fargo, ND, USA) or PlasmidFactory (PlasmidFactory GmbH & Co. KG, Bielefeld, Germany) or was purified with the EndoFree Plasmid Kit from Quiagen GmbH (Hilden, Germany).

Plasmid pEGFP-N1 (encoding enhanced green fluorescent protein (EGFP) under the control of the CMV promoter/enhancer were purchased from Clontech Laboratories, Inc. (Heidelberg, Germany) or Elim Biopharmaceuticals.

pCMV-CYP2B1 (rat cytochrome P450 under the control of CMV promoter/enhancer) described in (75) was produced endotoxin-free by Elim Biopharmaceuticals (San Francisco, CA, USA).

Hypoxia response element HRE–luciferase reporter constructs pHRE-LUC (firefly luciferase) were synthesized as described in (76).

Renilla LUC-expressing plasmid pRL-SV40, utilized as an internal control, was obtained from Promega GmbH (Mannheim, Germany). Both plasmids constructs were provided by Dr. A. Kurosh.

Plasmid pNFκB-LUC (Luciferase under control of a NF-κB level sensitive promoter/enhancer) was obtained from Clontech Laboratories, Inc. (CA, USA).

Negative control plasmid pTAL-LUC was also obtained from Clontech Laboratories, Inc. (CA, USA).

2.1.3 Recombinant proteins

Recombinant human FGF-basic growth factor was obtained from Peprotech, London UK and was added to M199 medium (Invitrogen) for the cultivation of HUVEC cells in a final concentration of 20ng/ml. Human recombinant TSP-1 was obtained from Immun Diagnostik, Bensheim, Germany.

2.1.4 Other reagents

Natriumthiosulfate, glycerine, natriumcarbonate, silvernitrate, 3-aminophenol, natriumchloride and DMSO for MTT assay, were obtained from Merck KGaA, Darmstadt, Germany. Acrolein and cyclophosphamide-monohydrate were obtained from FLUKA Chemika, Milwaukee, WI. Collagenase Type II was obtained from Biochrom AG, Berlin, Germany; Agarose Ultrapure and Geneticin G418 were obtained from Invitrogen, Oregon, USA. 4-Hydroperoxy-CPA was obtained from Dr. Ulf Niedermeyer (Tel. +49 01726611870 or +49 05212080977). All other reagents were obtained from Sigma-Aldrich, Taufkirchen, Germany.

2.1.5 Software

Evaluation of receptor status and analysis of polyplex cell association was carried out by using the WINMDI 2.8 software (Windows Multiple Document Interface for Flow Cytometry). The software is downloadable at http://facs.scripps.edu/software.html.

The MIPAV application (Medical Image Processing, Analysis, and Visualization) was used for measuring Hoechst33258 fluorescence levels in CT26 tumor slides after systemically application. The software was downloaded from http://mipav.cit.nih.gov/.

Axio vision and Axio vision LE (Carl Zeiss, Jena, Germany) was used for presenting immunohistochemical analysis and for measuring migration capability.

Microsoft Excel and WinStat (R. Fitch software, Bad Krozingen, Germany) were used for generating diagrams and performing statistical analysis.

2.1.6 Antibodies

Primary antibodies

Rabbit-anti-laminin antibody was obtained from Chemicon Europe, Hampshire, UK. The mouse-anti-human CD51/CD61 complex antibody, anti-human CD71 receptor antibody, mouse-anti human Epidermal growth factor receptor (EGF) clone H11 antibody and IgG1, negative control antibody were obtained from Dako, Copenhagen, Denmark.

The rat-anti-mouse CD31 antibody was obtained from CALTAG, Burlingame, USA;

PE rat IgG control antibody and PE rat anti-mouse antibody were both obtained from Pharmingen, BD Biosciences, Canada. The mouse-anti-ratCYP2B1 antibody was obtained from Oxfordbiomedical Research, Oxford, UK; rat-anti-mouse CD51 was obtained from Biolegend, Biozol, Eching, Germany; anti-acrolein-antibody ACR, monoclonal antibody was obtained from JaICA, Japane and the Mouse anti TSP-1 Ab-4 (Clone A6.1) was obtained from Lab vision, Neomarkers, Westinghouse, CA.

Secondary antibodies

Texasred labelled goat-anti-rabbit antibody was obtained from Vector, Burlingame, UK. The ALEXA488 labelled goat-anti-rat antibody and the ALEXA488 labelled goat –anti-mouse antibody were obtained from Invitrogen, Oregon, USA. ALEXA467-anti-rat antibody and the ALEXA488-anti-mouse were obtained from Invitrogen, Oregon, USA. The Cy5 labelled anti-mouse antibody was purchased from Jackson ImmunoResearch Laboratories, Inc., Newmarket, England.

2.1.7 Measurement of protein concentration

BIO-RAD protein assay (BIO-RAD, Munich, Germany)

The concentration of protein containing samples was measured with the BIO-RAD protein assay (BIO-RAD, Munich, Germany) according to the manufactures instructions. BSA was used for the protein standard curve.

BCA protein assay (Pierce, Rockford, IL)

The concentration of protein containing samples was measure with the BCA protein assay (Pierce, Rockford, IL) in the case of the TSP-1 induction experiment according to the manufactures instructions. BSA was used for the protein standard curve.

2.2 Cell biological methods

2.2.1 Cell culture

Cell culture media, antibiotics, fetal bovine serum (FBS), G148 (geneticin) and trypsin/EDTA solution were purchased from Invitrogen GmbH (Karlsruhe, Germany).

All cultured cells were grown at 37C in 5% CO_2 humified atmosphere in incubators (Heracell) obtained from Kendro Laboratory products, Langenselbold.

CT26/X39 cells were cultured in DMEM low glucose medium, supplemented with 10% FBS, whereas X39 were established from the CT26 murine colon carcinoma cells (ATCC CRL-2638) by stable transfection with linearised pCMV-CYP2B1 plasmid DNA. Neuro2A murine neuroblastoma cells (ATCC Cl-131) were cultured in DMEM

low glucose medium, supplemented with 10% FBS. 9L and 9L-2DB1 were obtained from D. Waxman and were cultured in DMEM low glucose medium, supplemented with 10% FBS.

HUH7 hepatocellular carcinoma (JCRB 0403; Tokyo, Japan) were grown in DMEM/F12 (1/1) with Glutamax I medium supplements with 10% FBS. PC3 human prostate carcinoma cells (CRL1435) were cultured in RPMI medium supplemented with 10% FBS.

Endothelial cells HUVEC (pooled human umbilical vein endothelial cells) were obtained from ATCC (Manassas, Virginia) and PEC cells, which were provided by J. Pelisek were cultured on collagen G coated plates in M199 medium supplemented with 20ng/ml human bFGF and 10% FBS. Isolated primary fibroblasts from NF-κB-luciferase-reporter mice, provided by C. Culmsee, were grown on collagen G coated plates in M199 medium supplemented with 10% FBS.

For in vitro experiments, all cell lines and primary cells were grown in medium, supplemented with 100 U/ml penicillin and 100µg/ml streptomycin.

2.2.2 Agarose overlay technique

Cells were seeded either in 24-well (Hoechst 33258 diffusion experiment) or 48-well plates (all other assays) 24 h prior to addition of the agarose overlay. Culture medium was removed and replaced with 345 µl medium (24-well plates) or 200 µl medium (48-well plates) containing 0.5% (w/v) agarose. The agarose-containing medium was obtained by stepwise dilution of complete medium with melted agarose (10% agarose in PBS, w/v). Before applying the agarose-containing medium to the seeded cells, the medium was allowed to cool to 37°C. After solidification of the agarose, 1040 µl (24 well-plate) or 600 µl (48-well plate) of complete culture medium without agarose (+/- CPA) was added to the cells.

2.2.3 Multicellular spheroid culture (Agarose suspension culture)

For generating agarose wrapped multicellular spheroids, a single cell suspension of the indicated tumor cells was mixed with 1% agarose (Ultrapure, Invitrogen) containing cell culture medium in a ratio of 1:1. 50µl of the obtained cell suspension was applied in an agarose coated 24 well plate (TPP, Switzerland). After solidification of the agarose, 500µl of the indicated standard cell culture medium was added to the well. Multicellular spheroids were cultured for several days, whereas replacement of cell culture medium was performed every third day.

2.2.4 Coculture in a transwell system

Coculture experiments were partly performed by using a transwell system. Therefore target cells were seeded in a 24 well plate (TPP, Switzerland) and producer cells (X39 tumor cells) were seeded in a transwell insert with a pore size of 8µm (NUNC, Denmark) about 24h prior to the administration of CPA. For performing the coculture, the inserts were transferred to the 24 well plate with a sterile tweezers.

2.2.5 Storage of isolated and other cells

Cells were harvested with trypsin/EDTA, followed by removing supernatant by centrifugation for 5min at 150g (Haereus, Megafuge 1.0 R). Cells were resuspended in FBS containing 10% DMSO (Sigma) and freezing was carried out, whereas the temperature dropped 1°C per minute, until -80°C was reached. Frozen cells were then transferred to a nitrogen storage tank for long term storage.

2.3 Molecular biological methods

2.3.1 Restriction digestion of plasmid DNA

pCMV-CYP2B1 plasmid DNA was incubated with restriction enzymes BamHI and XHO1 (Promega, Mannheim, Germany) for 2-3h. For digestion, 5 units of the desired restriction enzyme per µg DNA was used in the appropriate restriction enzyme buffer according to manufactures instructions. Success of digestion was tested by agarose gel electrophoresis.

2.3.2 Linearizing of plasmid DNA

Plasmid pCR3.1-CYP2B1 was linearized by digestion with XhoI, followed by agarose gel electrophoresis and Qiaprep® Spin MiniprepKit 250 (Qiagen) purification according to the manufacturer's instructions. Plasmid DNA content was evaluated by UV absorption measurement at 260nm and 280nm respectively.

2.3.3 Generation of stably transfected single cell clones

CT26 and Neuro2A cells were seeded and transfected in 24-well plates. The transfection complex of linearized pCR3.1-CYP2B1 plasmid with PEI was generated at an N/P ratio (nitrogen in PEI/phosphate in DNA) of 6 in HBS (HEPES buffered saline: 20mM HEPES pH 7.1, 150mM NaCl) at a final DNA concentration of 20 µg/ml. Forty eight h after transfection, cells were selected with 0.5 µg geneticin per ml culture medium. To obtain subclones, the surviving cells were re-seeded in a 96-well plate at 1 cell/well after 2 wk of geneticin selection. Subclones were analyzed and

characterized for CYP2B1 activity using 7-pentoxyresorufin as substrate. Clone X39 gave the highest P450 activity and was used in all subsequent experiments.

2.4 Polyplex formation and transfections

In general, polyplexes were generated by condensing plasmid DNA encoding luciferase, EGFP-N1 or pCMV-CYP2B1 with LPEI at a molar ratio of PEI nitrogen to DNA phosphate (N/P) of 6. For this reason, plasmid DNA and PEI or PEI conjugates were each diluted in HBS (HEPES buffered saline, and rapidly mixed by pipetting up and down 10 to 20 times. DNA/PEI polyplexes were prepared at a final DNA concentration of 20µg/ml. Polyplexes were allowed to stand for at least 20min at room temperature before use.

2.5 Gene expression assays

2.5.1 Luciferase reporter gene expression in vitro experiments

Cells were plated in the indicated densities either in 48 well- or in 24 well- plates 24h prior to transfection. In case of primary endothelial cells or fibroblasts well plates were coated with collagen G prior seeding. Transfection complexes with indicated amounts of plasmid DNA were added to the cells in 300µl of cell culture medium. Medium was replaced 4h after the transfection and gene expression was measured at the indicated time points (if not mentioned, measurement was performed 24h after transfection). Detection of luciferase activity was carried out as described recently (77). Luciferase activity levels were expressed as relative light units (RLU) per seeded cells (mean ± SD from n=3, n=4 or n=6) or were normalized on activity levels of control cells. 2ng of recombinant luciferase (Promega, Mannheim, Germany) correspond to 10^7 relative light units (RLU).

Detection of luciferase activity under the control of a NF-κB sensitive promoter in primary fibroblasts was carried out with a prolonged signal measure time of 30s.

In the case of hypoxia induction studies, cells were plated in the indicated density on 6 well plates prior to transfection. Detection of luciferase activity was carried out at the indicated time points with the Promega Dual Luciferase kit according to manufactures instructions.

2.5.2 EGFP reporter gene expression

Indicated number of cells was seeded 24 h prior to transient transfection in a 48-well plate (NUNC). Cells were transfected with the indicated amount of pCMV-EGFP-N1

using linear PEI (N/P 6 in HBS). Medium was replaced 4h after transfection. Forty eight h after transfection, the cells were washed with PBS and harvested by trypsin treatment. For analysis of EGFP expression, the cells were analyzed as described (78) or by counting GFP positive cells by fluorescence microscopical analysis.

2.5.3 CYP2B1 gene expression

Indicated number of cells was seeded 24 h prior to transient transfection in a 48-well plate (NUNC). Cells were transfected with the indicated amount of pCMV-CYP2B1 using linear PEI (N/P 6 in HBS). Medium was replaced 4h after transfection. Forty eight h after transfection, the cells were washed with PBS and harvested by trypsin treatment. For analysis of CYP2B1 expression, the cells were analyzed after antibody-staining by FACS analysis as described (79) or by counting positively stained cells by fluorescence microscopical analysis.

2.5.3.1 CYP2B1 Transgene expression analysis after transient transfection

HUH7 cells were seeded 24 h prior to transient transfection in a 48-well plate. Cells were transfected with 100 ng pCMV-CYP2B1 or pCMV-EGFPN1 using linear PEI (N/P 6 in HBS). Forty eight h after transfection, the cells were washed with PBS and harvested by trypsin treatment. For analysis of EGFP expression, the cells were analyzed as described (80). For analysis of CYP2B1 expression, cells were fixed with 2% paraformaldehyde in PBS, followed by permeabilization with 0.1% (w/v) Triton X-100 in PBS. Cells in 5% FBS in PBS were incubated with mouse monoclonal anti-rat CYP2B1 (Oxford Biomedical Research, Oxford, MI, USA) or, as a control, with non-specific mouse isotype control antibody. Alexa488-conjugated goat anti-mouse IgG (Molecular Probes) was used as second antibody. Cells were analyzed on a Cyan MLE flow cytometer (Dako Cytomation, Kopenhagen, Denmark). As an additional control, non-transfected cells were similarly stained and analyzed.

2.5.4 NF-κB activity studies

NF-κB levels in primary endothelial cells

Screening for NF-κB activity levels of primary endothelial cells (HUVECs) were performed in the absence or in the presence of different concentrations of acrolein in the medium. Therefore HUVEC cells were seeded on collagen coated (Collagen G, Biochrom) 24 well plates in a density of 15000 cells/well prior to transfection. HUVEC cells were transfected with LPEI polyplexes (N/P 6, HBS, 300ng/well) containing either pNFκB-LUC plasmid or pTAL-LUC plasmid DNA. Medium was replaced 4h

after transfection with 300µl of fresh medium and cells were cultivated for further 20h at standard conditions (37ºC, 5% CO_2, 20.9 %oxygen). 24h after the transfection different amounts of acrolein (dissolved in PBS) were added to the cells. Control cells were vehicle treated (PBS). Cells were cultivated for further 24h and detection of luciferase activity was carried out as described in 3.5.1.1. NF-κB induced luciferase expression was normalised on pTAL-LUC activity levels.

NF-κB levels in tumor cells (CT26)

Screening for NF-κB activity levels of CT26 tumor was performed in the absence or in the presence of different concentrations of Acrolein in the medium. Therefore CT26 cells were seeded on 24 well plates in a density of 15000 cells/well prior to transfection. CT26 cells were transfected with LPEI polyplexes (N/P 6, HBS, 400ng/well) containing either pNFκB-LUC plasmid or pTAL-LUC plasmid DNA. Medium was replaced 4h after transfection with 300µl of fresh medium and cells were cultivated for further 20h at standard conditions (37ºC, 5% CO_2, 20.9 %oxygen). 24h after the transfection different amounts of acrolein (dissolved in PBS) were added to the cells. Control cells were vehicle treated (PBS). Cells were cultivated for further 24h and detection of luciferase activity was carried out as described in 3.5.1.1. NF-κB induced luciferase expression was normalised on pTAL-LUC activity levels.

NF-κB levels in other tumor cells

Screening for NF-κB activity levels of PC3 and reisolated PC3ID3 and PC3ID4 as well as HUH7 and reisolated HUH7 REISO and Neuro2A and Neuro2A REISO cells was performed by transfection with a NF-κB sensitive luciferase encoding plasmid. Therefore all mentioned parental and reisolated cells were seeded on 24 well plates in a density of 15000 cells/well 24h prior to transfection. Cells were transfected with LPEI polyplexes (N/P 6, HBS, 400ng/well) containing either pNFκB-LUC plasmid or pTAL-LUC plasmid DNA. Medium was replaced 4h after transfection with 300µl of fresh medium and cells were cultivated for 44h at standard conditions (37ºC, 5% CO_2, 20.9 %oxygen). Detection of luciferase activity was carried out as described in 3.5.1.1. NF-κB induced luciferase expression was normalised on pTAL-LUC activity levels.

NF-κB levels in primary fibroblasts

Primary fibroblasts expressing luciferase under the control of a NFKB sensitive promoter were obtained from transgene animals (NFKB-LUC-Mice). Fibroblasts were

seeded on collagen coated (Collagen G, Biochrom) 24 well plates in a density of 15000 cells/well. 24h after the seeding cells were treated with different concentrations of acrolein (dissolved in PBS). Control cells were vehicle treated (PBS).

2.6 Assays for detection of CYP2B1 enzymatic activity

2.6.1 Resorufin assay

A modified form of a previously described assay (81) was used to assay CYP2B1 enzymatic activity. Cells were incubated in 48-well plates with 200 µl Optimem I medium containing 1.7 µM 7-pentoxyresorufin and 100 µM 3,3´-methylene-bis(4-hydroxycoumarin) ('substrate solution') for 20 to 120 min. Following incubation, the cells were subject to a freeze-thaw-cycle to stop the enzymatic reaction. The supernatant was transferred to a 1.5 ml reaction tube, centrifuged at 15,000 *g* for 10 min and 150 µl of the clear liquid was assayed for fluorescence using a Cary Eclipse fluorimeter (Cary, Mulgrave, Australia) with excitation and emission wavelengths set to 562 and 585 nm, respectively. Measurements were performed in triplicate and enzyme activity was expressed as relative fluorescence units (RFU).

When measuring CYP activity under the agarose layer 200µl substrate solution was injected between the adherent cells and the agarose layer after solidification of the agarose (200µl). After 40min of incubation at 37°C the agarose layer was removed and resorufin content quantified in the supernatant. In the "–gel" samples, 200µl substrate solution was added to the cells under standard conditions, incubated for 40min at 37°C and resorufin content quantified thereafter. In the case of the "gel removed" samples, cells were overlaid with 200µl agarose for 1h. Thereafter the gel was removed, 200µl substrate solution added to the cells and after incubation at 37°C for 40min resorufin was quantified in the supernatant. No significant amounts of resorufin were found in the agarose layer, indicating that the majority of resorufin is localized in the solution between the cells and the agarose overlay.

When performing the pentoxyresorufin assay in a hypoxia chamber, 100,000 X39 cells were seeded in a 3.5 cm culture dish. Twenty four h after seeding, the cells were incubated in the hypoxia chamber for 40 min with 500 µl of the substrate solution either under normoxia (21% O_2) or under various decreased O_2 concentrations, with O_2 replaced by a mixture of N_2 and CO_2. Oxygen partial pressure was measured with a digital oxymeter (GMH 3690, Greisinger Electronic,

Germany). Relative humidity and temperature (37°C) were similar under all conditions.

For validation recovery of resorufin in biological fluidics was investigated. Therefore different amounts of resorufin (solved in PBS) were added to the resorufin incubation solution. The detection of the added resorufin was performed by fluorescence measurement as described above.

Thereby, concentrations of added resorufin were chosen in an interval that is relevant for in situ released resorufin by CYP2B1 enzymatic reaction. FIG 2-1 demonstrates that measured fluorescence signal of the recovered resorufin in the incubation solution depends on its concentration in a linear manner.

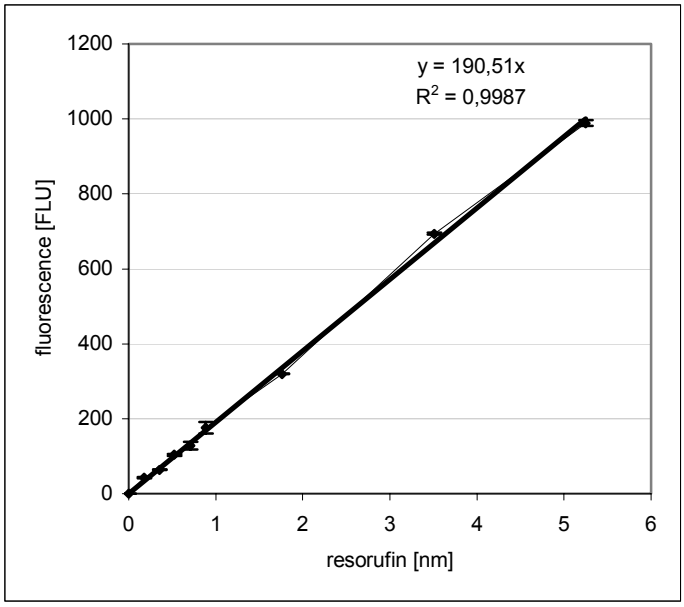

Fig.: 2-1 Validation of recovery of resorufin in biological fluidics. Different amounts of resorufin were added to the resorufin incubation solution in order to achieve cell culture medium with increasing concentrations of resorufin. Resorufin recovery was performed by fluorescence measurement (562nm/585nm). Values are means ±SE of duplicates

Further evaluation of the resorufin assay was performed on the X39 cell line because of the high CYP2B1 enzymatic activity of the cell line.

The amount of in situ produced resorufin was proportional to the incubation time (FIG 2-2 A) and proportional to cell count (FIG 2-2 B).

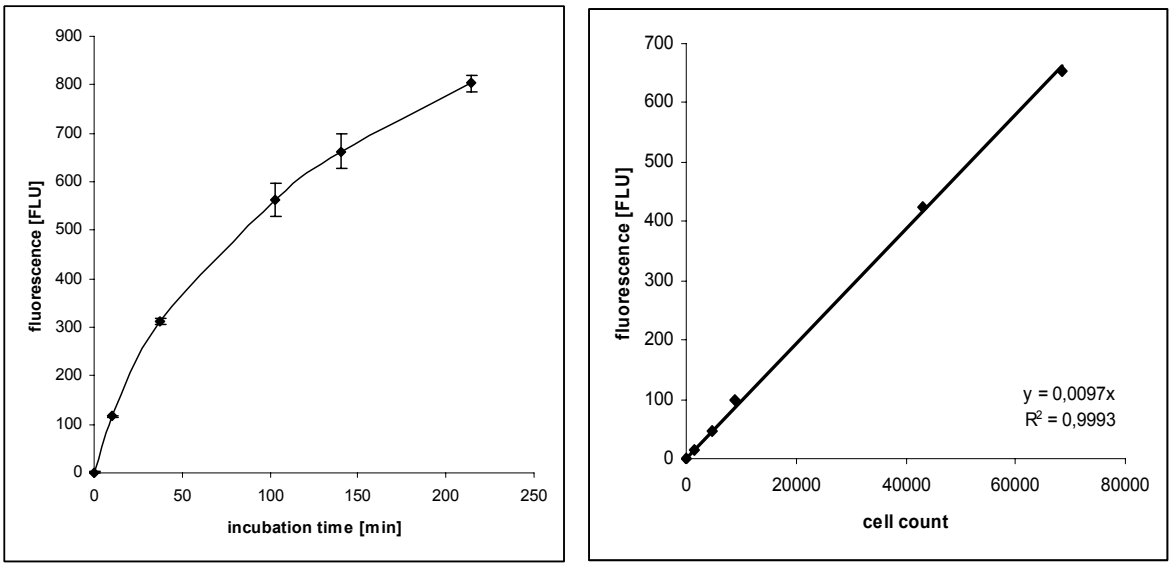

A B

Fig.: 2-2 Validation of the resorufin assay for detection of CYP2B1 activity in cultured cells. A) X39 cells were cultured with resorufin assay incubation solution for different incubation times. Resorufin in the supernatant was determined by fluorescence measurement after a freeze-thaw-cycle. Values are means ± SD of triplicates. B) Different amounts of X39 cells were cultured with resorufin incubation solution for 60min. After a freeze-thaw cycle resorufin was determined in the supernatant by fluorescence measurement. Values are means ±SE of duplicates.

2.6.2 Acrolein assay

A modified form of an previously described assay (82-84) was used to measure CYP2B1 enzymatic activity in the context of CPA conversion.

In contrast to the described assay, the cell incubation solution included 0.005M semicarbazide to reduce protein adduct forming in a FBS containing medium. After the incubation, cells were subjected to a freeze-thaw cycle, followed by removal of proteins by precipitation. Therefore, 500µl of the incubation solution was drugged with 200µl of a sated solution of barium hydroxide and 200µl of a sated solution of zinc chloride. After an centrifugation step, the acrolein in the supernatant was derivatized as described previously (85). Derivatised acrolein was detected by fluorescence measurement; measurements were performed by using a Cary Eclipse fluorimeter (Cary, Mulgrave, Australia) with excitation and emission wavelengths set to 350nm and 515nm, respectively. Measurements were performed in triplicate and enzymatic conversion capability was expressed as relative fluorescence units (RFU).

For validation, recovery of acrolein in cell culture medium was investigated. Therefore indicated amounts of acrolein (solved in PBS) were added to the incubation solution. Protein precipitation, derivatising and the detection of added acrolein was performed

by fluorescence measurement as described above. Thereby, concentrations of added acrolein were chosen in an interval that is relevant for in situ released acrolein by CPA conversion. FIG 2-3 demonstrates that measured fluorescence signal of the recovered acrolein in the incubation solution depends on its concentration in a linear manner up to 30µM.

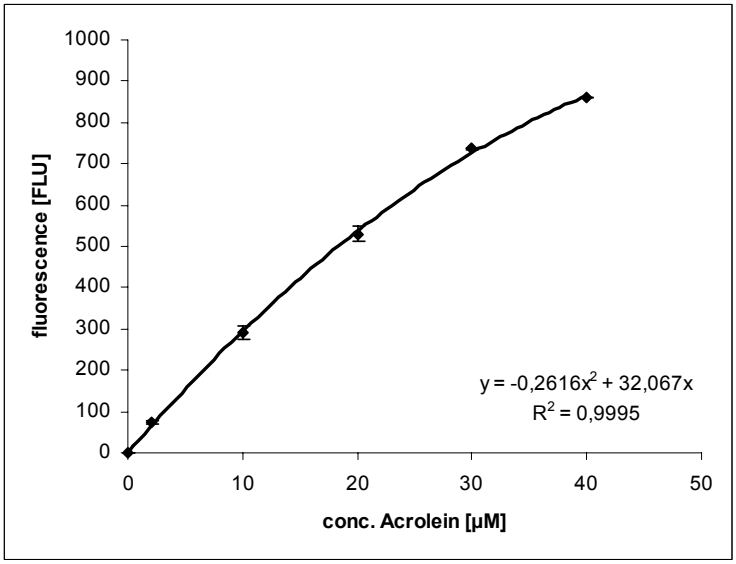

Fig.: 2-3 Validation of acrolein recovery in cell culture medium supplemented with 10% FBS. Different amounts of acrolein were added to cell culture medium (DMEM, low glucose, supplemented with 10% FBS) in order to achieve medium with increasing concentrations of acrolein. Acrolein recovery was performed with the acrolein assay described in materials and methods. Values are means ±SE of triplicates.

2.7 Hypoxia induced HRE-responsible gene expression

Control hypoxia induction studies were performed with CT26 and Neuro2A cells. 20.000 CT26 or Neuro2A cells were seeded in 6 well plates (NUNC). 24h after the seeding cells were transfected with LPEI polyplexes (N/P 6, HBS, 1000ng/well) containing pHRE-LUC and pRL-SV40 plasmid DNA (400:1 w/w). Medium was replaced 4h after transfection and cells were cultivated for 20h at standard conditions (37ºC, 5% CO_2, 20.9 %oxygen). Cells were cultured for further 24h at 37ºC in humified atmosphere containing either air (20.9% oxygen; normoxia) or air sufficient to give 1% oxygen. 5% CO2 was used in all normoxic and hypoxic incubators, with the balance being nitrogen in the hypoxic incubation. Oxygen partial pressure was measured with a digital oxymeter (GMH 3690, Greisinger Electronic, Germany).

Firefly and Renilla luciferase expression levels were determined by the Promega Dual Luciferase kit according to the manufactures instructions.

For hypoxia induction studies referring to the agarose overlay technique 200.000 CT26 or Neuro2A cells were seeded in 6 well plates (NUNC). 24h after the seeding cells were transfected with LPEI polyplexes (N/P 6, HBS, 1000ng/well) containing pHRE-LUC and pRL-SV40 plasmid DNA (400:1 w/w). Medium was replaced 4h after

transfection and cells were cultivated for 20h at standard conditions (37ºC, 5% CO_2, 20.9 %oxygen). 24h after the transfection agarose overlay was performed with 1.6ml agarose (0.5% w/w) containing medium. 5.2ml agarose free medium was added after solidification to the well plates. Cells were cultured for further 24h in a humified atmosphere at 37ºC, 5% CO_2, 20.9 %oxygen. Afterwards, agarose overlay was removed and cells were analyzed for firefly and renilla luciferase activity by the Promega Dual Luciferase kit according to manufactures instructions. The Renilla LUC-expressing plasmid pRL SV40 (Promega) was included in each transfection, as an internal control to normalize LUC expression.

2.8 Angiogenesis assays

2.8.1 Migration assay wound healing (scratch wound assay)

HUVEC and PEC cells were plated onto collagen G (Biochrom AG) coated chamber slides (IBIDI, Munich, Germany) or glass cover slips (15000 cells/well) 24h prior performing the scratch wound assay. When cells were confluent, the monolayer was scratched by a yellow pipette tip. Detached cells were rinsed away with PBS and the medium was changed. Digital image of cells was taken immediately after scratching (t=0) and after the incubation time. Cells were cultivated for further 24h in the presence of indicated concentrations of acrolein or in cocultivation with CYP2B1 expressing X39 cells with or without CPA. The distance between cells in the scratched area was measured using the Axio vision LE software (Zeiss, Jena, Germany). Ten measurements were performed for each data point. The results were calculated in% rate of migration, whereas time point 0 was considered as the starting point and the 24h time point in the control experiments was considered as 100% cell migration.

2.8.2 Tube formation assay

Cooled matrigel (Sigma, Germany) 50µl was added to each well of a 96 well plate (300µl to a 24well plate) and incubated at 37°C for 30min to allow polymerisation. HUVEC cells were harvested at a density of about 70% confluency and the cell suspension was added to each well of the plate and incubated for 4h in the absence or in the presence of indicated concentrations of CPA or acrolein, respectively. Cells were fixed with 4% paraformaldehyde (in PBS) and analyzed via transmitted light

microscopy. Total amount of tube like structures were detected, whereas only complete tubes were counted.

2.8.3 Staining for integrin αvβ3

Cells were cultured as described on collagen IV coated Lab-Tek chambered #1.0 Borosilicate cover glass system from NUNC. After treatment for 4h with indicated concentrations of acrolein the supernatant was removed and cells were washed with prewarmed PBS, followed by fixing with paraformaldehyde containing PBS (4% w/w) for 10min. In case of simultaneous staining of the F-actin cytoskeleton as well as integrin receptors the fixation was followed by a Triton-X 100 (0.1% in PBS) treatment for 5min. Thereafter, cells were washed two times with PBS containing 0.5% FCS. After the second washing step, cells were incubated for 10min with the FBS containing PBS to mask unspecific recognition sequences.

The supernatant was removed and replaced by 200µl of antibody containing (mouse-anti-human CD51/61 ((Dako, Copenhagen, Denmark)) PBS solution containing 0.5% FBS. The working dilution of the antibody was 1:200. After incubation for 2h at room temperature cells were washed for 3 times with PBS containing 0.5% FBS to remove unbound antibody. For simultaneous visualisation of the F-actin cytoskeleton and integrin receptors, cells were incubated with a solution containing Cy5 labelled anti mouse antibody (1:200) (Jackson ImmunoResearch Laboratories, Inc.) and Phalloidin-FITC with an end concentration of 0,165µM; the incubation was performed at room temperature for 1h in a humified atmosphere. Afterwards cells were washed repeatedly with PBS containing 0.5% FBS. Immediately after the washing procedure cells were embedded with vector shield mounting medium (Vector Labs, Burlingame, CA, USA) to avoid drying and bleaching processes. Pictures were obtained by using a Zeiss Axiovert 200 microscope. FITC-fluorescence was excited using a 470±20 nm bandpass filter and emission was collected using a 540±25 nm bandpass filter, whereas ALEXA467 was excited using a 640±20 nm bandpass filter and emission was collected using a 735±35 nm bandpass filter.

2.8.4 Staining for F-actin

Cells were cultured as described above on collagen IV coated Lab-Tek chambered #1.0 Borosilicate cover glass system from NUNC. After treatment for 4h with indicated concentrations of acrolein the medium was removed. Cells were fixed with PBS containing 4% (w/w) paraformaldehyde for 10min after washing with prewarmed

PBS. The fixing solution was removed completely and the cells were washed with prewarmed PBS again followed by a treatment with 0.1% Triton X-100 in PBS. After 5min of Triton X treatment, cells were washed two times with PBS containing 0.5% FCS. After the second washing step cells were incubated for 10min with PBS containing 0.5% FBS. Afterwards the supernatant solution was removed and replaced by 200µl of a 0,165µM phallotoxin-FITC (Sigma-Aldrich, Germany) containing PBS/FBS solution. After incubation for 30min at room temperature in the dark cells were washed again for 3 times with PBS containing 0.5% FBS to remove unbound phallotoxin-FITC. Immediately after the washing procedure cells were embedded with vector shield mounting medium (Vector Labs, Burlingame, CA, USA), to avoid drying and bleaching processes. Pictures were obtained by using a Zeiss Axiovert 200 microscope and using a 470±20 nm bandpass filter for excitation; emission was collected using a 540±25 nm bandpass filter.

2.8.5 Thrombospondin Elisa

HUVEC cells were seeded on collagen G (Biochrom AG) coated 24 well plates (TPP, Switzerland) in a density of 15000 cells per well. 24h after the seeding, cells were cultured with indicated concentrations of acrolein in the medium for further 24h. After the incubation, cells were washed with PBS followed by cell lyses with 100µl/well Millipore water and a freeze-thaw cycle. Subsequent centrifugation at 16,000g for 60min (4ºC) allowed removal of cell debris. 25µl of the supernatant was diluted with Diluent #2 (ChemiKine, Human TSP-1 EIA KIT, Chemicon, USA) to 100µl diluted sample. The samples were analyzed for TSP-1 level by the ChemiKine Human TSP-1 EIA KIT according to manufactures protocol.

Data thus obtained were normalized on protein content, measured by the BCA protein content assay (BCA, Protein Assay KIT, Pierce, Rockford, IL) according to manufactures protocol.

2.9 Proliferation and viability assays

2.9.1 Hoechst33258 DNA content assay

To assay for DNA content, culture medium and agarose layer were removed and cells were washed with PBS. After the washing procedure, cells were harvested with Trypsin-EDTA (100µl) and lysed with Millipore water (100µl) followed by freeze-thaw-cycle. 200µl of cell lyses buffer (20mM Tris, 2mM EDTA 5M NaCl, pH 7.4) containing

0.2µg/ml Hoechst 33258 dye were applied to each well, followed by another freeze-thaw-cycle. 200µl of the cell suspension were transferred to a black bottom 96 well plate (Greiner-Bio One, Frickenhausen, Germany). The DNA content was measured by quantifying fluorescence signal with a SPECTRAFluor Plus plate reader (Tecan, Grödig, Austria),using excitation and emission filters centered at 360nm (excitation) and 465nm (emission), respectively.

For verifying the qualification of this assay increasing cell numbers were transferred to Eppendorf tubes and centrifuged at 1000rpm. The pellets were analyzed by the Hoechst33258 based DNA content assay as described in materials and methods. Linear correlation between cell number and fluorescence signal in the DNA content assay was found. The correlation was verified for the following cell lines: 9L, 9L-D2B1, CT26, X39, Neuro2A and HUH7.

For safe cell count quantification at least 600 to 700 cells were required. (three fold fluorescence increase in comparison to signal to noise ratio)

FIG 2-4 demonstrates that the Hoechst 33258 based proliferation assay is reliable for cell numbers ranging from $1x10^3$ to $5x10^4$.

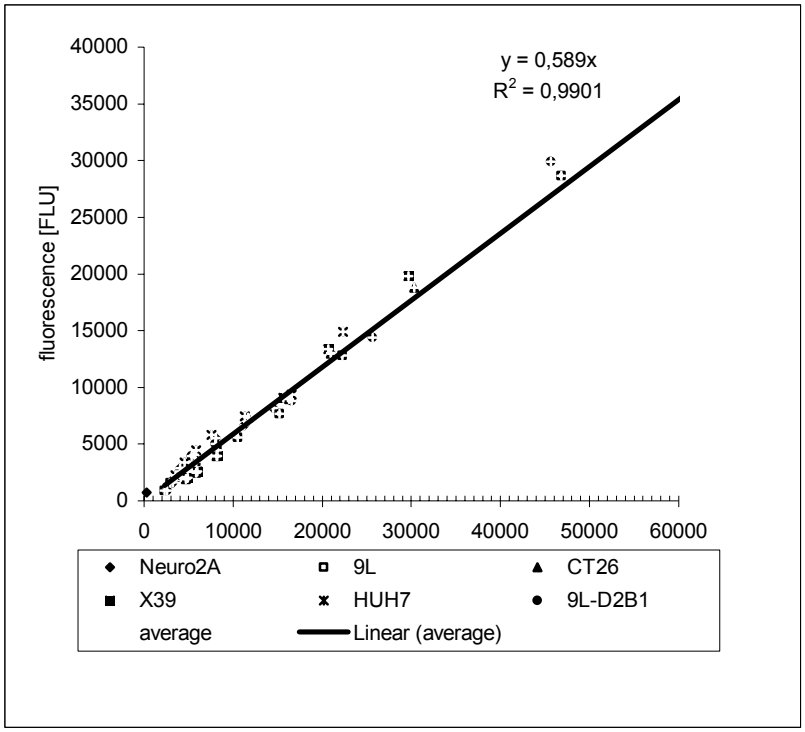

Fig.: 2-4 Validation of the Hoechst33258 based proliferation assay. Neuro2A, CT26, X39, 9L, 9L-D2B1 and HUH7 cells were harvested with trypsin/EDTA, followed by a freeze-thaw cycle. The assay was performed by incubating different cell numbers with TNE buffer containing Hoechst33258 in black bottom 96 well plates, fluorescence was determined at 465nm in a SPECTRAFluor Plus plate reader (excitation: 360nm). Values are means of duplicates.

Results obtained with the Hoechst33258 based DNA content assay correlate well with those of the MTT assay under normoxic conditions. However, cultivation of cells under long-term hypoxic conditions, results of the MTT assay were artificially low, indicating adaption mechanisms influencing metabolic activity in the MTT assay.

2.9.2 MTT assay

After removing the culture medium and, if applicable, the agarose layer, 300 µl of culture medium containing 0.25% MTT (w/v) was applied to each well after which the plates were incubated for 3 h at 37°C. MTT is converted to a colored, water insoluble formazan salt by the metabolic activity of viable cells. The culture medium was then removed and the cells were frozen at -80°C. After thawing the cells, 300 µl of DMSO was added to dissolve the insoluble formazan salt and absorbance at 590 nm was measured with a plate reader (Tecan, Grödig, Austria). A reference absorbance at 630 nm was subtracted from the absorbance at 590 nm for each well.

In order to verify the adequacy of this assay for the quantification of living cells different cell numbers were seeded and measured for metabolic activity by MTT assay as described above 24h after seeding. In a parallel experiment the seeded cells were harvested by treatment with trypsin/EDTA solution and cell number was determined by transmitted light microscopy.

The reliability of the MTT assay was verified for CT26, Neuro2A, 9L and HUH7 cells. Linear correlation between cell number (living cells) and MTT absorbance was found in all assayed cell lines.

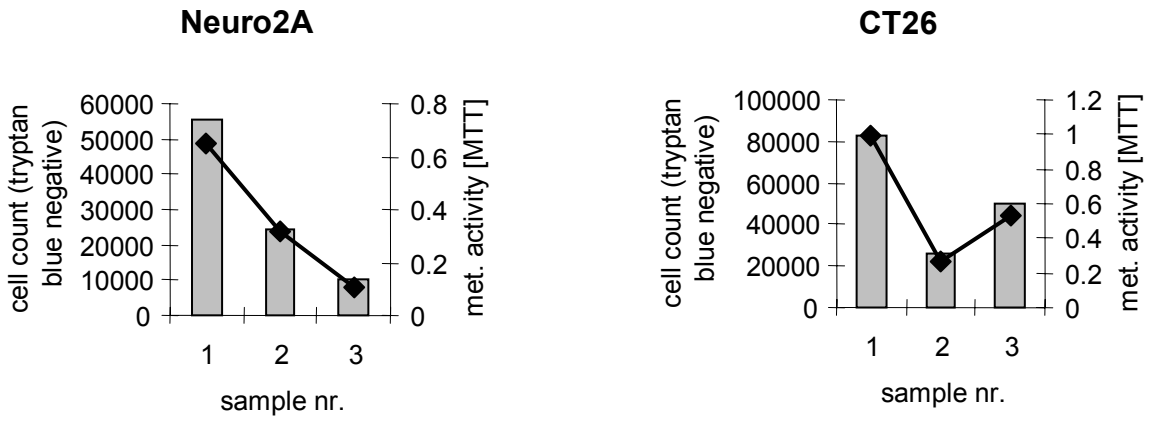

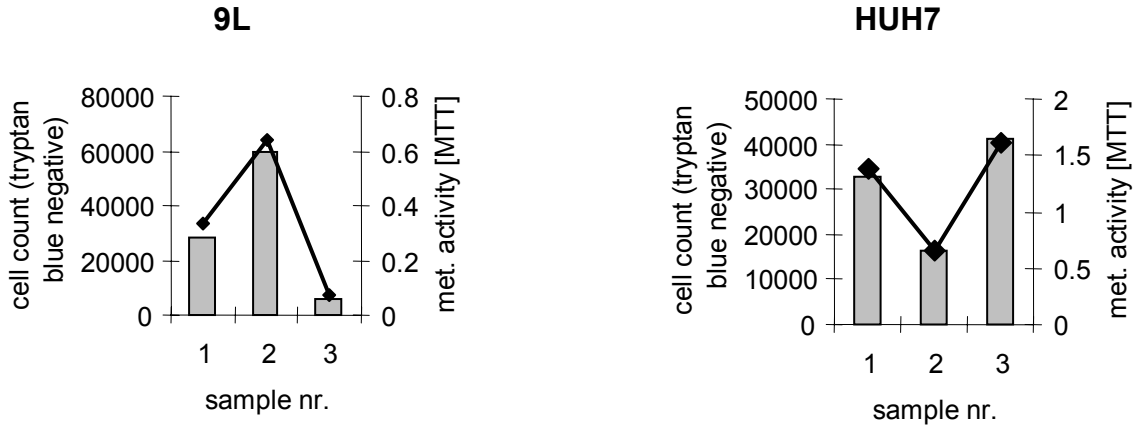

Fig.: 2-5 Validation of cell number (living cells) correlation with metabolic activity (MTT assay). Cell count of living cells was determined by transmitted light microscopy after addition of tryptan blue as a marker for viable cells. Values are means of duplicates. In a parallel performed MTT assay total metabolic activity of the cells was measured. Values are means of duplicates.

2.10 Flow cytometric analysis and microscopy

2.10.1 Flow cytometric analysis of EGF receptor and CD71 on reisolated tumor cells

Indicated reisolated tumor cells (PC3ID3, PC3ID4 and HUH7 REISO) and parental tumor cells (PC3 and HUH7) were seeded in 24 well plates (TPP, Switzerland) at a density of 40.000 cells per well 48h prior receptor status detection. Cells were washed with prewarmed PBS and harvested by treatment with trypsin/EDTA. The obtained cell suspensions were pooled and adjusted to 10^6 cells/ml with MACS buffer (PBS containing 2.5% FBS) after centrifugation for 5min at 150g (Haereus, Megafuge 1.0 R). The cell suspension was divided up and exposed to the following antibodies at 4°C for 1h; mouse-anti-human-EGF antibody (Dako) and mouse-anti-human CD71 antibody (Dako). Control staining was performed by using mouse IgG1, negative control antibody (Dako). All antibodies were applied at a total dilution of 1:200.

After primary antibody exposition, cells were washed repeatedly with prewarmed MACS buffer (PBS containing 2.5% FBS) to remove unbound antibody. Secondary antibody staining was performed by exposing the cell suspension to ALEXA488 labelled anti-mouse-antibody (Invitrogen), for 1h at 4°C. The secondary antibody was applied at a total dilution of 1:400.

Reisolated Neuro2A tumor cells and parental Neuro2A tumor cells were seeded in 24 well plates (TPP, Switzerland) at a density of 40.000 cells per well 48h prior receptor status detection. Harvesting and adjusting cell suspension to 10^6 cells/ml was

performed as described above. The cell suspension was divided up and exposed to the PE-labelled anti-mouse CD71 antibody (BD Pharmingen) at 4°C for 1h; control staining was performed by exposition to the corresponding PE-labelled rat-IgG-control antibody (BD Pharmingen). Both antibodies were applied at a total dilution of 1:200.

Samples were kept on ice until analysis. Receptor status was assayed by flow cytometry using a Cyan^{TM} MLE flow cytometer (Dako). The fluorophore of ALEXA488 labelled antibody was excited at 488nm and emission was detected by using a 530/40nm bandpass filter, whereas PE was excited through a 750nm longpass filter and emission was detected using a 613/20 bandpass filter.

To discriminate between viable and dead cells and to exclude doublets, cells were appropriately gated by forward/side scatter and pulse width. Antibody staining was evaluated via electronically analysis by using the WINMDI software.

2.10.2 Flow cytometric analysis of integrin receptor and aminopeptidase N on HUVEC cells

Cells were seeded in collagen G (Biochrome AG, Germany) coated 24 well plates (TPP, Switzerland) at a density of 20.000 cells per well 48h prior receptor status detection. Cells were washed with prewarmed PBS and harvested by treatment with collagenase (Biochrom AG) (625 U/ml). The obtained cell suspensions were pooled and adjusted to 10^5 cells/ml with MACS buffer (PBS containing 2.5% FBS) after centrifugation for 5min at 150g (Haereus, Megafuge 1.0 R). The cell suspension was divided up and exposed to the following antibodies at 4°C for 1h; mouse-anti-human CD51/61 antibody (Dako) and mouse-anti-human aminopeptidase N (CD13) (Dako). Control staining was performed by using the mouse specific antibodies rat-anti-mouse CD51 (Dako) and rat-anti-mouse CD13 (Biolegend). All antibodies were applied at a total dilution of 1:200.

Afterwards, cells were washed repeatedly with prewarmed MACS buffer (PBS containing 2.5% FBS) to remove unbound antibody. Secondary antibody staining was performed by exposing the cell suspension to ALEXA488 labelled anti-mouse- or anti-rat-antibody (Invitrogen), respectively for 1h at 4°C. The secondary antibody was applied at a total dilution of 1:400. Receptor status was assayed as described in 2.10.1.

2.10.3 Flow cytometric analysis of integrin receptor status on CT26 tumor cells

CT26 tumor cells were seeded in collagen G (Biochrome AG, Germany) coated 24 well plates (TPP, Switzerland) at a density of 30000 cells per well 24h prior receptor status detection. Cells were washed with prewarmed PBS and harvested by treatment with collagenase (Biochrom AG) (625 U/ml). The obtained cell suspensions were pooled and adjusted to 10^6 cells/ml with MACS buffer (PBS containing 2.5% FBS) after centrifugation for 5min at 150g (Haereus, Megafuge 1.0 R). The cell suspension was divided up and exposed separately to the following antibodies at 4°C for 1h; mouse-anti-human CD51/61 antibody (Dako), rat-anti-mouse CD51 (Dako) and rat-anti-mouse CD13 (Biolegend). All antibodies were applied at a total dilution of 1:200. Afterwards, cells were washed repeatedly with prewarmed MACS buffer (PBS containing 2.5% FBS) to remove unbound antibody. Secondary antibody staining was performed by exposing the cell suspension to ALEXA488 labelled anti-mouse- or anti-rat-antibody (Invitrogen), respectively for 1h at 4°C. The secondary antibody was applied at a total dilution of 1:400. Receptor status was assayed as described in 2.10.1.

2.10.4 Transmission light and epifluorescence microscopy

Transmission light microscopy of living cells growing as monolayers or multicellular microspheroids wrapped in agarose was performed using an Axiovert 200 microscope (Carl Zeiss, Jena, Germany) equipped with a Sony DSC-S75 digital camera (Sony Corporation, Tokyo, Japan). Light was collected through 5x0.12 NA, 10x0.25NA or 32x0.40Na objectives (Carl Zeiss, Jena, Germany), and images were captured using phase contrast.

Fluorescence microscopy of transiently EGFP expressing cells was carried out using an Axiovert fluorescence microscope (Carl Zeiss, Jena, Germany). CYP2B1 expressing cells were stained with the mouse-anti-ratCYP2B1 antibody (Oxfordbiomedical Research, Oxford) followed by visualisation by the secondary ALEXA488 labelled goat-anti-mouse antibody (Invitrogen, Oregon, USA). EGFP and ALEXA488-fluorescence were excited using a 470±20 nm bandpass filter and emission was collected using a 540±25 nm bandpass filter.

Fluorescence microscopy of stained cryosections was likewise carried out using an Axiovert 200 fluorescence microscope (Carl, Zeiss, Jena, Germany) equipped with a Zeiss Axiocam camera. Light was collected through a 20x0.4 NA or 63 x 1.4 oil

immersion objective (Zeiss). Hoechst33258 fluorescence was excited using a 365 nm bandpass filter and emission was collected using a 420 nm bandpass filter. ALEXA 488 and FITC-fluorescence were excited using a 470±20 nm bandpass filter and emission was collected using a 540±25 nm bandpass filter, whereas ALEXA467 was excited using a 640±20 nm bandpass filter and emission was collected using a 735±35 nm bandpass filter. Texas Red fluorescence was excited using a 530-585 nm bandpass filter and emission was collected by using a 615nm longpass filter.
Cy3 fluorescence was excited using a 546 nm bandpass filter and emission was collected by using a 610±30 nm bandpass filter. Digital image recording and image analysis were performed with the Axiovision 3.1 software (Zeiss) or the Axiovision LE software (Zeiss), respectively.

2.11 In vivo/ex vivo experiments

2.11.1 Animals

Mice were obtained either from breeders for lab animals (Harlan-Winkelmann, Borchen or Charles River, Sulzfeld) or own breeding. Up to 5 animals were kept in single individually ventilated cages (Type II, long, Techniplast ICV System, Buguggiate, Italy) under specified pathogen free conditions. Room temperature was 21ºC, humidity was 60% and the night/day stages were 12h each. Food (Sniff) and water were autoclaved before use and were available for the mice ad libitum.
The litter in the cages was saw mill waste (3/4 fiber, Abedd Koeflach, Austria); additionally cages were equipped with pulp, a red mouse house (Techniplast, Italy) and a tube of wood (Abedd, Koeflach, Austria). The cages were loaded with the equipment and autoclaved prior use.
Mice obtained from breeders were kept at least one weak in the new environment for acclimatisation before admitting them to the experiments.
The experiments with animals were approbated by the Bavarian government. All performed experiments were in line with the request for animal experiments “Gentherapeutische Behandlung von Tumoren im Tier-Model-System” (209.1/211-2531-5/03, project leaders Prof. E. Wagner/Dr. M. Ogris and “Elektroporation zur Behandlung von Tumoren mit therapeutischen Nukleinsäuren“ (209.1/211-2531-63/03) project leaders Dr. C. Culmsee/Dr. M. Ogris.

2.11.2 Providing tumor cells for in vivo implantation

CT26 mouse colon carcinoma cells (ATCC CRL-2638), Neuro2A mouse neuroblastoma cells (ATCC CCl-131) and X39 CYP2B1 expressing CT26 cells were cultured as described above in DMEM low glucose supplemented with 10% FBS.

HUH7-human hepatocellular carcinoma cells (JCRB 0403; Tokyo, Japan) were cultured in DMEM/F12 with Glutamax I medium supplemented with 10% FBS.

PC3 human prostate carcinoma cells (CRL-1435) were cultured in RPMI medium supplemented with 10% FBS.

All cell lines were cultured without antibiotics for at least 3-4 passages, before tumor implementation. Cells were harvested with trypsin/EDTA when confluency was about 70%.

2.11.3 Tumor cell implantation and tumor models

The tumor cells were cultivated as described above. When a confluency of about 70% was reached, medium was removed and cells were washed 2 times with 37C warm PBS, followed by harvesting with trypsin/EDTA (Invitrogen, Germany).

The obtained cell suspension was mixed with medium containing 10% FBS in order to inactivate the present trypsin. Cells were counted by transmitted light microscopy with a Rosenberg count plate. Afterwards, the cell suspension was centrifuged 5min with 150g and resuspended in fresh PBS. This washing procedure was repeated before cells were suspended with PBS to the desired concentration.

Mice were shorn before application of the tumor cell suspension with an electrical razor (Braun, Germany). 100µl of the tumor cell suspension was applicated subcutaneously with a 25G needle (Braun, Melsungen, Germany) into the flank of the animals.

Animals were controlled regularly for tumor growth. When the tumor volume reached a size of at least 10mm^3, tumor progression was monitored with a digital measuring slide (Digi-Met, Preisser, Gammertingen). For determination of tumor growth 3 parameters (length, width and height) were measured and tumor volume was calculated via the following formula: a x b x c x 0.4 (whereas a, b and c are the measured parameters length, width and height). Accounting for measured thickness of the skin the correction factor 0.4 is required in order to calculate real tumor volume.

Syngeneic tumor models

Neuro2A cells ($1x10^6$ tumor cells per animal) were applicated subcutaneously to about 8 to 9 weeks old A/J mice. The cells were suspended in PBS; total subcutaneous injection volume per animal was 100µl.

Xenograft tumor models

SCID mice were used for the CT26/X39, HUH7 and the PC3 tumor model due to disturbed function of the immune system (86). For establishing subcutaneous CT26, X39 and HUH7 tumors, male and female SCID mice were used when they were about 8 to 9 weeks old.

For establishing the CT26/X39 tumor model 100 000 cells, for the HUH7 tumor model $5x10^6$ cells and for the PC3 tumor model 10^6 were applicated subcutaneously. The PC3 human prostate xenograft model was solely established on male SCID mice. All tumor cells were suspended in PBS. The total injected volume per animal was 100µl.

2.11.4 Systemic application of Hoechst dye 33258

For systemic application of the Hoechst33258 dye (2.5 mg/ml Hoechst33258 in PBS), as a marker for blood flow, procedure of injection was similar to the application of the polyplex formulations described above. After the injection mice were removed from the tube. 5min after the application of the Hoechst dye mice were sacrificed.

2.11.5 Intraperitoneal application of CPA

The chemotherapeutical drug CPA (Cyclophosphamide, Sigma, Taufkirchen) was solved in PBS at a concentration of 10mg/ml followed by steril filtration (0.22µm sterilfilter, Millex-GV, Millipore Carrigtwohill, Ireland). Application was performed intraperitoneally. Therefore mice were fixed by hand and turned in order to allow access to the ventral side. The CPA solution was administered with a 25G needle (Braun, Melsungen). The application of the CPA solution was carried out every 4th, 6th or 7th day, respectively. The applicated volume was 80 to 350µl. The single dose of each application was based on animal body weight. Toleration of the treatment with CPA was monitored by regular measurement of body weight.

2.11.6 Isolation of tumors/organs for histology

For histological investigation of tumor and organs mice were sacrificed with CO_2. Before organs were removed the vein to the liver was cut in order to reduce rest blood. After the removal, the organs were embedded in OCT Tissue Tek (Sakura,

USA) and frozen at -80C. In the case of fluorescence microscopic analysis of GFP expression tissue was fixed with 4% paraformaldehyde in PBS for 1 day prior to embedding in OTC medium and freezing.
For immune histology, organs/tumor was cut into slides of 5 to 7µm thickness with a kryomicrotome (Leica CM 3050s) at -20C. For HE staining organs/tumor were cut into slides of 5 to 10µm thickness. Slides were transferred to a microscope slide and fixed with 4% paraformaldehyde (in PBS). Immune histological staining was performed as described.

2.11.7 Haematoxilin/Eosin stain

Cryosections of the tissue was fixed with 4% paraformaldehyde and stained with Haematoxilin (Sigma, St. Loius, USA) for 30 min. After a washing step with PBS and aqua dest., sections were incubated with a 1:100 dilution of Eosin (Sigma, St. Louis, USA) for 4 min. Afterwards, sections were washed with aqua dest., embedded with PBS and analyzed by transmission light microscopy.

2.11.8 Vessel perfusion with fluorescent dye

Hoechst 33258 was used as a marker for blood perfused areas in the tumor. After a 1 min exposure to 200µl of 7.5mg Hoechst 33258 in PBS (given intravenously) the mice were sacrificed and the tumors were resected. Tumors were wrapped in OTC and immediately frozen. Frozen sections (10µm) were cut on a cryostat at three different levels between one pole and the equatorial plane. The slides were viewed in a light microscope under ultraviolet illumination. Blood perfusion was observed by Hoechst33258 stained nuclei and quantified by image-analysis. Nine sections per tumor were examined and 5 fields per section were randomly selected for image analysis. Fluorescence levels were analyzed with the MIPAV software.

2.11.9 Antibody stain

2.11.9.1 Staining for vascular markers

Cryosections (5µm) were transferred to a microscope slide and fixed with 4% paraformaldehyde (in PBS) for 5min. Afterwards, tissue sections were rehydrated and washed with MACS buffer (PBS containing 5% FBS) prior to antibody incubation.

Simultaneous staining for laminin and endothelial marker CD31
Staining was performed with the rabbit-anti-laminin antibody (Chemicon Europe, Hampshire, UK) and simultaneous with the rat-anti-mouse CD31 (CALTAG,

Burlingame, USA) antibody; both antibodies were used in a 1:200 dilution (in MACS buffer). After an incubation time of 12h at 4ºC in a humified atmosphere sections were washed repeatedly with MACS buffer followed by secondary antibody staining. Therefore the sections were incubated with the Texasred labelled goat-anti-rabbit antibody (Vector, Burlingame, UK) and the ALEXA488 labelled goat-anti-rat antibody (Invitrogen, Oregon, USA); the staining was performed with a 1:200 dilution (in MACS buffer) of both antibodies for 2h at room temperature in a humified atmosphere.
Before analysis by fluorescence microscopy, sections were washed with MACS buffer repeatedly.

Simultaneous staining for laminin and CD13

Staining was performed with the rabbit-anti-laminin antibody (Chemicon Europe, Hampshire, UK) and simultaneous with the rat-anti-mouse CD13 (Dako, Copenhagen, Denmark) antibody; both antibodies were used in a 1:200 dilution (in MACS buffer). After an incubation time of 12h at 4ºC in a humified atmosphere sections were washed repeatedly with MACS buffer followed by secondary antibody staining. Therefore the sections were incubated with the Texasred labelled goat-anti-rabbit antibody (Vector, Burlingame, UK) and the ALEXA488 labelled goat-anti-rat antibody (Invitrogen, Oregon, USA); the staining was performed with a 1:200 dilution (in MACS buffer) of both antibodies for 2h at room temperature in a humified atmosphere.
Before analysis by fluorescence microscopy, sections were washed with MACS buffer repeatedly.

2.11.9.2 Staining for other epitopes

Staining for expressed CYP2B1 protein in tumor tissue

Cryo sections (5µm) were transferred to a microscope slide and fixed with 4% paraformaldehyde (in PBS) for 5min, followed by treatment with Triton X (0.1% in PBS) for further 5min. Afterwards, tissue sections were rehydrated and washed with MACS buffer (PBS containing 5% FBS). Washing procedure was repeated for 2 times. Surplus supernatant was removed and the rehydrated tissue sections were incubated with the mouse-anti-ratCYP2B1 antibody (Oxfordbiomedical Research, Oxford, UK), used as a 1:200 dilution in MACS buffer (PBS containing 5% FBS). Control antibody staining was performed by the mouse IgG1, negative control antibody (Dako, Copenhagen, Denmark). Antibody binding was carried out in a

humified atmosphere at room temperature for 2h, followed by a washing procedure with MACS buffer. For secondary antibody staining, tissue sections were incubated with ALEXA488 labelled goat –anti-mouse antibody (Invitrogen, Oregon, USA), used as a 1:200 dilution in MACS buffer, for 1h in a humified atmosphere at room temperature. Before analysis by fluorescence microscopy, sections were washed with MACS buffer (repeated for 2 times).

Staining for integrin αv

Cryo sections (5µm) were transferred to a microscope slide and fixed with 4% paraformaldehyde (in PBS) for 5min, followed by treatment with Triton X (0.1% in PBS) for further 5min. Afterwards, tissue sections were rehydrated and washed with MACS buffer (PBS containing 5% FBS). Washing procedure was repeated for 2 times. Surplus supernatant was removed and the rehydrated tissue sections were incubated with the rat-anti-mouse CD51 antibody (Dako), used as a 1:200 dilution in MACS buffer (PBS containing 5% FBS). Control antibody staining was performed by the mouse-anti-human CD51/61 antibody (Dako, Copenhagen, Denmark). Antibody binding was carried out in a humified atmosphere at room temperature for 2h, followed by a washing procedure with MACS buffer. For secondary antibody staining, tissue sections were incubated with the appropriated ALEXA488 labelled antibodies (Invitrogen, Oregon, USA), used as a 1:200 dilution in MACS buffer, for 1h in a humified atmosphere at room temperature. Before analysis by fluorescence microscopy, sections were washed with MACS buffer (repeated for 2 times).

Staining for acrolein-adducts in tumor tissue

Cryo sections (5µm) were transferred to a microscope slide and fixed with 4% paraformaldehyde (in PBS) for 5min, followed by treatment with Triton X (0.1% in PBS) for further 5min. Afterwards, tissue sections were rehydrated and washed with MACS buffer (PBS containing 5% FBS). Surplus supernatant was removed and the rehydrated tissue sections were incubated with the anti-acrolein-antibody (ACR, monoclonal antibody, JaICA, Japane) and simultaneous incubation was performed with the rat-anti-mouse-CD31 antibody (CALTAG, Burlingame, USA). Both antibodies were used in a 1:100 dilution (in MACS buffer). Antibody binding was carried out in a humified atmosphere at 4ºC over night. Control antibody staining was performed by the mouse IgG1, negative control antibody (Dako, Copenhagen, Denmark) instead of

the anti-acrolein-antibody (ACR) in the same manner. After removing of antibody containing supernatant, tissue sections were washed with 1ml MACS buffer. The washing procedure was repeated for five times. For visualizing binding of the firstly antibodies, staining was performed with a 1:200 dilution (in MACS buffer) of secondary antibodies, ALEXA467-anti-rat and ALEXA488-anti-mouse. Incubation was carried out for 2h at room temperature in a humified atmosphere. Before analysis by fluorescence microscopy, sections were washed with MACS buffer, followed by an additional washing step with demineralised water and embedding in glycerine.

2.11.10 Reisolation of tumor cells

For the reisolation of tumor cells, mice were sacrificed with CO_2. The skin was cleaned and sanitized by isopropanol (70% in water V/V) followed by drying under steril conditions. Tumors were collected and immediately inserted in the indicated Penstrep (Biochrome, Germany) containing medium. In the case of Neuro2A tumors, DMEM low Glucose medium was used, whereas DMEM high glucose/F12 medium was used for HUH7 tumors and in the case of PC3, tumor tissue was inserted in RPMI medium.

Tumor tissue was reduced to small pieces under steril conditions with a scalpel. This procedure was repeated until tumor tissue was homogenized. In the case of reimplantation of PC3 tumor cells, homogenized tumor tissue was directly injected subcutaneously to male SCID mice by use of a 25G needle (Braun, Mesungen, Germany) into the flank of the animals.

The obtained homogenized cell suspension was diluted with fresh medium, followed a centrifugation step (150g/5min). The supernatant was removed and resuspension of the tumor cell containing pellet was performed with fresh, Penstrep containing medium. The tumor cell containing suspension was transferred to collagen coated (Collagen G, Biochrom) tissue flasks (TPP, Switzerland) and incubated under standard conditions (37ºC, 5% CO_2) in a humified atmosphere for 2-3 days. When cells were attached to the bottom of the flasks, medium was replaced every second day, until cells reached a confluency of about 70%. Obtained cells were cultured for 2 passages before harvested by tyrpsin/EDTA treatment and placed in storage as described in 2.2.5.

2.11.11 Isolation of PEC cells

Pig aortas were obtained from the local slaughterhouse (Munich, Germany) and immediately inserted in Penstrep (Biochrome, Germany) containing medium (M199, Invitrogen). Adipose and loose tissue was removed carefully and the aorta was cut lengthwise into two pieces. Aortic tissue was fixed with the luminal, endothelial cell containing layer to the upper side and washed with prewarmed (37ºC) PBS. Afterwards, 5ml of collagenase type II CLS (625U/ml) (Biochrome, Germany) and trypsin/EDTA (Invitrogen, Germany) containing solution was added to the aortic tissue, followed by an incubation step at 37ºC for 15 to 20 minutes.

The incubation solution was removed carefully and replaced by 5ml of M199 medium, containing 10% FCS (Invitrogen, Germany). Endothelial cells were obtained by repeated replacement of fresh M199 medium. Cell containing medium was pooled and the procedure was followed by a centrifugation step (150g, 8min) and resuspension of the obtained pellet in fresh, Penstrep containing M199 medium. Cells were seeded in tissue flasks (75 cm^2, Costar, Sigma-Aldrich, USA) and incubated under standard conditions (37ºC, 5% CO_2) in a humified atmosphere for 2 to 5 days. When cells began to proliferate, medium was replaced every second day, until cells reached a confluency of 80 to 90%. Obtained PEC cells were harvested by tyrpsin/EDTA treatment and placed in storage as described in 3.2.5.

2.11.12 Isolation of fibroblasts / NF-κB Animals

NF-κB-luciferase-reporter mice were bred and used for the measurement of changes in NF-κB transcriptional activity as described previously (87). The NF-κB-luciferase transgene contained the firefly luciferase gene, driven by two NF-κB sites responding to p65/p50, p50/cRel and other dimer combinations of NF-κB as established in previous studies (88;89)

Primary fibroblast cultures were obtained following a standard protocol for skin biopsies with slight modifications. Briefly, skin biopsies of E15 luciferase-reporter mouse embryos were placed in a culture dish containing 1 ml Dulbecco's minimal essential medium supplemented with 10% FBS. Using two sterile scalpels and a crisscrossing motion the skin was cut into small pieces, not greater than 1 mm X 1 mm. Afterwards media and tissue pieces were transferred as a suspension into a T25 vented flask. The petri dish was rinsed with additional 1 ml medium and then transferred to the T25 flask. The T25 flask was then placed in a 5% CO 2 incubator at 37°C, and the media was changed weekly until the fibroblast layer in the flask was

confluent. Confluent cultures were trypsinized following standard methods and grown in Dulbecco's minimal essential medium supplemented with 10% FBS at 37°C in a humidified atmosphere with 5% CO_2 in air. Cells were routinely seeded at a density of $10^4/cm^2$ and subcultured every 7 days upon reaching confluence.

3 Results

3.1 Evaluation of tumor cells as producer cells in the standard GDEPT concept

3.1.1 Endogenous P450 activity of the used cancer cell lines

The family of cytochrom P450 enzymes include isoforms that metabolize the anticancer prodrugs CPA (cyclophosphamide) and IFO (ifosphamide) by a hydroxylation reaction. This activation is the basic requirement for their antitumoral and cytotoxic activity. CYP2B1 is one of the P450 isoforms that convert CPA and IFO. Yet tumor cells usually exhibit rather low expression of endogenous CYP2B1 activity (90); bioactivation of the prodrugs CPA and IFO is mainly localized in the liver so that the activated drugs have to be distributed over the blood stream to reach the tumor tissue.

Localized activation of the prodrug in the context of GDEPT concept as studied in the current thesis would be more effective and less toxic and can be obtained by transfer of CYP2B1 encoding plasmid DNA into tumor cells. As a first step, endogenous CYP2B1 activity of the wild type (wt) cancer cell lines used in this thesis was evaluated by the acrolein assay and resorufin assay.

3.1.1.1 Acrolein assay

The acrolein assay is based on the detection of acrolein in biological fluids. Acrolein is one of the metabolites that is released by activated cyclophosphamide or ifosphamide, respectively. The amount of acrolein in the supernatant of cultured cells reflects therefore cellular cytochrom P450 enzymatic activity when cells are grown in the presence of CPA or IFO, respectively.

Acrolein was not evident in the supernatant of the wt tumor cells CT26, Neuro2A HUH7 and 9L, indicating low cytochrom P450 enzymatic activity in terms of CPA or IFO conversion capability (FIG 3-1).

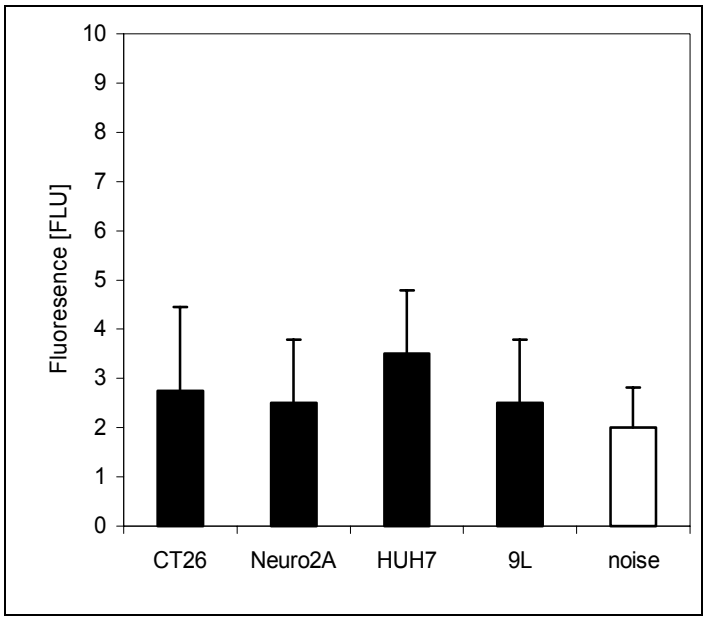

Fig.: 3-1 Conversion of CPA by wt tumor cell lines (acrolein assay). Detection of the metabolite acrolein was performed in the supernatant of cells incubated with 2.0mM CPA for 24h. Values are means ± SE of triplicates.

3.1.1.2 Resorufin assay

The different P450 cytochrom isotypes are catalysts for different biochemical reactions. The isoenzyme cytochrom P4502B1 exhibit also alkoxy-o-dealkylase activity. This catalytic activity provides the reaction of 7-pentoxyresorufin to the fluorescent compound resorufin (91). The CYP2B1 activity of cultivated cells is therefore reflected by the amount of in situ produced resorufin, which can be easily measured in the supernatant by its fluorescence signal.

The tumor cell lines CT26, Neuro2A, HUH7 and 9L were again analyzed for their CYP2B1 enzymatic activity by the resorufin assay. Alkoxy-o-dealkylase activity was detected in HUH7 cells, whereas no enzymatic activity was evident in CT26, Neuro2A and 9L cells (FIG 3-2).

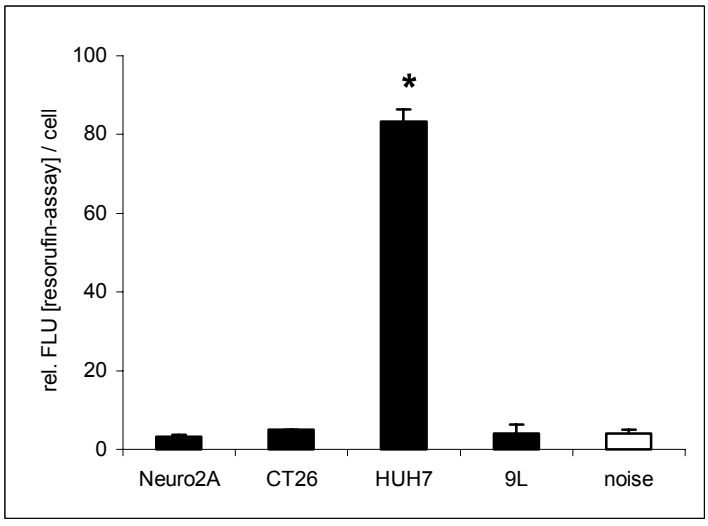

*Fig.: 3-2 Detection of CYP2B1 enzymatic activity in wt tumor cells by the resorufin assay. Cells were incubated with resorufin incubation solution and in situ released resorufin was detected in the supernatant of the cells after a freeze-thaw cycle by fluorescence measurement Measurements were normalized on cell count. Values are means ±SD of triplicates. *p<0.05, compared to vehicle treated system (Mann-Whitney U-test).*

For further investigation of endogenous CYP2B1 activity in wt tumor cells, detected fluorescence signal was normalized for total metabolic activity measured by the MTT assay.

CYP2B1 enzymatic activity of wt HUH7 cells was about 16 fold higher than CYP2B1 activity of Neuro2A, CT26 and 9L cells, whereas total metabolic activity of HUH7 cells was about 4 times higher than metabolic activity of the other assayed cell lines (9L, CT26, Neuro2A). Therefore, HUH7 cells exhibited a higher specific endogenous alkoxy-o-dealkylase enzymatic activity than the other wt cell lines Neuro2A, CT26 and 9L. Alkoxy-o-dealkylase level of the CT26, 9L and the Neuro2A cell line were on similar low levels and not detectable in the resorufin assay (FIG 3-3).

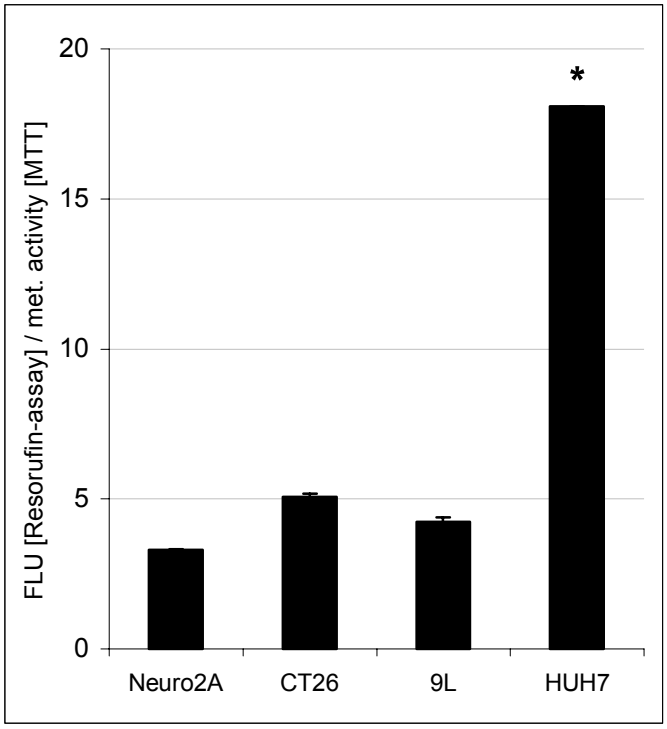

*Fig.: 3-3 CYP2B1 alkoxy-o-dealkylase activity (resorufin assay) normalized on total metabolic activity (MTT assay). The wt cell lines Neuro2A, CT26, 9L and HUH7 were analyzed for CYP2B1 alkoxy-o-dealkylase activity by the resorufin assay. In a parallel experiment the mentioned cell lines were analyzed for metabolic activity by the MTT assay. Values are means ±SE of duplicates (resorufin assay) or triplicates (MTT assay). *p<0.05, compared to vehicle treated system (Mann-Whitney U-test).*

3.1.1.3 Comparison of the acrolein and the resorufin assay

The acrolein assay is based on the detection of acrolein as a metabolite released by activated cyclophosphamide and ifosphamide and reflects therefore directly CPA or IFO conversion capability. Yet, the resorufin assay exhibits higher sensitivity and lower signal to noise ratio. Moreover, enzymatic activity of the CYP2B1 may be decreased or regulated by cytotoxic metabolites over the time when cells are incubated with CPA or IFO. For that reason the resorufin assay was preferred in order to detect CYP2B1 activity in the following experiments.

3.1.2 Sensitivity of wt tumor cells against CPA treatment

3.1.2.1 Assays for determination of cell survival and proliferation

For investigation of biological activity of CPA and IFO, respectively, different concentrations of the anticancer drugs were assayed for reduction in proliferation and survival of each cell line. Proliferation and survival were investigated by the Hoechst33258 based DNA content proliferation assay and the MTT assay.

Reliability and correlations of the used assays were verified (compare materials and methods).

3.1.2.2 Survival and proliferation of CT26 and Neuro2A cells after CPA or IFO treatment

To determine the relevant CPA and IFO concentration range for further experiments wt CT26 and Neuro2A cells were treated with different concentrations of CPA and IFO ranging from 0.05mM to 10.0mM. The level of cell proliferation was determined on day 3 after the beginning of the treatment by the Hoechst 33258 based DNA content assay. The results demonstrate that CPA had no significant antiproliferative effects up to 1.0 mM on both tested wt cell lines. However IFO treatment resulted in decreased cell proliferation when IFO concentration was 0.25mM or higher, indicating a higher unspecific toxicity of the inactivated prodrug (FIG 3-4A and 3-4B). For that reason all further experiments with CYP2B1 expressing cells were performed with CPA.

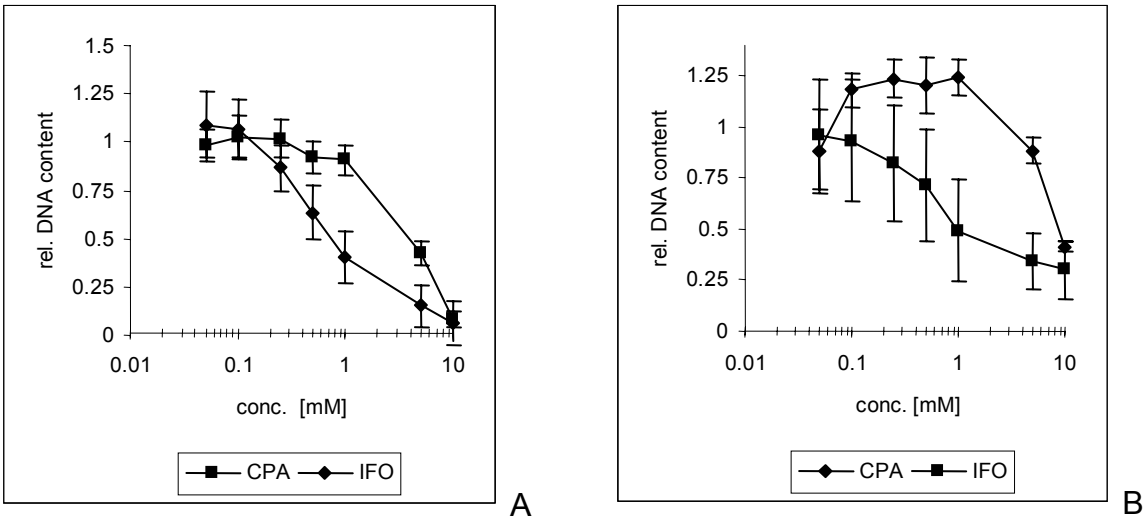

Fig.: 3-4 Decrease in proliferation rate by a 3 day treatment of wt CT26 and wt Neuro2A cells with either CPA or IFO. Wt CT26 and wt Neuro2A cells were treated for with increasing concentrations of CPA or IFO. Proliferation rate was determined by Hoechst 33258 based DNA content assay. Measurements were normalized on untreated control cells. A) wt CT26 cells, B) wt Neuro2A cells. Values are means ±SD of triplicates.

3.1.3 Generation of CYP2B1 expressing tumor cells

3.1.3.1 Stable Transfection

3.1.3.1.1 Generation of the stably transfected X39 cell line

The CT26 and the Neuro2A cell line were chosen for stable transfection due to their low endogenous CYP2B1 enzymatic activity. The cell lines were transfected with LPEI polyplexes (N/P=6, HBS) containing a linearized form of the pCMV-CYP2B1 expression vector. G418-selected colonies were chosen for expansion and further evaluation for CYP2B1 activity.

3.1.3.1.2 Pre-evaluation of CYP2B1 activity of the G418 resistant CT26 and Neuro2A clones

G418 resistant CT26 and Neuro2A clones were expanded and CYP2B1 enzymatic activity was pre-evaluated by the resorufin assay. Measurements were normalized on cell count. G418 resistant CT26 clones exhibited higher enzymatic activity in the resorufin assay compared to the not transfected wt CT26 cell line (FIG 3-5). CYP2B1 activity of Neuro2A sublines were on lower levels compared to stable transfected CT26 cells (data not shown). The highest expressing CT26 clone called X39 was chosen for further investigation.

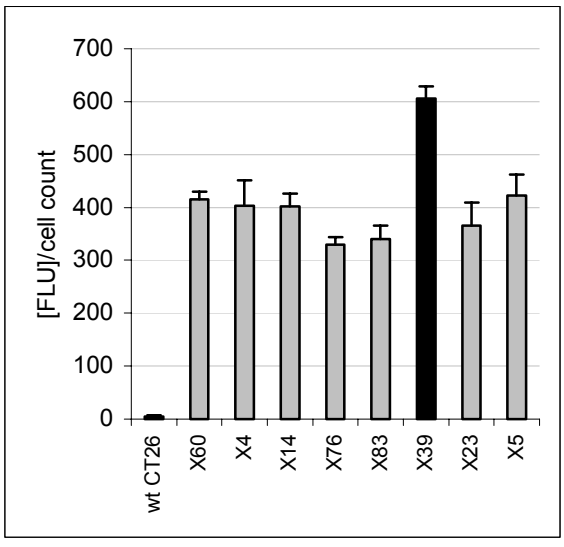

Fig.: 3-5 CYP2B1 enzymatic activity of different stable transfected CT26 clones. CT26 cells were transfected with LPEI polyplexes containing a linearized form of the pCMV-CYP2B1 expression vector, followed by selection via G418 treatment. Resistant cells were subcloned and analyzed for CYP2B1 activity by the resorufin assay. Measurements were normalized on cell count. Values are means ±SE of duplicates.

3.1.3.1.3 Confirmation of continuity of CYP activity

In order to confirm constant CYP2B1 activity, enzymatic activity was correlated to the total metabolic activity of the X39 cells over a culture period of 7 days. Therefore CYP2B1 enzymatic activity and total metabolic activity were measured in parallel experiments on days 1, 3, 6 and 7 after seeding of the cells. The experiment was

performed in the absence of G418 in the culture medium. CYP2B1 enzymatic activity and total metabolic activity were correlating at every analyzed time point, indicating continued high CYP2B1 enzymatic activity of the X39 cells (FIG 3-6).

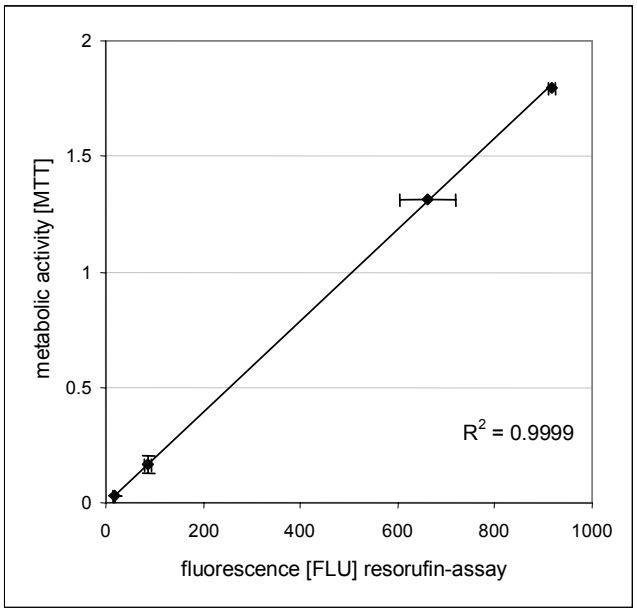

Fig.: 3-6 CYP2B1 enzymatic activity is continuous in X39 cells. CYP2B1 activity and total metabolic activity were analyzed at over a period of 7 days in cultured X39 cells. CYP2B1 enzymatic activity was determined on day 1, 3, 6 and 7 by performing the resorufin assay. In a parallel experiment total metabolic activity of the cultured X39 cells was determined by MTT assay. Values of CYP2B1 enzymatic activity are means ± SE of duplicates. Values of total metabolic activity (MTT assay) are means ± SD of 6 values.

3.1.3.1.4 Confirmation of CYP2B1 protein in X39 by antibody staining

X39 cells were cultivated in G418 free medium for at least 5 passages. Expression of rat CYP2B1 protein in the X39 clone was confirmed by specific antibody staining against rat CYP2B1 protein, followed by FACS analysis. X39 cells showed a homogenous population of CYP2B1 expressing cells, indicated by one peak in the histogram, shifted in comparison to CT26 control cells. In this context, >80% of analyzed X39 cells were positive for CYP2B1 protein expression (FIG 3-7).

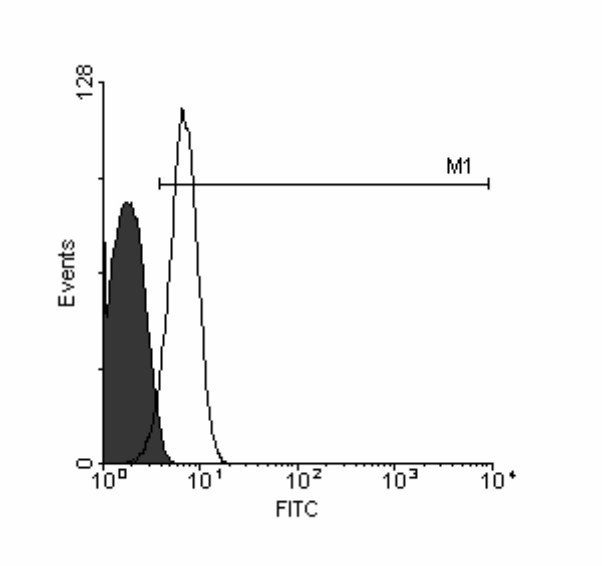

Fig.: 3-7 Antibody staining of ratCYP2B1 expression, followed by analysis via cell flow cytometry. Wt CT26 and CYP2B1 expressing X39 cells were subjected to antibody staining for ratCYP2B1 protein. Antibody staining was performed as described in materials and methods, followed by FACS analysis.

3.1.3.1.5 Characterisation of the X39 clone for CYP2B enzymatic activity by resorufin assay and CPA conversion

Alkoxy-o-dealkylase enzymatic activity of the stably transfected X39 cells was measured by the resorufin assay and compared to CYP2B1 expressing 9L-D2B1 and wt tumor cell lines.

The highest alkoxy-o-dealkylase activity was detected for stably transfected X39 and 9L-D2B1 tumor cells. Enzymatic activity of X39 cells were about 100 fold higher than the parental CT26 wt cells. In comparison to stably CYP2B1 expressing 9L-D2B1 cells, alkoxy-o-dealkylase activity of X39 cells was about two times higher (FIG 3-8).

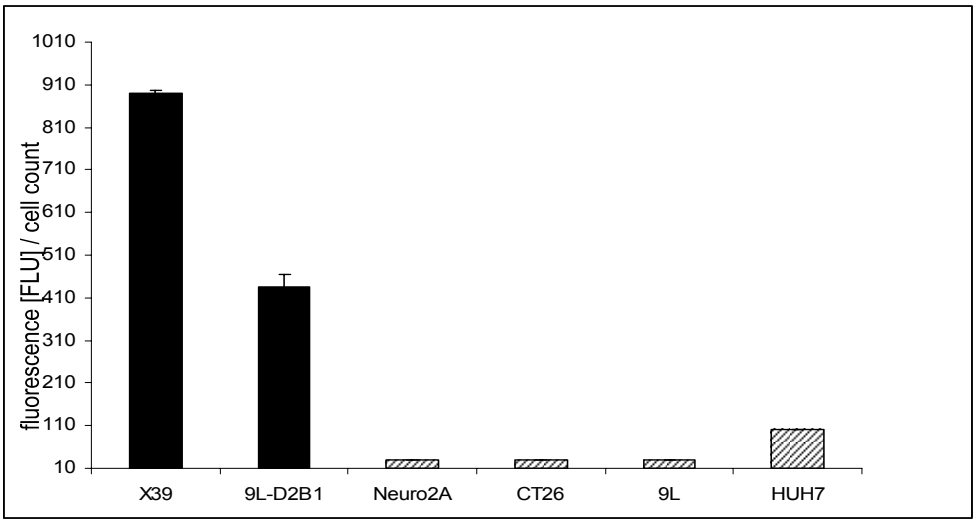

Fig.: 3-8 Detection of CYP2B1 enzymatic activity in the stable transfected X39 and 9L-D2B1 cells. Cells were incubated with resorufin incubation solution and in situ released resorufin was detected in the supernatant of the cells after a freeze-thaw cycle by fluorescence measurement. Black bars: stable CYP2B1 expressing cells; hatched bars: wt tumor cell lines. Measurements were normalized for cell count. Values are means ± SD of triplicates.

CYP2B1 enzymatic activity was further evaluated by the acrolein assay in the supernatant of cells. The concentration of acrolein reflects directly the ability of the stable transfected cells to activate the prodrug by enzymatic hydroxylation.

Similar to the results of the resorufin assay, X39 cells showed highest enzymatic activity for CYP2B1. The stably transfected 9L-D2B1 cells were about half times less effective in converting CPA. No acrolein was detectable in the supernatant of CT26 wt and all other wt cells (FIG 3-9).

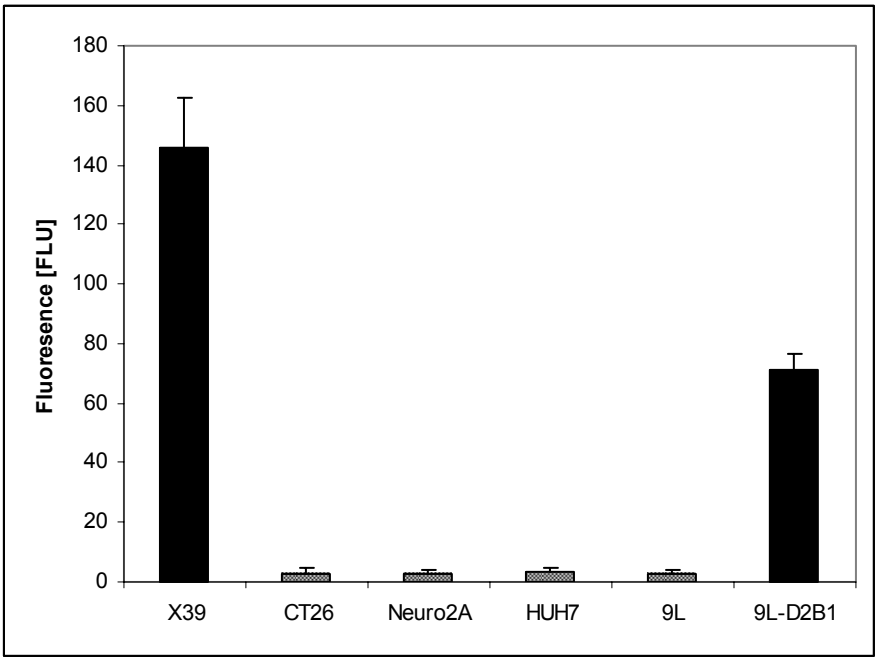

Fig.: 3-9 Detection of the metabolite acrolein in the supernatant of cells. Cells were grown in the presence of 2.0mM CPA for 24h. Supernatant was analyzed by the acrolein assay. Measurements were normalized on cell count. Values are means ± SD of triplicates.

3.1.3.1.6 Suicidal effects of CYP2B1 expressing X39 and 9L-D2B1 tumor cells

In order to compare suicidal effects in CYP2B1 stable expressing cell lines, CYP2B1 expressing X39 and 9L-D2B1 cells were cultured in the absence or in the presence of 0.5mM CPA. Suicidal effects (decrease in proliferation and metabolic activity) were determined by Hoechst33258 based DNA content assay and by MTT assay. Control experiments were performed with the wt cells lines 9L and CT26. Suicidal effects in X39 cells were not significantly distinctive in comparison to the suicidal effects in 9L-D2B1 cells at the same CPA concentration and incubation time. However, X39 as well as 9L-D2B1 exhibited increased sensitivity towards CPA treatment compared to the corresponding parental cell lines at 0.5mM CPA (FIG 3-10).

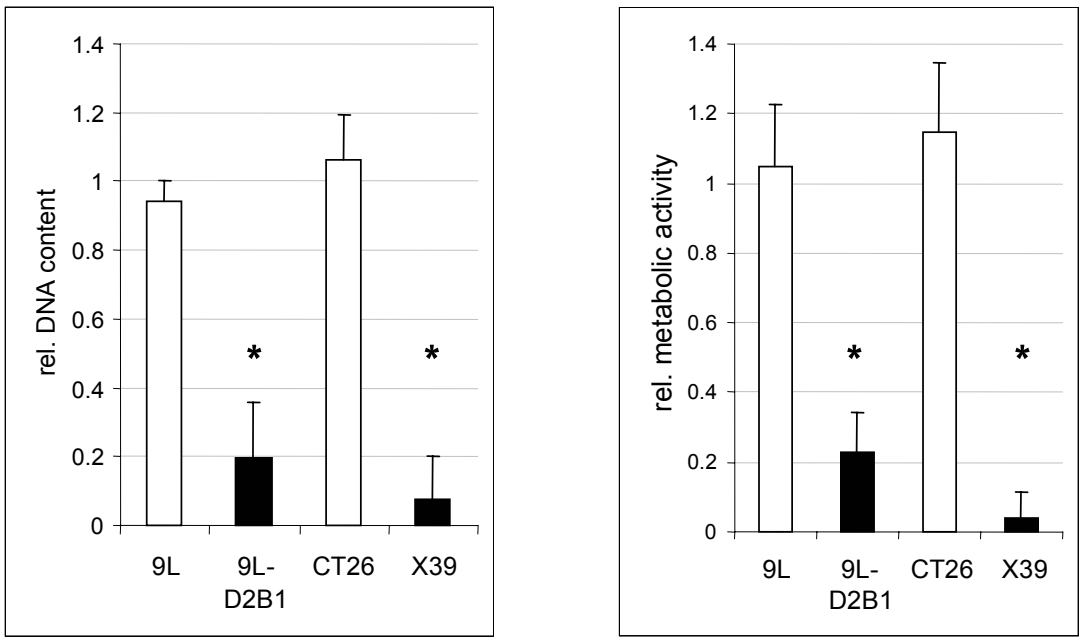

A B

*Fig.: 3-10 Suicidal effects of stable CPY2B1 expressing tumor cells cultured in the presence of 0.5mM CPA. X39 and 9L-2B1 tumor cells were cultured in the absence or in the presence of 0.5mM CPA. After an incubation time of 3 days, suicidal effects were determined by Hoechts33258 based proliferation assay (A). Additionally metabolic activity was measured by MTT assay (B). Control experiments were performed with wt CT26 and 9L tumor cells. Open bars: 0mM CPA, black bars: 0.5mM CPA. Values are means ±SD of triplicates. *p<0.05, compared to vehicle treated system (Mann-Whitney U-test).*

Moreover, CYP2B1 expressing X39 tumor cells were cultivated with different concentrations of CPA that did not show any anti-proliferative effects on the CT26 wt cell line. Concentrations for CPA included in vivo relevant concentrations (0.05mM to 1.0mM). Suicidal effects were quantified by DNA content (Hoechst33258 based DNA content assay) and total metabolic activity (MTT assay). Without CPA treatment X39 cells grew to a confluent monolayer. X39 cells incubated with CPA showed significant decrease in cell proliferation (FIG 3-11). Decrease in metabolic activity was similar to the decrease in proliferation rate (data not shown).

Sensitivity of the CYP2B1 stable expressing X39 cells towards CPA treatment was significantly increased in comparison to the CT26 wt cells (compare FIG 3-4). This indicates that the expression of the CYP2B1 in X39 cells catalyses the reaction of the non-toxic prodrug CPA to toxic metabolites and leads to reduction in proliferation and survival of the tumor cells.

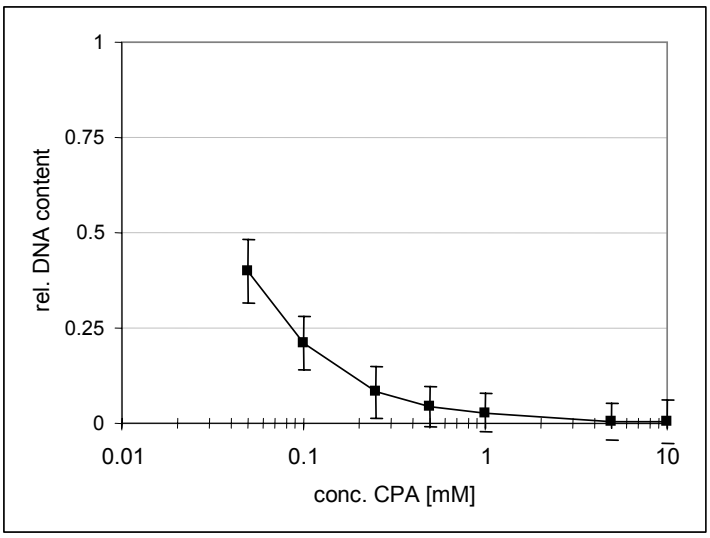

Fig.: 3-11 High sensitivity of cultured CYP2B1 expressing X39 cells towards CPA treatment in terms of cell proliferation. X39 cells were treated with different concentrations of CPA in the medium for 3 days. Proliferation rate was determined by Hoechst33258 based DNA content assay. Measurements were normalized on DNA content of non treated X39 tumor cells. Values are means ± SD of triplicates.

3.1.3.1.7 Suicidal effects of CPA treatment in comparison to IFO treatment

The prodrugs cyclophosphamide and ifosphamide are both metabolized by CYP2B1 enzymatic activity to the active cytotoxic compounds. X39 cells were utilized to investigate the potential of CPA and IFO regarding to suicidal effects on CYP2B1 expressing tumor cells.

CPA treatment and IFO treatment did not show a significant difference in the inhibition of proliferation (FIG 3-12). However, non-activated CPA exhibited less unspecific toxicity to tumor cells than IFO (compare FIG 3-4). For that reason all further studies were carried out with CPA.

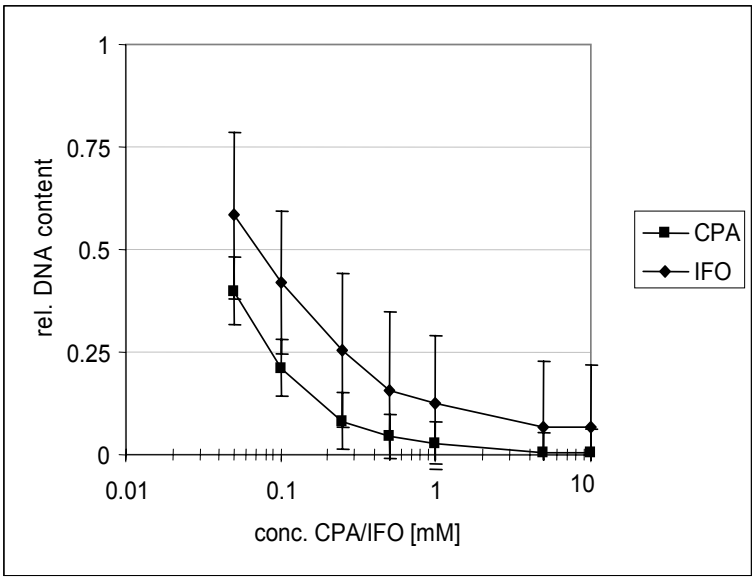

Fig.: 3-12 Sensitivity of stable CYP2B1 expressing X39 cells towards CPA and IFO treatment. X39 cells were cultured for 3 days either in the absence of CPA/IFO or in the presence of different concentrations of CPA/IFO (0.05mM, 0.25mM, 0.5mM 1.0mM, 5.0mM and 10.0mM). Cell proliferation was determined by Hoechst 33258 based DNA content assay. Measurements were normalized on DNA content of non-treated X39 tumor cells. Values are means ±SD of triplicates.

3.1.3.1.8 Verification the presence of soluble cytotoxic metabolites (Transwell system)

In the GDEPT concept the bystander effect is one of the crucial factors for efficient antitumoral effects in the context of the CPA/CYP2B1 concept. In order to verify the presence of soluble cytotoxic metabolites, cells were cultured in a transwell system to avoid cell-cell contacts. Biological effects that occur in a transwell system are therefore caused by soluble compounds that are able to pass the porous membrane.

To verify the presence of diffusible metabolites in this work, CYP2B1 expressing X39 cells were cocultivated with wt CT26 cells in a ratio of 1:1, whereas the CPA concentration in cell culture medium was adjusted to 0.5mM. Control experiments were performed by replacement of X39 tumor cells by corresponding wt CT26 cells. After an incubation time of 3 days cell proliferation was separately assayed for cells at the bottom of the well plate (target cells) and in the well plate insert (producer cells). CPA did not show any anti-proliferative effects on the wt CT26 cells, when no CYP2B1 expressing X39 tumor cells were present in the coculture system. In the presence of 0.5mM CPA CT26 cells exhibited decreased proliferation rate when cocultivation was performed with X39 cells in the transwell system. No reduction in proliferation rate occurred when CT26 cells were cocultured with X39 cells in the absence of CPA (FIG 3-13).

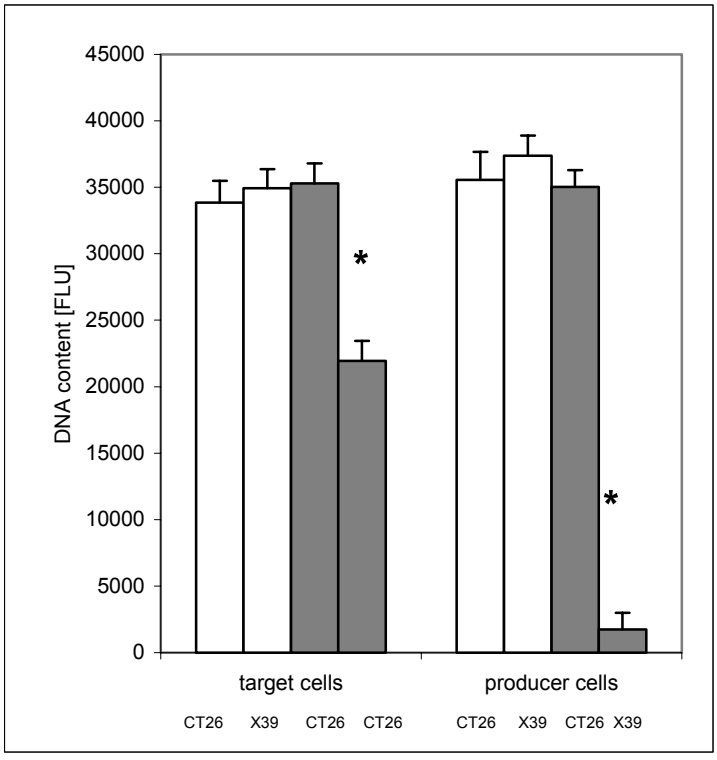

*Fig.: 3-13 Evidence of soluble cytotoxic compounds by in situ activated CPA. Wt CT26 cells were cultivated with stably CYP2B1 expressing X39 cells in (ratios 1:1) in the absence or in the presence of 0.5mM CPA in a transwell coculture system. Control experiments were performed by exchange of X39 cells by wt CT26 cells. After an incubation time of 3 days, proliferation rate for cells in each compartment was performed separately by Hoechst33258 based DNA content assay. Open bars: vehicle treated. Black bars: 0.5mM CPA. Values are means ± SD of triplicates. *p<0.05, compared to vehicle-treated system (Mann-Whitney U-test).*

3.1.3.2 Transient transfection

3.1.3.2.1 Expression kinetics and expression levels after transient transfection

Wt tumor cell lines CT26, Neuro2A, and 9L were transfected with pCMV-CYP containing polyplexes (LPEI, N/P=6, 300ng total plasmid DNA/well, HBS). Control transfection experiment was performed with pEGFN1 plasmid DNA containing LPEI polyplexes. CYP2B1 enzymatic activity was determined at different time points after the transfection by the resorufin assay. Highest CYP2B1 enzymatic activity was detected about 60 hours after the transfection in Neuro2A cells (FIG 3-14 A). A moderate increased CYP2B1 enzymatic activity was detected in transiently transfected 9L cells 24h after the transfection. Transient CYP2B1 enzymatic activity in 9L cells was stable for 70h after transfection (FIG 3-14 B). No enzymatic CYP2B1 activity was detectable in transiently transfected CT26 cells by the resorufin assay (data not shown).

Control transfection with LPEI polyplexes containing plasmid DNA encoding for EGFP resulted in 38.5% transfection efficiency in Neuro2A cells, 8% in 9L and 8.5% in CT26 tumor cells (data not shown).

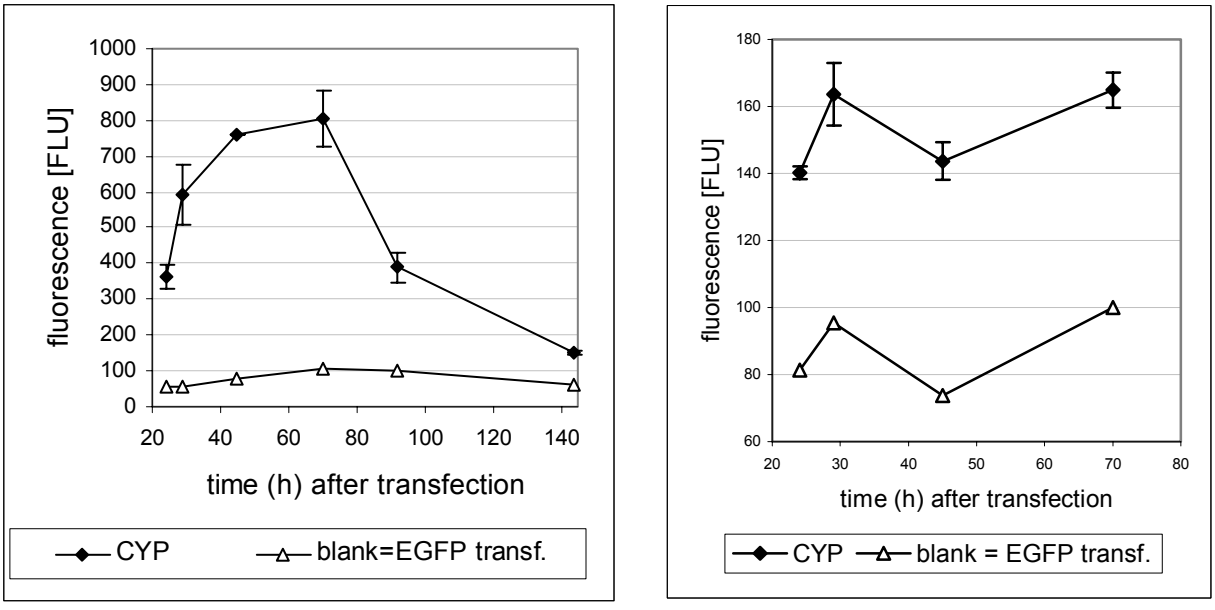

A B

Fig.: 3-14 CYP2B1 enzymatic activity after transient transfection with pCMV-CYP2B1 containing LPEI polyplexes. Wt cells (A) Neuro2A and (B) 9L were transfected transiently with pCMV-CYP2B1 containing LPEI polyplexes. Control transfection experiments were performed with pCMV-EGFP containing LPEI polyplexes (300ng/well, N/P=6, HBS). CYP2B1 enzymatic activity was determined at different time points after the transfection by resorufin assay. Values are means ±SD of triplicates.

3.1.3.2.2 Evaluation of CYP2B1 dependent activation of CPA in vitro

For the detection of CYP2B1 dependent activation of CPA in wt cell lines after transient transfection with LPEI polyplexes containing pCMV-CYP2B1 plasmid DNA (N/P=6, HBS) the acrolein assay was performed. Detection of acrolein was performed for transiently transfected Neuro2A and 9L cells. Acrolein was not detectable in the supernatant of pCMV-CYP2B1 transfected cells (data not shown), indicating that activation of the prodrug CPA did not occur at considerable amounts.

3.1.3.2.3 Evaluation of sensitizing tumor cells against CPA after transient transfection (conventional cell culture)

Transient CYP2B1 expressing Neuro2A cells were analyzed for sensitization towards CPA treatment after transient transfection with pCMV-CYP containing LPEI polyplexes (N/P=6, HBS, 300ng DNA/well). Control experiment was performed with pCMV-LUC and pCMV-EGFP (EGFPN1) plasmid DNA.

Forty eight hours after the transfection, when CYP2B1 enzymatic activity measured by the resorufin assay reached maximum values (compare FIG 3-14 A), CPA was administered. Cells were cultured for further 3 days in the absence or in the presence of 0.5mM CPA. Sensitivity against CPA treatment was determined by measuring total metabolic activity by the MTT assay.

Transiently transfected cells were not sensitized against CPA treatment. No increase in sensitivity towards CPA was detectable in comparison to transfection with the control plasmids (FIG 3-15).

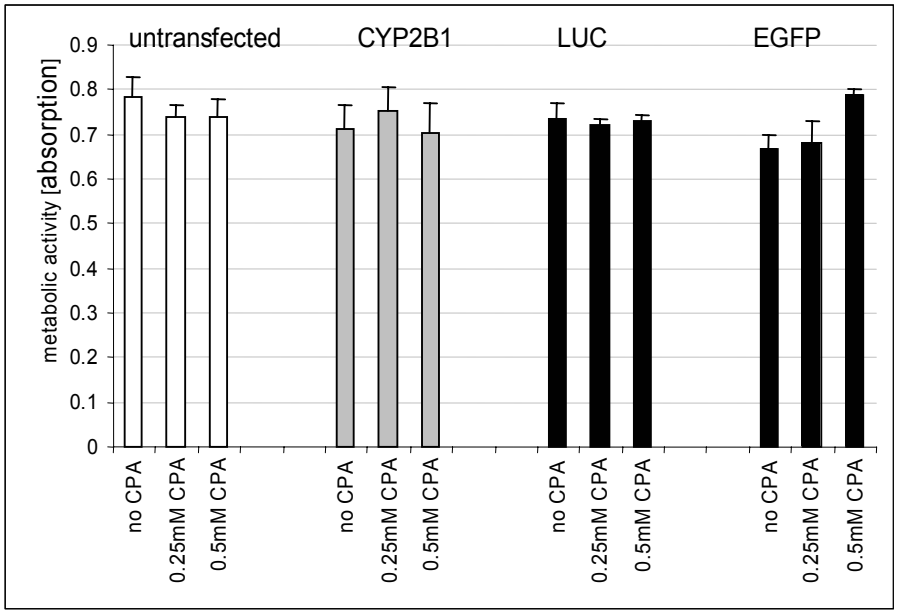

Fig.: 3-15 Transient transfection of Neuro2A tumor cells with LPEI polyplexes containing CYP2B1 encoding plasmid DNA did not result in increased sensitivity towards CPA treatment. Cells were treated with indicated concentrations of CPA for 3 days. Metabolic activity was determined by MTT assay. Values are means ± SD of triplicates.

Despite CYP2B1 enzymatic activity as measured by the resorufin assay no sensitizing towards CPA treatment was evident after transient transfection in conventional cell culture. Due to the reason that this failure might result from the artificial cell culture environment, development of a new cell culture technique was essential for further evaluation of the GDEPT concept.

3.1.3.3 Bystander effect in a tumor environment mimicking cell culture system: Agarose overlay technique

Diffusion of drugs is far more limited within a tumor in vivo than in tumor cells cultured in vitro. In addition, tumor cells are often subjected to a hypoxic environment. These factors are both likely to affect CYP prodrug activation and bystander cytotoxicity. To better mimic the tumor microenvironment, tumor cells seeded in tissue culture plates were covered with a thin layer of agarose dissolved in cell culture medium. Oxygen, nutrients and drugs can reach the cells by diffusion through the agarose layer. We anticipated that the activated metabolites of CPA would form a concentration gradient in the vicinity of the drug-activating cells, similar to the situation in a solid tumor.

3.1.3.3.1 Diffusion in the agarose layer

To test the agarose overlay technique in terms of limited diffusion, a small amount of the membrane-permeable DNA stain Hoechst 33258 was added to the cells (FIG. 3-16). When the stain was added to normal culture medium, the concentration was too low for detection of fluorescent cell nuclei by fluorescence microscopy. However, when a similar amount of Hoechst stain was injected in the agarose layer covering the cells, bright fluorescent nuclei were observed near the injection site. More distant cells were less fluorescent but still visibly stained. Thus, the agarose layer is likely to limit diffusion of low molecular weight drugs and their metabolites, thereby establishing a concentration gradient. Hoechst33258 is indeed a good model for CPA in terms of diffusion within a gel as both drugs have a low molecular weight, (Hoechst33258 624Da, CPA 250Da) and are both hydrophilic.

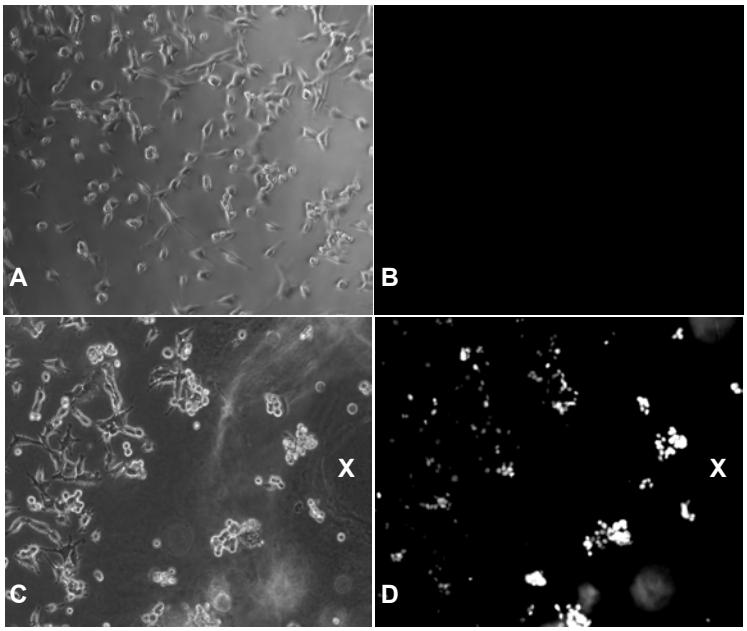

Fig.: 3-16 Diffusion and concentration effects of an agarose overlay using Hoechst 33258. CT26 cells were seeded at 40,000 cells per well of a 24-well plate 24 h before addition of an agarose overlay. The agarose was added as described in materials and methods. Hoechst 33258-containing solution (1 µl at 0.02 ng/ml in PBS) was injected into the agarose layer and cellular fluorescence was monitored 30 min after the injection using a Zeiss Axiovert 200 microscope equipped with appropriate excitation (365 nm) and emission (420 nm long pass) filters. Cells were viewed with a 10X objective and phase contrast pictures were obtained for transmitted light. A control experiment was performed without agarose overlay, with the same amount of Hoechst 33258 dye added to a similar volume of culture medium. Application of Hoechst 33258 without agarose overlay (A: transmitted light, B: fluorescence); injection of Hoechst 33258 into the agarose layer (C: transmitted light, D: fluorescence). Similar exposure times were used for B and D (X: point of dye injection).

3.1.3.3.2 Cell morphology under the agarose layer

CT26 cells and Neuro2A cells were grown in conventional cell culture and under an agarose layer (0.5% agarose distributed in cell culture medium, 200µl/well, 48 well plate). After 3 days cell morphology was assayed by transmitted light microscopy. No obvious differences in cell morphology were detected when cells were grown under the agarose layer in comparison to cells cultured in conventional cell culture systems.

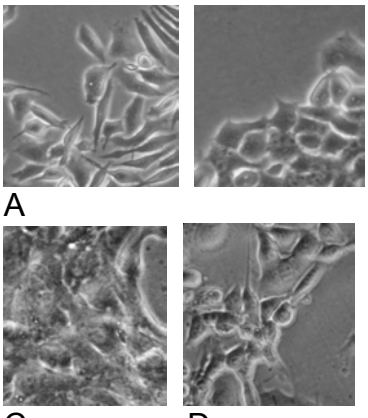

Fig.: 3-17: Cell morphology is not significantly influenced by the agarose overlay. Neuro2A (A and B) and CT26 cells (C and D) were cultured either under conventional cell culture conditions (A and C) or with agarose overlay for 3 days (B and D). Cells were viewed with a 20X objective and phase contrast pictures were obtained for transmitted light.

3.1.3.3.3 Influence of the agarose layer on cell proliferation

In order to evaluate the impact of the agarose overlay on cell proliferation and survival, CT26 and Neuro2A cells were cultured either with or without the agarose overlay technique. Cell proliferation and survival were assayed at several time points by the Hoechst33258 based DNA content assay and by MTT assay over a period of 5 days. In the case of the agarose overlay, the agarose layer was removed just before performing Hoechst33258 based DNA content and MTT assays.

Both cell lines exhibited decreased proliferation rates in the Hoechst33258 based DNA content assay as well as in the MTT assay when cell culturing was carried out under an agarose layer (FIG 3-18). Additional performed analysis by transmitted light microscopy did not give any evidence for cell death (data not shown) indicating the decrease in metabolic activity resulted from decreased proliferation rate.

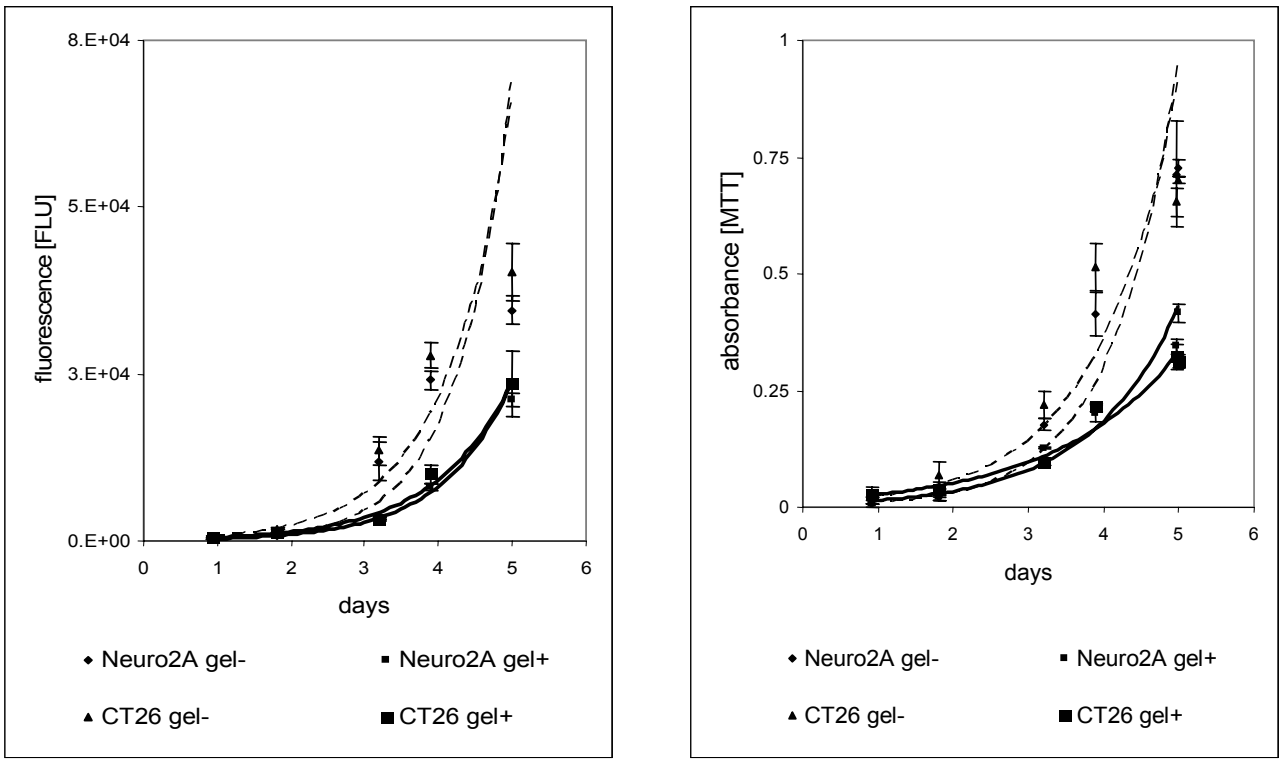

A B

Fig.: 3-18 Influence of the agarose overlay on proliferation and survival of CT26 and Neuro2A cells. CT26 and Neuro2A cells were cultured for 5 days either under standard cell culture conditions or with the agarose overlay. Cell proliferation and survival were measured at several time points by (A) Hoechst33258 based DNA content assay and (B) by determination of metabolic activity (MTT assay). Values are means ± SD of triplicates.

3.1.3.3.4 Investigation of the agarose overlay technique in terms of hypoxic stress

Hypoxic environment might change gene expression profiles and therefore influences sensitivity of tumor cells to chemotherapeutic drugs. Therefore, it was essential to investigate if hypoxia responsive gene expression was evident under the agarose overlay. Therefore CT26 and Neuro2A cells were transfected in a cotransfection experiment with LPEI polyplexes (N/P=6, HBS) containing two different luciferase encoding plasmid constructs. Expression of the Renilla luciferase plasmid was controlled by the CMV promoter, a hypoxia unresponsible promoter, whereas the expression of the firefly luciferase was under the control of a hypoxia responsible promoter HRE (hypoxia responsive element). After the removal of medium or agarose layer, respectively, luciferase activity was measured in a dual-luciferase assay.

No hypoxia induced increase in firefly luciferase activity was detected. The ratio of CMV-controlled luciferase expression and HRE controlled luciferase expression was not changed by the agarose layer within 24h, indicating that gene expression was not strongly influenced by the potential hypoxic environment under the agarose layer. Control experiments for positive activation of the hypoxia responsible promoter were performed in an atmosphere with 1% O_2 in a hypoxia chamber (data not shown).

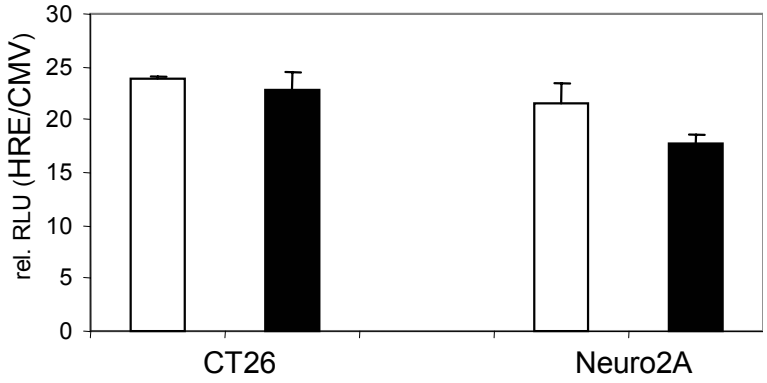

Fig.: 3-19 Regulation of hypoxia responsible elements under conditions of the agarose overlay. Activation of hypoxia responsible elements in cells cultured under the agarose layer was investigated by a dual luciferase assay. Cells were transfected in a cotransfection experiment with 2 different luciferase encoding plasmids. Expression of firefly luciferase encoding plasmid was therefore controlled by a hypoxia sensitive promoter, whereas the expression of the Renilla luciferase encoding plasmid was controlled by the CMV promoter. The diagram shows the relative ratios between both luciferase levels controlled by hypoxia-sensitive and hypoxia insensitive CMV-promoter controlled expression.Open bars: conventional cell culture, black bars: agarose overlay. Values are means ± SE of duplicates.

3.1.3.3.5 Dependency of the CYP2B1 on sufficient oxygen supply

The CYP2B1 enzyme exhibits monooxidase enzymatic activity. Therefore its functionality critically depends on the presence of oxygen. CPY2B1 enzymatic activity in X39 cells was assayed under different oxygen partial pressures. Therefore cells were incubated with the CYP2B1 substrate 7-pentoxyresorufin in a hypoxia chamber under defined ambient oxygen concentrations. Temperature was adjusted to 37°C and humidity was kept constant during incubation time. CYP2B1 enzymatic activity was directly dependent on the oxygen content, as indicated by the near linear correlation between O_2 concentration and fluorescence signal, resulting from in situ converted 7-pentoxyresorufin (Fig. 3-20). Based on this calibration curve, CYP2B1 enzymatic activity was reduced to ~25% of the normoxic control level at 5% O_2, and to 7% in the absence (<0.1%) of O_2.

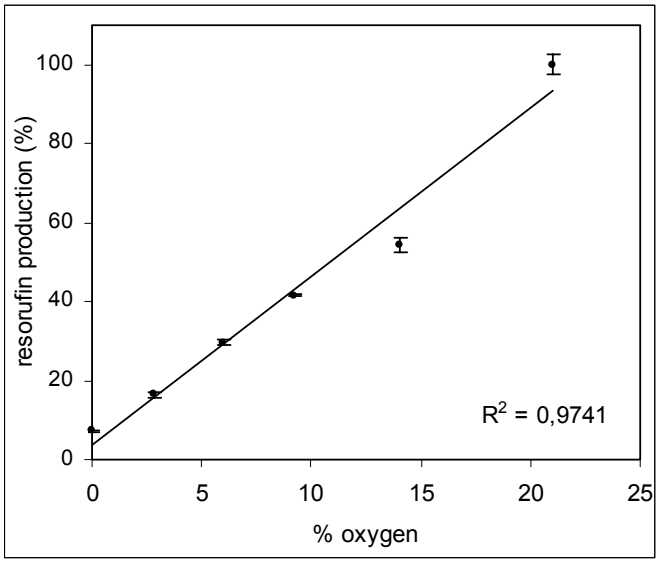

Fig.: 3-20 Influence of oxygen concentration on CYP metabolic activity. CYP2B1 enzymatic activity was measured in X39 cells under different concentrations of O_2 as described in materials and methods. Resorufin production determined at 21% O_2 was set to 100%; mean values from triplicates ± SD are shown.

3.1.3.3.6 CYP2B1 enzymatic activity under the agarose layer

To evaluate CYP2B1 enzymatic activity under the agarose layer, X39 cells, cultured under standard conditions or under an agarose layer, respectively, were assayed for CYP2B1 activity by the resorufin assay.

The substrate, 7-pentoxyresorufin: 1) was added directly to the culture medium ('- gel'); 2) was carefully injected into the space between the cells and the agarose overlay ('+ gel'); or 3) was added to cells cultured under agarose after the gel was removed ('gel removed'). The DNA content of each well was quantified to ensure that similar cell numbers were present in the individual wells. The CYP activity of cells grown under standard conditions was similar to that of cells cultured under agarose with removal of the agarose prior to substrate incubation. In contrast, CYP activity

assayed in cells under the agarose layer was reduced to 12% compared to cells without the agarose (FIG 3-21), despite the presumed substrate concentration effect of the agarose overlay. This CYP activity level corresponds to an oxygen concentration of about 1-2% based on the calibration curve shown in FIG. 3-20. To rule out artifacts due to diffusion of resorufin into the agarose gel, a control experiment with resorufin injected under the agarose layer in the absence of cells was carried out. Approximately 83% of the fluorescent dye was found in the solution under similar incubation conditions (data not shown). CYP2B1 protein levels were not influenced by the agarose overlay, as determined by antibody staining and flow cytometry analysis (data not shown). Hence, the agarose layer does not influence expression of CYP2B1. Thus, the agarose overlay technique apparently mimics the tumor environment regarding hypoxic conditions.

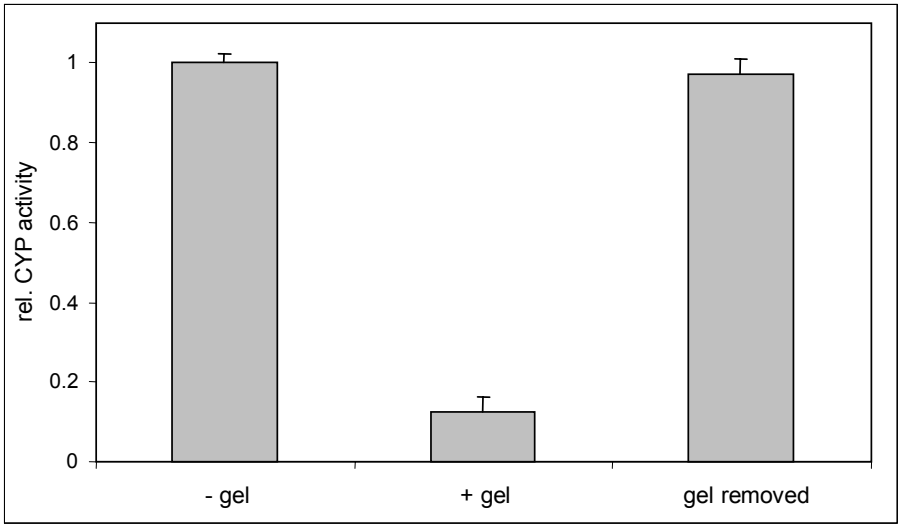

Fig.: 3-21 Twenty four h prior to agarose overlay, 30000 X39 cells were seeded per well of a 48-well plate. CYP activity was measured as described in materials and methods ('- gel'). When performing the resorufin-assay under the agarose overlay ('+ gel'), 200 µl of the incubation solution was injected under the agarose layer 1 h after solidification of the agarose overlay. After the incubation, fluorescence measurements were performed in the same way as described above. In 'gel removed' samples, CYP activity with pentoxyresorufin was determined for cells cultured under agarose after removal of the agarose overlay. Resorufin production by cells without agarose overlay ('-gel') was set to 100%. Mean values from triplicates ± SD are shown.

3.1.3.3.7 Enhancement of bystander activity by the agarose overlay technique in a coculture system

Coculture experiments were carried out to determine the impact of the conditions imposed by the agarose overlay, i.e., limited drug and metabolite diffusion and hypoxic conditions, on bystander anti-tumor activity. Different ratios of X39 and CT26 cells (FIG. 3-22A and 3-22B) or X39 and murine neuroblastoma Neuro2A cells (FIG. 3-22C and 3-22D) were seeded in multi well plates. The cells were treated with 0.5

mM CPA in standard cell culture medium (A and C) or after coating the cells with a layer of 0.5% agarose (B and D). After CPA treatment for 5 days, cell proliferation was measured using the DNA content assay. Under standard culture conditions, CT26 cells were quite resistant to the cytotoxic effects of CPA activated by X39 cells. Thus, 50% killing of the overall cell population was only achieved when the population was comprised of 75% CYP2B1-expressing (X39) cells (FIG. 3-22A). Neuro2A cells exhibited somewhat greater sensitivity to activated CPA, with 50% cell killing achieved in cocultures containing ~60-65% X39 cells (FIG. 3-22C). By contrast, a remarkable bystander effect was achieved when agarose overlaid cocultures were treated with CPA. In particular, CPA killed ~ 80% of the Neuro2A + X39 mixed cell population in cultures containing 25% CYP-expressing cells, and almost complete eradication of the Neuro2A + X39 mixed cell population was achieved in cultures containing 50% CYP-expressing cells (FIG. 3-22D; also see CT26 cells in FIG. 3-22B).

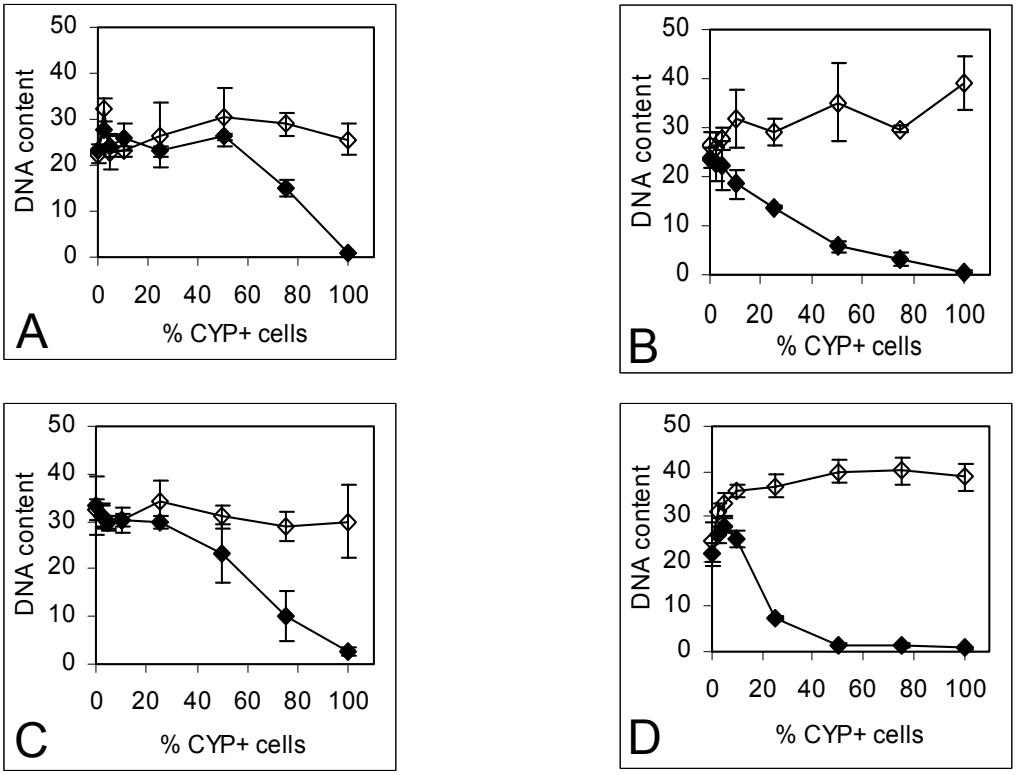

Fig.: 3-22 Impact of agarose overlay on bystander effect in mixed cell populations: Different ratios of CT26 cells (A and B) or Neuro2A cells (C and D) mixed with the CYP2B1-expressing X39 cells were treated for 5 d with 0.5 mM CPA. The DNA content of each well was assayed, and absolute DNA content values expressed as RFU x 1000 are shown on the y-axis. A and C: conventional cell culture; B and D: agarose overlay cell culture; mean values from triplicates ± SD are shown. Open symbols, no CPA treatment; closed symbols, treatment with 0.5 mM CPA

3.1.3.3.8 Kinetic of cell death induced by CPA treatment

To investigate if the agarose layer has an influence on the kinetic of cell death by in situ activated CPA, coculture experiments were performed with and without the overlay technique. CT26 cells and Neuro2A cells were grown as a coculture system with 25% of CYP2B1 expressing X39 cells. The medium was removed 24h after the seeding and exchanged by either 200µl of fresh medium or the agarose layer was applied. Afterwards 600µl CPA containing medium was added to each well; the resulting concentration of CPA was 0.5mM CPA. Cell proliferation and survival was analyzed for the following 6 days by Hoechst33258 based DNA content assay and a parallel performed MTT assay. Analysis was performed every 24h.

The coculture systems without the overlay technique showed the most distinctive decrease in cell survival at day 3 after the CPA administration, indicated by decreased fluorescence signal in the Hoechst33258 based proliferation assay and a decreased absorbance in the MTT assay. Likewise, the coculture systems with the agarose layer showed a decrease in proliferation at day 3 of treatment. Yet, reduction in proliferation and survival was more pronounced in the system with the agarose layer. Beside detection of pronounced reduction on cell proliferation in the coculture systems with the agarose overlay, no time dependent effects regarding cell death in comparison to conventional cell culture technique were evident in the agarose overlay system.

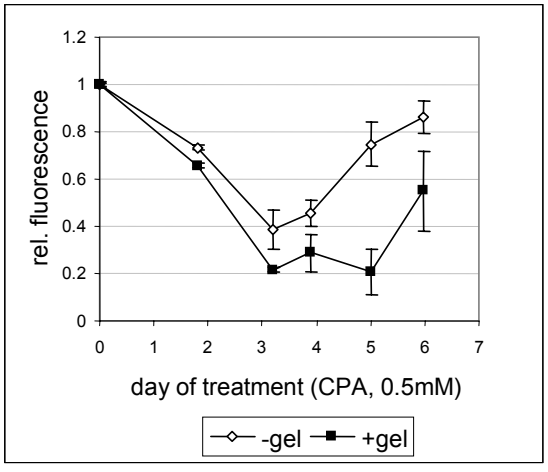

A

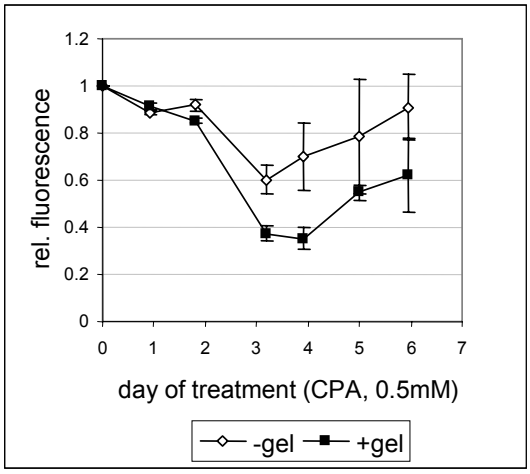

B

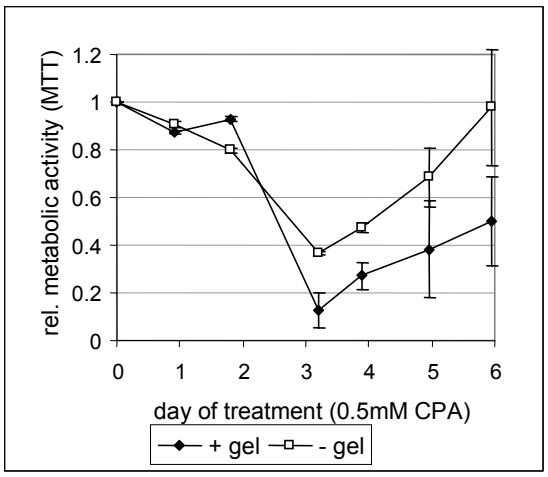

C

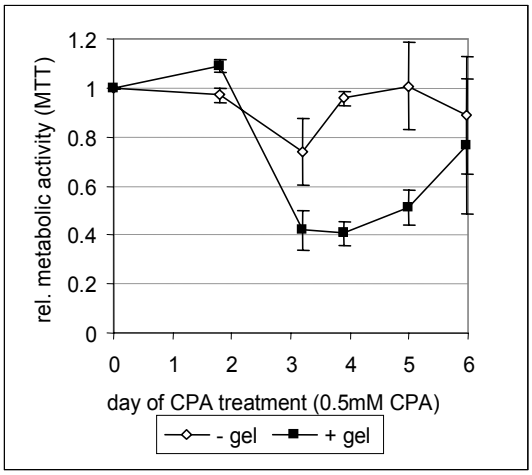

D

Fig.: 3-23 Time dependency of CPA based reduction in tumor cell proliferation in cocultures with CYP2B1 expressing cells (A: Neuro2A/X39; B: CT26/X39; C: Neuro2A/ X39; D: CT26/X39). Cocultures were treated with 0.5mM CPA for 6 d in conventional environment or under an agarose layer. Proliferation was determined by (A and B) DNA content measured or by (C and D) performing the MTT assay. Relative DNA content or metabolic activity is shown, with control levels set tovehicle treated cells. Black symbols: cells cultured with agarose overlay; white symbols: cells cultured without agarose overlay; mean values from triplicates ± SD are shown.

3.1.3.3.9 Bystander effect in cocultures with a fixed ratio of CYP2B1 expressing cells

The CPA concentration achieved in tumor tissue *in vivo* can be quite low (< 0.5 mM) due to rapid clearance of the drug from the blood stream (half-life <30 min (92)). We therefore investigated if a bystander effect of activated CPA can also be obtained at low CPA concentrations. CT26, HUH7 and X39 cells, and mixtures of X39 cells and either CT26 cells or HUH7 cells (25%/75%) were treated for 5 days with 0.01 to 10.0 mM CPA in culture medium, with or without an agarose overlay. The CYP2B1-deficient CT26 and HUH7 cells were quite resistant to CPA, both in the absence and in the presence of the agarose layer, and significant cell killing was only observed at CPA concentrations $\geq$3 mM (FIG. 3-24). No beneficial effect of the agarose layer was observed in cultures conatining X39 cells alone, as all the cells express CYP2B1 and generate 4-OH-CPA intracellularly, and thus no bystander effect is required for cell killing (Fig. 3-24C). In cocultures of 25% X39 cells and 75% CT26 cells, the presence of an agarose overlay markedly increased CPA-induced cell killing (FIG. 3-24D). At 0.05 mM CPA, ~40% cell killing was observed, both with and without the agarose overlay. As the X39 cells grow slightly faster than the parental cell line (data not shown), the 40% reduction in DNA content most probably reflects the killing of the 25% X39 cells seeded initially. A clear bystander effect was observed for the cells under the agarose layer at CPA concentrations between 0.1 and 1.0 mM, which

corresponds to a pharmacologically relevant concentration range. In cocultures of X39 cells with HUH7 hepatoma cells, 50% cell killing was achieved at very low concentrations of CPA (0.05 mM) and this effect was further enhanced by the agarose overlay (Fig. 3-24E).

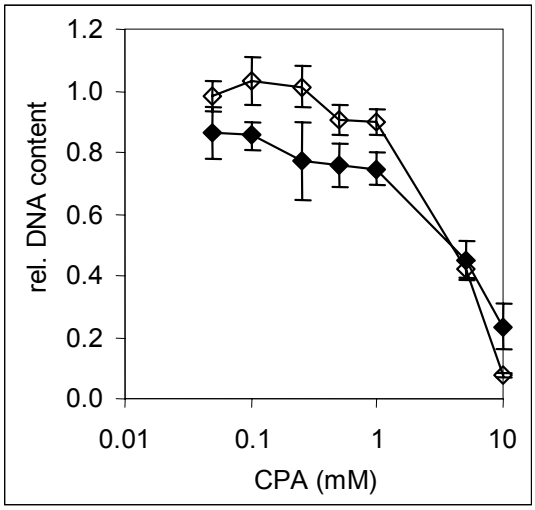

A

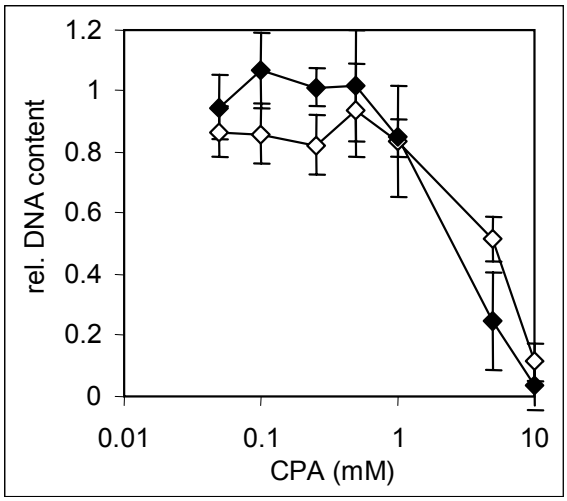

B

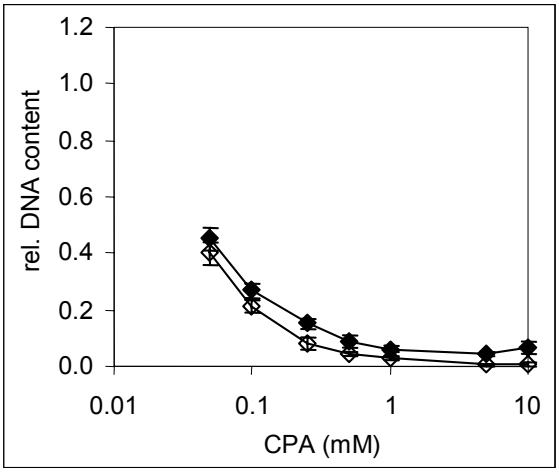

C

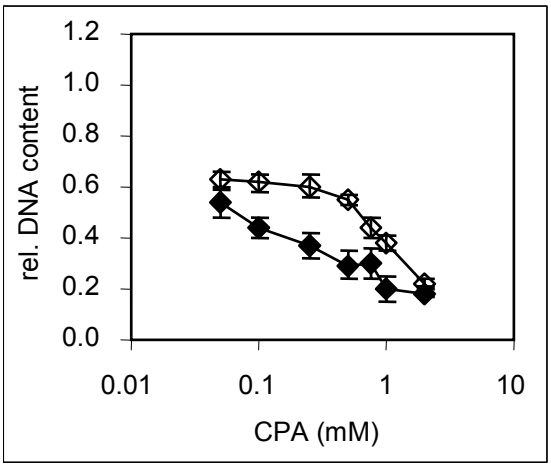

D

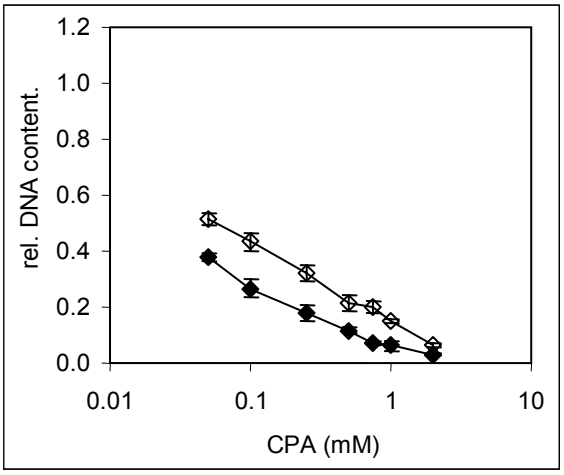

E

Fig.: 3-24 Effect of CPA concentration on tumor cell proliferation in cocultures with CYP2B1 expressing cells (A: CT26; B: HUH7; C: X39; D: CT26/X39 75%/25%; E: HUH7/X39 75%/25%) were treated with different concentrations of CPA for 5 d and the DNA content measured thereafter. Relative DNA content is shown, with the cells without CPA treatment set to 100%. Black symbols: cells cultured with agarose overlay; white symbols: cells cultured without agarose overlay; mean values from triplicates ± SD are shown.

3.1.3.3.10 Enhancement of bystander activity by the agarose overlay technique in transient transfection experiments

To investigate the impact of the agarose overlay on bystander activity under conditions where CYP2B1 encoding plasmid DNA is expressed in tumor cells after transient transfection, HUH 7 cells were transfected with CYP2B1 encoding plasmid DNA using LPEI; transient transfection resulted in ~13 % transfection efficiency, as shown by using EGFP as a reporter gene and confirmed by antibody staining for CYP2B1 (data not shown). Using similar conditions, HUH7 cells were transfected with plasmid encoding CYP2B1, or luciferase, followed by treatment with 0.5 mM CPA.

In cells transfected with CYP2B1 and agarose overlay, >90% of the cells were killed after only a 5 h CPA treatment, as judged in by MTT assay 3 days after the treatment. Control cells, transfected with luciferase, exhibited non-significant increased sensitivity.

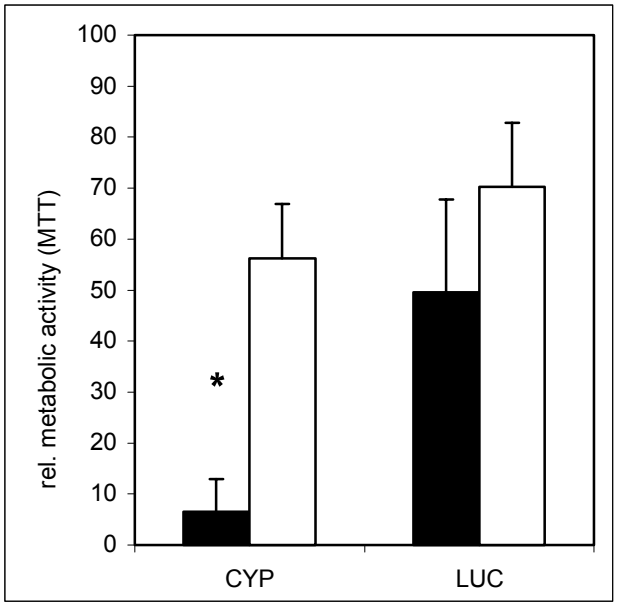

*Fig.: 3-25 Influence of agarose overlay on cytotoxicity of CPA toward transiently transfected tumor cells. HUH7 cells were transfected with LPEI polyplexes containing either pCMV-LUC (Luc) or pCMV-CYP2B1 (CYP). Forty eight h after transfection, the cells were treated for 5 h with 0.5 mM CPA either with agarose overlay (black bars) or under standard culture conditions (white bars). Culture medium and agarose overlay were then removed and replaced by CPA free medium. Three days after CPA treatment, cell viability was measured by the MTT assay.. Data are normalized to control cells treated in the same way but without CPA. Open bars: vehicle treated, black bars: 0.5mM CPA. Data shown are mean values for triplicates, ± SD. *p<0.05, compared to vehicle treated system (Mann-Whitney U-test).*

For further investigation of the GDEPT concept, with attention to transient transfection and short CPA exposure time, in vivo experiments were performed. In this context, the therapeutic gene pCMV-CYP2B1 was delivered to the tumor tissue of established subcutaneous CT26 tumors by electroporation, followed by systemic CPA treatment.

3.1.4 In vivo approach

The in vivo studies were performed in SCID mice bearing subcutaneous CT26 tumors to evaluate effects of local CPA prodrug activation after gene transfer in

addition to liver metabolism. Therefore the subcutaneous CT26 tumor model in SCID mice was chosen because of low endogenous cytochrom enzymatic activity of CT26 cells and already established efficient gene transfer via electroporation in the subcutaneous CT26 tumor model.

3.1.4.1 Characterisation of tumor histology and tumor growth

For the in vivo investigation of CPA treatment after CYP2B1 gene transfer, the subcutaneous CT26 tumor model was established in SCID mice to avoid possible immune response on expressed rat CYP2B1 protein. Tumor growth was initialized by implantation of 100000 CT26 cells in the flank of the animals and tumor growth was determined; additionally mice were monitored for body weight loss.

3.1.4.1.1 Tumor histology

For characterization of the established subcutaneous CT26 tumors, tumor tissue was collected and analyzed by Haematoxylin/Eosin staining. Positively charged haematoxilin binds to DNA resulting in blue stained nuclei, whereas negatively charged eosin binds to plasma proteins and is therefore used as plasma stain. CT26 xenografts own a very compact and homogenous tissue structure. Tumor cell nuclei are large in comparison to the cytoplasm. The tumor tissue was encased in a layer of connective tissue (FIG 3-26A). In tumors of an average cross section dimension of 10mm and larger necrotic areas were detected in the central areas of the tumors.

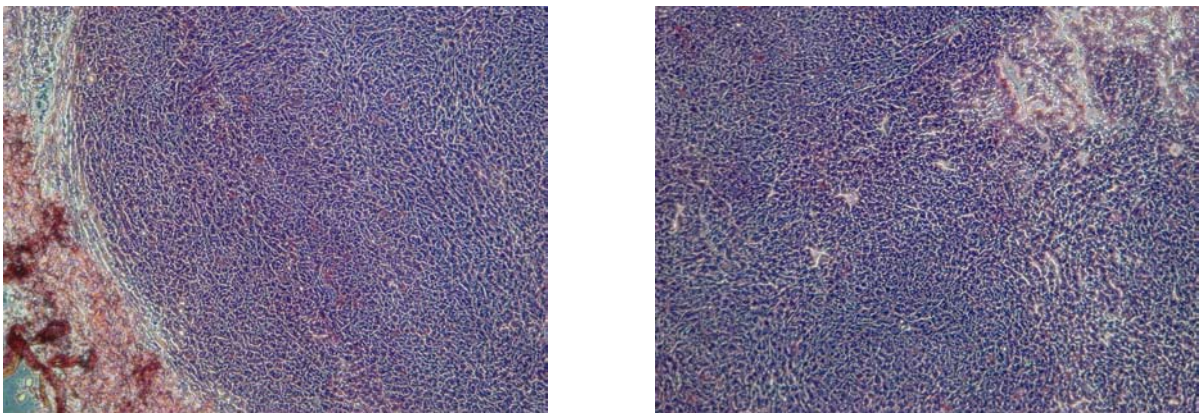

A B

Fig.: 3-26 Histology of subcutaneous CT26 xenografts in SCID mice (H/E stain). Cryosections (8µm) were fixed with 4% paraformaldehyde and subjected to H/E staining. Sections were viewed on a Zeiss Axiovert 200 transmitted light microscope and pictures were taken by a Sony DSC-S75 digital camera. A, B) 20x0.4 NA objective

3.1.4.1.2 Tumor growth and body weight

In order to initialize growth of CT26 xenografts in SCID mice, CT26 tumor cells were implanted subcutaneously in the flank of SCID mice as described in materials and

methods. After a lag time of about 7 days tumors were palpable in most of the mice. At this stage tumor volume increased in an exponential manner for the next two weeks (FIG 3-27A). Average tumor volume doubling time was 3.5 days. When the tumors reached a cross section dimension of 15mm in one of the measured variables, mice were sacrified.

Tumor bearing mice were additionally monitored for changes in body weight over the time of tumor growth. Body weight was constant for about 20 days after tumor implantation (FIG 3-27F). When average tumor size reached 300 to 400 mm^3 mice began to loose body weight (data not shown). At more than 20% loss of body weight mice were sacrified.

3.1.4.2 Tumor response to metronomic scheduled CPA treatment

In order to find a dose interval for metronomic scheduled CPA that is adequate for combination with CYP2B1 gene transfer, CPA dose response rates were determined in the CT26 SCID xenograft model. When the average tumor size reaches $40mm^3$ at day 9 after the tumor implantation CPA treatment was started. Different doses (mg/kg) CPA were administered in a 6 day schedule. Tumor size and body weight were monitored over the time of treatment. When tumors reached a cross section dimension of 15mm in one of the measured variables or when body weight loss was more than 20%, mice were sacrified.

Metronomically scheduled CPA treatment in a 6 day regime caused a slower increase in tumor volume of the treated tumors in comparison to the untreated control group. The tendency of decreased tumor growth was already evident when mice were treated with 75mg/kg CPA intraperitoneally every 6 days. Average tumor volume double time was 6 days versus 3.5 days of the non-treated control group (FIG 3-27C). When animals were treated with 50mg/kg CPA every 6th day, influence on tumor volume doubling time was slight (FIG 3-27B). Treatment of mice with 120mg/kg and 150mg/kg CPA intraperitoneally resulted in pronounced decrease in tumor growth. Average tumor double time was increased up to 13 to 14 days at both CPA dosages (FIG 3-27D and 3-27E). Average loss in body weight was not detectable in any treated group up to day 23 after tumor cell implantation (FIG 3-27 F).

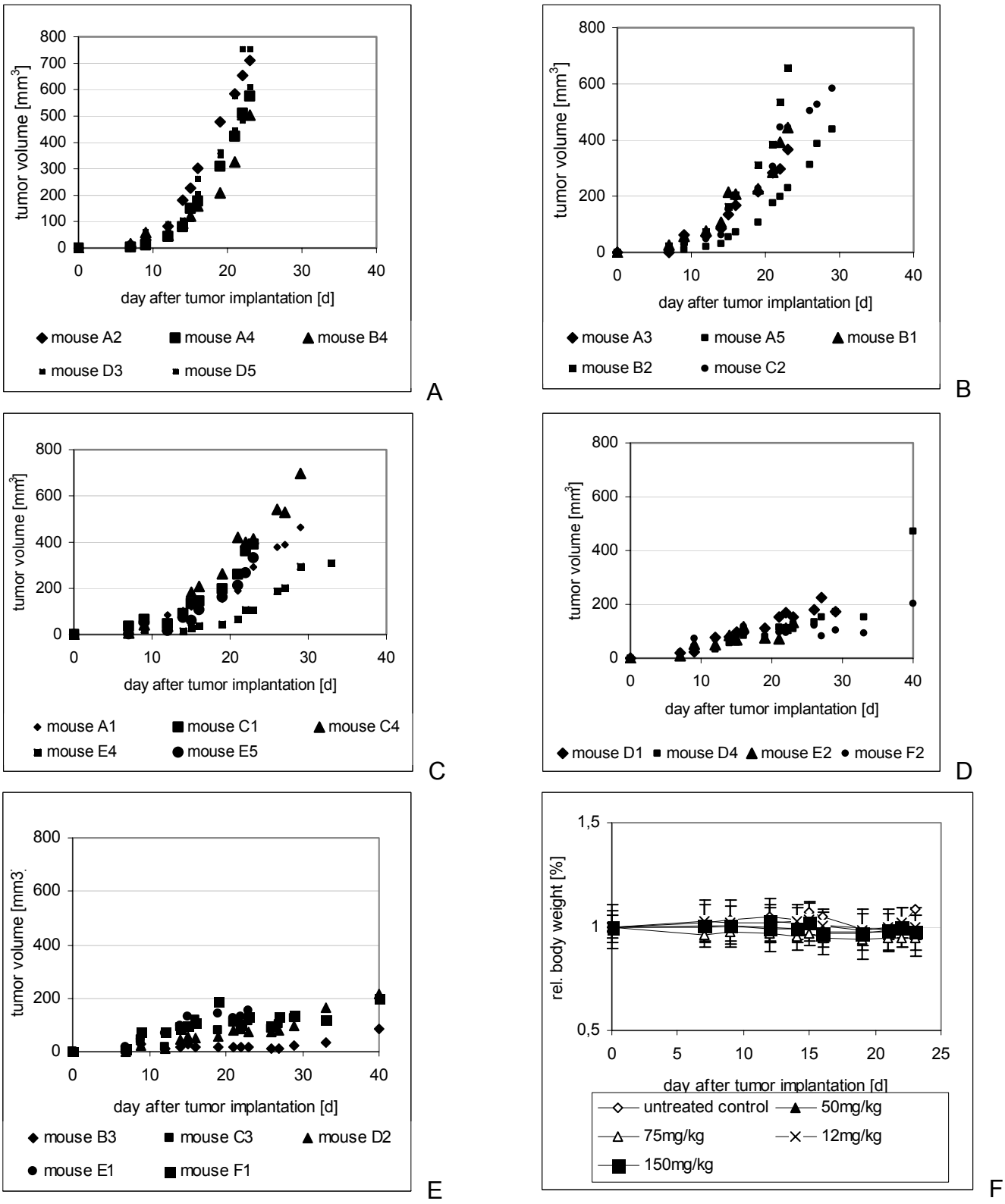

Fig.: 3-27 Tumor growth curves of CT26 xenografts in SCID mice and body weight analysis. CPA administration, tumor volume measurement and body weight elevation were carried oust. (A) untreated control; (B) treated with 50mg/kg CPA; (C) treated with 75mg/kg CPA; (D) treated with 120mg/kg CPA; (E) treated with 150mg/kg CPA; (F) average changes in body weight. (n=5 or n=4 for 120mg/kg group)

To further evaluate suitable CPA treatment regimes for gene therapy combinations, the treatment free interval between CPA applications was shorted to 3 days with half dosage of the 6 day schedule. Subcutaneous CT26 bearing mice were treated with either 40mg/kg every third day or 80mg/kg every 6th day. Tumor growth and body weight was monitored over the time of treatment.

No difference was evident in the 3 day regime with 40mg/kg in comparison to the 6 day schedule with 80mg/kg in terms of tumor growth and body weight (FIG 3-28C and 3-28D). Therefore the time between the CPA applications was shortened for the combination with CYP-gene therapy in the following experiment.

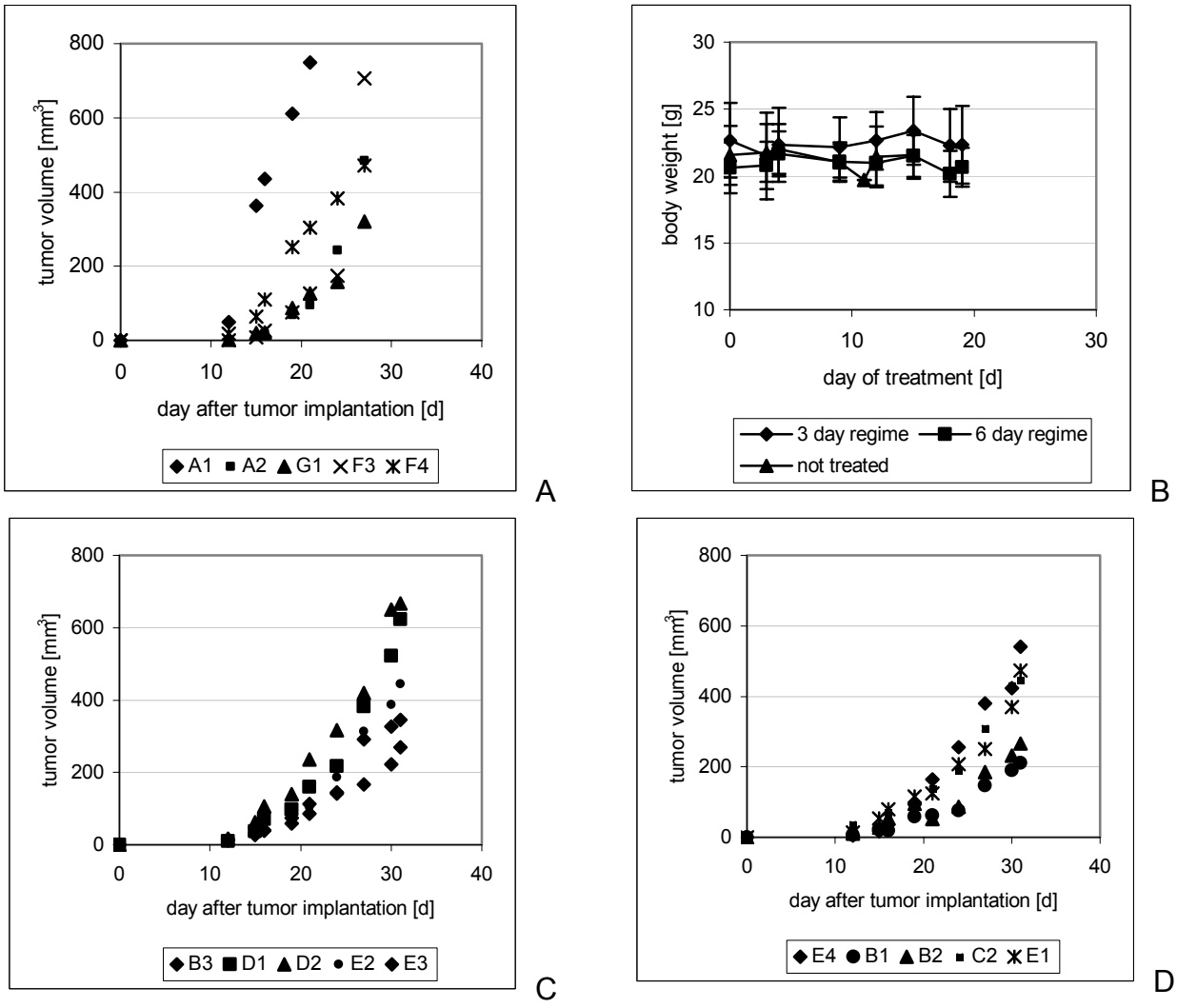

Fig.: 3-28 Tumor growth curves of CT26 xenografts in SCID mice and body weight analysis. CPA administration, tumor volume measurement and body weight elevation were carried out. (A) untreated control; (B) average body weight (C) treated with 40mg/kg CPA every third day; (D) treated with 80mg/kg CPA every 6th day.

3.1.4.3 Metronomic scheduled CPA treatment combined with precedent CYP2B1 gene transfer

CT26 tumors were initialized in SCID mice as described in materials and methods. In separately performed studies parameters for electroporation were optimized via luciferase reporter gene expression (S. van der Piepen and M. Ogris, unpublished). When average tumor volume reached 40mm^3 on day 11, the combined gene transfer plus CPA treatment regime was started. Intratumoral injections of plasmid (either pCYP2B1 or an empty control plasmid (pNull) with subsequent electroporation were performed to achieve transgene expression within the tumor tissue. Animals were treated with low dose CPA (40mg/kg) on both following days after the gene transfer. In addition to the control electroporation group a further control group with animals which were not subjected to the electroporation procedure was set; CPA application was performed as in both electroporation groups. Tumor growth and body weight was monitored over the whole period of treatment. The schedule was repeated every 4 days. No significant change in body weight was observed for all treated groups compared to the control (data not shown). From day 17 on, after tumor cell implantation, CPA treated tumors showed a decreased growth rate to untreated control. The decrease in tumor growth was more pronounced for the combination of electroporation and CPA treatment. Interestingly also the transfection with the control plasmid (pNull) had a similar effect on growth retardation. There was no significant difference in tumor growth retardation between the pCYP4502B1 and pNull groups (FIG 3-29).

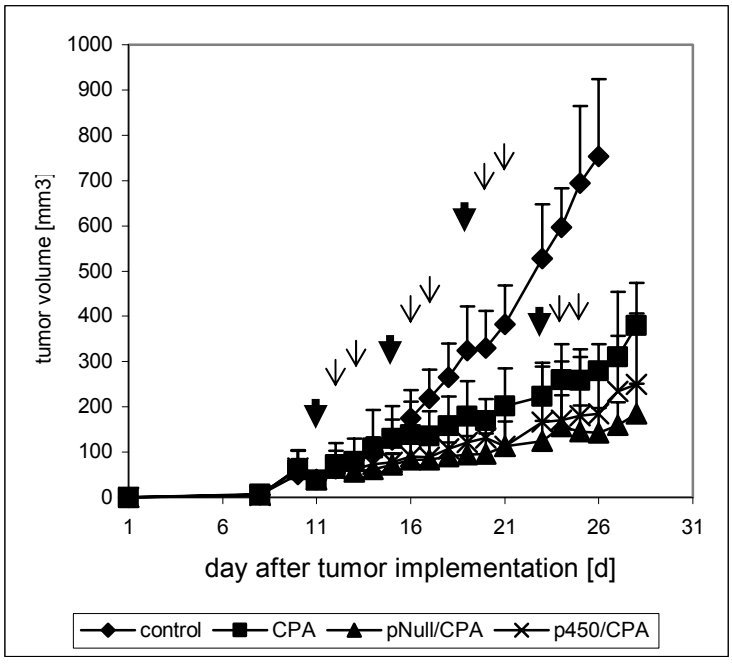

Fig.: 3-29 Tumor growth of subcutaneous CT26 tumors, treated with CPA only or in combination with pP450CYP2B1/pcontrol gene transfer by electroporation. SCID mice bearing subcutaneous CT26 tumor were treated either a combination of gene transfer via electroporation (pP4502B1 or pNull) and CPA treatment on both following days or only CPA treatment. Broad arrows indicate days of gene transfer via electroporation, light arrows indicate days of CPA application (40mg/kg, intraperitoneally).

3.2 Evaluation of tumor cells as producer cells in the antiangiogenic GDEPT concept

3.2.1 Endogenous CYP activity in endothelial cells

In order to evaluate endothelial cells for endogenous CYP activity, HUVEC and PEC cells were evaluated for enzymatic activity by the resorufin assay. Measured fluorescence signal was on background levels; no enzymatic activity was detectable in HUVEC and in PEC cells by the resorufin assay (data not shown).

3.2.2 Sensitivity of primary endothelial cells against CPA treatment

To determine the toxic profile of the prodrug CPA on endothelial cells, HUVEC and PEC cells were incubated for 3 days with different concentrations of CPA (0.05mM, 0.5mM, 1.0mM and 10.0mM) in the medium. Sensitivity against CPA treatment was then evaluated by measuring proliferation rate by the DNA content assay. Additionally total metabolic activity was determined by the MTT assay (data not shown). Reduction in proliferation rates of HUVEC and PEC cells were not observed when CPA concentrations were adjusted up to 1.0mM CPA in the cell culture medium, indicating low unspecific toxicity of the prodrug on primary endothelial cells. However, treatment with 10.0mM CPA resulted in significantly decreased proliferation rates due to relevant unspecific toxic effects of CPA prodrug at this concentration.

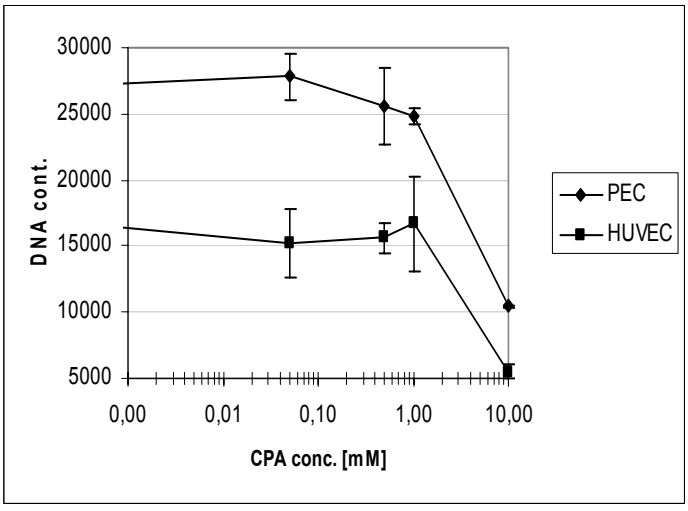

Fig.: 3-30 Effects of the prodrug CPA on the proliferation rate of endothelial cells. HUVEC and PEC cells were incubated for 3d with different concentrations of CPA. Proliferation levels were determined by the Hoechst33258 based proliferation assay. The values are means ± SD of triplicates.

3.2.3 Coculture of endothelial cells with CYP2B1 expressing tumor cells

3.2.3.1 Evaluation of proliferation and survival

The sensitivity of endothelial cells to in situ activated CPA was evaluated in coculture experiments with CYP2B1 expressing tumor cells (X39). Coculture experiments were performed in conventional coculture systems (cell-cell-contacts between tumor and endothelial cells were possible) and in transwell systems with prevented cell-cell-contacts.

3.2.3.1.1 Proliferation of endothelial cells in a coculture

HUVEC cells and PEC cells were cocultured with different rates of CYP2B1 expressing tumor cells (X39) at a constant CPA concentration of 0.5mM for 3 days. The concentration of 0.5mM CPA in the medium was chosen because proliferation rate of evaluated endothelial cells was not influenced at this concentration in a monoculture system. After the incubation time of 3 days, proliferation rate of the coculture system was determined by measuring DNA content by the Hoechst33258 based proliferation assay. X39 cells are nearly completely removed by suicidal effects when treated with 0.5mM CPA for 3 days. Measurements were corrected for background by remaining X39 DNA content. The resulting DNA, measured by the Hoechst33258 based proliferation assay therefore reflects the proliferation of the endothelial cells in the coculture system.

In HUVEC cells, 50% of CYP2B1 expressing tumor cells were required in order to decrease total proliferation rate in the coculture system extending suicidal effects of X39 cells (FIG 3-31). In PEC cells, 25% of CYP2B1 expressing tumor cells decreased total proliferation rate extending suicidal effects of X39 cells (FIG 3-32). This indicates higher sensitivity of PEC cells to treatment with in situ activated CPA in terms of proliferation.

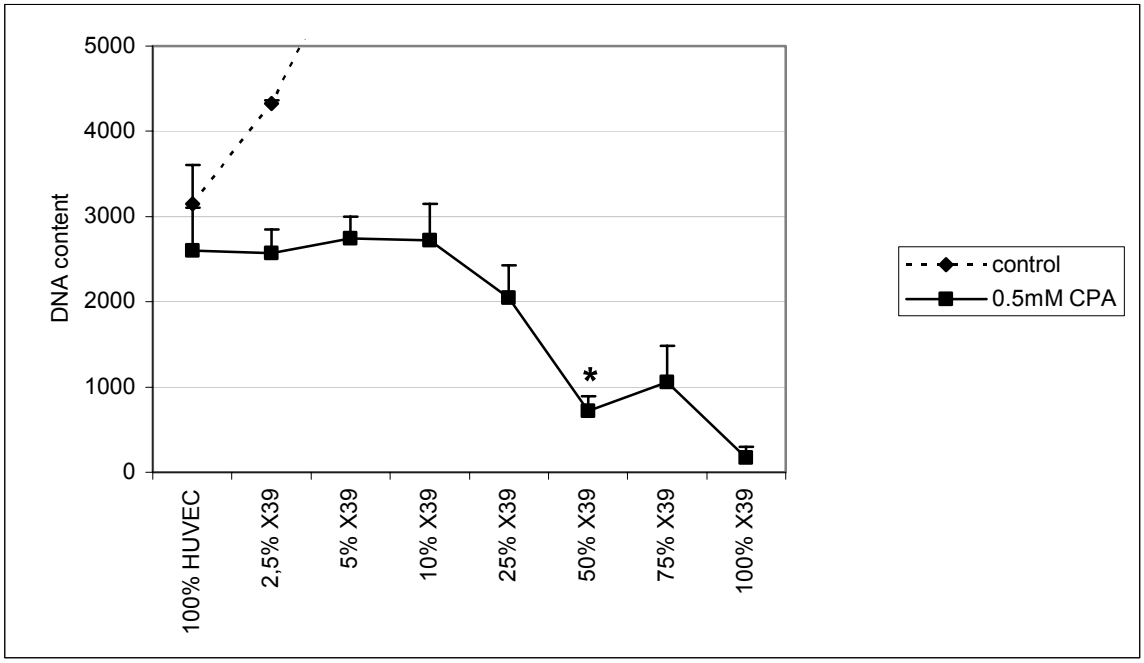

*Fig.: 3-31 Proliferation levels of coculture systems with different rates of endothelial HUVEC and CYP2B1 expressing tumor cells in the presence of 0.5mM CPA. Cocultures were treated in the presence of CPA for 3 days. Proliferation rate was determined by DNA content based Hoechst33258 proliferation assay. Measurements are corrected for X39 DNA content. Values are means ± SD of triplicates. *p<0.05, compared to the HUVEC monoculture system (Mann-Whitney U-test).*

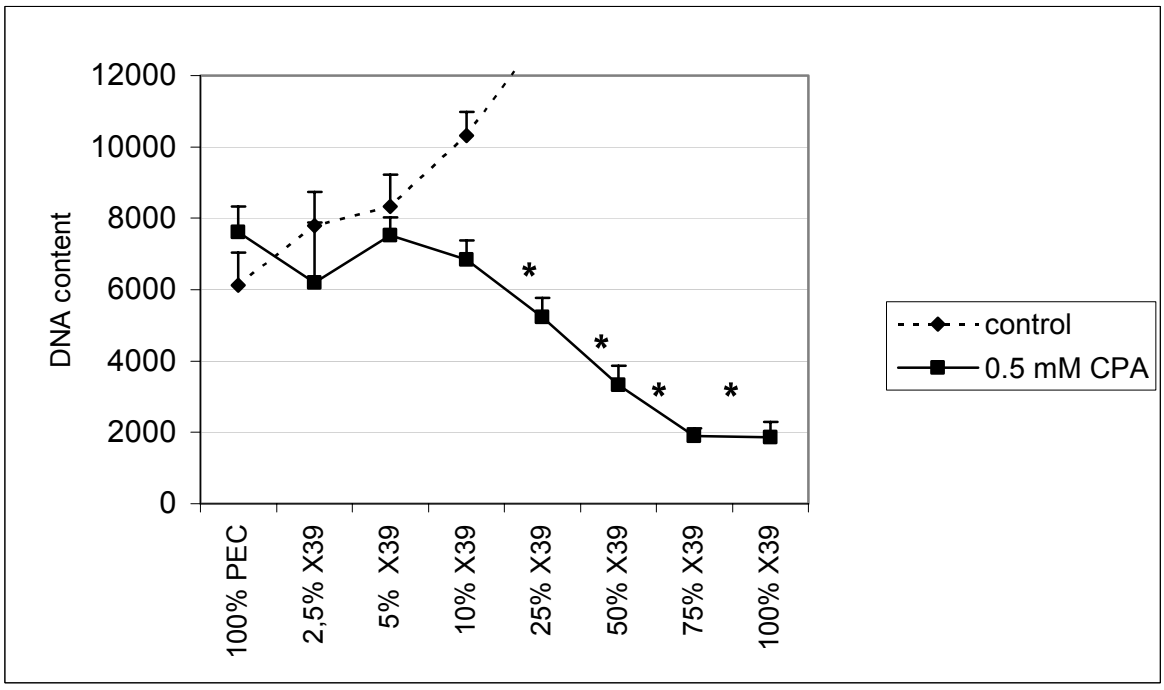

*Fig.: 3-32 Proliferation levels of coculture systems with different rates of endothelial PEC and CYP2B1 expressing tumor cells in the presence of 0.5mM CPA. Cocultures were treated in the presence of CPA for 3 days. Proliferation rate was determined by DNA content based Hoechst33258 proliferation assay. Measurements are corrected for X39 DNA content. Values are means ± SD of triplicates. *p<0.05, compared to the HUVEC monoculture system (Mann-Whitney U-test).*

3.2.3.1.2 Proliferation and survival in a transwell system

For further evaluation of in situ activated CPA on primary endothelial cells, coculture studies were performed in a transwell system preventing direct cell-cell contacts; antiproliferative effects of soluble CPA metabolites should be detectable. Therefore endothelial cells (HUVECs and PECs) were cultured in the bottom chamber of the transwell system (target cells). CYP2B1 expressing X39 and CT26 control tumor cells were seeded in the insert of the transwell system (producer cells).

Culturing was performed in the absence or in the presence of 0.5mM CPA. After an incubation time of 3 days, proliferation rate of endothelial cells in the bottom compartment was determined by the Hoechst33258 based proliferation assay. Additionally metabolic activity of endothelial cells was measured in a parallel experiment.

Proliferation rate of PEC cells was decreased when the coculture was performed in the presence of CYP2B1 expressing X39 cells and 0.5mM CPA for 3 days (FIG 3-33). In contrast, coculturing with wt CT26 cells in the absence or in the presence of 0.5mM CPA did not result in antiproliferative effects on PEC cells. Also, no antiproliferative effects were detectable when the coculture experiment was performed with X39 cells in the absence of CPA. Decrease in metabolic activity of PEC cells cocultured with X39 cells in the presence of 0.5mM CPA was in the same range than the decrease in proliferation rate (data not shown).

The incidence of antiproliferative effects in the coculture system with CYP2B1 expressing X39 cells in the presence of 0.5mM CPA indicates in situ activation of CPA and soluble CPA metabolites bothering the proliferation of cocultured PEC cells.

When HUVECs were cocultured in the transwell system with CYP2B1 expressing X39 cells for 3 days in the absence or in the presence of 0.5mM CPA, no anti-proliferative effect was evident in comparison to the control system with wt CT26 cells (FIG 3-34). Moreover no decrease in metabolic activity was detectable when HUVEC cells were cocultured with X39 cells in the presence of 0.5mM CPA (data not shown).

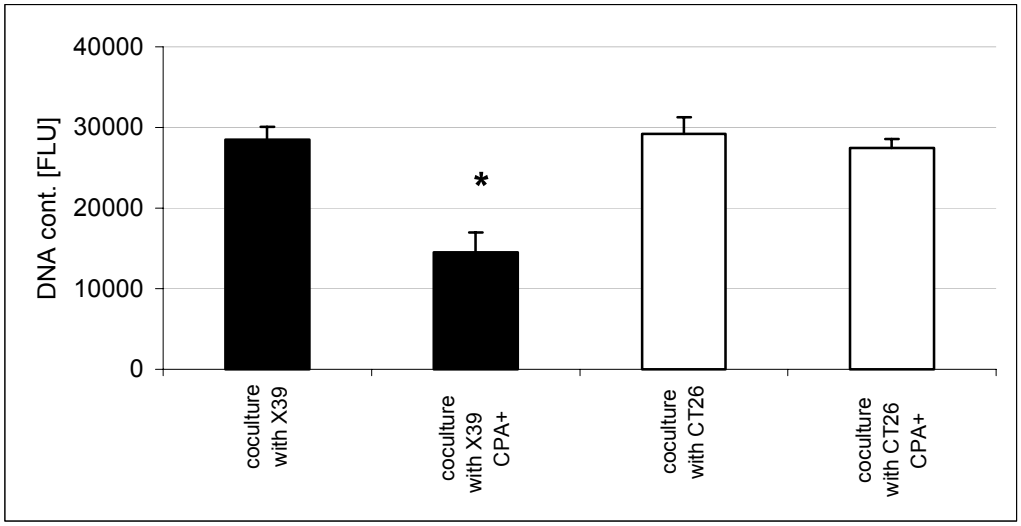

*Fig.: 3-33 In situ activated CPA decreases proliferation rate of PEC cells in a transwell system. PEC cells were cocultured with CYP2B1 expressing X39 and wt CT26 tumor cells in the absence or in the presence of 0.5mM CPA. Proliferation rate of the PEC cells was determined by Hoechst 33258 proliferation assay. Open bars: Cocultivation with wt CT26 cells; black bars: Cocultivation with CYP2B1 expressing X39 tumor cells. Values are means ± SD of triplicates. *p<0.05, compared to control systems (Mann-Whitney U-test).*

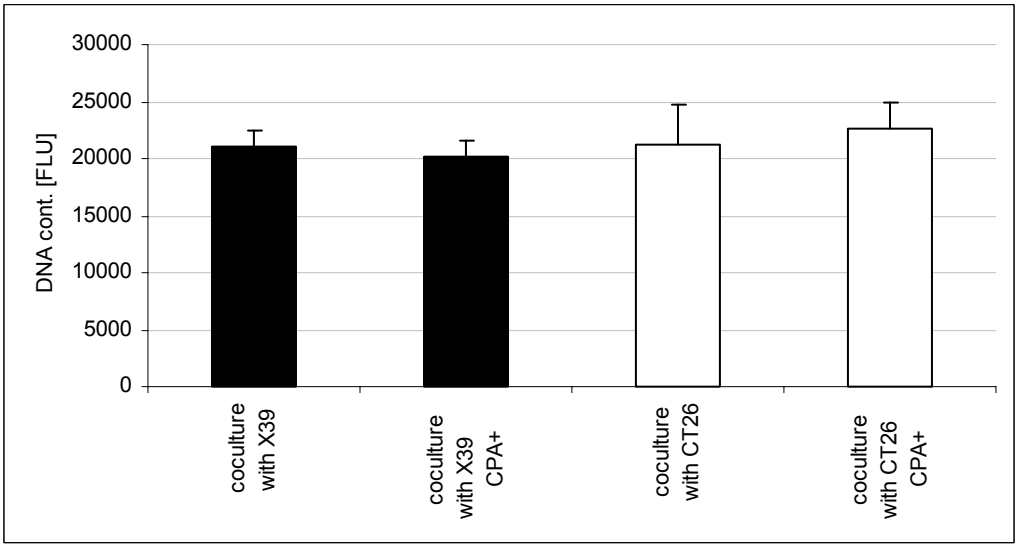

Fig.: 3-34 In situ activated CPA did not decrease proliferation rate of HUVEC cells in a transwell system. HUVEC cells were cocultured with CYP2B1 expressing X39 and wt CT26 tumor cells in the absence or in the presence of 0.5mM CPA. Proliferation rate of the HUVEC cells was determined by Hoechst 33258 proliferation assay. Open bars: Cocultivation with wt CT26 cells; black bars: Co-cultivation with CYP2B1 expressing X39 tumor cells. Values are means ± SD of triplicates.

3.2.3.2 Anti-migrative effects in an endothelial cell – tumor cell coculture system

Anti-migrative effects of in situ activated CPA by CYP2B1 expressing X39 tumor cells was evaluated by performing the wound scratch assay in an endothelial – tumor – cell coculture system. Migration rate of HUVEC and PEC cells was decreased when

the coculture was performed with X39 cells in the presence of 0.5mM CPA. No antimigrative effects were evident when the migration assay was performed in the absence of CPA or when the coculture was carried out with wt CT26 cells. HUVEC cells and PEC cells exhibited similar decrease in mean migration rates when cocultured with X39 cells in the presence of 0.5mM CPA. Yet, these antimigrative effects were not statistically significant (data not shown).

3.2.3.3 Coculturing endothelial cells with X39 cells in the presence of CPA disturbed the tube forming process

PEC cells were cocultured with CYP2B1 expressing X39 cells and with control wt CT26 tumor cells on collagen coated glass dishes. The mixed coculture (75% PEC, 25% tumor cells) was seeded in the presence of 0.5mM CPA in the cell culture medium. Control experiments were performed in the absence of CPA.

When PEC cells were cultured as a monoculture system on collagen coated glass dishes a monolayer was formed and no tube forming process was evident within 24h (FIG 3-35A). However, endothelial cells exhibited tube forming processes when co-culturing was performed with wt CT26 or X39 cells within 24h (FIG 3-35B and FIG 3-35C) in the absence of CPA.

In the presence of CYP2B1 expressing X39 cells the process of tube formation was disturbed significantly in the presence of 0.5mM CPA. Further on, the intensity of F-actin staining was decreased, indicating degradation of the F-actin cytoskeleton (FIG 3-35E). Tube forming process was not negatively influenced by coculturing PEC cells with control wt CT26 cells in the absence or in the presence of 0.5mM CPA (FIG 3-35 B and FIG 3-35D).

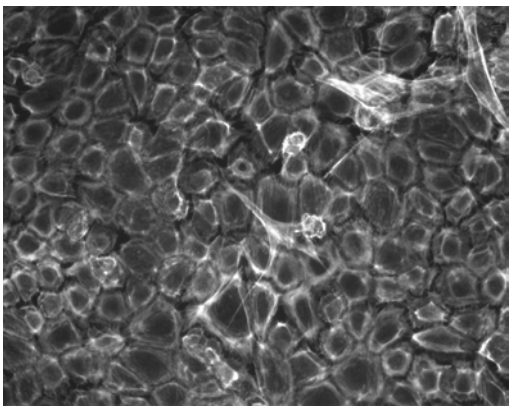

A

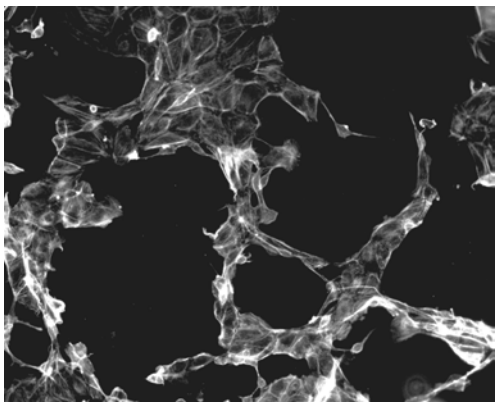

B

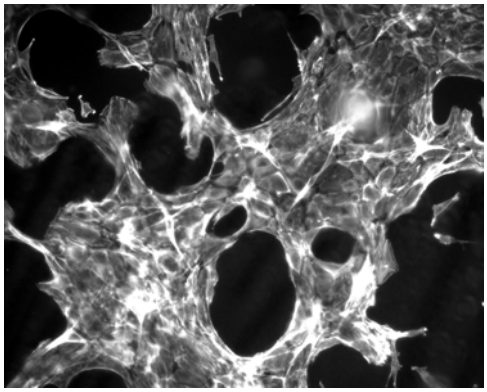

C

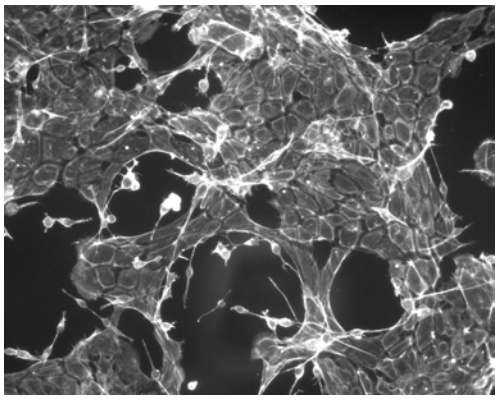

D

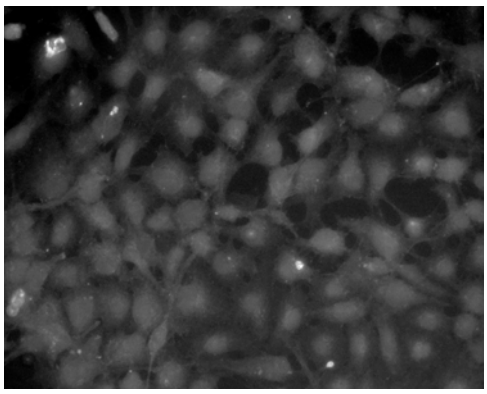

E

Fig.: 3-35 Tube forming and F-actin staining of PEC cells cultured on collagen coated glass dishes. A) PEC cells in the absence of X39/CT26 cells, B) PEC cells cocultured with 25% wt CT26 cells in the absence of CPA, C) PEC cells cocultured with 25% CYP2B1 expressing X39 cells in the absence of CPA, D) PEC cells cocultured with 25% wt CT26 cells in the presence of 0.5mM CPA and E) PEC cells cocultured with 25% CYP2B1 expressing X39 cells in the presence of 0.5mM CPA. The experiment was performed in duplicates. Figures show representative sections.

3.2.3.4 Coculturing of endothelial cells with CYP2B1 expressing tumor cells in the presence of CPA results in modifications of the F-actin cytoskeleton

The F-actin cytoskeleton of PEC and HUVEC cells showed modifications, when coculturing with CYP2B1 expressing X39 cells was performed in the presence of CPA. Therefore F-actin filaments were further analyzed by epifluorescence microscopy after staining. F-actin staining did not result in distinguishable F-actin fibres, indicating a breakdown of the endothelial F-actin cytoskeleton when coculturing was performed in the presence of CYP2B1 expressing tumor cells and CPA (FIG 3-36D and 3-36H). No breakdown of the F-actin cytoskeleton was detectable when endothelial cells were cocultured with X39 in the absence of CPA (FIG 3-36C and 3-36G). Further on endothelial cells cocultured with wt CT26 cells in the absence or in the presence of 0.5mM CPA did not result in disturbance in the F-actin cytoskeleton (FIG 3-36A, 3-36B and 3-36E, 3-36F).

This finding indicates that in situ activated CPA or metabolites of activated CPA, are responsible for the disturbance in the F-actin cytoskeleton of the endothelial cells.

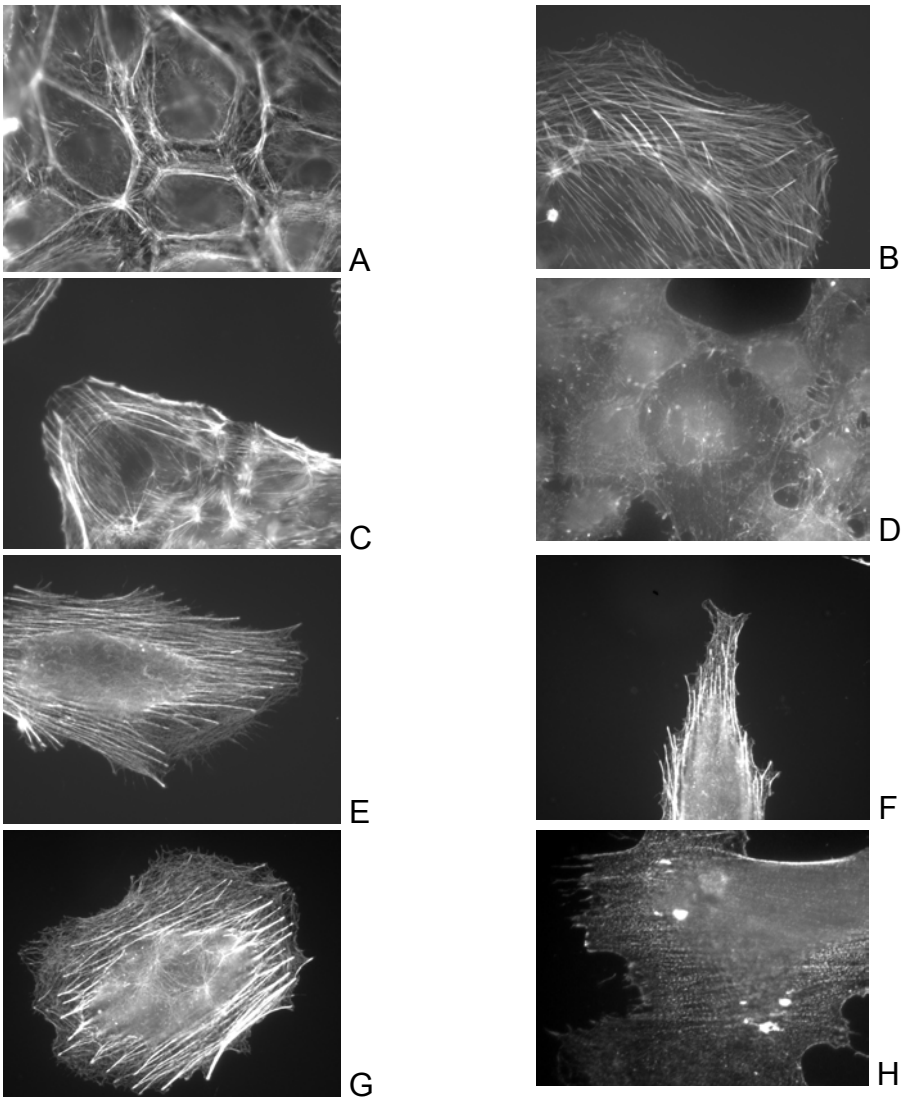

Fig.: 3-36 F-actin cytoskeleton of endothelial cells after coculturing with CYP2B1 expressing X39 or wt CT26 cells in the absence or in the presence of 0.5mM CPA for 24h. For optimal visualization of F-actin fibres light was collected through a 63x1.4 NA oil immersion objective (Zeiss). A) PEC cells cocultured with CT26 cells in the absence of CPA, B) PEC cells cocultured with CT26 cells in the presence of 0.5mM CPA, C) PEC cells cocultured with X39 cells in the absence of CPA, D) PEC cells cocultured with X39 cells in the presence of 0.5mM CPA, E) HUVEC cells cocultured with CT26 cells in the absence of CPA, F) HUVEC cocultured with CT26 cells in the presence of 0.5mM CPA, G) HUVEC cells cocultured with X39 cells in the absence of CPA and H) HUVEC cells cocultured with X39 cells in the presence of 0.5mM CPA. Figures show representative sections.

3.3 Role of acrolein in CPA therapy at metronomic schedule

Acrolein is one of the metabolites released by in situ activated CPA. This metabolite is considered to be very toxic; however, no impact on tumor growth is accredited to acrolein, at least in conventional high dose CPA regimes. In order to investigate a possible role for contribution of acrolein to the total antitumoral effect in metronomic scheduled CPA therapy, in vivo and in vitro experiments were performed.

3.3.1 Significant reduction in tumor blood flow and tumor growth in CPA treated mice

The ability of CPA to delay tumor growth in a metronomic schedule was evaluated in colon carcinoma CT26. Treatment of mice bearing CT26-tumors with CPA (40mg/kg on two consecutive days followed by two days without treatment) resulted in a significant growth delay as indicated by a lagged increase in tumor volume compared to the untreated control (FIG 3-29). Treatment was well tolerated as no significant decrease in body weight was observed (data not shown).

Changes in blood supply were measured by using Hoechst33258 as a tracer. This method was preferred because previous results showed a great discrepancy comparing CD31 antibody staining with actual functional blood flow (data not shown). Measurements were performed either at the end of the experiment (day 28 after tumor setting) or when tumor size exceeded 15mm in one dimension. CPA treatment resulted in a decreased blood supply in all three indicated areas of the tumors. The decrease in fluorescence was significant, indicating reduced blood flow compare to untreated animals.

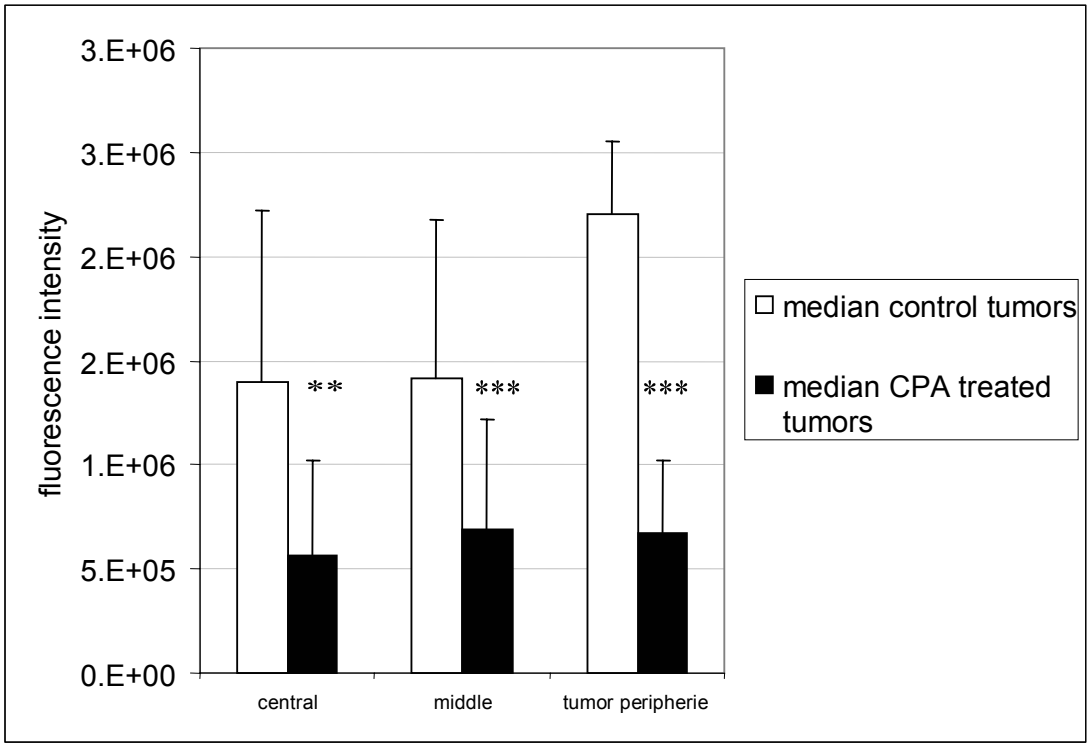

*Fig.: 3-37 Decrease in blood supply induced by low dose scheduled CPA treatment of SCID mice bearing subcutaneous CT26 tumors. Cryo-sections (10µm) were humidified with a drop of PBS, provided with a cover slip and immediately analyzed for fluorescence signal of intravenously injected Hoechst 33258 stain. For analysis 5 sections of the tumor regions (central, middle and tumor periphery) of each tumor, and 5 areas of each section were chosen in a randomized assortment. Analysis was performed with a Zeiss Axiovert 200 fluorescence microscope equipped with a 20x0.4 Zeiss objective and a Zeiss Axiocam. Quantification was performed with the MIPAV (Medical Image Processing, Analysis and Visualisation) software. Values are medians ± SD of six animals in the control group and ten animals in the CPA treated group. ***p<0.001; **p<0.01; *p<0.05, compared to control tumors (Mann-Whitney U-test).*

3.3.2 Acrolein adducts in tumor tissue of treated mice

Conversion of CPA to its activated metabolites is mainly taking place in the liver. In situ activated CPA and metabolites are then distributed all over the body via the blood stream. In order to investigate if relevant amounts of acrolein reach the tumor, cryosections were screened for acrolein adducts by specific antibody staining. Cryo-sections (5µm) of two randomly chosen CPA treated tumors of the experiment described in 3.3.1 were stained with an antibody that is specific for acrolein modified protein structures. In addition tumor sections were stained for endothelial cells with a rat-anti-mouse CD31 antibody in order to visualize tumor blood vessels.

Acrolein protein adducts were detected in both CPA treated tumor tissues by antibody staining, in tumor cells and in endothelial cells (FIG 3-38B). No staining was detectable with the control IgG (data not shown) and only slight staining appeared in the untreated control tumors (FIG 3-38A). It is noteworthy that acrolein adducts were

often localized in tumor areas of low blood supply, indicated by low Hoechst33258 signal.

Staining for acrolein adducts in the liver did not give a significant difference in CPA treated versus untreated animals. In both groups only slight positive staining for acrolein-protein adducts was detectable (data not shown). These results indicate that the metabolite acrolein reaches the tumor site via blood stream in detectable amounts and therefore may contribute to antitumoral effects of metronomic scheduled CPA therapy.

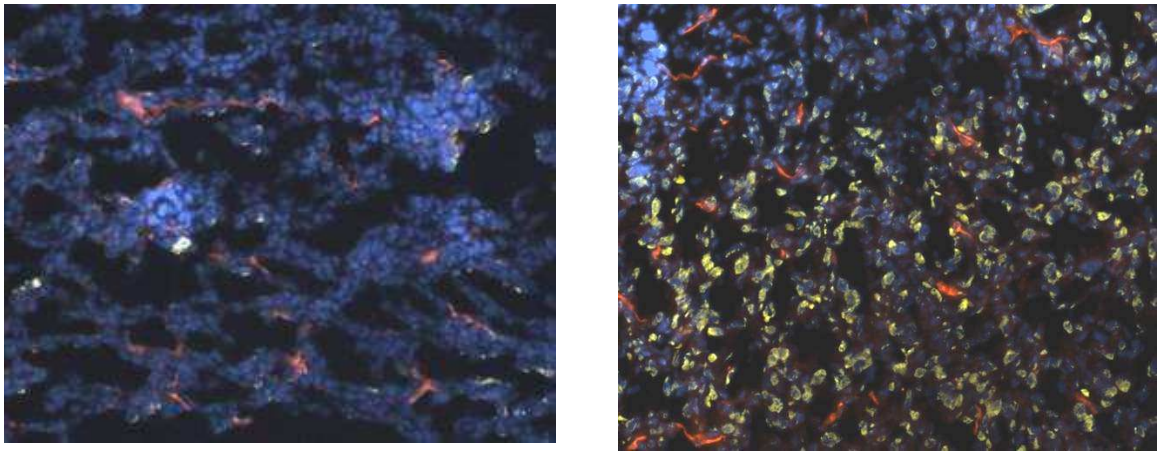

A B

Fig.: 3-38 Distribution of acrolein modified proteins in the tumor tissue of CPA treated (B) versus untreated control tumors (A). Cryo-sections (5µm) were fixed with 4% paraformaldehyde and stained with specific antibodies for endothelial cells (rat-anti-mouse CD31 (red)) and acrolein modified proteins (yellow). The intravenously injected Hoechst 33258 stain was visualized as well (blue). Analysis was performed with a Zeiss Axiovert 200 fluorescence microscope equipped with a 20x0.4 Zeiss objective and a Zeiss Axiocam.

3.3.3 Antiangiogenic properties of acrolein in vitro

For further investigation of possible antiangiogenic properties of acrolein, effects of this metabolite were investigated on primary endothelial cells regarding proliferation, migration and differentiation. In addition, effects of acrolein on NF-κB levels in endothelial cells and tumor cells were investigated because NF-κB seems to be a key regulator in angiogenic processes. Moreover, acrolein was evaluated for the potential of modulation on thrombospondin-1 levels due to thrombospondin-1 was identified as a possible mediator of antiangiogenic scheduled CPA therapy (93).

3.3.3.1 Changes of cell morphology

Primary endothelial cells (HUVECs) were analyzed for morphological changes due to acrolein treatment. Therefore, HUVEC cells were seeded 24h prior treatment at a density of 15000 cells/well on collagen G coated 24 well plates. Cells were cultured

with acrolein containing medium for 24h and morphology of cells was analyzed by transmitted light microscopy. Cell morphology was different in comparison to the control, when cell culture was performed in the presence of 30µM and 40µM acrolein (FIG 3-39 D and E) whereby cells appeared spindle-shaped at 30µM and rounded at 40µM Acrolein. Morphological changes were not evident when HUVEC cells were cultured in the presence of 10µM and 20µM acrolein (FIG 3-39 B and C).

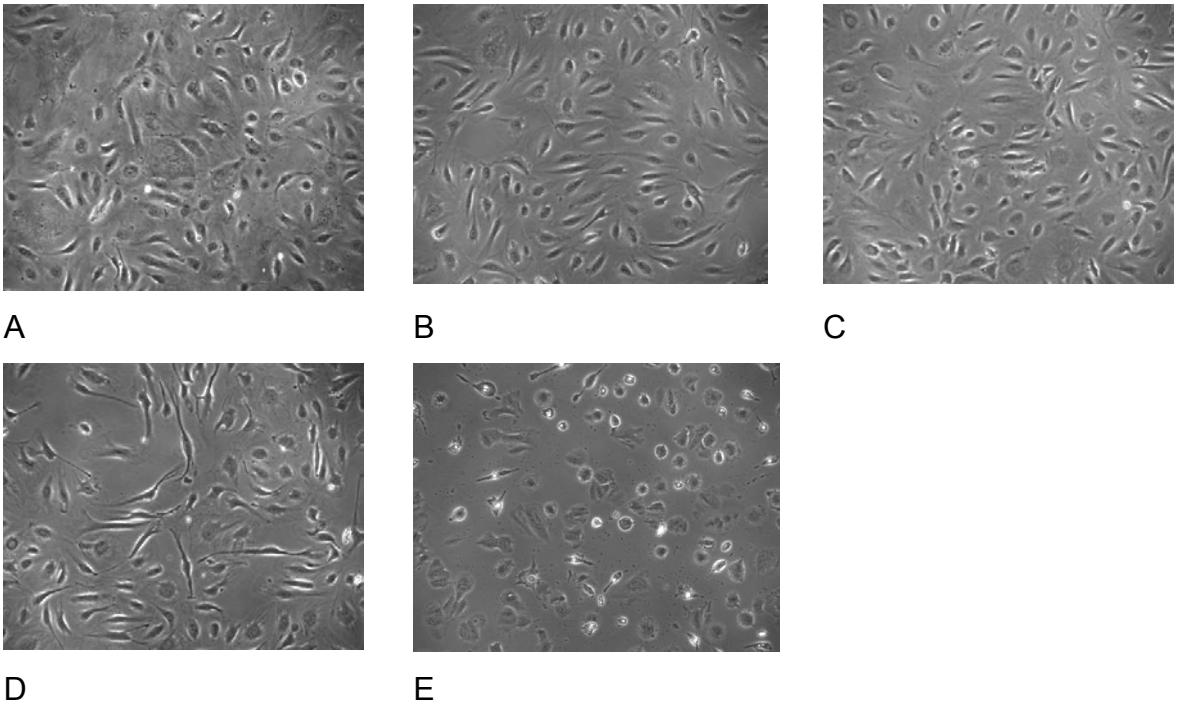

Fig.: 3-39 Morphology of HUVEC cells cultured in the presence of different concentrations of acrolein for 24h. 15000 HUVEC cells were seeded on collagen coated 24 well plates. 24h after the seeding different amounts of acrolein (dissolved in PBS) were added to the wells to adjust increasing concentrations of acrolein in the medium; (A) vehicle (PBS) 0µM acrolein, (B) 10µM acrolein, (C) 20µM acrolein, (D) 30µM acrolein and (E) 40µM acrolein. Cells were visualized 24h after the acrolein addition by transmitted light microscopy.

3.3.3.2 Acrolein is antiproliferative on endothelial cells

Primary endothelial cells (HUVECs and PECs) were investigated for antiproliferative properties of acrolein. Therefore cells were cultured for 24h in the absence or in the presence of different concentrations of acrolein in the medium (7.5µM, 10µM, 12.5µM, 25µM and 50µM). Survival and proliferation was determined by MTT assay as described in materials and methods.

Acrolein inhibited the proliferation and survival of vascular endothelial cells in a dose dependent manner. Effects in HUVEC cells were less pronounced than in PEC cells. (FIG 3-40)

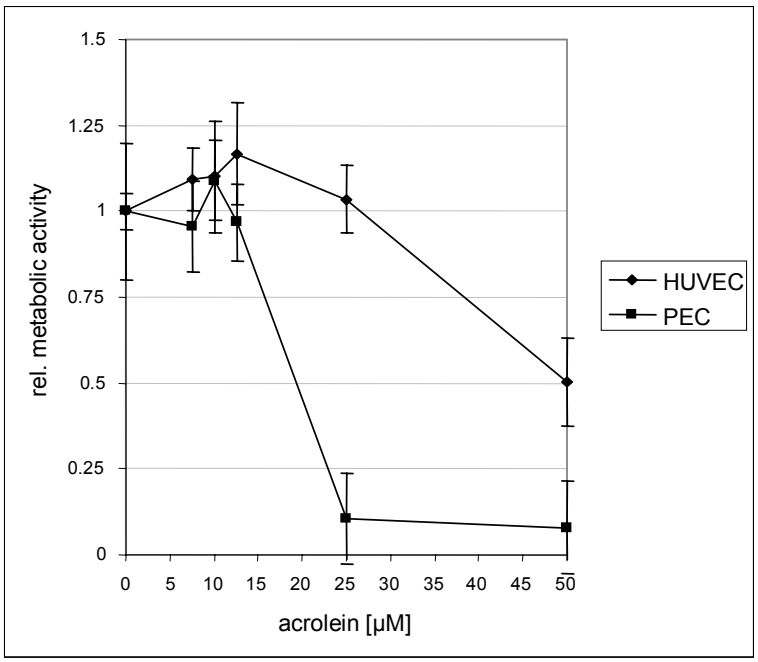

Fig.: 3-40 Proliferation and survival of primary endothelial cells cultured with different concentrations of acrolein. HUVEC and PEC cells were cultured in the absence or in the presence of 7.5 to 50µM acrolein in the medium. Proliferation and survival was determined by MTT assay. Values are means ±SD of triplicates.

3.3.3.3 Acrolein inhibits endothelial cell migration

Primary endothelial cells were further analyzed for sensitivity towards acrolein regarding migration. Migration of cells HUVEC cells was decreased by 50% in the presence of 20µM acrolein and even to 80% when the scratch wound assay was performed in the presence of 25µM acrolein (FIG 3-41A). In the case of the PEC cells migration decreased to 40% when the scratch wound assay was performed in the presence of 15µM acrolein (FIG 3-41B).

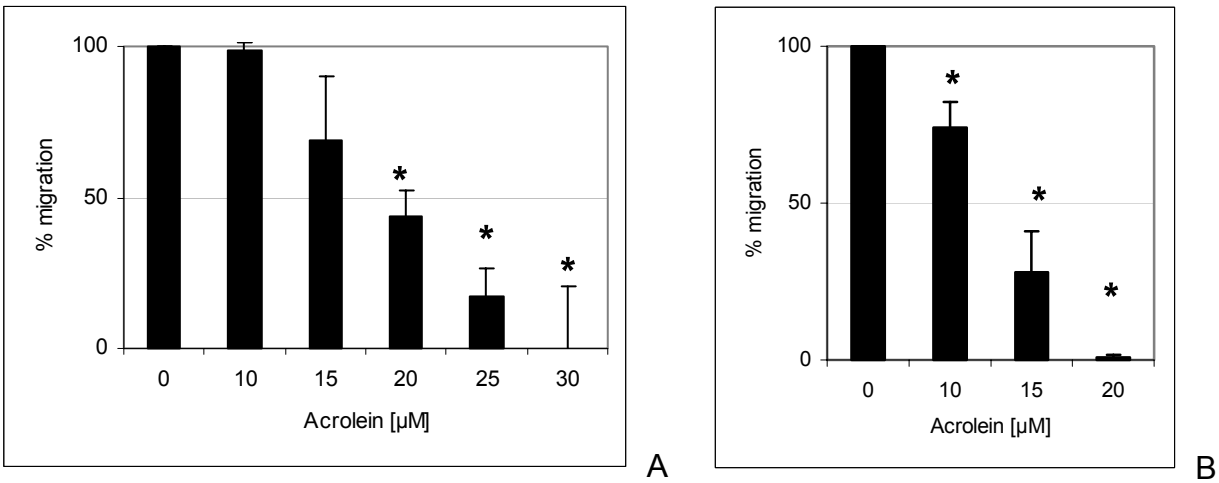

*Fig.: 3-41 Treatment of HUVEC cells (A) and PEC cells (B) for 24h with increasing concentrations of acrolein resulted in a dose dependent inhibition of migration in the scratch wound assay. A confluent cell layer of endothelial cells was scratched with a pipette tip and analyzed by transmitted light microscopy (t=0). After 24 h of incubation with increasing concentrations of acrolein cells were fixed and analyzed again (t=24). In the absence of acrolein HUVEC cells as well as PEC cells grow to a confluent monolayer. Values are means ± SD of ten values. *p<0.05, compared to untreated control cells (Mann-Whitney U-test).*

3.3.3.4 Acrolein inhibits endothelial tube formation

The ability of primary endothelial cells to differentiate and form vessel like structures was analyzed in the matrigel tube formation assay. HUVEC cells usually form tube like structures within 4h when seeded on the polymerised matrigel. Performing the tube formation assay in the presence of acrolein inhibited the formation of tube like structures in a dose dependent manner (FIG 3-42).

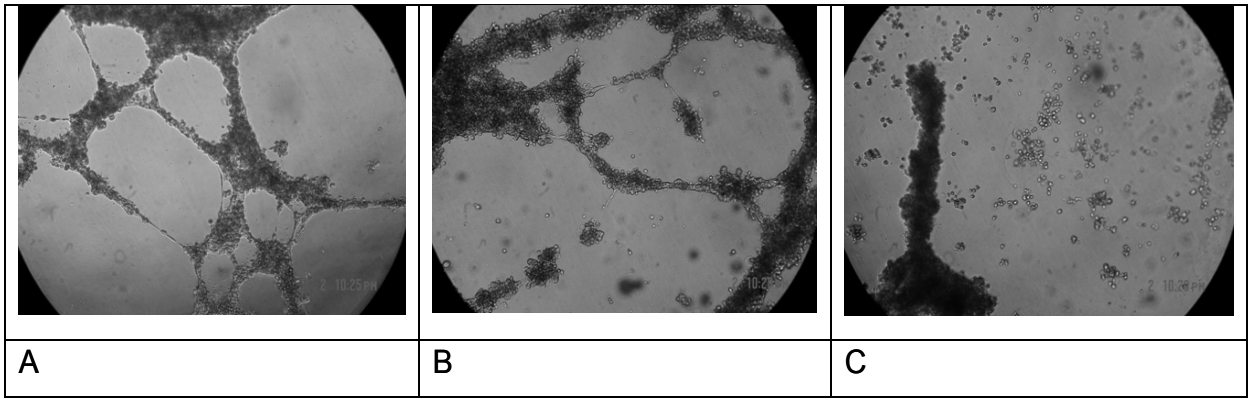

Fig.: 3-42 Matrigel tube formation assay in the presence of acrolein. The matrigel tube formation assay was carried out in the absence (A) or in the presence of 10µM (B) and 30µM (C) acrolein. Tube formation was analyzed by transmitted light microscopy.

Quantification of tube like structures was carried out; only tube like structures, without interruptions, were counted in each well. Even at 10µM acrolein the number of tube like structures without defects decreased by approximately 70% (FIG 3-43).

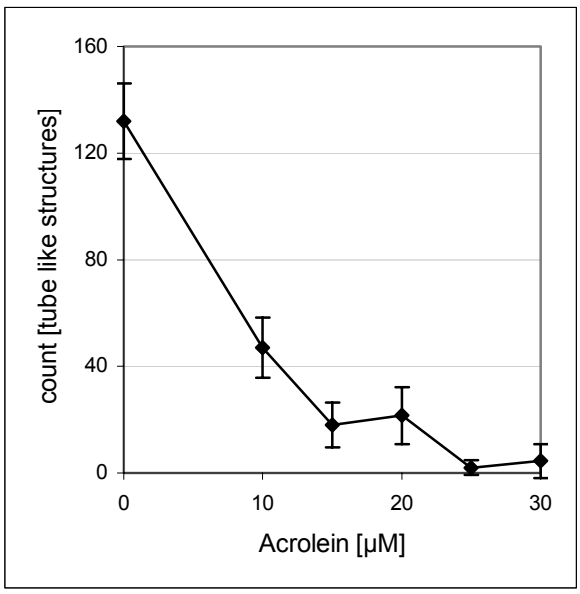

Fig.: 3-43 Disturbance of tube like structure formation in the matrigel assay. Matrigel tube formation assay was performed with HUVEC cells in the absence or in the presence of 10µM to 30µM acrolein in the medium. Forming of tube like structures was quantified by transmitted light microscopy. Values are means ±SE of duplicates

3.3.3.5 Subacute cytotoxic acrolein concentrations disrupt endothelial F-actin cytoskeleton

To further investigate the impact of acrolein on migration of primary endothelial cells, F-actin cytoskeleton analysis was performed. HUVEC cells were seeded 24h before treatment. Cells were cultured for further 12h in the absence or in the presence of different concentrations of acrolein (5µM to 20µM). Afterwards cells were fixed and staining of the F-actin cytoskeleton was performed. Control cells contained thick long fibres of actin filaments, often spanned across the entire cytoplasm. Incubation of proliferating HUVECs with non acute cytotoxic concentrations of acrolein (0-20µM) resulted in cytoskeletal disorganisation and disruption of F-actin filaments within 12h of incubation. The extent of cytoskeleton damage was dose dependent (FIG 3-44). Damaged cells were able to remodel F-actin cytoskeleton to a certain degree within 24h after acrolein removal (data not shown).

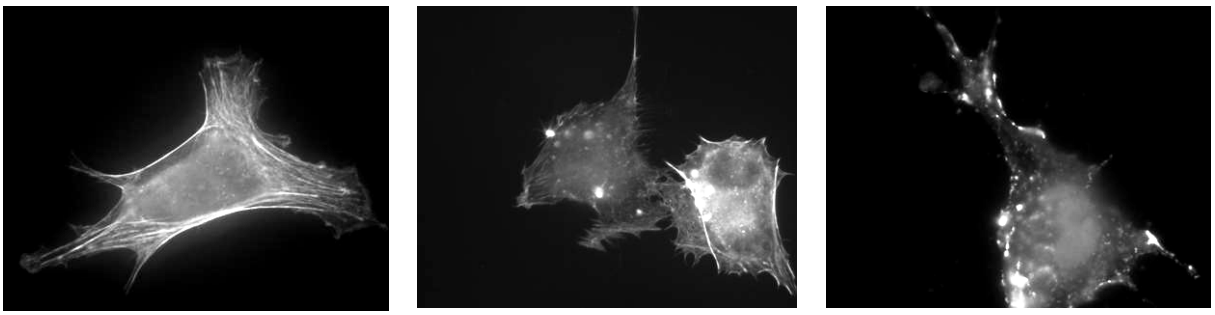

A B C

Fig.: 3-44 Disorganisation of F-actin cytoskeleton in primary endothelial cells (HUVECs) due to acrolein treatment. F-actin cytoskeleton of cultured HUVEC cells on a collagen G coated glass surface in the presence of 10% FBS and 10ng/ml bFGF is well organized (A). Treatment of HUVEC cells with acrolein leads to disruption of the F-actin cytoskeleton and F-actin plugs are formed in the cells (10µM acrolein (B) and 20µM acrolein (C)).

3.3.3.6 Acrolein inhibits integrin αvβ3 clustering on endothelium filopodiae

Integrin αvβ3 plays a crucial role in the angiogenic process. Clustering of the integrin αvβ3 receptor induces several signalling cascades in endothelial cells, regulating cell survival, migration and differentiation properties of angiogenic endothelial cells (94;95).

Therefore the impact of acrolein on the integrin αvβ3 receptor systems of primary endothelial cells (HUVECs) was investigated. Cells were screened for integrin αvβ3 clustering and total receptor levels on the surface of the cells were determined.

HUVEC cells were seeded on collagen IV coated Lab-Tek slides 24h before treatment. Cells were cultured for further 12h in the absence or in the presence of

different concentrations of acrolein (5µM to 20µM). Afterwards cells were fixed and staining of the integrin αvβ3 receptor was performed. Additionally cells were stained for F-actin cytoskeleton. Integrin clustering and changes in the cytoskeleton were analyzed by fluorescence microscopy.

Incubation of HUVECs with acrolein for 12h leads to disarrangement of integrin αvβ3 receptors and clustering at the filopodia of the cells was inhibited (FIG 3-45). Additionally F-actin staining consolidated the absence of functional filopodia when the cells were cultured with 20µM acrolein in the medium.

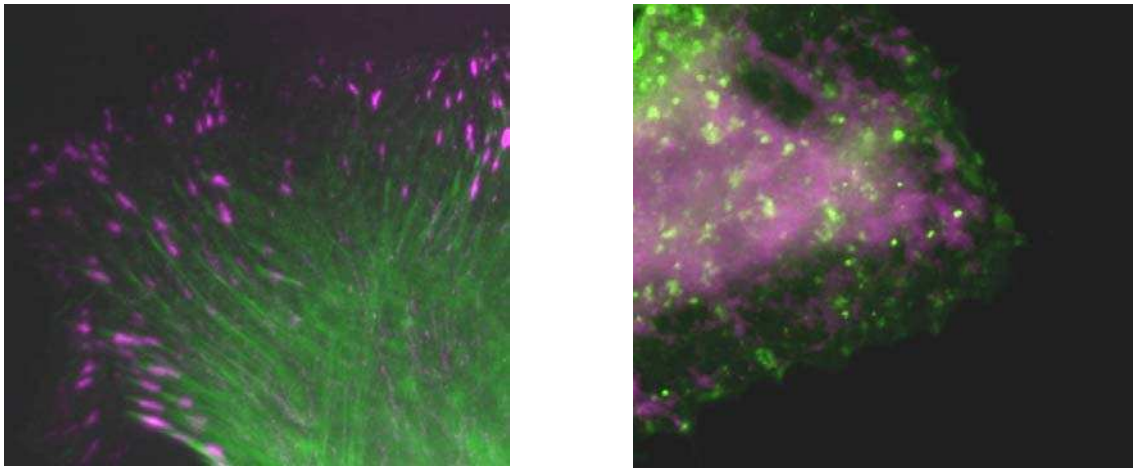

A B

Fig.: 3-45 Acrolein treatment disturbs integrin αvβ3 (violet) receptor clustering and the formation of focal adhesions in primary endothelial cells (HUVECs). (A) Vehicle (PBS) treated HUVEC on a collagen coated surface show a well organized F-actin cytoskeleton (green) with F-actin accumulations in the area of focal adhesions). Moreover, clustering of integrin αvβ3 receptors at focal adhesions is seen. (B) Incubation of HUVEC with 20µM acrolein for 12h results in destruction of the F-actin cytoskeleton in the area of focal adhesion and as well in a disturbance of integrin αvβ3 receptor clustering.

Integrin αvβ3 receptor status was also determined by flow cytometry. HUVEC cells were cultured for 12h in the absence or presence of 20µM acrolein, and antibody staining was carried out, followed by FACS analysis. No change in total amount of integrin αvβ3 receptor on the surface of the endothelium cells was detectable when cells were cultured for 12h with 20µM acrolein (data not shown).

3.3.3.7 Acrolein modulates NF-κB activity in cultured human endothelial cells

NF-κB plays a crucial role in angiogenesis and cell survival. Therefore, effects of acrolein on NF-κB activity levels in primary endothelial cells were determined. HUVEC cells were transiently transfected with LPEI polyplexes (HBS, N/P 6) containing an NF-κB dependent expression vectors for luciferase (pNFκB-LUC).

Control experiments were performed with similar LPEI polyplexes (HBS, N/P 6) containing a luciferase encoding plasmid without NF-κB enhancer areas in the promoter region (pTAL-LUC). Twenty four hours after transfection acrolein was added to the supernatant and luciferase activity was measured 48h after the transfection.

Treatment of HUVEC cells with 10µM and 20µM acrolein decreases basal NF-κB activity within 24h of acrolein treatment (FIG 3-46). Interestingly, NF-κB activity was upregulated after cells were treated with 30µM acrolein for 24h.

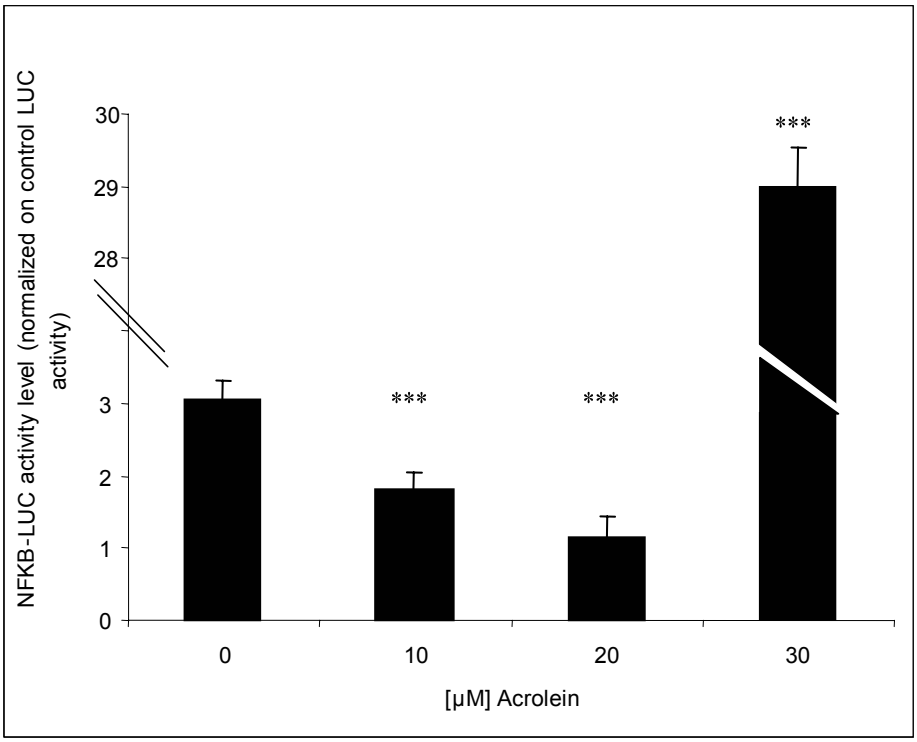

*Fig.: 3-46 Modulation of NFKB activity in HUVEC cells by acrolein. HUVEC cells were transfected with LPEI polyplexes contained an expression vector for luciferase with NFKB sensitive binding sites in the promoter region. Control experiments were performed with a similar vector, yet without NFKB binding sites. 24 h after the transfection cells were cultured for further 24h in the absence or in the presence of 10µM, 20µM or 30µM acrolein. Luciferase measurement was performed as described in materials and methods. Ratios of luciferase expression obtained with pNFκB-LUC and control plasmid pTAL-LUC in HUVEC cells are shown. Mean values of eight transfections per condition ± SD are shown. ***p<0.001, compared to control tumors (Mann-Whitney U-test).*

3.3.3.8 Acrolein modulates thrombospondin-1 levels in primary endothelial cells (HUVECs)

For investigation of modulation effects on thrombospondin-1 levels by acrolein in HUVEC cells, thrombospondin-1 levels were analyzed in HUVEC cell lysates by a competitive ELISA. Moreover total protein content was measured by the BCA-protein-content assay (Pierce). Thrombospondin-1 levels were modulated by acrolein in cultured primary HUVEC cells. Interestingly, incubation of HUVECs with only 5µM

acrolein for 24h results in highly increased thrombospondin-1 levels (11-fold). High induction of TSP-1 levels was also evident when cells were treated with 10µM and 20µM acrolein. Decreasing Thrombospondin-1 levels were detected when cells were cultured in the presence of 30µM acrolein and higher. The total protein content (BCA assay) was similar at all indicated concentrations.

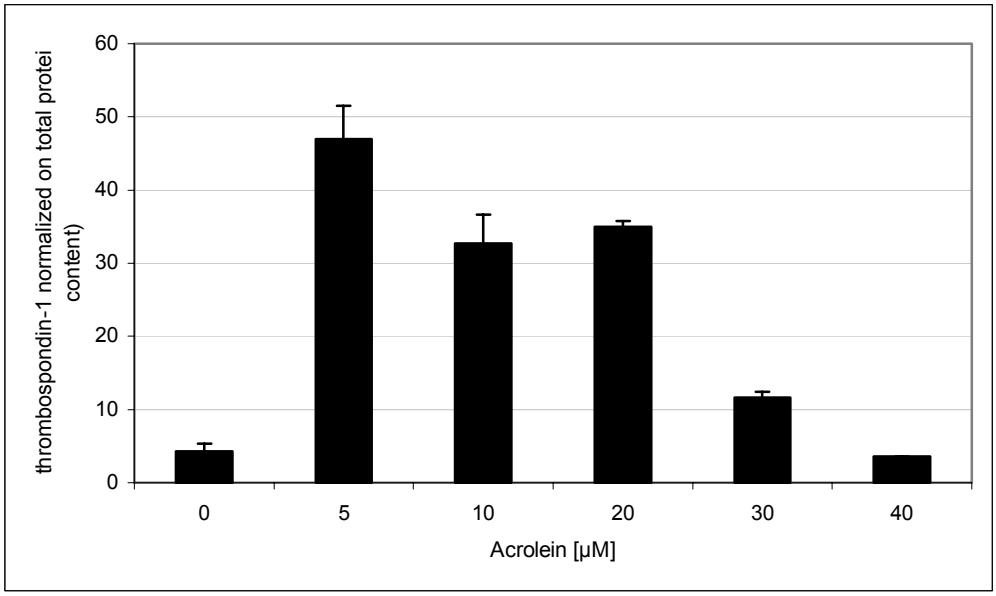

Fig.: 3-47 Modulation of thrombospondin-1 levels in HUVEC cells by acrolein. HUVEC cells were cultured in the presence of different concentrations of acrolein for 24h. After the incubation time, cells were washed with PBS and 100µl/well water was added, followed by a freeze-thaw-cycle. thrombospondin-1 contents were determined by the competitive thrombospondin-1 ELISA (Chemicon). Moreover cell lysates were analyzed for total protein content (BCA-protein-assay). Thrombospondin-1 levels were normalized on total protein content. Values are means ± SE of duplicates.

3.3.4 Impact of acrolein on CT26 tumor and tumor stroma cells (fibroblasts)

3.3.4.1 Proliferation and survival of CT26 tumor cells

In order to evaluate direct antitumoral effects of acrolein on tumor cells, CT26 cells were cultured in the absence or in the presence of different concentrations of acrolein (5µM to 40µM). After 24h of incubation survival and proliferation was determined by measuring total metabolic activity via MTT assay as described in materials and methods. Values were normalized to vehicle treated cells (PBS).

Total metabolic activity was decreased in a dose dependent manner. When CT26 cells were cultured with 40µM acrolein in the medium, metabolic activity was decreased to 50% compared to vehicle treated cells (FIG 3-48).

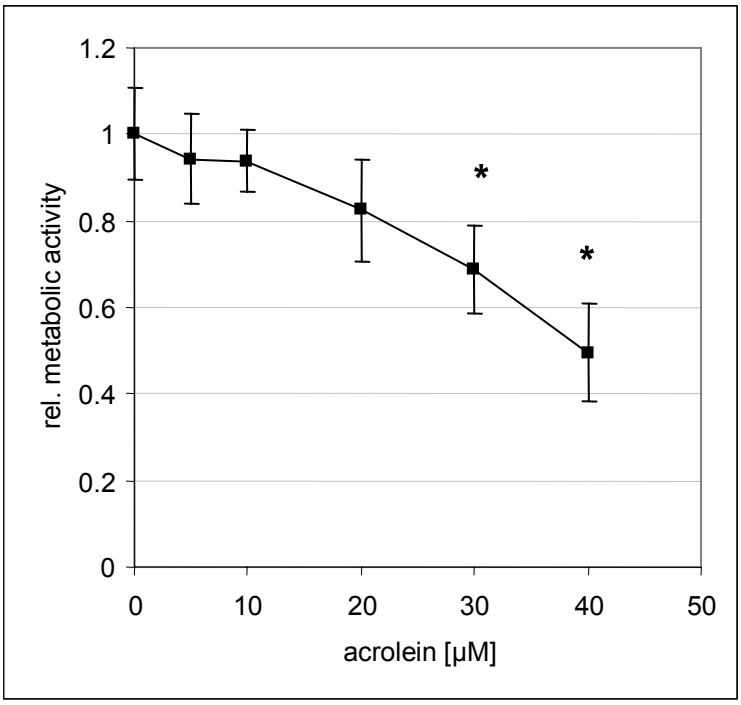

*Fig.: 3-48 CT26 cells were cultured with increasing concentrations of acrolein (0µM to 40µM) for 24h. Survival was determined by measuring total metabolic activity via MTT assay. Values are means ±SD of four samples. *p<0.05, compared to untreated control cells (Mann-Whitney U-test).*

3.3.4.2 Regulation of NF-κB activity levels in CT26 tumor cells

Several tumor relevant cytokines regulating angiogenic processes, like VEGF or bFGF, are also controlled by NF-κB activity (96-98). Therefore the impact of acrolein on NF-κB activity levels was investigated in CT26 tumor cells. In contrast to the effects of acrolein on NF-κB levels in HUVEC cells, no obvious modulatory effects were detected in CT26 tumor cells.

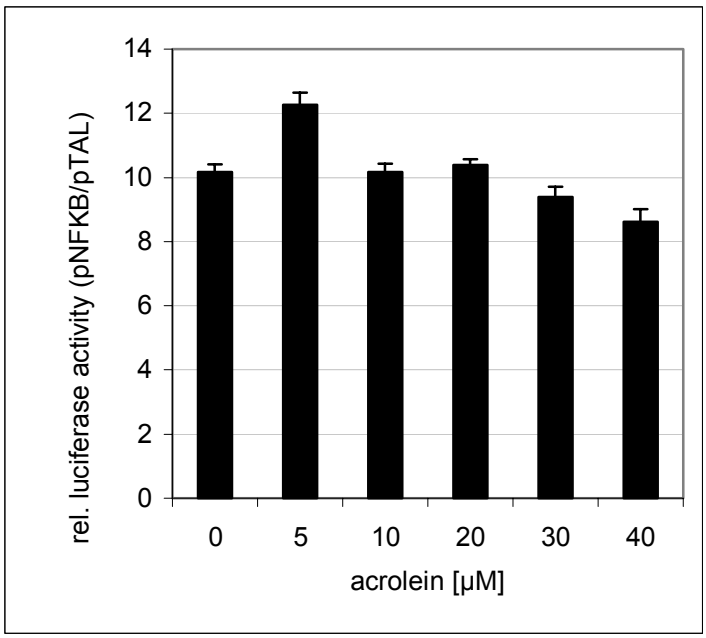

Fig.: 3-49 Modulation of NF-κB activity in CT26 tumor cells by acrolein. CT26 cells were transfected with LPEI polyplexes containing an expression vector for luciferase with NF-κB sensitive binding sites in the promoter region (pNFκB-LUC). Control experiments were performed with a similar vector, but without NF-κB binding sites (pTAL-LUC). 24 h after the transfection cells were cultured for further 24h in the absence or in the presence of 5µM or 40µM acrolein. The ratio of luciferase expression obtained by pNFκB-LUC to pTAL-LUC is shown. Values ± SD are means of eight values.

3.3.4.3 NF-κB regulation and survival of fibroblasts

Tumor stroma cells, particularly fibroblasts, have great influence on the angiogenic process in tumors due to their output of proangiogenic cytokines such as bFGF. NF-κB is a crucial factor in the regulation of these cytokines. Therefore the influence of acrolein treatment on NF-κB levels in fibroblasts was evaluated. Moreover, cell survival was investigated and correlated with NF-κB activity levels.

Fibroblasts expressing luciferase under the control of a NF-κB sensitive promoter were obtained from transgenic animals (NF-κB-LUC mice) (99;100). The luciferase expressing fibroblasts were cultured with different concentrations of acrolein for 6 and up to 24h. Luciferase expression levels were measured by performing a luciferase assay after 6 and 24h of treatment; in a parallel experiment cell survival was determined by performing the MTT assay.

Decreased NF-κB activity levels were detected after 6h of acrolein treatment at 30µM and above. Cell survival was not influenced at this time point, indicated by constant total metabolic activity (FIG 3-50A).

After 24h of acrolein treatment NF-κB levels and cell survival were decreased when the acrolein concentration in the medium was beyond 20µM (FIG 3-50 B). Correlation of NF-κB activity, indicated by luciferase expression levels, and cell survival, indicated by metabolic activity was evident after 24h, but not after 6h of treatment, indicating that decrease in NF-κB levels occur prior to cell death.

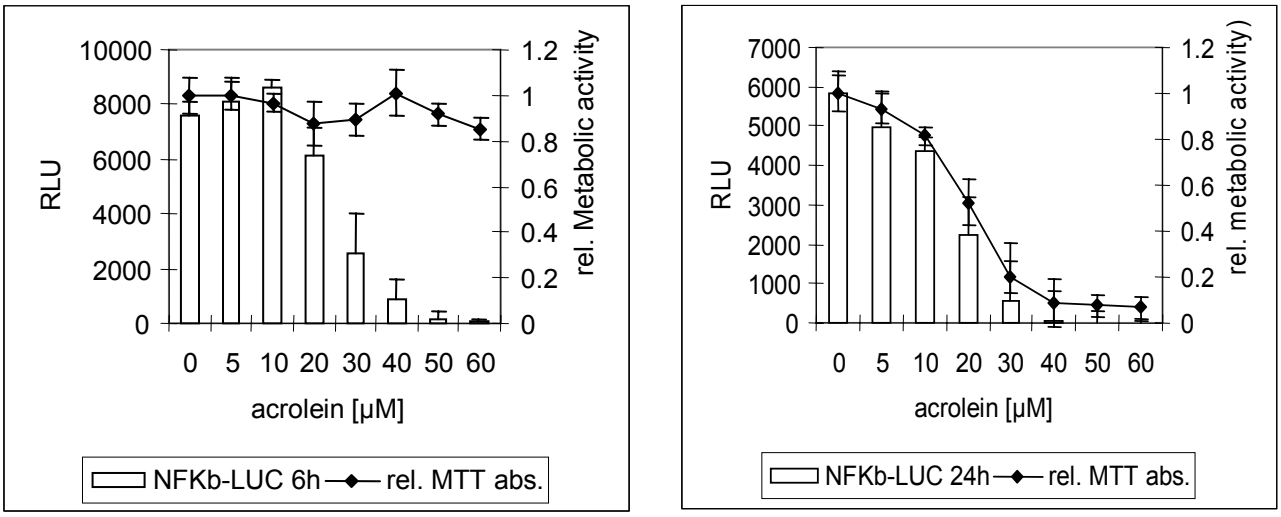

A B

Fig.: 3-50 NF-κB activity levels, indicated by luciferase expression levels and cell survival, indicated by metabolic activity (MTT) of mouse fibroblasts treated with different concentrations of acrolein. Fibroblasts were obtained from transgenic mice expressing luciferase under the control of a NF-κB sensitive promoter. Luciferase levels were analyzed after 6h (A) and 24h (B) of treatment with acrolein. Total metabolic activity (MTT) was monitored in a parallel experiment also after 6h (A) and 24h (B) of acrolein treatment. Values are means ± SD of 6 measurements.

3.4 Chemoresistance in metronomic CPA therapy

Resistance to chemotherapy is a major hindrance for classical chemotherapy and also occurs in metronomic scheduled chemotherapy. Therefore investigating mechanisms of chemoresistance is an important objective. During evaluation of different CPA regimes in this thesis, chemoresistance occurred in different syngeneic and xenograft in vivo tumor models. Moreover, primary chemoresistance occurred when chemosensitive X39 tumor cells were grown in a three dimensional cell culture model or in SCID mice as subcutaneous tumors. For investigation of resistance in CPA treated tumors, histological changes were analyzed and tumor cells were isolated of for further characterisation.

3.4.1 Resistance in the CT26/X39 tumor model

3.4.1.1 CT26/X39 sensitivity to CPA treatment in a coculture system

In order to evaluate primary resistance of CYP2B1 expressing X39 tumor cells, their sensitivity towards CPA treatment was determined both in a multicellular spheroid culture model and in standard monolayer culture. CT26 cells were cocultured with X39 cells at different ratios in a system combining monolayer and spheroid culture in the absence or in the presence of 0.5mM CPA. For three dimensional cell culture system, different ratios of CT26 and X39 cells were suspended in agarose containing medium. After solidification of the agarose, medium was added and spheroids were grown for 10 days (FIG 3-51).

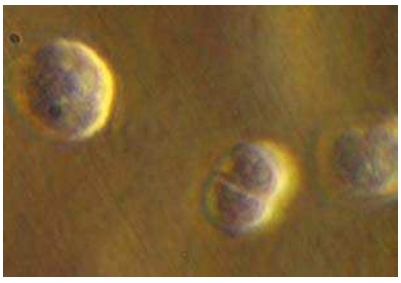

X39 cells day 3

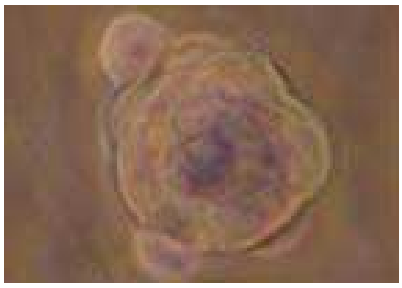

X39 cells day 10

Fig.: 3-51 X39 and CT26 tumor cells, suspended in agarose containing medium, grow to multicellular spheroids within 10 days.

Similar ratios of CT26 and X39 cells were cultivated as a standard monolayer. Twenty four hours after monolayer culture ten day old spheroids were added to the monolayer cultures. Thereafter the mixture was treated for 3 days with 0.5 mM CPA.

This combination of monolayer culture and spheroid culture in the same incubation medium ensured similar concentration of metabolites for monolayers and spheroids.
Cell proliferation and survival was determined by measuring total metabolic activity by the MTT assay. Analysis of metabolic activity were performed separately for monolayer and spheroid cultures.
An increasing ratio of X39 cells resulted in elevated sensitivity of the coculture in the monolayer. Coculturing 25% X39 cells in the system reduced metabolic activity of the monolayer to 50%. When 50% of X39 were present in the system, metabolic activity of the monolayer was even reduced to 25% compared to the control system without CPA treatment. The strong reduction in the monolayer may result from additional diffusible CPA metabolites produced by the spheroids. In a pure monolayer system reduction in metabolic activity was not as pronounced (FIG 3-27).
In contrast, metabolic activity of cells in the microspheroid section was decreased in a lesser degree by the CPA treatment. Even when 100% of CYP2B1 expressing X39 cells were present in the system, decrease in total metabolic activity was only 40% (FIG 3-52).

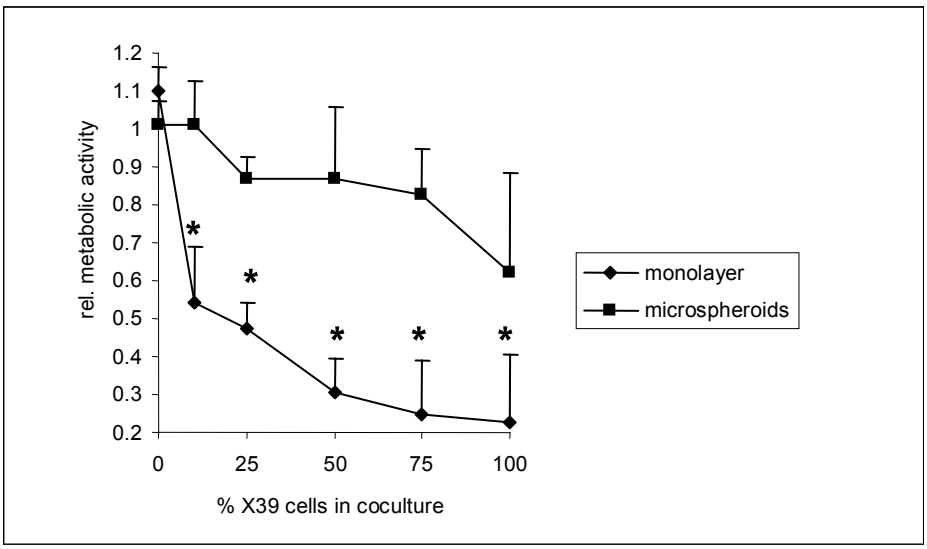

*Fig.: 3-52 Sensitivity of wt CT26 tumor cells, cocultured with CYP2B1 expressing X39 cells in a combined system of monolayer and multicellular microspheroids, against CPA treatment. Metabolic activity was determined separately for the monolayer and for the agarose wrapped spheroids by MTT assay. The values are means ±SD of triplicates. *p<0.05, compared to untreated control cells (Mann-Whitney U-test).*

When agarose embedded CYP2B1 expressing X39 cells were treated with CPA prior to spheroid forming, X39 cells were as sensitive towards treatment as X39 cells in a standard monolayer system (data not shown). This indicates that diffusion of CPA and decreased enzymatic activity of CYP2B1 are not limiting factors in the three

dimensional system, but rather decreased sensitivity that results from modifications of the tumor cells when they grow as multicellular spheroids.

3.4.1.2 CYP2B1 expression of X39 microspheroids

To further investigate the mechanism of resistance towards CPA treatment in the three dimensional cultivated X39 cells, antibody staining against CYP2B1 protein was performed after the CPA treatment. Therefore X39 cells were grown as microspheroids in agarose containing medium. Agarose wrapped microspheroids were subject to CPA treatment for 3 days. Afterwards agarose wrapped spheroids were embedded in OTC medium and frozen at -80°C. Frozen spheroids were cut with a cryostat to slides of 5µm thickness, following antibody staining against CYP2B1 protein as described in materials and methods. Cell nuclei were stained with Hoechst 33258. Control spheroids were treated in the same manner except for the CPA treatment. CYP2B1 expression was evident both in CPA treated and in control spheroids (FIG 3-53), indicating that decreased sensitivity does not result from downregulation of CYP2B1 or selection processes by the CPA treatment.

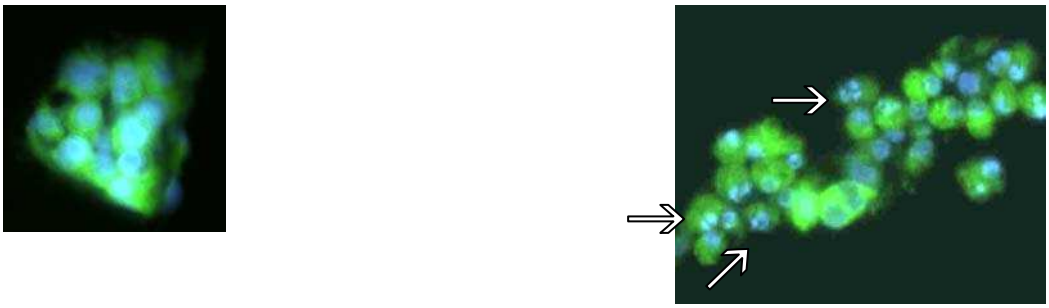

control spheroid CPA treated spheroid

Fig.: 3-53 CYP2B1 expression in CYP2B1 expressing X39 cells grown as multicellular spheroids in the absence (control) or in the presence of 0.5mM CPA for 3 days. Cell nuclei were stained by Hoechst33258, fragmented nuclei are marked (⟹)

In CPA treated X39 microspheroids DNA fragmentation was detected by fluorescence microscopy after staining with Hoechst 33258 dye. According to these results resistance of three dimensional grown X39 cells to CPA treatment is not due to decreased CYP2B1 expression.

3.4.1.3 Decreased sensitivity of CT26 microspheroids towards treatment with 4OOH-CPA

CT26 cells were analyzed for changes in sensitivity towards 4OOH-CPA treatment comparing cells were grown as microspheroids or monolayer. Established CT26

microspheroids wrapped in agarose and CT26 cells grown as a monolayer were treated with medium containing different concentrations of 4OOH-CPA.

After incubation for 3 days metabolic activity of CT26 cells was significantly reduced even at the lowest 4OOH-CPA concentration tested whereas CT26 microspheroids did not show response to the treatment up to concentrations of 20µM 4OOH-CPA (FIG 3-54).

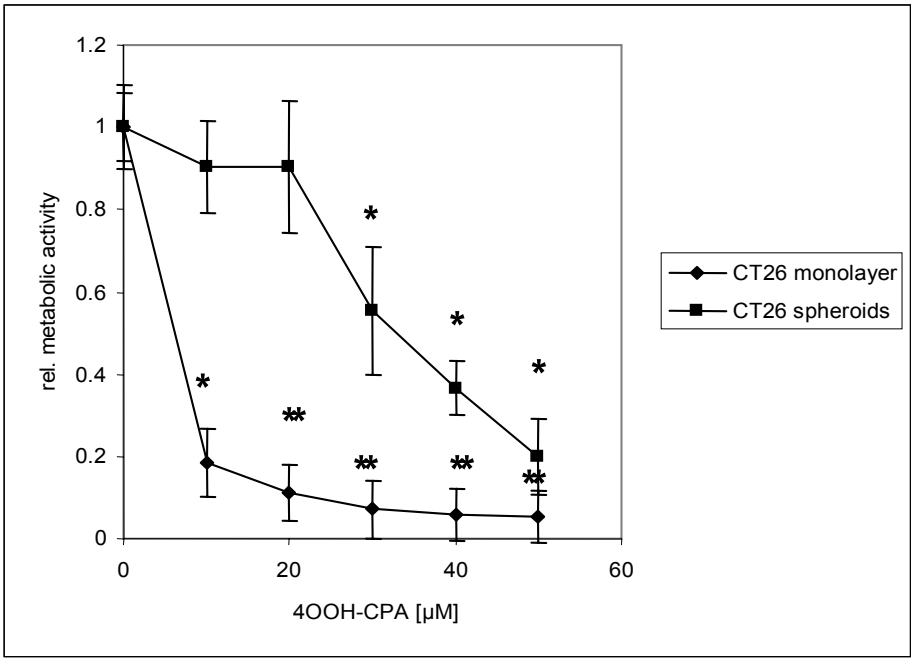

*Fig.: 3-54 Sensitivity of CT26 cells towards CPA treatment, cultivated either as multicellular spheroids or as a monolayer. Metabolic activity was measured by MTT assay and normalized to cell without CPA treatment. Values are means ± SD of four measurements. *p<0.05, **p<0.01, compared to untreated control cells (Mann-Whitney U-test).*

3.4.1.4 Sensitivity of established X39 tumors in vivo

In order to investigate sensitivity of CYP2B1 expressing tumor cells in vivo, subcutaneous CT26 and X39 tumors were established in SCID mice.

Before implantation of X39 cells into the flank of the SCID mice CYP2B1 expression was confirmed by antibody staining followed by FACS analysis (data not shown). Further on X39 cells were analyzed for sufficient CYP2B1 enzymatic activity by the resorufin assay; fluorescence levels in the resorufin assay indicated sufficient CYP2B1 activity (FIG 3-55).

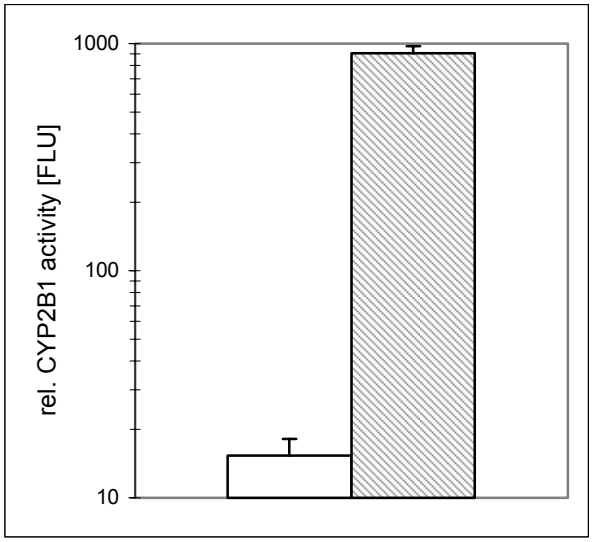

Fig.: 3-55 Confirmation of CYP2B1 enzymatic activity in stable transfected X39 cells prior to implantation. Cells were incubated with resorufin incubation solution and in situ released resorufin was detected in the supernatant of the cells after a freeze-thaw cycle by fluorescence measurement. Hatched bars: stable CYP2B1 expressing cells; open bars: wt CT26 tumor cell line. Measurements were normalized to cell count. Values are means ± SD of triplicates.

The X39 tumors showed later onset of tumor growth compared to CT26 tumors. When tumors reached a volume of 35mm^3 80mg/kg CPA was administered every sixth day intraperitoneally. Tumor size and body weight was measured regularly during treatment period.

Treatment was well tolerated in CT26 and in X39 tumor bearing mice indicated by no significant weight loss (data not shown). Despite high CYP2B1 expression in X39 tumors the response to the CPA treatment was not significantly different from CPA response in CT26 tumors (FIG 3-56).

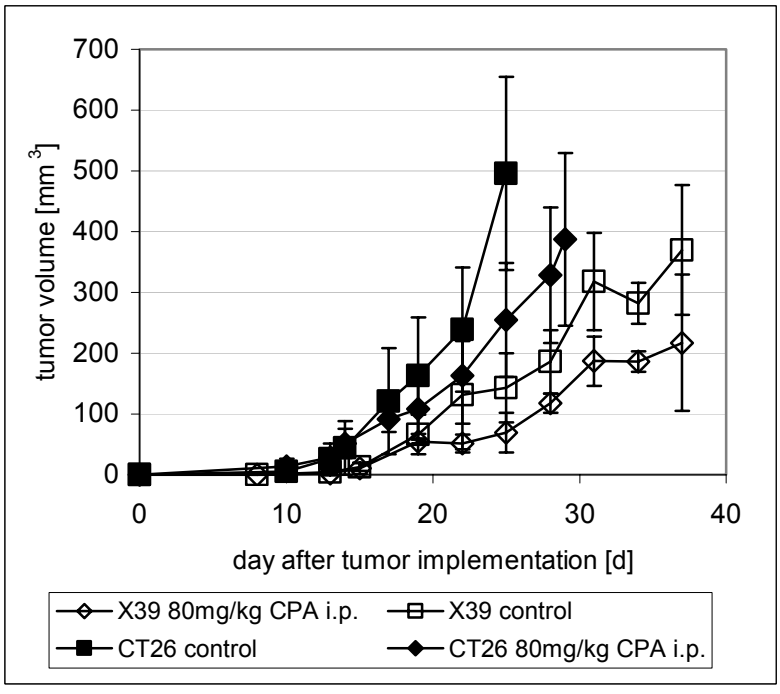

*Fig.: 3-56 Growth delay of subcutaneous CT26 and CYP2B1 expressing X39 tumors in SCID mice treated with 80mg/kg intraperitoneally every 6th day. (n=5 for CT26 bearing animals and n=3 for X39 bearing mice) *p<0.05, compared to untreated control cells (Mann-Whitney U-test).*

3.4.1.5 Detection of CYP2B1 expression in CPA treated X39 tumors

To clarify if the moderate response to CPA treatment in terms of tumor growth delay is due to in vivo selection of CYP2B1 negative tumor cells, antibody staining against ratCYP2B1 protein was performed at the endpoint of the treatment. No difference in CYP2B1 expression was detectable in CPA treated X39 tumors compared to untreated X39 tumors (FIG 3-57).

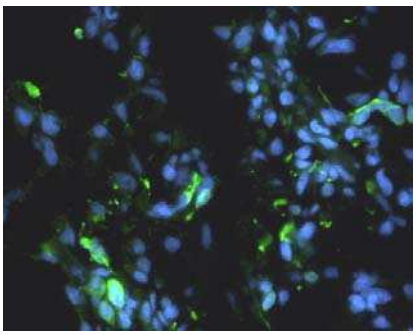

Control tumor

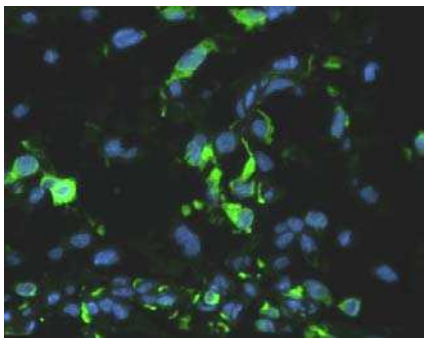

CPA treated tumor

Fig.: 3-57 CYP2B1 expression in subcutaneous grown X39 tumors after CPA treatment with 80mg/kg CPA every six days. Control tumors were obtained of non-treated SCID mice.

3.4.1.6 Integrin αv expression in subcutaneous CT26 xenografts

Integrins were shown to modulate apoptotic signaling (101) and preventing CPA induced cell death in endothelial and epithelial cells (102). Therefore integrin expression levels of subcutaneous grown CT26 tumors were compared to monolayer cultured CT26 cells. Interestingly, αv expression was detectable in tumors in vivo but not on the cell surface of cultured CT26 tumor cells.

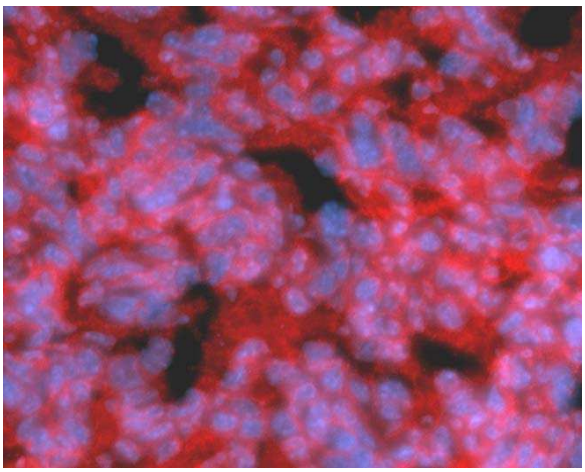

A

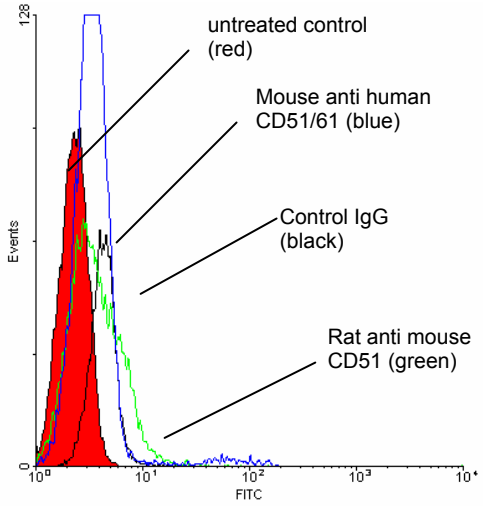

B

Fig.: 3-58 (A) Cryo sections (5µm) were fixed with 4% PFA and stained with specific antibodies for rat-anti-mouse CD51 (red). Secondary antibodies were labelled with Alexa 488. The intravenously injected Hoechst 33258 stain was visualized as well (blue). (B) CD51 expression levels on in vitro cultured CT26 cells. Staining was performed with the indicated antibody, followed by FACS analysis. Secondary antibodies were labelled with Alexa 488.

3.4.2 Resistance in the PC3 tumor model

Subcutaneous human PC3 tumors were established in male SCID mice by injection of $1x10^6$ PC3 cells in the flank of the animals. CPA treatment was started on day 11 after tumor implantation when tumors reached an average volume of 37 mm^3. Tumor bearing mice were treated with 120mg/kg CPA every six days. Metronomic scheduled CPA treatment resulted in a significant tumor growth delay. Tumor volume of treated mice was constant up to day 50 after the tumor cell implantation whereas tumors in the control group exhibited a tumor volume doubling time of 2.5 days. Around day 50 after tumor implantation tumor volume began to increase in the CPA treated group despite ongoing treatment with a tumor doubling time of 9 days (FIG 3-59).

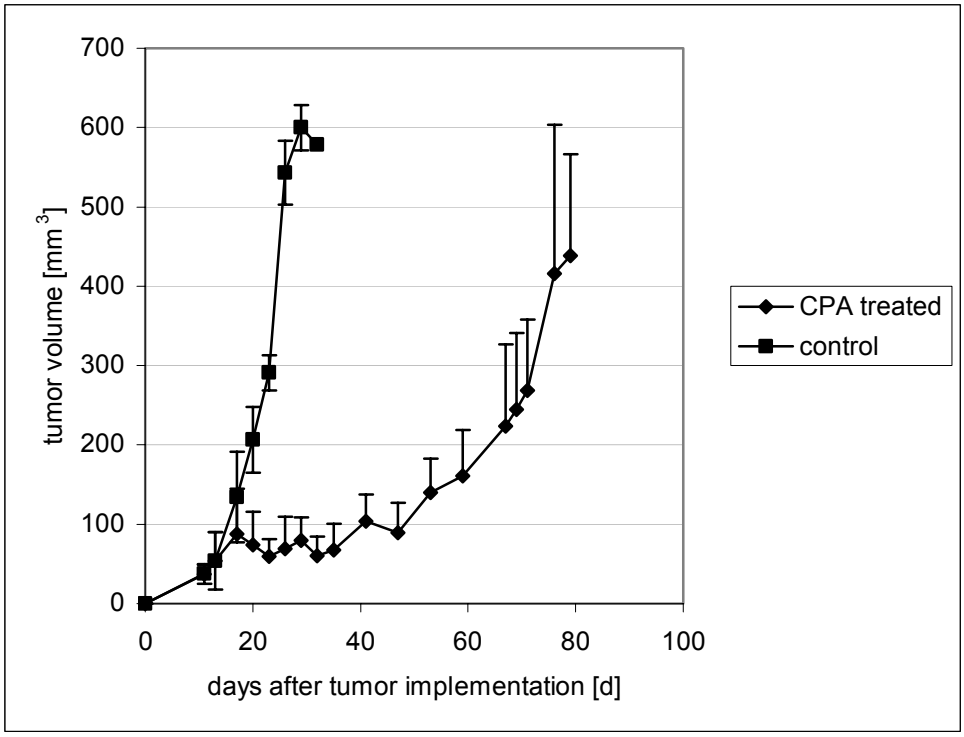

Fig.: 3-59 Tumor growth in a human PC3 xenograft model with and without metronomic scheduled CPA treatment. Tumor bearing SCID mice were treated intraperitoneally with 120mg/kg CPA every sixth day. (n=4 for untreated control animals and n=6 for CPA treated animals)

Metronomic scheduled CPA therapy was well tolerated indicated by constant animal body weight up to day 67. Further CPA treatment resulted in significant loss of body weight observed in all CPA treated animals. Treatment was stopped and animals were sacrificed when average loss in body weight reached 20%.

For further investigation tumors were collected and subject to histological analysis. Further on, tumor cells were extracted from tumor tissue for characterisation and cell

culture experiments. Part of the reisolated tumor cells were reimplanted into male SCID mice.

3.4.2.1 Histological analysis of PC3 tumors

For characterisation and evaluation of histological changes induced by CPA treatment, tumors were collected, embedded in OTC medium and frozen at -80ºC. Cryostat were stained with Haematoxylin/Eosin and analyzed by transmitted light microscopy. Untreated PC3 xenografts own a very compact tissue structure and only small areas of condensed and fragmented cell nuclei were detected (FIG 3-60A). In contrast, CPA treated tumors exhibited larger areas of condensed and fragmented cell nuclei, indicating a higher degree of cell death (FIG 3-60B).

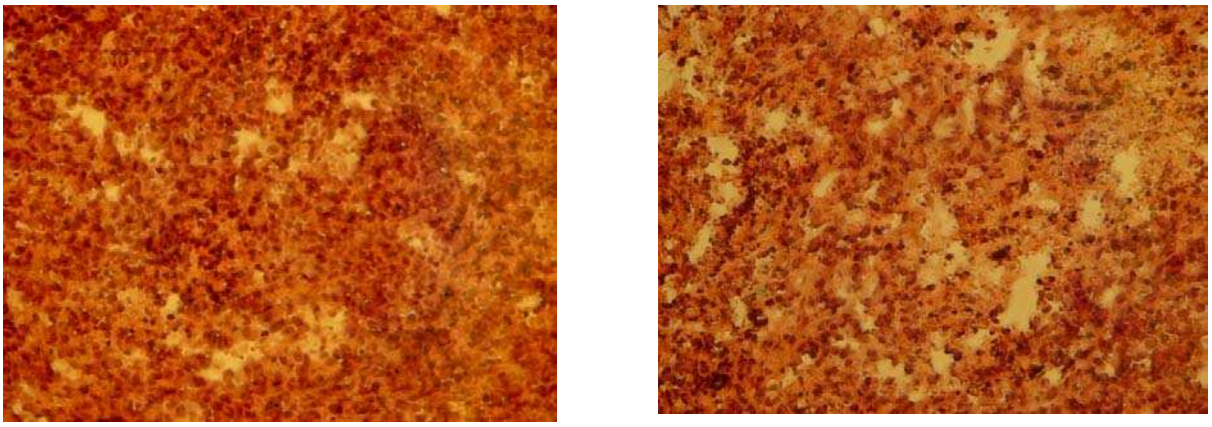

A B

Fig.: 3-60 Histology of subcutaneous PC3 xenografts in male SCID mice (H/E stain). Control tumors were collected at day 32 (A), CPA treated tumors on day 67 (B) after tumor setting. Cryosections (8µm) were fixed with 4% paraformaldehyde and subjected to H/E staining. Sections were viewed on a Zeiss Axiovert 200 transmitted light microscope with a 20x0.4 NA objective. Pictures were taken by a Sony DSC-S75 digital camera.

3.4.2.2 Immunohistological analysis of PC3 tumors

To further evaluate possible reasons for the occurred resistance towards CPA treatment, PC3 tumors were analyzed for immunohistological changes. Due to the antiangiogenic metronomic schedule of CPA, attention was focussed on vascular markers. Functional blood flow was visualized by intravenous application of Hoechst 33258 dye and antibody staining against laminin, CD31 and CD13 was performed. Functional blood flow was decreased in CPA treated tumors, indicated by decreased Hoechst33258 fluorescence signal within the tumor tissue (FIG 3-61B and D). No significant changes in the arrangement of laminin and CD31 positive endothelial cells was detected in CPA treated tumors in comparison to control tumors. Moreover, colocalisation of laminin and CD31 positive endothelial cells remained unchanged (FIG 3-61A and B). Tendency of tumor cell lined vessels (vascular mimicry) was not

detected. However staining for CD13 positive cells, a marker for angiogenic active endothelial cells, was increased in CPA treated tumors, whereas colocalisation of laminin and CD13 staining was decreased compared to untreated control (FIG 3-61C versus 3-61D).

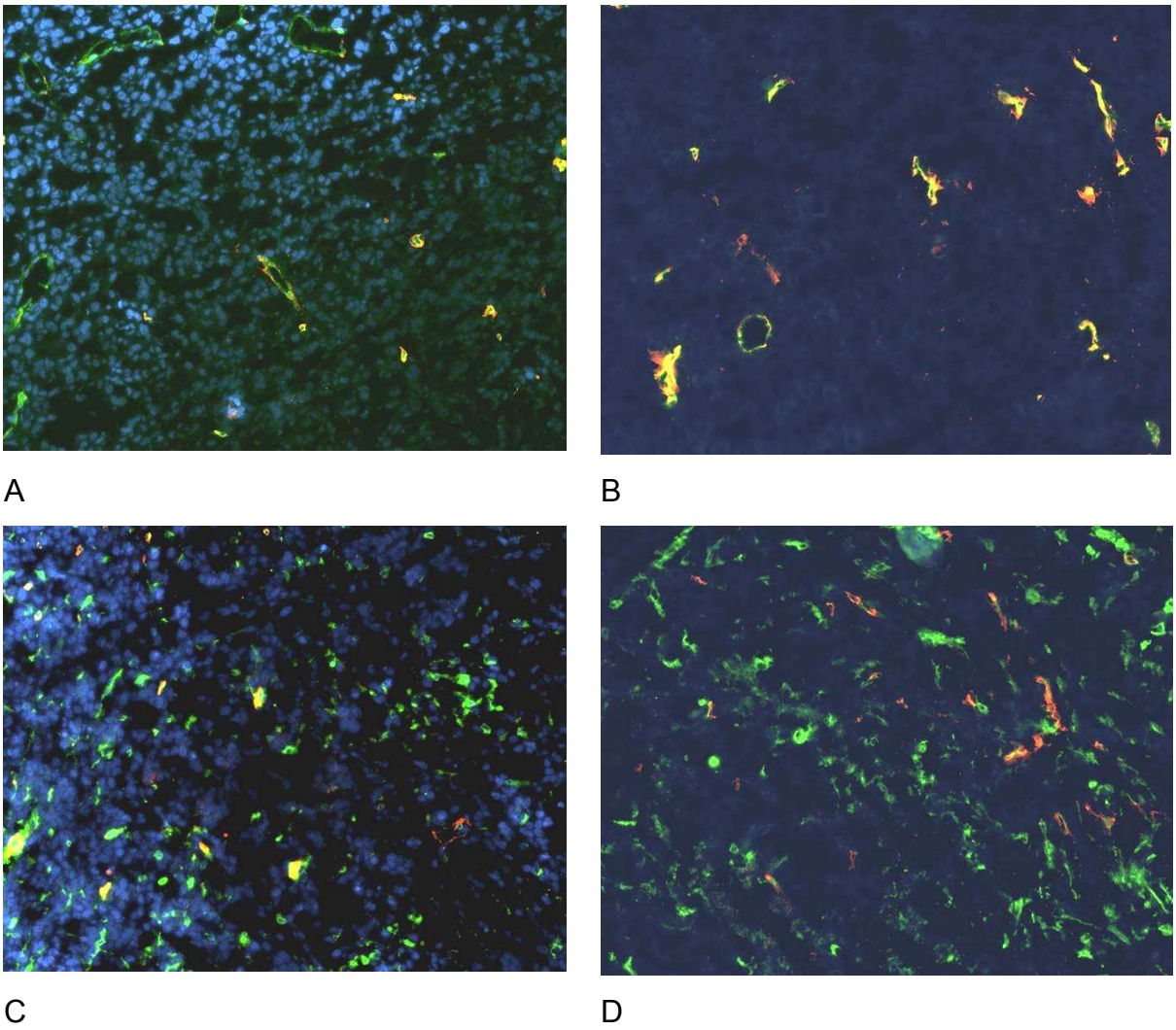

A B C D

Fig.: 3-61 Cryo sections (5µm) of untreated (A and C) and CPA treated tumors (B and D) were fixed with 4% paraformaldehyde and stained with specific antibodies for rat-anti-mouse CD31 (green) and anti laminin (red) (A and B), or for rat-anti-mouse CD13 (green) and anti laminin (red) (C and D). Secondary antibodies were labelled with Alexa 488 (CD31/CD13) or Texasred (laminin). The intravenously injected Hoechst 33258 stain was visualized as well (blue).Analysis was performed with a Zeiss Axiovert 200 fluorescence microscope equipped with a 10x 0.4 Zeiss objective and a Zeiss Axiocam.

3.4.2.3 Characterisation of reisolated tumor cells

3.4.2.3.1 Morphology

Reisolated PC3 tumor cells (PC3ID3 and PC3ID4) and parental PC3 cells were analyzed for cell morphology by transmitted light microscopy. Twenty four hours after seeding no obvious changes in cell morphology were detectable (FIG 3-62).

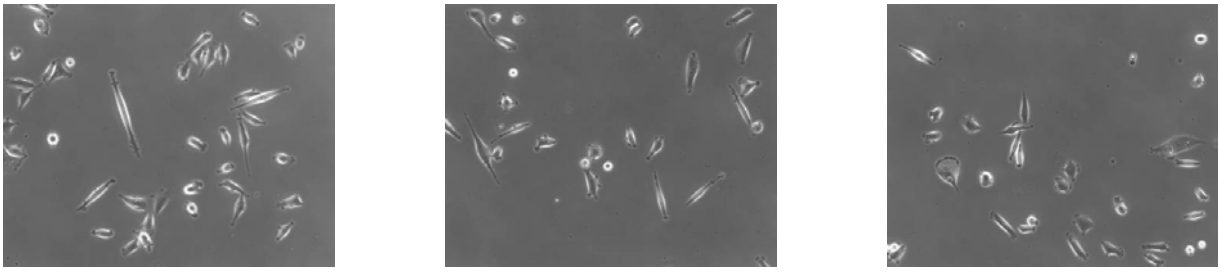

A B C

Fig.: 3-62 Morphologies of wt PC3 cells (A) and reisolated PC3ID3 (B) and PC3ID4 cells (C).

3.4.2.3.2 EGF and CD71 status

To verify the identity of reisolated PC3 cells, antibody staining against huEGFR and human CD71 was performed and analyzed by cell flow cytometry. Receptor status of reisolated cells was similar to the receptor status of wt PC3 cells regarding EGF receptor and human CD71 expression (FIG 3-63).

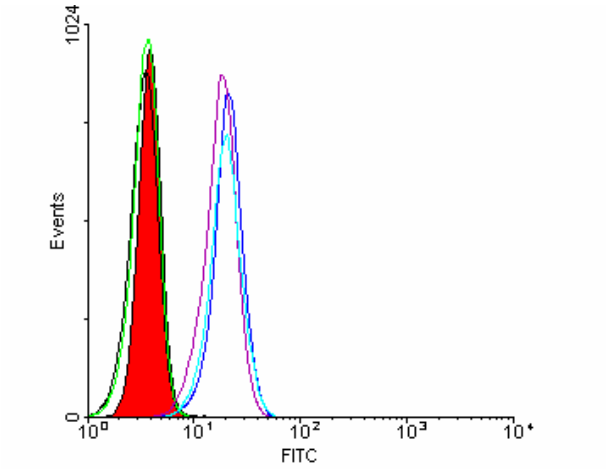

A

red: parental PC3 cells; control IgG
black: PC3Id4 control; IgG
green: PC3Id3 control; IgG
dark blue: parental PC3; anti human-EGF
violet: PC3ID3; anti human-EGF
light blue: PC3ID4; anti human-EGF

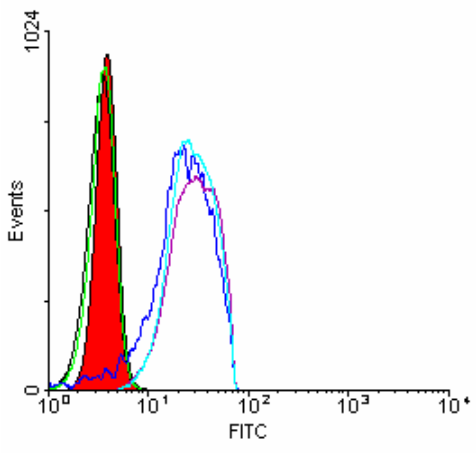

B

red: parental PC3 cells; control IgG
black: PC3ID4; control IgG
green: PC3ID4; control IgG
dark blue: parental PC3; anti human CD71
violet: PC3ID3; anti human CD71
light blue: pc3id4; anti human CD71

Fig.: 3-63 Antibody status for EGF- (A) and transferrin receptor (CD71) (B) on parental and reisolated PC3 cells. Parental and reisolated PC3 tumor cells were stained for human EGF- and human transferrin-receptor, followed by FACS analysis.

3.4.2.3.3 Proliferation rate

In order to investigate whether the resistance towards CPA treatment occurred due to changes in the proliferation rate, reisolated tumor cells were compared to parental PC3 cells in terms of proliferation by the Hoechst 33258 based DNA content assay. The proliferation rate was determined over a period of 5 days. Reisolated tumor cells PCID3 and PCID4 exhibited a slightly increased proliferation rate compared to the parental PC3 cells, however increase in proliferation rate was not significant ($p>0.05$, Mann-Whitney U-test).

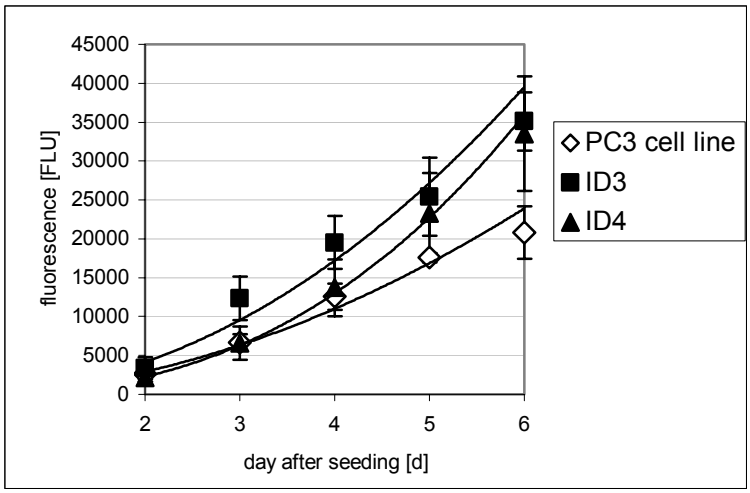

Fig.: 3-64 Proliferation of parental and reisolated PC3 cells (PCID3 and PCID4). Parental PC3 and reisolated tumor cells were seeded in a 48 well plate (1500 cells/well) and medium was changed every second day. Proliferation was determined by Hoechst33258 based DNA content assay over a period of 5 days. Open symbols: parental PC3 cells, closed symbols: reisolated PC3 cells. Values are means ± SD of four measurements.

3.4.2.3.4 NF-κB expression level

NF-κB is reported to be a critical factor in the response of tumors to chemotherapy; increased expression levels of NF-κB are able to protect tumor cells from drug induced cell death (68-71). Therefore, reisolated cells PC3ID3 and PC3ID4 were compared to the parental PC3 cell line in terms of NF-κB expression levels.

Parental and reisolated cells were transiently transfected with LPEI polyplexes (LPEI, N/P=6, HBS, 400ng/well) containing an NF-κB sensitive luciferase encoding plasmid. Control experiments were performed with similar LPEI polyplexes (HBS, N/P 6) containing a luciferase encoding plasmid without NF-κB enhancer areas in the promoter region. The reisolated cells PC3 ID3 and PC3 ID4 showed a significant increase in NF-κB activity in comparison to the parental PC3 cell line.

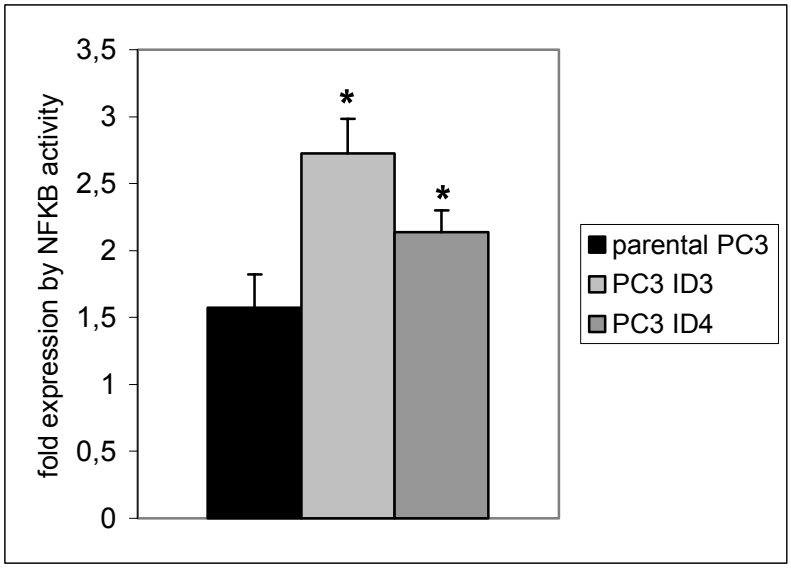

*Fig.: 3-65 Increased NF-κB activity levels in reisolated PC3ID3 and PC3ID4 cells. Data were corrected by control luciferase expression of parental PC3 cells. Mean values ± SD of four measurements are shown. *p<0.05, compared to parental PC3 NF-κB levels (Mann-Whitney U-test).*

3.4.2.3.5 Sensitivity to 4OOH-CPA treatment

For further investigation of secondary resistance, the effect of 4OOH-CPA treatment on survival of parental PC3 cells and reisolated PC3ID3 and PC3ID4 tumor cells was investigated. Therefore parental PC3 cells and reisolated tumor cells were seeded as a monolayer and incubated with different concentrations of 4OOH-CPA for 3 days. Survival was analyzed by measuring total metabolic activity (MTT assay). The reisolated PC3ID3 and PC3ID4 cells exhibited comparable sensitivity to the 4OOH-CPA induced reduction of cell survival as the parental PC3 cells in the monolayer system (FIG 3-66).

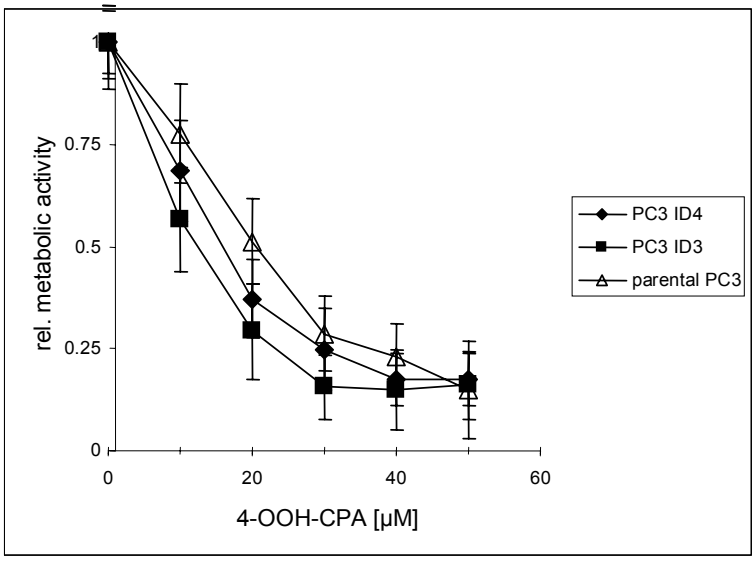

Fig.: 3-66 Sensitivity of parental PC3 and reisolated PC3ID3 and PC3ID4 cells towards treatment with 4-OOH-CPA. Parental and reisolated cells were treated with different concentrations of 4-OOH-CPA for 3 days. Survival was determined by measuring total metabolic activity. Control experiments were performed in the absence of 4-OOH-CPA. Mean values ± SD of four measurements are shown.

3.4.2.3.6 Tumor growth of reimplanted PC3 tumor cells

For further evaluation of resistance phenomena, in vivo experiments were performed. Reisolated PC3 tumor cells were again implanted in the flank of other male SCID mice. On day 17 after the tumor implantation, when average tumor volume reached 28mm^3, mice were subject to CPA treatment (120mg/kg, every six days).

Tumor volume and body weight were measured regularly over the period of the treatment. In contrast to the achieved growth delay of the tumors in the first CPA treatment (see FIG 3-59), no difference in tumor growth between the treated group and the control group was detectable. Control tumors as well as treated tumors had an average tumor volume doubling time of approximately three days (FIG 3-67). Metronomic scheduled CPA was again well tolerated, indicated by no significant loss in body weight (data not shown).

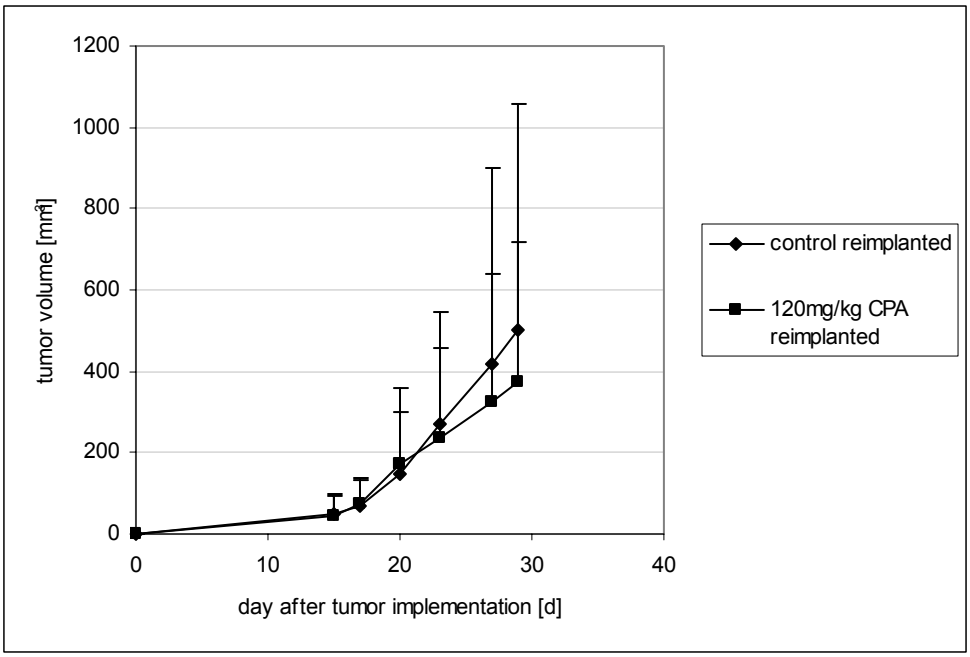

Fig.: 3-67 Tumor growth of reisolated PC3 tumor cells. Cells from resistant CPA treated tumors were obtained and again implanted subcutaneously in male SCID mice. Mice were treated again with 120mg/kg every sixth day. (n=4 for untreated control animals, n=5 for CPA treated animals)

3.4.2.4 Immunohistochemical analyses of reimplanted tumors

Reimplanted PC3 xenografts were analyzed for immunohistological changes in comparison to parental PC3 tumors. Again, attention was concentrated on vascular markers. Functional blood flow was visualized by intravenous application of Hoechst 33258 dye and antibody staining against laminin, CD31 and CDE13 was performed. Blood supply in reimplanted PC3 tumors was homogenous, indicated by homogenous staining of cell nuclei by systemically applied Hoechst 33258 dye. No significant changes in the arrangement of laminin and CD31 positive endothelial cells

was detected in reimplanted tumors in comparison to parental control tumors. Moreover, colocalisation of laminin and CD31 positive endothelial cells remained unchanged (FIG3-68A). Tendency of structural modifications or tumor cell lined vessels (vascular mimicry) as a possible mechanism of resistance were not detected. In parental PC3 tumors CD13 positive cells and laminin staining was partly colocalized (FIG 3-61C), whereas in the reimplanted tumors no colocalisation was detectable (FIG 3-68B).

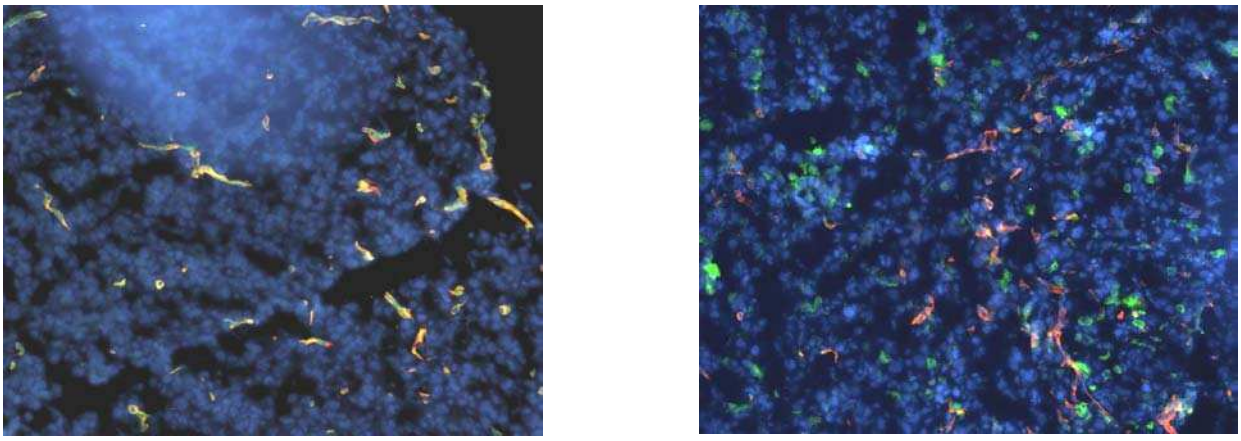

A B

Fig.: 3-68 Immunohistochemical analysis of reimplanted PC3 tumors. Cryo sections (5µm) were fixed with 4% paraformaldehyde and stained with specific antibodies for A) rat-anti mouse CD31 (green) and anti laminin (red), respectively for B) rat-anti mouse CD13 (green) and anti laminin (red). Secondary antibodies were labelled with Alexa 488 (CD31/CD13) or Texasred (laminin). The intravenously injected Hoechst 33258 stain, indicating functional blood flow, was visualized as well (blue).

3.4.3 Resistance in the HUH7 tumor model

3.4.3.1 HUH7 tumor model

Subcutaneous human HUH7 tumors were established in SCID mice by injection of $5x10^6$ HUH7 cells in the flank of the animals. When tumors reached an average tumor volume of 32 mm^3 CPA treatment was started on day 12 after the tumor implantation. Tumor bearing mice were treated with 75mg/kg CPA every 6th day. Tumor volume and body weight was measured over the time of CPA treatment. Metronomic scheduled CPA treatment resulted in a significant delay in tumor growth. Tumor volume was constant up to day 75 after the tumor cell implantation, whereas tumors in the control group showed tumor progression. When CPA treated HUH7 tumor began to grow despite ongoing CPA therapy, tumor double time was 3.5 days.

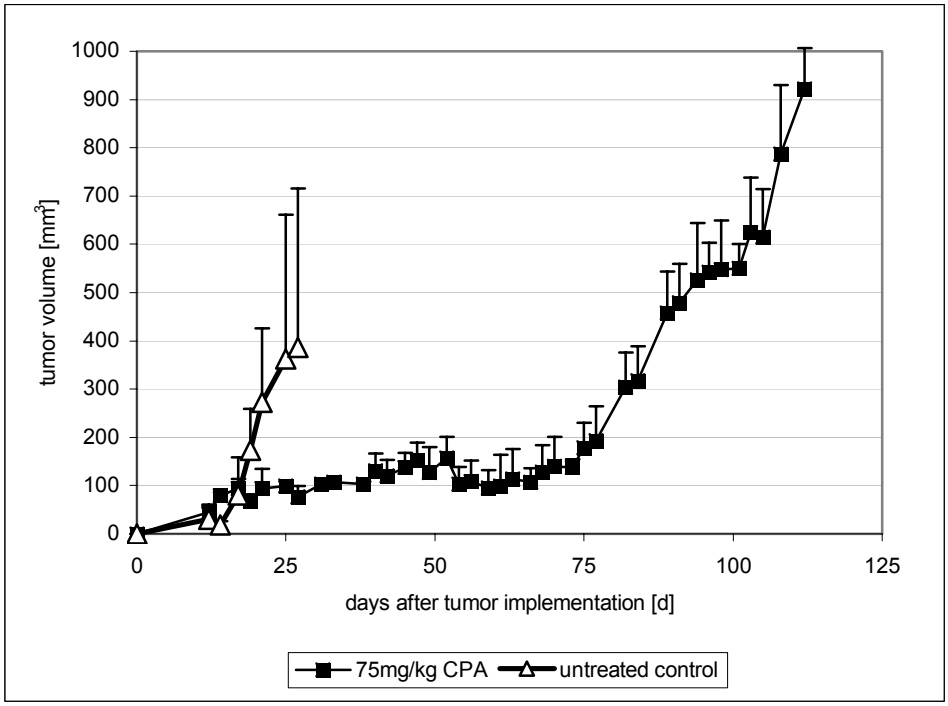

Fig.: 3-69 Tumor growth in a human HUH7 xenograft model with and without metronomic scheduled CPA treatment. Tumor bearing SCID mice were treated with 75 mg/kg CPA every 6th day. (n=3 animals per group)

Metronomically scheduled CPA therapy was well tolerated indicated by constant animal body weight up to day 85. Further CPA treatment resulted in significant loss of body weight pertaining to all CPA treated animals (data not shown). Treatment was stopped and animals were sacrified when average loss in body weight reached 20%. Tumors were collected and subjected to histological analysis. Further on, tumor cells were extracted from rebounded tumors for characterisation and cell culture experiments.

3.4.3.1.1 Macroscopic differences between tumors

The embedded and frozen tumor tissue was analyzed for macroscopical changes because treated tumors were obviously different in their appearance compared to non-treated control. The tumor tissue of non-treated tumors was compact and homogenous (FIG 3-70A and B), whereas resistant CPA treated tumors exhibited an inhomogeneous and sponge like structure. Moreover the tissue of treated tumors appeared darker resulting from incorporated blood lakes within the tissue (FIG 3-70C, D, E and F).

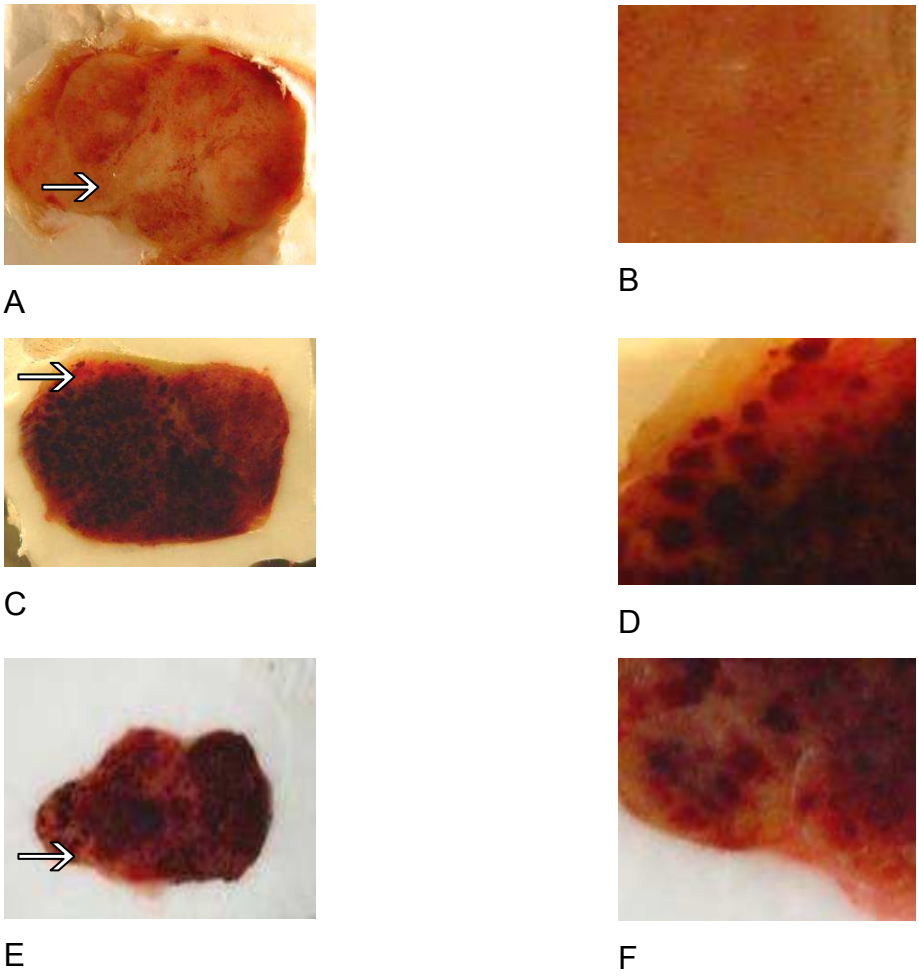

Fig.: 3-70 Macroscopic appearance of relapsed CPA treated HUH7 tumors. Tumor tissue was collected on day 112 after implantation in case of treated tumors (C, D, E and F) and on day 27 in the case of control tumors (A and B). Frozen, embedded tumor tissue was cut with a cryostat until the centre of the tumors was reached. Photos were taken with a SONY DSC-75 digital camera. Pictures B, D and F are enlarged details from overview pictures A, C and E (⟹)

3.4.3.1.2 Histology (HE)

For characterisation and evaluation of histological changes induced by CPA treatment, tumors were collected and histological analyses by H/E staining and transmission light microscopy were performed.

Untreated HUH7 xenografts own a very compact and homogenous tissue structure (FIG 3-71 A). In contrast, relapsed CPA treated tumors appeared inhomogeneous and exhibited a spongy structure with large cell free areas (FIG 3-71 B). These cell free areas were identified as intratumoral blood lakes, characterized by the presence of erythrocytes. Interestingly, larger areas of condensed or fragmented cell nuclei were neither found in control tumors nor in relapsed CPA treated tumors, indicating a similar degree of cell death (FIG 3-71A and B).

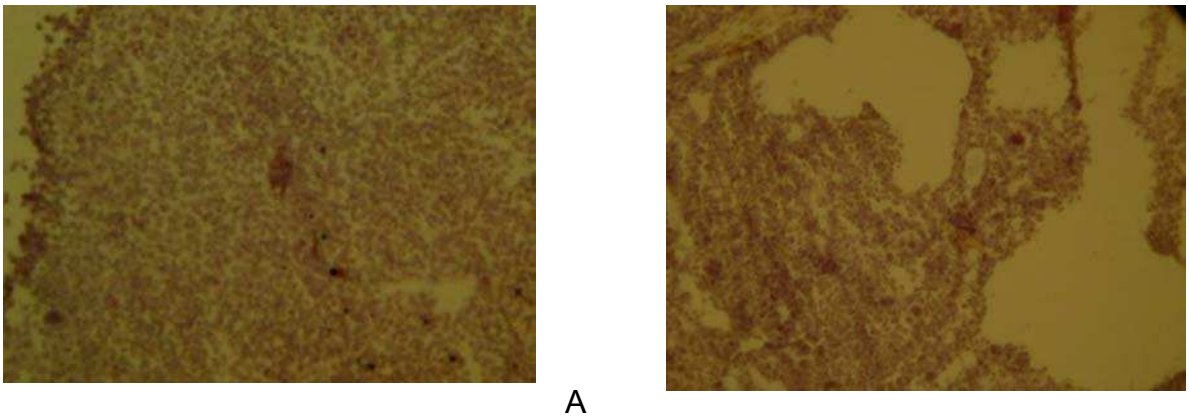

A B

Fig.: 3-71 Histology of subcutaneous HUH7 xenografts in male SCID mice (H/E stain). Control tumors were collected at day 27 (A) and CPA treated tumors on day 112 (B) after tumor cell implantation. Cryosections (10µm) were fixed with 4% paraformaldehyde and subjected to H/E staining as described in materials and methods. Sections were viewed on a Zeiss Axiovert 200 transmitted light microscope with a 20x0.4 NA objective. Pictures were taken by a Sony DSC-S75 digital camera.

To evaluate, if integrated blood lakes contribute to blood supply Hoechst33258 was applied systemically as a tracer. Several blood lakes exhibited Hoechst 33258 stained lining (blue), indicating connection with systemic blood supply (FIG 3-72B). Blood supply of non treated HUH7 tumors was investigated with the same technique (FIG 3-72A). Counterstain of nuclei was performed with propidium iodide.

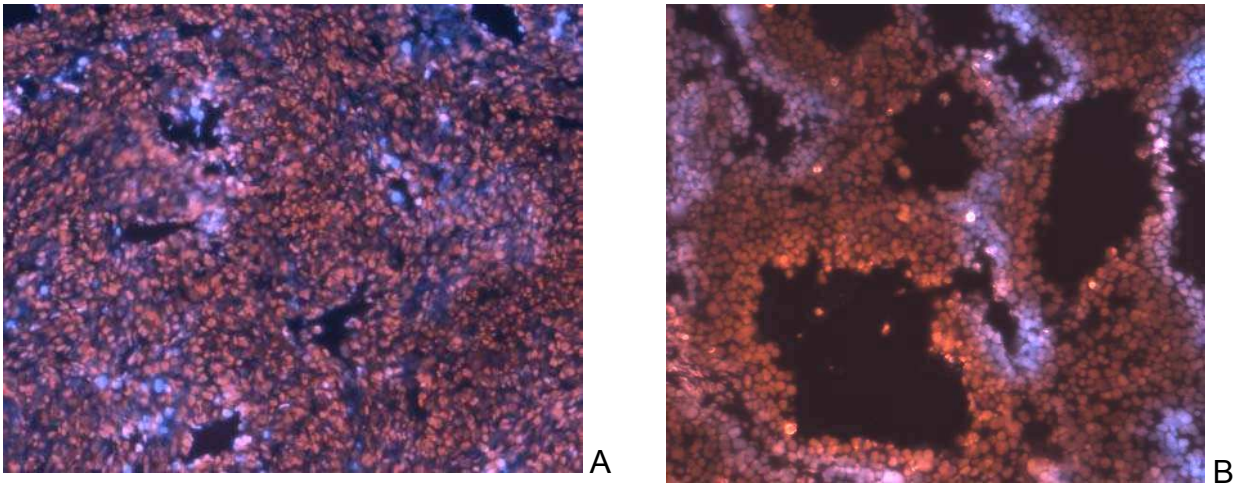

A B

Fig.: 3-72 Blood supply in HUH7 xenografts. Cryo sections (10µm) were fixed with 4% paraformaldehyde and counter stain was performed with propidium iodide (red). Blood supply is indicated by blue staining of intravenously applied Hoechst 33258 dye. Analysis was performed with a Zeiss Axiovert 200 fluorescence microscope, equipped with a 10x0.4 Zeiss objective and pictures were taken with a Zeiss Axiocam.

3.4.3.1.3 EGF-receptor status

For further evaluation of potential changes responsible for resistance against CPA treatment, HUH7 tumors were analyzed for immunohistological modifications. Due to the antiangiogenic metronomic schedule of CPA, attention was focussed on vascular

markers. Functional blood flow was visualized by intravenous application of Hoechst 33258 dye and antibody staining against laminin, CD31 and CD13 was performed. Functional blood flow was decreased in relapsed CPA treated tumors, indicated by decreased Hoechst33258 fluorescence signal within the tumor tissue (FIG 3-73 B and D); moreover vessel density was decreased. Less CD31 and laminin positive vessels were detected in comparison to the control tumors. Colocalisation of laminin and CD31 positive endothelial cells remained unchanged (FIG 3-73A and B). However, in contrast to control tumors, in CPA treated tumors vessels were not continuously lined with CD31 positive endothelial cells. Tumor cell lined vessels (vascular mimicry) for a possible reason of resistance towards the metronomic scheduled CPA treatment was evident in these relapsed tumors.

Staining for CD13 positive cells, a marker that indicates angiogenic active endothelial cells, resulted in slightly decreased fluorescence signal compared to non-treated control tumors. Similar to evaluated PC3 tumors, colocalisation of laminin and CD13 staining was decreased in relapsed CPA treated HUH7 tumors. In the case of HUH7 tumors colocalisation was even completely diminished. In contrast to organized structures of CD13 positive cells in the control tumors, CD13+ endothelial cells exhibited manifest trappings of disorganisation. In treated tumors CD13+ cells were scattered distributed over the tumor tissue whereas CD13+ cells were colocated with the established vessel network in control tumors (FIG 3-73C and D).

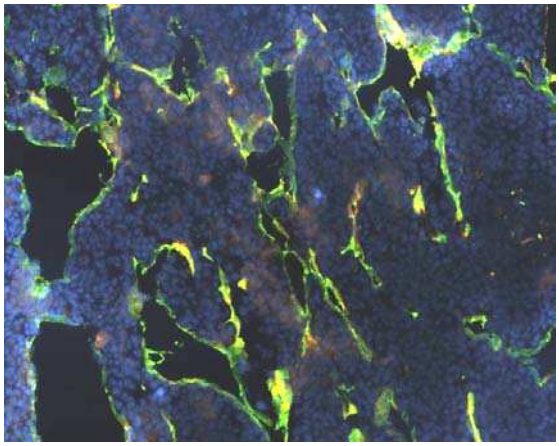

A

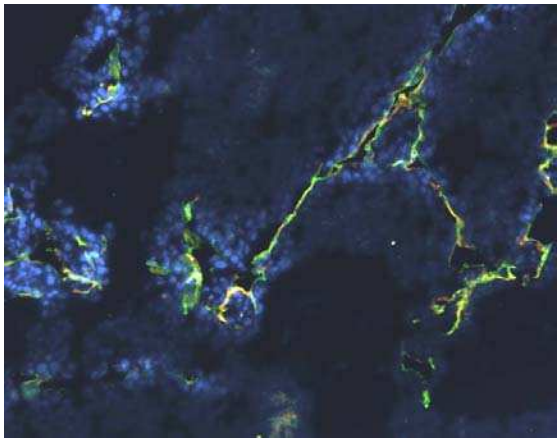

B

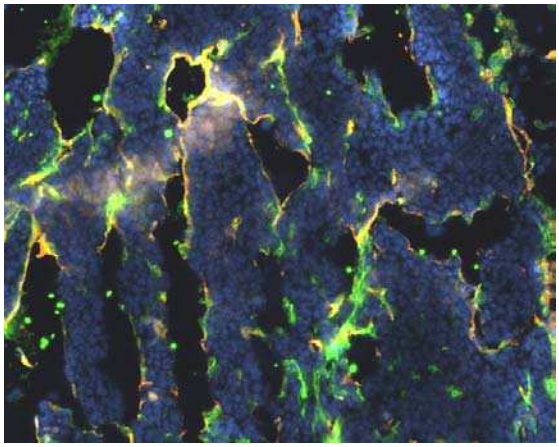

C

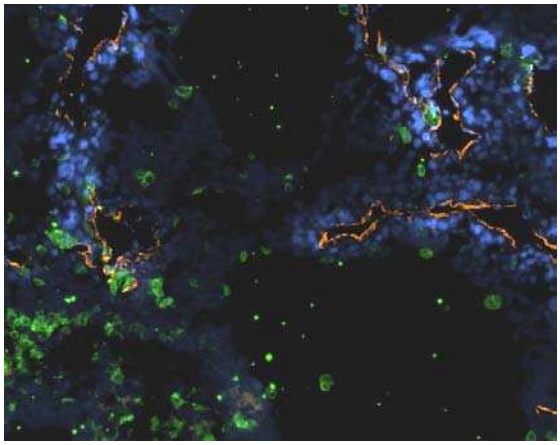

D

Fig.: 3-73 Immunohistochemical analysis of HUH7 tumors (A,C) untreated control tumors and (B,D) CPA treated. Cryo sections (5µm) were fixed with 4% paraformaldehyde and stained with specific antibodies for A,B rat-anti mouse CD31 (green) and anti laminin (red), respectively for C,D rat-anti mouse CD13 (green) and anti laminin (red). Secondary antibodies were labelled with Alexa 488 (CD31/CD13) or Texasred (laminin). The intravenously injected Hoechst 33258 stain was visualized as well (blue).

3.4.3.1.4 Morphology of reisolated HUH7 tumor cells

Reisolated HUH7 tumor cells and cells from the HUH7 parental cell line were analyzed for cell morphology by transmitted light microscopy. Parental HUH7 cells and reisolated cells from relapsed CPA treated tumors were seeded in well plates. 24h after the seeding pictures were taken. No obvious changes in cell morphology were detectable.

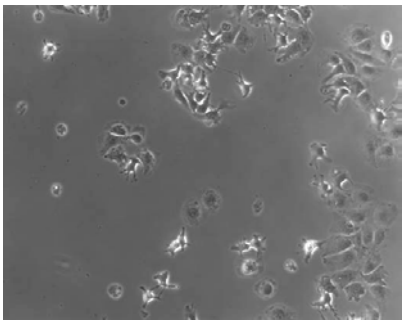

A

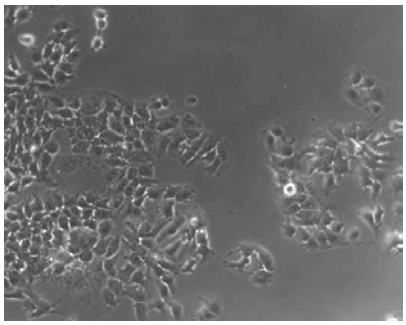

B

Fig.: 3-74 Morphology of parental HUH7 cells (A) and reisolated HUH7 (HUH7 REISO) cells (B).

3.4.3.1.5 EGF-receptor expression

To verify the identity of reisolated human HUH7 tumor cells, antibody staining against human EGFR receptor was performed and analyzed by cell flow cytometry.

Receptor status of reisolated cells was very similar to the receptor status of parental HUH7 cells regarding human EGF receptor. The EGF receptor was detected in a similar density on the reisolated cells compared to parental HUH7 cells (FIG 3-75).

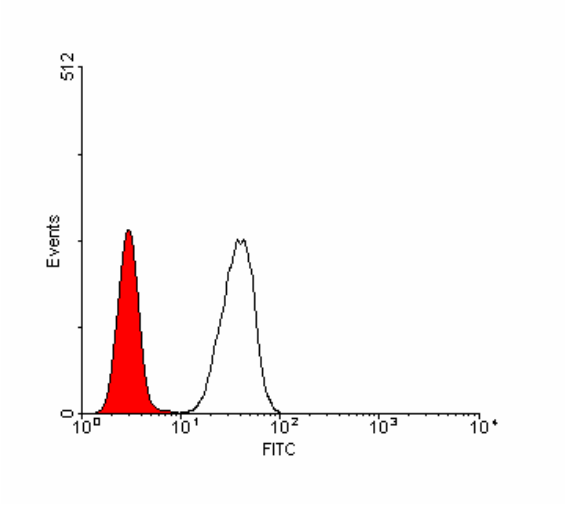

red: parental HUH7; control IgG
black: parental HUH7; anti huEGF

A

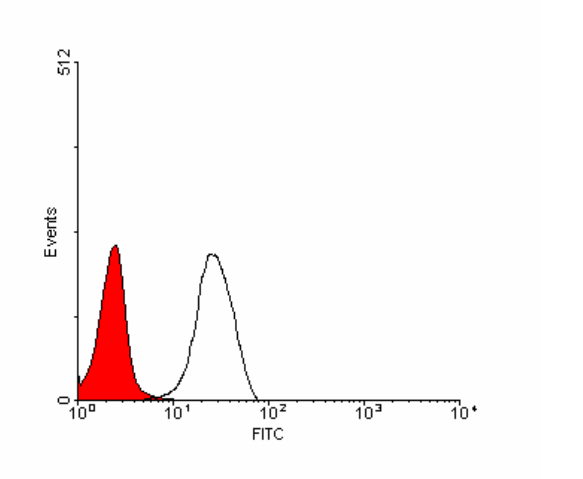

red: HUH7 REISO; control IgG
black: HUH7 REISO; anti huEGF

B

Fig.: 3-75 Antibody status for human EGF receptor on parental and reisolated HUH7 cells. Parental and reisolated PC3 tumor cells were stained for human EGF- and human Transferrin-receptor as described in materials and methods, followed by FACS analysis. A) parental HUH7 cells, B) reisolated HUH7 cells.

3.4.3.1.6 Proliferation rate of reisolated HUH7

In order to test whether the non response towards CPA treatment is due to changes in the proliferation rate, reisolated tumor cells were compared to the parental cell lines in terms of proliferation rate by the Hoechst DNA content assay. Proliferation rate was determined over a period of 4 days. No difference in proliferation rate was found in the reisolated HUH7 cells compared to proliferation rate of parental HUH7 cells.

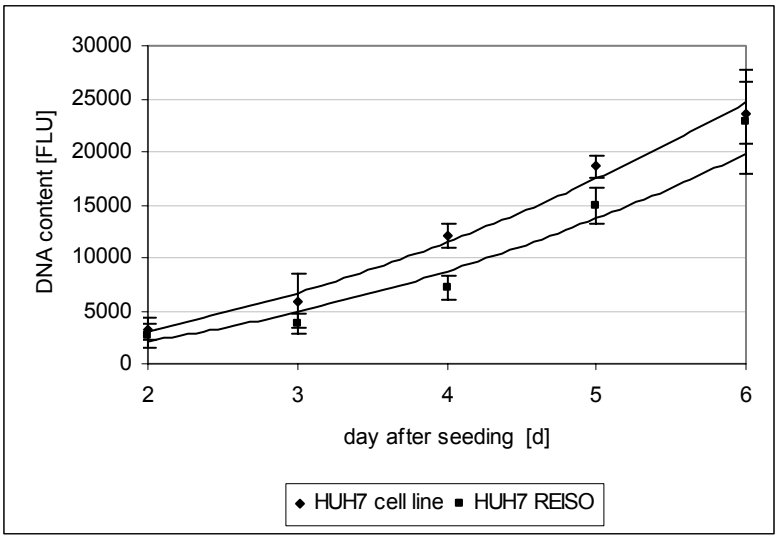

Fig.: 3-76 Proliferation of parental and reisolated HUH7 cells (HUH7 REISO). Parental HUH7 and reisolated tumor cells were seeded in a 48 well plate (1500 cells/well). Medium was changed every second day. Proliferation was determined by Hoechst33258 based DNA content assay over a period of 4 days. Values are means ± SE of five measurements.

3.4.3.1.7 CYP activity in HUH7

Since HUH7 cells have endogenous CYP enzymatic activity in the resorufin assay, non response to CPA therapy might be a result of changes in endogenous activity. Therefore HUH7 REISO cells were compared to parental HUH7 cells in terms of endogenous CYP enzymatic activity in the resorufin assay. Enzymatic CYP activity was indeed reduced in the HUH7 REISO cells in comparison to the HUH7 parental cell line (FIG 3-77). The reduction of CYP2B1 enzymatic activity leads to decreased CPA activation in the cells and therefore may contribute to a non CPA responsive phenotype. Reduction in endogenous CYP2B1 activity was significant referring to cell count and total metabolic activity. (p=0.049; Mann-Whitney U-test).

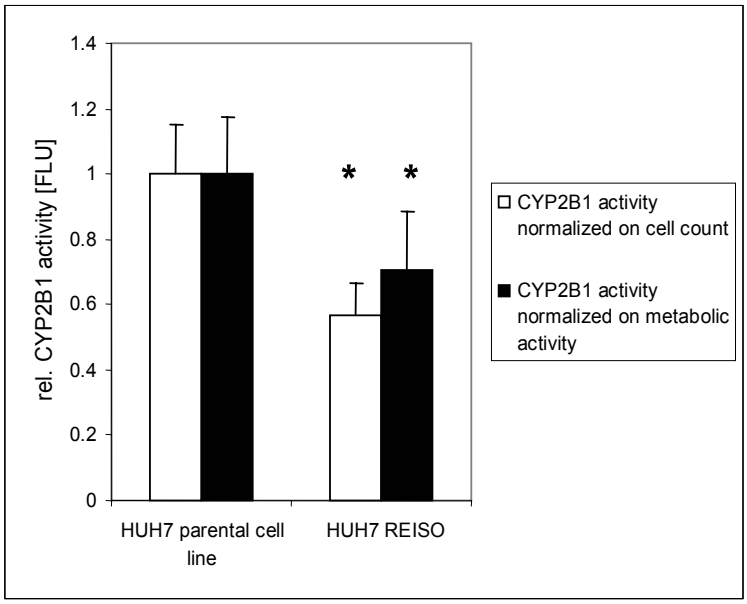

*Fig.: 3-77 Decreased CYP2B1 activity levels in reisolated HUH7 tumor cells. Data were corrected by cell count or metabolic activity (MTT) of parental HUH7 cells. Mean values ± SD of triplicates are shown. *p<0.05, compared to parental HUH7 CYP activity levels (Mann-Whitney U-test).*

3.4.3.1.8 NF-κB activity

Reisolated HUH7 tumor cells were compared to parental cells in terms of NF-κB activity levels. Determination of NF-κB activity levels was performed similar as in PC3 and Neuro2A cells. The increase in luciferase expression by transfection with the plasmid containing NF-κB responsive elements in the promoter region was most pronounced in HUH7 cells compared to other cell lines (see chapters 2 CT26:10,1 and chapter 4, Neuro2A: 2,2 , PC3: 1,6). Moreover reisolated cells HUH7 REISO shows a significantly increased NF-κB activity in comparison to the parental HUH7 cell line, indicating that NF-κB activity might contribute to decreased sensitivity towards cytotoxic treatment.

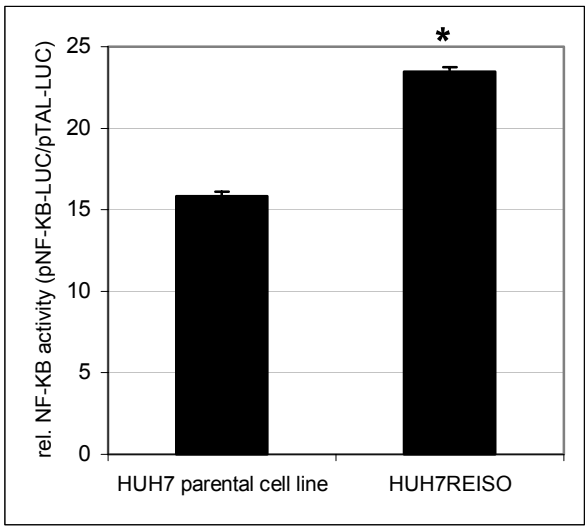

*Fig.: 3-78 Increased NF-κB activity levels in reisolated HUH7 tumor cells. Data were corrected by control luciferase expression of parental HUH7 cells. Mean values ± SD of four measurements are shown. *p<0.05, compared to parental HUH7 NF-κB activity levels (Mann-Whitney U-test).*

3.4.3.1.9 Sensitivity of HUH7 towards CPA treatment in a coculture model

For further investigation of resistance phenomena, reisolated HUH7 cells were exposed to in situ activated CPA in a coculture system with CYP2B1 expressing X39 tumor cells. Reisolated or parental HUH7 cells were seeded with X39 cells in a ratio of 75:25 and incubated with different concentrations of CPA for 5 days. Control experiments were performed in the absence of CPA. Cell survival was analyzed by measuring total metabolic activity (MTT assay). The reisolated cells exhibited comparable sensitivity to the CPA induced reduction of cell survival as the parental HUH7 cells in a monolayer system.

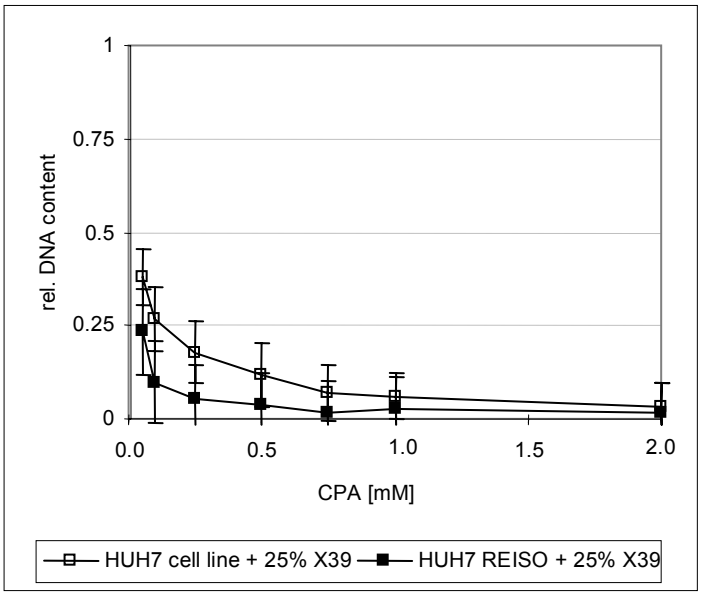

Fig.: 3-79 Sensitivity of parental HUH7 and reisolated HUH7 REISO cells towards treatment with in situ activated CPA. Parental and reisolated cells co-cultivated with X39 cells and treated with different concentrations of CPA for 5 days. Survival was determined by measuring Hoechst DNA content assay. Control experiments were performed in the absence of CPA. Mean values ± SD of six measurements are shown.

3.4.3.2 Reimplantation of reisolated HUH7 cells

For the reimplantation of HUH7 tumors, cells obtained from one relapsed CPA treated tumor were isolated, passaged four times in vitro and injected in the flank of SCID mice. On day 12 when average tumor volume reached 40mm^3 CPA treatment was started (75mg/kg, every sixth day).

In contrast to significant growth delay of tumors established with parental HUH7 cells due to CPA treatment, tumor progression of treated and control animals were not significantly different when tumors were established with reisolated HUH7 tumor cells (Mann-Whitney U-test). Metronomic scheduled CPA was again well tolerated indicated by no significant loss in body weight (data not shown).

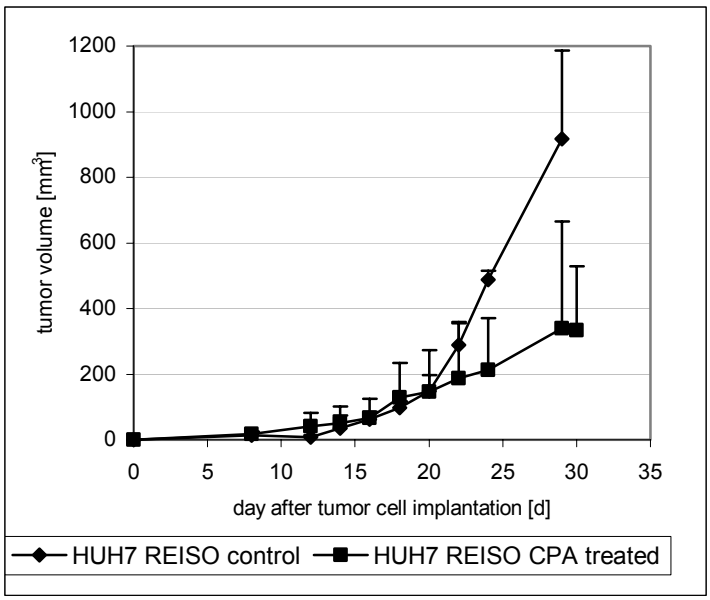

Fig.: 3-80 Tumor growth of reisolated HUH7 tumor cells. Cells from relapsed CPA treated tumors were obtained and reimplanted subcutaneously in SCID mice. Mice were treated with 75mg/kg every sixth day. (n=3 for untreated control group, n=4 for CPA treated group).

3.4.3.3 Histology of reimplanted tumors

Reimplanted HUH7 xenografts were analyzed for immunohistological changes in comparison to parental HUH7 tumors. Blood supply in reimplanted HUH7 tumors was heterogeneous and insufficient, indicated by large areas without staining after systemic application of Hoechst 33258 dye. Moreover, a considerable fraction of tumor vessels was dilated and tissue structure was rather spongy in comparison to parental HUH7 tumors. No significant changes in the arrangement of laminin and CD31 positive endothelial cells was detected in reimplanted tumors in comparison to parental control tumors. Moreover, colocalisation of laminin and CD31 positive endothelial cells remained unchanged (FIG 3-81A). Tendency of tumor cell lined vessels (vascular mimicry) for a possible reason of resistance towards the metronomic scheduled CPA treatment was detected in some tumor areas (FIG 3-81B). Colocalization of CD13 positive cells and laminin was detectable in some tumor areas (FIG 3-81C). However, colocalisation of laminin and CD13 staining was significantly decreased in considerable areas of tumor tissue in comparison to parental HUH7 tumors (FIG 3-81D).

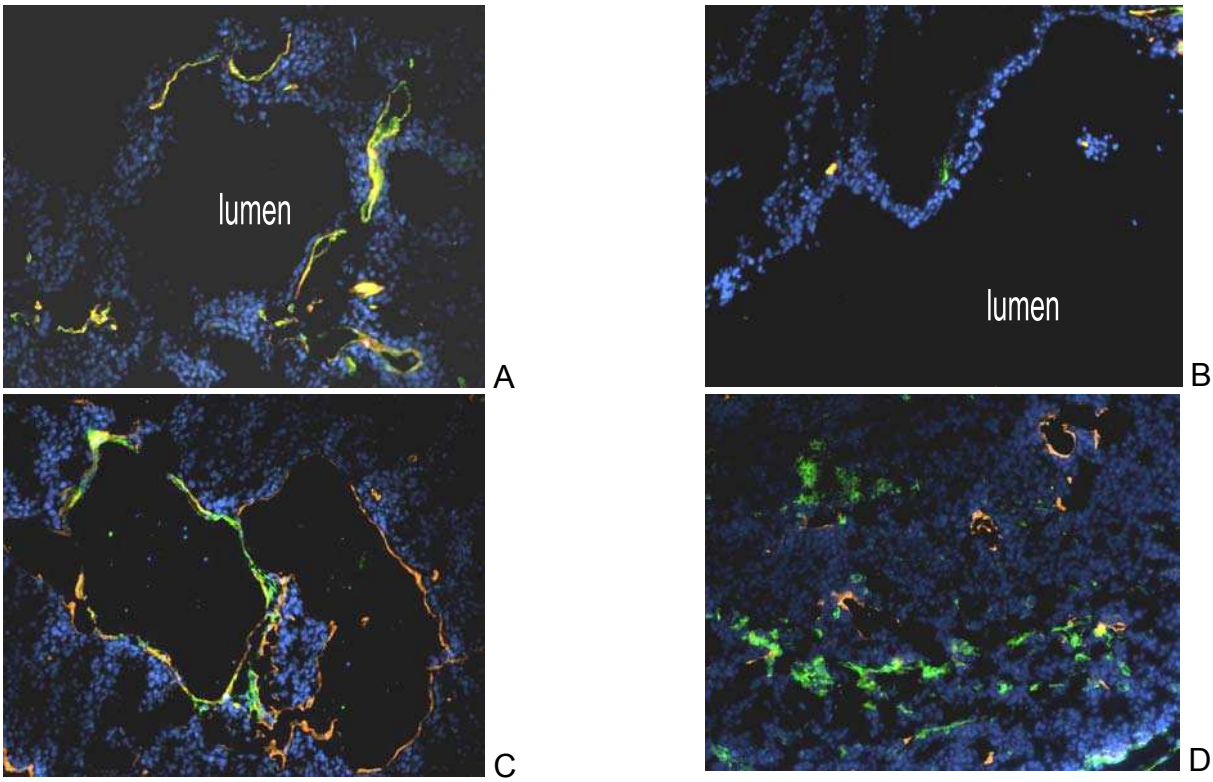

Fig.: 3-81 Cryo sections (5µm) were fixed with 4% paraformaldehyde and stained with specific antibodies for rat-anti mouse CD31 (green) and anti laminin (red) (A and B), respectively for rat-anti-mouse CD13 (green) and anti laminin (red) (C and D). Secondary antibodies were labelled with Alexa 488 (CD31/CD13) or TexasRed (laminin). The intravenously injected Hoechst 33258 stain was visualized as well (blue).

3.4.4 Resistance in the syngeneic Neuro2A tumor model

3.4.4.1 In vivo treatment of Neuro2A tumors

Subcutaneous Neuro2A tumors were established in A/J mice by subcutaneous injection of $1x10^6$ Neuro2A cells in the flank of the animals. On day 11 after the tumor implantation when tumors reached an average tumor volume of $50mm^3$, combined electroporation with plasmid DNA encoding for CYP2B1 enzyme and CPA treatment (75mg/kg every seventh day) was started (GDEPT concept, chapter 1). Tumor volume and body weight was measured at constant intervals during CPA treatment. Electroporation combined with metronomic scheduled CPA treatment (application two day after electroporation) resulted in a significant delay in tumor growth. Tumor progression of the treated animals was diminished up to day 62 after the tumor cell implantation whereas tumors of the control group showed an average tumor doubling time of about 3 days. When electroporated and CPA treated Neuro2A tumors began to re-grow despite ongoing therapy tumor doubling time was 6 days.

Combined electroporation with metronomic scheduled CPA therapy was well tolerated indicated by constant animal body weight up to day 65. Further treatment resulted in significant weight loss in all treated animals. Treatment was stopped and animals were sacrified when average weight loss reached 20% (data not shown).

For further investigation of treatment non-responding, tumors were collected and cells were extracted from the tumor tissue for further characterisation.

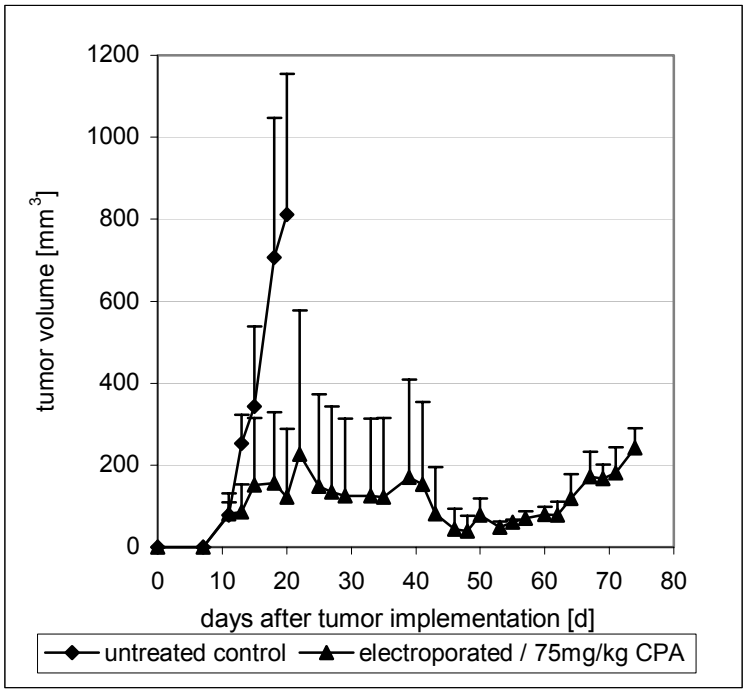

Fig.: 3-82 Tumor growth in a Neuro2A tumor model with and without metronomic scheduled CPA combined with electroporation treatment. (n=3 animals per group)

3.4.4.2 Morphology of reisolated Neuro2A tumor cells.

Reisolated Neuro2A tumor cells and parental cells from the Neuro2A cell line were analyzed for cell morphology by transmitted light microscopy. Therefore parental cells and reisolated cells, obtained from the treatment non responsive tumors, were seeded in well plates. 24h after the seeding pictures were taken. No obvious changes in cell morphology were detectable.

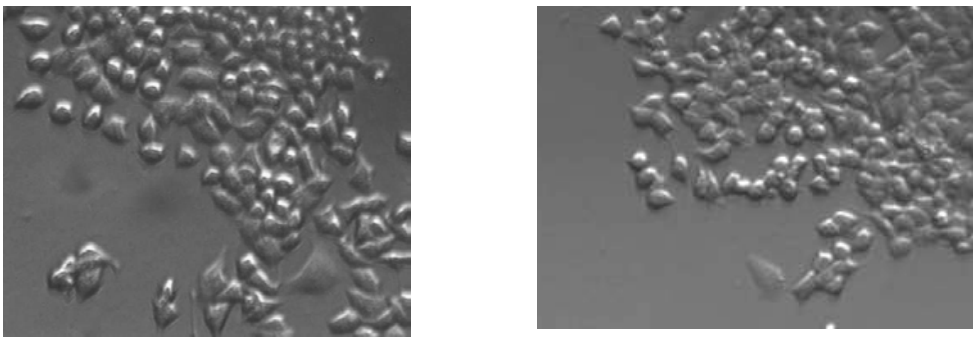

A B

Fig.: 3-83 Morphology of parental Neuro2A cells (A) and reisolated Neuro2A cells (Neuro2A REISO) (B).

3.4.4.3 CD71 status of reisolated Neuro2A tumor cells

To verify the identity of reisolated Neuro2A tumor cells, antibody staining against CD71 was performed and analyzed by cell flow cytometry. The parental Neuro2A cells and as well the reisolated cells were positively stained for CD71 receptor. A slightly increased CD71 density was detected on Neuro2A REISO cells compared to parental Neuro2A cells.

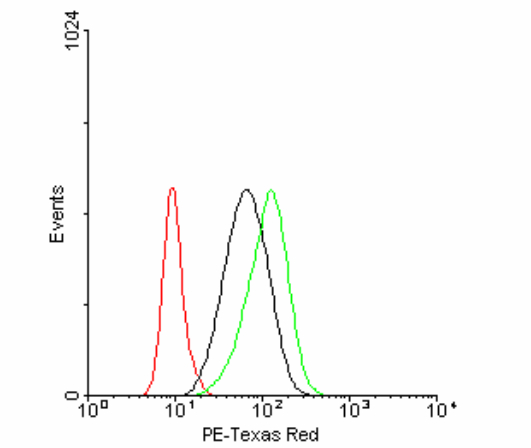

red: isotype control IgG-PE

black: parental Neuro2A; anti mouse CD71-PE

green: Neuro2A REISO; anti mouse CD71-PE

Fig.: 3-84 Antibody status for mouse CD71 on parental and reisolated Neuro2A cells. Parental and reisolated Neuro2A tumor cells were stained for mouse transferrin receptor (CD71) as described in materials and methods, followed by FACS analysis.

3.4.4.4 Proliferation rate of reisolated Neuro2A cells

In order to test whether the non response towards CPA treatment is due to changes in the proliferation rate, reisolated tumor cells were compared to the parental cell lines in terms of proliferation rate by the Hoechst DNA content assay. Proliferation rate was determined over a period of 4 days. No difference in proliferation between reisolated and parental Neuro2A was detected.

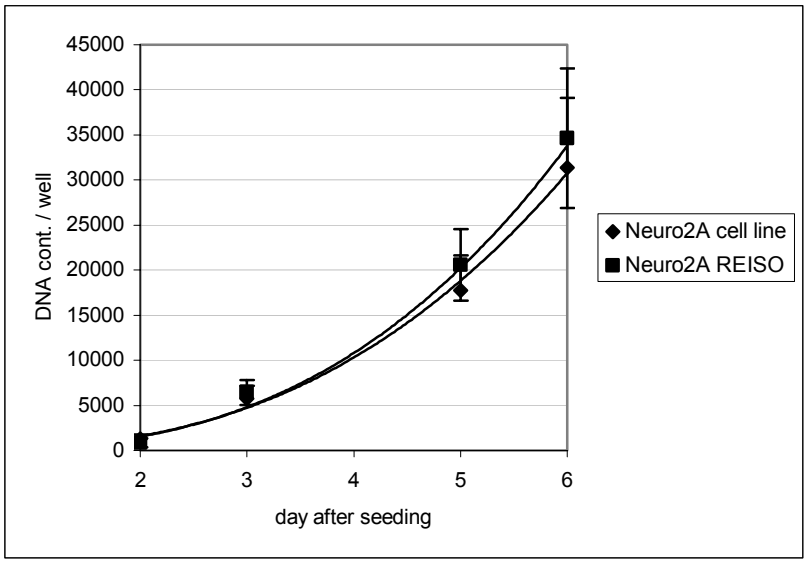

Fig.: 3-85 Proliferation of parental and reisolated Neuro2A cells (Neuro2A REISO). Parental Neuro2A and reisolated tumor cells were seeded in a 48 well plate (1500 cells/well). Medium was changed every second day. Proliferation was determined by Hoechst33258 based DNA content assay over a period of 4 days. Values are means ± SD of six measurements.

3.4.4.5 CYP activity in reisolated Neuro2A tumor cells

Due to the fact that mice were treated with a combination of CYP2B1 gene transfer and metronomic scheduled CPA therapy, reisolated tumor cells were analyzed for CYP activity by the resorufin assay. Neuro2A REISO cells did not exhibit increased CYP activity in comparison to parental Neuro2A cells (data not shown).

3.4.4.6 NF-κB expression levels

To evaluate a potential role of NF-κB activity in resistance of the Neuro2A tumor model, reisolated Neuro2A tumor cells were investigated regarding to their NF-κB activity levels. Determination of NF-κB levels was performed similar as in PC3 and HUH7 cells. Reisolated Neuro2A cells exhibited no significantly increased NF-κB activity in comparison to parental Neuro2A cells ($p=0.078$, Mann-Whitney U-test).

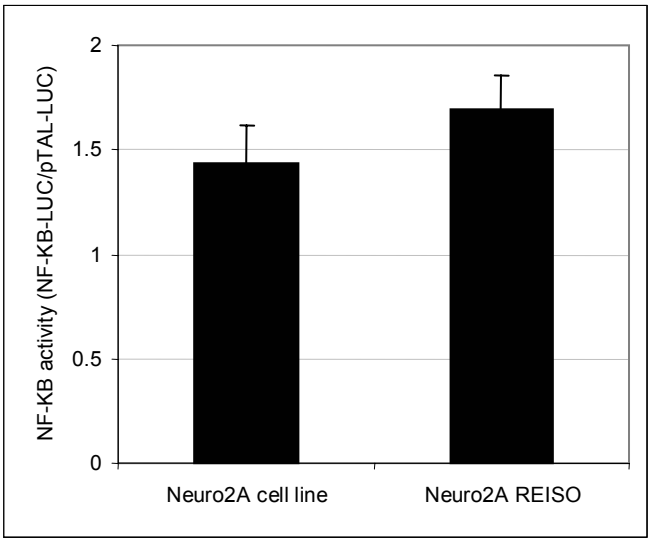

Fig.: 3-86 NF-κB activity levels in parental Neuro2A and reisolated Neuro2A (Neuro2A REISO) cells. Mean values ± SD of six measurements are shown.

3.4.4.7 Sensitivity towards 4OOH-CPA treatment

For further evaluation of resistance in the Neuro2A tumor model, the effect of 4OOH-CPA treatment on the survival of parental Neuro2A and reisolated Neuro2A REISO cells was investigated in vitro. Therefore, parental Neuro2A cells and reisolated tumor cells were seeded as a monolayer and incubated with different concentrations of 4OOH-CPA for 3 days. Survival was analyzed by measuring total metabolic activity (MTT assay).

Reisolated cells exhibited comparable sensitivity to the 4OOH-CPA induced reduction of cell survival as the parental Neuro2A cells in a monolayer system.

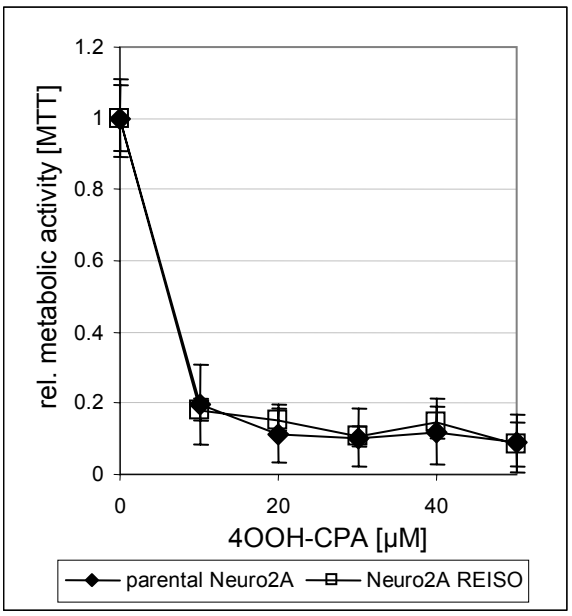

Fig.: 3-87 Sensitivity of parental Neuro2A and reisolated Neuro2A REISO cells towards treatment with 4-OOH-CPA. Parental and reisolated cells were treated with different concentrations of 4-OOH-CPA for 3 days. Survival was determined by measuring total metabolic activity. Control experiments were performed in the absence of 4-OOH-CPA. Mean values ± SD of four measurements are shown.

3.4.5 CPA treatment of reimplanted Neuro2A REISO cells

For the reimplantation of Neuro2A tumors, cells from one CPA treated tumor were recultivated and 10^6 cells were injected subcutaneously in the flank of A/J mice.

When the average tumor volume was 46.5 mm^3 on day 8 after tumor implantation, mice were subjected to CPA treatment (75mg/kg, every 6th day). Electroporation prior to CPA application was not performed in this experiment. Tumor volume and body weight were measured regularly over the period of the treatment.

CPA treated tumor bearing mice exhibited a strong decrease in tumor growth whereas control tumors exhibited an average tumor volume double time of 2 days.

Metronomic scheduled CPA was again well tolerable, indicated by no significant loss in body weight (data not shown).

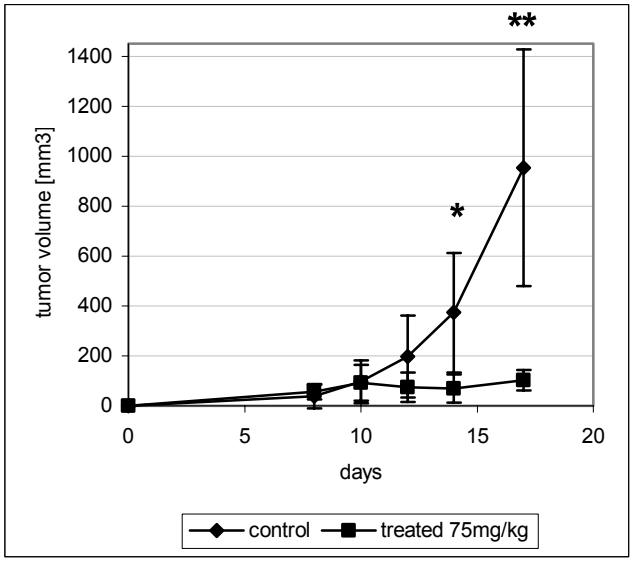

*Fig.: 3-88Tumor growth of reimplanted Neuro2A tumor cells in A/J mice. Cells from one rebounded CPA treated tumor were obtained and subjected to recultivation. 10^6 reisolated tumor cells were again implanted subcutaneously. Mice were treated with 75mg/kg every 6th day. Difference in tumor volume was significant at day 14 and day 17 after tumor cell implantation. (n=4 for the control group and n=5 for treated group) **p<0.01; *p<0.05, compared to non treated control tumors (Mann-Whitney U-test).*

4 Discussion

Therapy of malignant diseases was continuously improved over the last decades. Drugs and treatment regimes were optimized in order to achieve adequate anti cancer activity combined with tolerable side effects. However, treatment with conventional antitumor drugs is still marked by a balance between antitumoral and side effects due to insufficient specificity. In particular, widely used low molecular drugs are distributed in similar quantity in healthy tissue, when administration is performed systemically.

Recently, a change towards more specific drugs is noticeable. Moreover, tumor vasculature as a promising target in anticancer strategies emerged in the last years. According, investigation of tumor angiogenesis and antiangiogenic approaches was a main issue in new antitumor strategies. Treatment regimes with conventional cytotoxic antitumoral drugs were evaluated and changed experimentally from high dose therapies to low dose metronomic schedules. In addition more specific approaches with antibodies, e.g. Herceptin® and Avastin®, thyrosin kinase inhibitors (Clivec®), or proteasom inhibitors (Velcade®) were recently developed and entered the clinic. New treatment regimes such as nucleic acid therapies including siRNA and gene therapy are investigated because of their potential of selectivity.

However, several limitations for cancer therapy exist up to now. The occurrence of primary and secondary resistance towards treatment regimes is still a major obstacle in tumor therapy. Approaches for cancer therapy have to be further improved regarding to specificity, antitumoral efficiency and resistance. A major obstacle for evaluation of new therapeutic strategies is the lack of reliable model systems and/or evaluation of potential strategies without incorporating tumor specific environmental properties.

Main issues in this thesis were therefore the evaluation of a potential specific gene therapeutic approach (GDEPT) in a tumor mimicking environment. Moreover, attention was turned towards metronomic scheduled CPA and acrolein as one of the metabolites that potentially support antiangiogenic activity. During the investigations chemoresistance towards CPA therapy was observed in tumor models in vitro and in vivo and was characterized by histological analysis and evaluations in reisolated tumors.

4.1 Classic GDEPT concept

A major obstacle for the improvement of CPA/IFO treatment regimes in regards to specificity and side effects is activation of CPA/IFO prodrug by liver enzymes and the systemic distribution of cytotoxic metabolites via the vasculature. Enzymatic conversion of CPA/IFO in the tumor site is in general prevented due to low endogenous CYP P450 activity in tumor cells. Conversion of CPA prodrug in the tumor area would result in relocation of cytotoxic metabolites in terms of high local concentrations of antitumoral active metabolites combined with a lower systemic burden compared to conventional CPA/IFO treatment regimes. Therefore, delivery of plasmids encoding for CPA/IFO converting enzymes to tumor cells, is a promising approach in improving CPA/IFO treatment (GDEPT, gene directed enzyme prodrug therapy).

While several hundreds of isoenzymes pertain to the family of **P450 enzymes**, only some of them contribute to the conversion of CPA and IFO. Primary, CPA/IFO activation by 4-OH hydroxylation reaction is catalyzed by P4502B and P4502C isoforms (103). P4502C isoforms exhibit fast conversion, however, application in the classic GDEPT concept is prevented due to saturation effects (104). Human CYP3A4 and CYP2B6 were found to activate the CPA prodrug very efficiently (105), however, CYP3A4 conversion resulted beneath hydroxylation of CPA in neurotoxic and nephrotoxic side products. In contrast, enzymatic activity of CYP2B1 and CYP2B6 is restricted on hydroxylation reaction, leading to the antitumoral active phosphoramid mustard (106).

In the context of this thesis, evaluation of this approach was performed with plasmid DNA encoding for rat CYP2B1 enzyme, due to substantial evaluations and characterizations of prior studies (107-111). For sufficient expression levels of the therapeutic gene in tumor cells, CYP2B1 expression was regulated by a highly efficient CMV-promoter/enhancer.

Evaluation of sensitizing tumor cells towards CPA/IFO treatment via CYP2B1 expression was performed in standard cell culture and additionally in the agarose overlay system, mimicking tumor environmental characteristics. Finally this GDEPT approach was investigated in vivo by intratumoral CYP2B1 gene transfer followed by CPA treatment in a CT26 xenograft tumor model.

Conventional cell culture

Evaluation of sensitizing tumor cells towards CPA/IFO treatment via CYP2B1 expression was performed on transiently transfected cells as well as on stably transfected cell lines. Different from prior studies on the CYP/CPA combination, attention was focused to low CPA concentrations, reflecting the metronomic scheduled CPA treatment regimes and not high dose therapy.

Beside assurance of expressed CYP2B1 protein in transfected cells via specific antibody staining, special attention was set to the evaluation of **enzymatic activity**. Enzymatic activity does not directly correlate, of necessity, on CYP protein content. Beneath environmental conditions (50) other factors are crucial for CYP2B1 enzymatic activity (112-114). Therefore two different **assays** for detecting CYP2B1 enzymatic activity were performed. The acrolein assay that directly reflects conversion of CPA/IFO was found to suffer from low signal to noise ratios, especially in culture systems with low CPA concentrations. Low detection rate of free acrolein in supernatants may be due to covalent reaction to serum proteins, present in the cell culture medium. To circumvent low sensitivity of the acrolein assay a modified resorufin assay was used for evaluation of CYP enzymatic activity. Resorufin recovery in serum containing biological fluids was easily detectable due to high sensitivity and sufficient signal to noise ratio. Therefore the resorufin assay was used by default to evaluate CYP2B1 enzymatic activity in the thesis.

In following studies, **wt tumor** cell lines and the CYP2B1 expressing X39- and 9L-D2B1 cells were analyzed on CYP2B1 enzymatic activity via resorufin assay. In line with literature, wt tumor cell lines exhibited only very low conversion capability (115); however, compared to CT26, 9L and Neuro2A, HUH7 cells exhibited 10-fold higher CYP activity in the resorufin assay (FIG 3-2). Elevated conversion capability of HUH7 cells can be explained by their origin on human hepatocytes, whereas enzymatic activity of severally CYP P450 systems were detected (116).

Stabely transfected **CYP2B1 expressing** cell lines X39 and 9L-D2B1 showed high enzymatic activity, whereas resorufin conversion capability of X39 cells was about twice as high in comparison to 9L-D2B1. This result was confirmed by the acrolein assay, indicating high relevance of the resorufin assay in terms of CPA metabolism (FIG 3-8 and 3-9).

Further on, sensitivity of wt CT26 and Neuro2A tumor cells towards **CPA** and **IFO** treatment was investigated. Treatment with IFO resulted in enhanced antiproliferative

effects compared to CPA; low CYP2B1 levels in this wt cancer cell lines indicate higher unspecific toxicity of the IFO prodrug (FIG 3-4). This phenomena may be based on the non-enzymatic hydrolysation reaction of IFO that is catalyzed by anorganic phosphates and results in the formation of cytotoxic chlorethylamine (117-119). No enhanced sensitivity of stable expressing CYP2B1 X39 tumor cells towards IFO treatment was detected (FIG 3-12). Enhanced sensitivity towards CPA treatment was detected when stable CYP2B1 expressing tumor cell lines X39 and 9L-D2B1 were cultured with CPA compared to the corresponding wt tumor cells (FIG 3-10). This indicates in situ conversion of CPA to cytotoxic metabolites and is a **proof of principle** for this GDEPT concept.

Even at low concentrations, relevant for the in vivo situation significantly decreased proliferation and survival was detected for both CYP2B1 expressing cell lines. In this context CYP2B1 high expressing X39 tumor cells tended to exhibit enhanced suicidal effects compared to 9L-D2B1 cells. However, due to predominantly apoptotic processes, induced by the in situ formed phosphoramid mustard (120;121), correlation of enzymatic activity and suicidal effects are not necessary direct. Beside the delivery of stably transfected, encapsulated, CYP2B1 expressing cells (31), in vivo approaches within the GDEPT concept includes strategies with tumor targeted gene transfer vehicles leading to transient expression of the therapeutic gene in tumor cells. **Transient transfection** of Neuro2A and 9L cells resulted in detectable enzymatic activity of the expressed CYP2B1 enzyme within 20h after the transfection. Maximum enzymatic activity was measured in Neuro2A tumor cells 60h after the transfection, whereas activity levels in transfected 9L cells were more constant over the observation period (FIG 3-14).

CYP2B1 enzymatic activity levels of Neuro2A cells were about two times (at maximal enzymatic activity, 60h after the transfection) compared to 9L cells when total transfection rates (measured by EGFP reporter gene expression) were considered. In the case of CYP2B1 plasmid DNA delivery to CT26 tumor cells no enhanced enzymatic activity was detectable in the resorufin assay despite similar transfection rates as detected in 9L cells via EGFP reporter gene expression.

Differences in CYP2B1 enzymatic activity after gene delivery are critically depending on several cellular characteristics. Beside influences on protein expression levels, several factors are crucial for enzymatic activity. Predominately, supply with NADH reduction equivalents by the P450 reducase were described for the 9L cell line (122);

additional effects on CYP2B1 activity might result form differences of total metabolic activity and characteristics of the endoplasmatic reticulum (123).

After transient transfections with LPEI polyplexes only a part of the cell population is transfected successfully. Thus, **bystander** activity is crucial. Malfunction can therefore result, beneath insufficient CYP2B1 expression and activity, from dilution effects in conventional cell culture. This effect seem to play an important role when enzymatic activity is rather low (50). In transwell coculture systems of wt CT26 and CYP2B1 expressing tumor cells influence of proliferation and survival was detected in both compartments when culturing was performed in the presence of 0.5mM CPA (FIG 3-13). In contrast to other GDEPT-based enzyme/prodrug combinations, e.g. herpes simplex virus thymidine kinase/ganciclovir, 4-OH-CPA readily diffuses across cell membranes and is not dependent on direct cell-cell contact for bystander killing (50).

However, strong cytotoxic effects were only detected for the 4-OH-CPA producing X39, whereas the wt CT26 acceptor cells only exhibited a moderate response in terms of proliferation and survival. This result indicates the importance of dilution effects especially in a low dose CPA GDEPT concept in vitro. In addition, 4-OH-CPA is very unstable and breaks down with a half-life time of only 17 min at 37ºC in serum containing medium (50). Efficiency of bystander effect seems to be dramatically linked to degrading of 4-OH-CPA and dilution effects. In vitro artifacts were circumvented by the development of the agarose overlay technique, mimicking limited diffusion effects of tumor tissue.

Evaluation of the CPA GDEPT approach in the agarose overlay system

Drug diffusion and concentration effects within the tumor tissue play an important role in the action of drugs such as CPA due to the short half-life of its active metabolites (124). Tumor cell uptake of CPA and 4-OH-CPA is facilitated by the low extracellular pH associated with tumors, which may increase intracellular accumulation of this weakly acidic drug and its metabolite by an ion trapping mechanism (125). The tumor microenvironment has a substantial impact on the response of tumor cells to cytotoxic agents (126). The diffusion of nutrients, drugs and metabolites within a solid tumor is limited. Moreover, most solid tumors are characterized by extended hypoxic regions and areas with an acidic microenvironment (127).

In addition to the level of CYP gene expression, the extent of CPA activation is highly dependent on the **availability of oxygen**, which is a cosubstrate for all CYP-catalyzed monooxygenation reactions. Low oxygen pressure resulting from insufficient blood supply is a hallmark of solid tumors (128). Despite the limited oxygen supply, excellent antitumor activity was reported in mouse and rat models of GDEPT using CYP2B enzymes (122;129), with some indications of efficiency reported in initial clinical trials after local delivery of a CYP gene (130).
Results obtained in bystander experiments of prior studies may be non-physiological and reflect the unnatural environment of conventional cell culture. Therefore, the CYP-CPA-GDEPT strategy was evaluated by using an **agarose overlay technique** to study the effect of limited diffusion and reduced oxygen supply on the bystander cytotoxicity of CYP activated CPA.

Agarose has been described as a suitable material for simulation of diffusion within a solid tumor (131). This effect was confirmed by injecting the membrane-permeable DNA dye Hoechst 33258 into the agarose layer. The **limited diffusion** of this dye led to the formation of a concentration gradient and the staining of tumor cell nuclei in the immediate vicinity of the injection site (FIG 3-16).
Beside bystander activity in the environment mimicking cell culture model, the impact of the agarose layer was evaluated in terms of cell morphology, proliferation rate and induction of hypoxia sensitive gene expression.
Within 24h of agarose overlay no obvious changes in cell morphology (FIG 3-17) and no induction of hypoxia induced gene expression was detected (FIG 3-19). However, cell proliferation rate was influenced when cells were cultured under an agarose layer for several days (FIG 3-18). Oxygen deprivation under the agarose layer was not leading to hypoxia induced gene expression within 24h, measured by luciferase expression under control of a HRE (hypoxic responsive element) containing promoter. This indicates that the agarose overlay reflects areas in the tumor with moderate hypoxia. Despite the lack of hypoxia induced gene expression, the agarose overlay imposed an apparent **hypoxic environment** on the cells, as shown by the 88% decrease in CYP metabolic activity of X39 tumor cells cultured under an agarose layer, which corresponds to the CYP activity at an ambient oxygen content of 2% (v/v) (FIG 3-21).
Regardless of reduced CYP activity, however, the CYP-expressing tumor cells cultured with the agarose overlay exhibited an **enhanced bystander** cytotoxic effect.

The increased bystander activity was seen in experiments with cocultures of CYP-expressing cells and CYP-deficient cells, and in experiments where the CYP gene was introduced by transient transfection.

Thus, with the agarose overlay, a population of 25% CYP-expressing X39 cells killed 80% of the overall tumor cell population compared to only 13% tumor cell killing in the absence of the overlay. Of note, X39 cells exerted greater bystander toxicity in HUH7 hepatoma cells compared to CT26 cells. The enhanced sensitivity of the HUH7 cells towards CPA may in part be due to the intrinsic CYP activity of HUH7 cells, which is ~2% of that seen with the X39 clone.

CPA induced decrease of cell survival in the agarose overlay model resulted in similar kinetics as in conventional cell culture when CYP2B1 expressing X39 tumor cells were cocultured with CT26 or Neuro2A cells. However, decrease in survival was more pronounced and was maximal at the third day of treatment under the agarose layer. The similar kinetic indicates that the mechanism of induced cytotoxicity is not influenced by the agarose overlay. The latency period of one to two days concede the case for maintaining an induction of apoptotic cell death also in the tumor environment mimicking cell culture model (FIG 3-23).

Short-term treatment (5 h) with 0.5 mM CPA should mimic the in vivo situation, where short exposures to CPA at peak levels of <1 mM can be found in tumor tissue, even after a high dose bolus of CPA (132). In the transient transfection studies, where only a limited number of cells expressed CYP2B1 (13%, estimated based on CYP2B1 antibody staining and EGFP as reporter gene in a parallel experiment), a clear CPA-induced killing effect was only observed for cells cultured under an agarose layer (FIG 3-25).

In conclusion, the present studies highlight the utility of an agarose overlay method that mimics moderate hypoxic areas in the tumor tissue and restricted diffusion of activated drug metabolites. In the case of CYP2B1-dependent CPA activation, the restricted diffusion of activated metabolites out from the tumor cell microenvironment is likely to prolong the exposure to elevated concentrations of active metabolites that play a crucial role in enhancing bystander cytotoxicity. Despite the fact that CYP activity, and therefore prodrug activation, is substantially reduced under the hypoxic conditions imposed by the agarose overlay, a strong bystander effect could nevertheless be observed as a consequence of the restricted diffusion of active metabolites. This bystander effect becomes even more important at low oxygen

concentrations and under conditions where only a limited fraction of the tumor cells express the *CYP* gene, as is likely to be the case in any in vivo gene delivery situation.

In vivo evaluation of the CPA GDEPT approach

For further evaluation of the CYP-CPA GDEPT strategy, CYP2B1 plasmid DNA was delivered to **subcutaneous CT26 tumors** via electroporation, followed by systemic CPA treatment on 2 consecutive days after gene transfer. Pronounced decrease in tumor growth was observed for CPA treatment regime combined with gene transfer (FIG 3-29). Interestingly, also transfection with an empty control plasmid increased antitumoral effects of treatment, which can be explained by several factors. Already electroporation of the tumor alone led to reduced tumor growth in certain cases (Silke van der Piepen, unpublished results). Moreover, local application of plasmid DNA can evoke enhanced immune response due to non methylated CpG sequences (133).
Control experiments with subcutaneous CYP2B1 expressing X39 cells in SCID mice with a similar CPA treatment regime (without gene transfer via electroporation) did not result in enhanced antitumoral activity compared to wt CT26 xenografts. Therefore, primary resistance was supposed in the CT26 xenograft model.

4.2 Extended GDEPT concept – antiangiogenic approach

Antiangiogenic approaches exhibit several advantages in comparison to conventional strategies in tumor treatment, e.g. reduced side effects. Therefore the CYP/CPA GDEPT approach was extended on endothelial cells and the strategy of locally activated CPA was evaluated with attention to **antiangiogenic effects**.
The bystander effect of in situ activated CPA via CYP2B1 expressing X39 tumor cells (producer) on primary endothelial cells (acceptor) was investigated in terms of critical key steps in the angiogenic process. Endothelial cells exhibit only low CYP activity and are therefore not able to contribute to CPA conversion. This results in low sensitivity towards CPA treatment (FIG 3-30). In prior studies, however, impact on proliferation and migration capability were detected when primary endothelial cells were cultured with 4-OH-CPA (20). Coculturing endothelial cells with CYP2B1 expressing tumor cells resulted in increased sensitivity in terms of **proliferation** and survival towards CPA treatment. Interestingly, PEC cells exhibited pronounced sensitization compared to HUVEC cells (FIG 3-31 and 3-32). In the case of coculturing producer and acceptor cells in a transwell system, bystander activity was

evident on PEC but not on HUVEC cells (FIG 3-33 and 3-34). Differences in sensitivity in the context of proliferation and survival are supposed to be provoked by higher proliferation rate of PEC cells due to certain cell cycle specificity of the phosphoramid mustard. However, several other factors including phenotype and species might be involved in the difference of sensitization towards CPA and its metabolites. In particular, differences in cellular GSH levels are crucial in the detoxification of the metabolite acrolein (134); interestingly, treatment of primary PEC and HUVEC cells with acrolein alone resulted in similar difference in sensitivity (FIG 3-40); in this context HUVEC cells were shown to exhibit an adaptive protection system (135). In addition, acrolein was shown to exhibit a more potent impact on cell death in the case of endothelial cells than the metabolite phosphoramid mustard (136).

Further on, the impact of in situ activated CPA was evaluated in terms of **antimigrative** effects on primary endothelial cells by coculturing with CYP2B1 expressing X39 cells. HUVEC as well as PEC cells exhibited decreased migration capabilities, however, antimigrative effects were less distinctive compared to treatment with 4-OH-CPA (20). Reasons for non significant effects on migration might result from different pharmacokinetics of in situ activated CPA and 4-OH-CPA administered directly to the cell culture medium. However, CPA conversion by CYP2B1 expressing X39 tumor cells is sufficient to inhibit endothelial **differentiation** processes via bystander activity (FIG 3-35). Control experiments with wt CT26 tumor cells indicate that disturbance of differentiation processes are specific in terms of CYP2B1 expression in the presence of CPA. Moreover, changes in the rearrangement of endothelial **F-actin cytoskeleton** was only detected in coculture systems with CYP2B1 expressing tumor cells in the presence of CPA (FIG 3-36).

In the GDEPT strategy, CYP2B1 expressing tumor cells can be utilized as producer cells for activated CPA metabolites, inhibiting crucial key steps in the angiogenic process. The bystander principle can therefore be extended on endothelial acceptor cells in terms of an antiangiogenic treatment approach.

4.3 Acrolein – unwanted side product or contribution to antiangiogenic properties of metronomic CPA therapy?

Metronomically scheduled CPA has been linked to antiangiogenic effects, reduced tumor blood supply and decreased side effects compared to conventional high dose CPA therapy (19). Moreover, activated CPA was shown to inhibit endothelial cell proliferation and migration in vitro and endothelial cell apoptosis in experimentally in vivo tumors (17;20). Modulation of endogenous antiangiogenic cytokines like thrombospondin-1 by metronomic scheduled CPA was described and is discussed as a potential mediator of antiangiogenic effects of this approach (21;22;93;137).

CPA is an anticancer prodrug that is dependent on cytochrom P450 metabolism to be activated to the first metabolite 4-OH-CPA. In vivo, this hydroxylation reaction is predominantly conducted by liver P450 cytochrom systems. The activated drug is released to the blood stream and distributed systemically over the body including the tumor site. 4-OH-CPA exists in equilibrium with aldophosphamide that releases spontaneously the phosphoramid mustard and **acrolein**. Antitumor activity was accredit to the phosphoramid mustard whereas acrolein was considered as a **side product**, responsible for unwanted side effects (138). However, some recent studies certify antitumor modulating effects, e.g. over modulation of the immunosystem, to acrolein, predominantly within low dose CPA therapy regimes (139-142).

For in vivo evaluation, CT26 xenografts were treated with a metronomic low dose CPA therapy regime (40mg/kg on two consecutive days, followed by two days without treatment). CPA treatment resulted in significant decreased tumor growth compared to the untreated control group (FIG 3-29). Possible antiangiogenic effects of this treatment regime were analyzed by intravenously injection of Hoechst33258 dye as a tracer. By performing this method only **functional tumor blood vessels** are visualized. In recent studies, tumor vessels are quantified after visualizing vessel cell markers by antibody staining, e.g. CD31. However, staining for vessel markers and quantification of anatomically present tumor blood vessels does not give evidence for the contribution of indicated vessels on tumor blood supply. Even in non treated experimental subcutaneous tumors, great discrepancy between CD31 stained tumor vessels and functional vessels was detected (not shown). Due to the fact that blood supply in tumors is very heterogeneous and experimentally subcutaneous grown tumors are often characterized by a necrotic central area and highly proliferating regions in the periphery, measurements were performed separately for three different areas (central, middle and peripheral area). Tumor blood supply of the peripheral

area of the tumors tended to be higher than in the central parts of the analyzed tissue, indicated by enhanced Hoechst33258 fluorescence signal. CPA treatment resulted in decreased tumor blood supply in all three tumor areas , whereas reduction was most pronounced in the peripheral areas. Tumor cell proliferation and angiogenic processes are most active in the peripheral areas of experimental subcutaneous tumors. Distinct reduction of **blood supply** in this proliferation zones indicated that the performed low dose CPA treatment regime indeed affected the forming of new functional blood vessels in terms of antiangiogenic therapy (FIG 3-37). For further investigation of a possible contribution of acrolein to antiangiogenic properties of low dose CPA scheduling, tumor tissue was analyzed for the presence of **acrolein adducts** by specific antibody staining against mouse CD31. Indeed, acrolein modified proteins were detected within the tumor tissue of CPA treated CT26 tumors. Moreover, colocalisation of CD31 and acrolein adduct antibody staining was evident, indicating a possible impact of acrolein on tumor endothelial cells (FIG 3-38). Acrolein adducts were also detected in prior studies far away form the site of CPA activation; e.g. acrolein-lysin adducts were located in aorta walls of CPA treated rats (143). Delivery of acrolein towards the tumor site can occur directly by 4-OH-CPA or aldophosphamide, respectively, due to relevant concentrations of these metabolites in peripheral blood (144). A second pathway of acrolein transport to the tumor tissue may be supported via thiol conjugates. In this context, these metabolites are described for transporting and releasing acrolein via β-elimination and were identified for delivery of toxic side effects of acrolein to distant organs like lung and bladder (145;146). Notably, tumor regions with increased acrolein adduct content displayed reduced tumor blood supply as identified by low Hoechst33258 staining. The in vivo results initiated further in vitro studies to evaluate a possible role for contribution of acrolein to the antiangiogenic effects of metronomic CPA therapy.

Antiangiogenic properties of acrolein on **primary endothelial** cells were evaluated in terms of classical antiangiogenic assays including proliferation, migration and differentiation studies. Further on, the impact of acrolein was assayed in terms of crucial cellular mechanisms that are linked to cell survival, migration and angiogenic phenotype.

Proliferation

Growing tumors require flexible adaptation and expanding tumor vessel networks. A basic requirement for the expansion of the vessel network is therefore the entrance of usually resting endothelial cells into cell cycle. The switch from resting endothelial cells to an angiogenic active phenotype is driven by several factors like hypoxia, released proangiogenic factors and other tumor environmental conditions. Culturing of primary endothelial cells in the presence of acrolein resulted in decreased proliferation and survival (FIG 3-40). In prior studies it was shown that acrolein is the crucial metabolite affecting endothelial cells survival; the metabolite phosphoramid mustard was recognized in this context to exhibit a minor role (147). Moreover, acrolein was shown to have the potential of inhibiting cell cycle regulating proteins (148).

Migration

Cell motility and migration are critical aspects in tumor progression influencing the sprouting of new blood vessels in the angiogenic process, cancer cell invasion and metastasis (149). During tumor blood vessel formation angiogenic endothelial cells migrate towards the direction of the angiogenic stimuli (chemotaxis). During the migration process further proliferation of endothelial cells can occur. Prior studies exhibited antimigrative effects of 4-OH-CPA on primary endothelial cells (20). However, treatment with acrolein alone inhibited endothelial cell migration in a dose dependent manner (FIG 3-41). Disturbance of cell migration by acrolein was more pronounced than in experiments with enzymatically in situ activated CPA. This difference in migration capability might result from different pharmacokinetics of acrolein which is released by enzymatic activated CPA and acrolein which is administrated directly to the cell culture medium.

Differentiation

Another crucial step in the angiogenic process is the endothelium specific differentiation of vascular cells in order to form lumen and functional blood vessels. Therefore potential antiangiogenic active drugs are evaluated for disturbing this differentiation processes. The matrigel assay operates on the capability of primary endothelial cells to form tube-like structures when cultured on a supportive matrix (150). The differentiation processes are promoted by different protein structures in the gel; laminin and to a lesser extend collagen IV seem to be the key regulator elements which interact with cellular surface receptors. Moreover, several

proangiogenic factors and growth factors like bFGF and EGF are embedded in the matrix. Morphological differentiation is rapid and occurs within several hours (151). Performing the matrigel tube formation assay in the presence of indicated concentrations of acrolein in the medium resulted in a pronounced and dose dependent inhibition of tube forming (FIG 3-42 and 3-43).

In summary, acrolein **disturbs crucial key steps** in the angiogenic process including proliferation, migration and differentiation

Actin cytoskeleton and integrin αvβ3 receptors

Dynamics of the actin cytoskeleton is a key element in cell migration and differentiation processes of endothelial cells (152). VEGF induces angiogenic activation of endothelial cells by assessing endothelial stress fiber assembly and **F-actin** cytoskeletal rearrangements are a very early step in the angiogenic process (153). While cell cycle proteins and apoptosis have been under investigation for anti-cancer drug development for several years, processes involved in controlling actin cytoskeleton dynamics, responsible for cell motility and cell shape, receives increasing attention. Actin cytoskeleton of endothelial cells and inhibitors for actin based endothelial cell migration are mainly investigated in the context of developing new antiangiogenic drugs or in mechanistic evaluation of already known antiangiogenic compounds. Disturbance of the endothelial F-actin cytoskeleton results in decreased migration and tube/capillary forming ability.

Actin has several nucleophilic reaction sites and can be targeted for Michael adduction. Acrolein was shown to react with actin in cell free systems in a dose dependent manner, leading to structural distortions and changes in polymerization rates. Moreover, it was shown that acrolein leads to the breakdown of the actin cytoskeleton in fibroblasts (154).

In this thesis a breakdown of the F-actin cytoskeleton was detected in primary endothelial cells when coculture experiments with CYP2B1 expressing X39 tumor cells were performed in the presence of CPA (FIG 3-36). Further, acrolein interacted with F-actin of HUVEC cells in a dose dependent manner and leads to the breakdown of the F-actin cytoskeleton (FIG 3-44), accounting for the ability of acrolein to inhibit cell migration and tube forming morphogenesis.

Endothelial cell adhesion molecules of the **integrin** family are critical mediators and regulators in the angiogenic process. Integrins are heterodimeric cell surface molecules consisting of two associated subunits (α and β) providing physical interaction with the extracellular matrix and are linked with the F-actin cytoskeleton (94;155); therefore integrins exhibit a crucial role for adhesion and migration processes. Especially, integrin αvβ3 is one of the central surface molecules in capillary forming during the angiogenic process (156). Moreover, integrins interact with several signaling pathways via cytoplasmic domains and are necessary for signaling events essential for cell survival, proliferation, migration and differentiation of endothelial cells (157). Following adhesion, integrin receptor clustering occur which recruit cytoskeletal and cytoplasmatic proteins to link the new formed integrin complexes to the actin cytoskeleton. The integrin signaling leads to cytoskeletal rearrangements, entry into S-phase of the cell cycle and as well to integrin mediated gene transcription (94). Several studies showed that disturbance of integrin αvβ3 clustering results in antiangiogenic effects in vitro and in vivo.
Specific antibody staining for integrin αvβ3 receptors exhibited dramatically changes in cell surface distribution on cultured primary endothelial cells after treatment with acrolein. Notably, integrin receptor clustering, being essential for signal transduction, was diminished. Moreover, accumulation of integrin αvβ3 receptors at filopodia structures, providing adhesion in migration processes, were prevented (FIG 3-45). Total expression levels, analyzed by antibody staining followed by FACS analyses, however, were not changed during observation period.

In summary, disturbance of integrin αvβ3 clustering by acrolein and the influence on regulation of F-acting cytoskeletal rearrangements indicate profound interference of acrolein with angiogenic processes. Additionally, results suggest possible mechanistic insights in the direct effects of acrolein on endothelial cell migration and differentiation.

NF-κB levels

Besides direct interference of acrolein with integrins and the F-actin cytoskeleton, modulation of NF-κB levels by acrolein was assayed. **NF-κB** signaling plays a critical role in cancer development, progression, angiogenesis and influences response to chemotherapy. In this context hypoxia (158) but also hormones (159) and growth

factors like EGF (160) were identified as important triggers of NF-κB activity. High levels of NF-κB were shown to be linked with cancer cell survival, expression of proteases (e.g. MPPs) and upregulation of proangiogenic cytokines (161;162).
Several proangiogenic factors and extracellular matrix degrading enzymes are not only secreted by tumor cells themselves but additionally by stromal fibroblasts in the vicinity of tumor cells. Also in fibroblasts the expression of critical proangiogenic genes are regulated by NF-κB and fibroblasts NF-κB activity levels are in turn regulated by cytokines released from tumor cells (163).

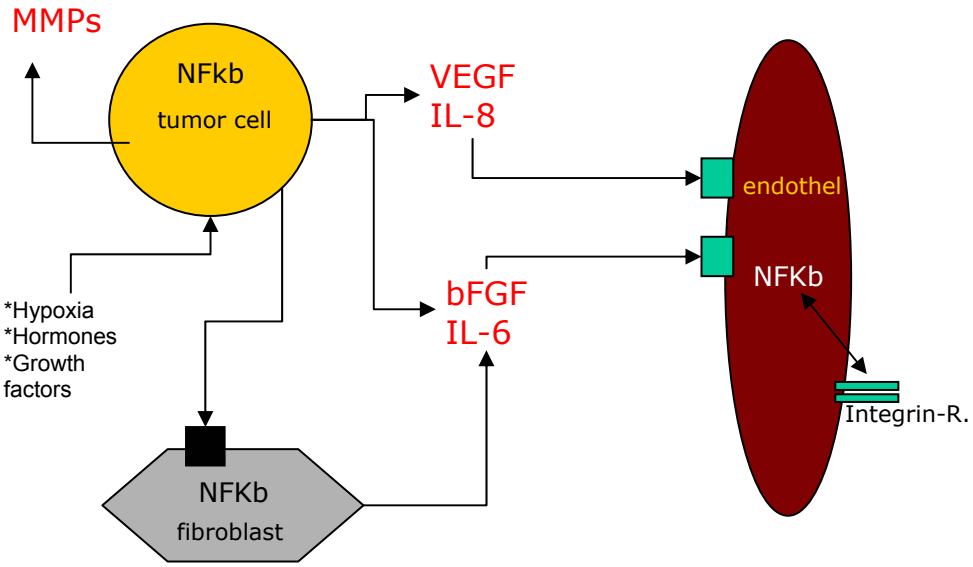

Fig.: 4-1 Network of tumor, tumor stroma and endothelial cells in the regulation of proangiogenic processes, leading to tumor progression and neovascularisation.

This network of paracrine effects, based on NF-κB mediation, indicates NF-κB as a promising target in tumor therapy. Therefore contribution of acrolein on antiangiogenic effects regarding metronomic CPA treatment was assayed in the context of NF-κB regulation in CT26 tumor cells, primary fibroblasts and as well in primary endothelial cells (HUVECs). Downregulation of NF-κB activity levels by acrolein was described for human A549 lung **tumor cells** (164); however modulation of NF-κB was not evident in CT26 tumor cells (FIG 4-50). Therefore it is assumed that effects of acrolein on CT26 tumors are not based on NF-κB dependent pathways. However, influence of acrolein on other pathways in terms of the expression of proangiogenic cytokines, have to be evaluated.
Analyzing primary **fibroblasts** in terms of modulation on NF-κB activity levels due to acrolein treatment resulted in a dose dependent inhibition of NF-κB activity within 6h (FIG 3-51A). Moreover, acrolein treatment reduced fibroblast cell survival within 24h (FIG 3-52B). Therefore, it is assumed that acrolein can interact with tumor supportive

stromal fibroblasts and may contribute to antiangiogenic effects of CPA therapy by reducing NF-κB regulated output of proangiogenic factors.

NF-κB activity is crucial for regulation of angiogenic or resting phenotype in **endothelial cells**. Autocrine expression of several proangiogenic factors are modulated by NF-κB (165;166). On the other hand proangiogenic factors like VEGF (167) can in turn activate NF-κB signaling in endothelial cells. Moreover, inhibition of NF-κB signaling inhibits bFGF induced angiogenesis (168) and resulted in inhibition of tube formation in in vitro matrigel assays (169). Another potential mechanism by which NF-κB may promote angiogenesis is via autocrine effects inducing endothelial VEGF expression. (170). In addition, NF-κB was identified as an important signaling molecule in integrin αvβ3 mediated endothelial cell survival (171) and was linked to the PI3K/Akt pathway (172), influencing survival, proliferation and differention. As tumor derived endothelial cells show upregulation of the PI3K/Akt pathway, suppression of TSP-1 expression was functionally linked to an upregulated PI3K/Akt pathway (173).

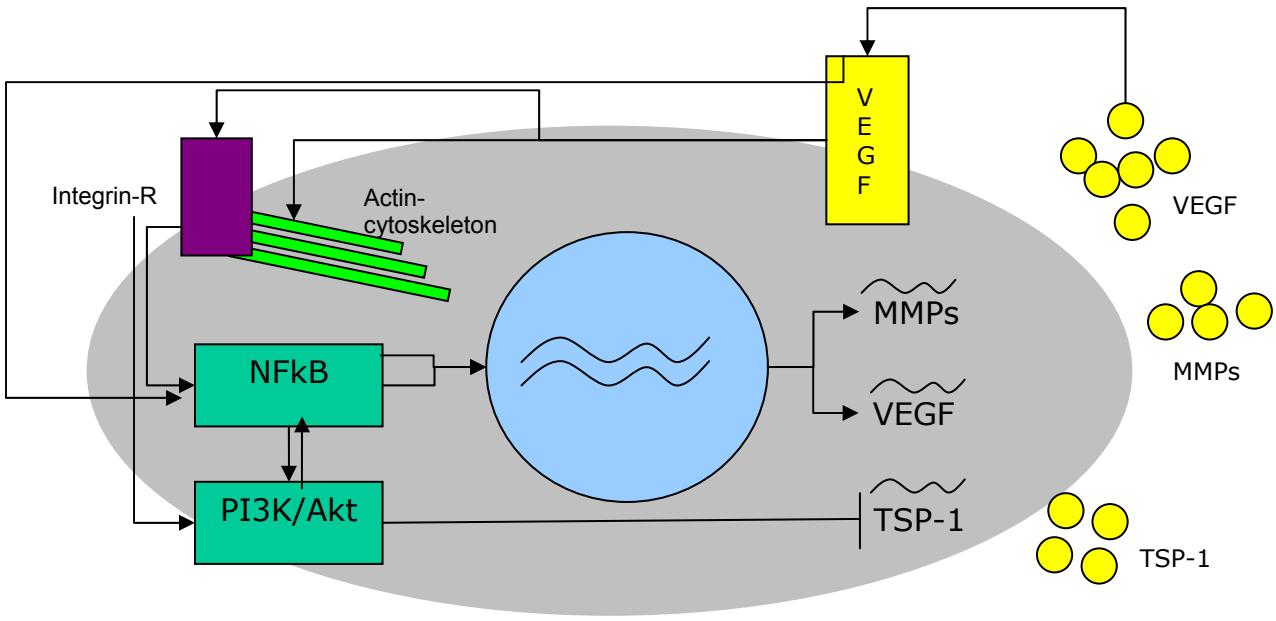

Fig.: 4-2 Interplay of important receptors, cytokines, pathways and the cytoskeleton in an angiogenic active endothelial cell

Reduction of NF-κB activity was significant when HUVEC cells were treated with 10µM acrolein for 24h. Decrease in NF-κB activity was even more pronounced when treatment was carried out with 20µM acrolein. Interestingly, culturing HUVEC cells with 30 µM acrolein resulted in highly increased NF-κB activity levels (FIG 3-46). This increase, however, seems to be not relevant in the context of angiogenesis, due to

the fact that treatment of HUVEC cells with 30µM or higher concentrations of acrolein were shown to interfere with cell survival after 3 days of treatment (unpublished results).

Thrombospondin-1

The hypothesis that acrolein interferes partly via NF-κB in the regulation of endothelial angiogenic phenotype may be assured by the expression profile of TSP-1 in HUVEC cells. **TSP-1 expression** was found to be highly upregulated in HUVEC cells cultured with 5, 10, and 20µM acrolein for 24h (FIG 3-48). TSP-1 expression falls back to control levels when treatment was carried out with 30µM acrolein and above. However, the strongest induction in TSP-1 expression was detected at a concentration of 5 µM, whereby NF-κB activity levels were reduced in a dose dependent manner with minimal activity levels at 20.0µM acrolein. These data suggest participation of other pathways involved in the acrolein affected regulation of TSP-1 expression. Other regulatory proteins affected by acrolein might be AP-1 (activator protein 1) (148;174), or the modulation of JNK- (175;176) and PKC pathways (177;178). Enhanced TSP-1 expression levels, however, seems to be specific, as general protein expression is downregulated, indicated by decreased luciferase expression levels after transfection with pCMV-LUC and acrolein treatment (not shown).

In conclusion, acrolein was shown to **inhibit several crucial steps** of the angiogenic process. Further on, disturbance of integrin clustering and reorganization processes of the F-actin cytoskeleton was detected in acrolein treated primary endothelial cells. Modulation of endothelial NF-κB regulated gene expression by acrolein and induction of TSP-1 expression was evident. Due to prior studies, TSP-1 is one of the most important endogenous inhibitors of angiogenesis and was functionally linked to metronomic CPA therapy regimes. The detection of acrolein protein adducts in tumors and especially acrolein modified endothelial cells suggest an important contribution of acrolein to antiangiogenic effects of metronomic CPA treatment regimes.

4.4 Resistance towards CPA treatment

Chemotherapy is the standard treatment in metastasized cancers. A major drawback of such treatment regimes, however, is resistance that either exists from the beginning of treatment (primary resistance) or is developed during chemotherapy (secondary resistance).

4.4.1 Primary resistance

Primary resistance is an existing obstacle in several types of cancer. Interestingly, drug resistant phenotypes described in several studies occur in multicellular tumor spheroids or in in vivo tumor models but not in monolayer cultures (179).

As described in chapter 1, CT26 tumor cells were highly sensitized towards CPA treatment in **monolayer cultures** when CYP2B1 gene expression was evident. However, this sensitizing effect was diminished when CYP2B1 expressing CT26 tumor cells (X39) were grown as subcutaneous tumors **in vivo** from the beginning of CPA treatment (FIG 3-56). Therefore, failure of sensitizing towards CPA treatment was classified as primary resistance.

In order to exclude the possibility of downregulation of therapeutically expressed CYP2B1 protein or to recognize possible selection effects occurring under CPA treatment, tumor tissue was collected and analyzed for CYP2B1 expression by specific antibody staining at the end of treatment. CYP2B1 expression was evident in control as well as in CPA treated tumors, indicating that the non-response towards treatment is not based on changes in expression levels or selection processes (FIG 3-57).

For further evaluation of this effect, CYP2B1 expressing X39 tumor cells were cultured in a combined cell culture system including a monolayer section as well as three dimensional grown X39 **spheroids**. The compartments in the system were connected over a joint medium reservoir to assure the exchange of free diffusible metabolites occurring in CPA prodrug conversion. Reduction in cell survival and proliferation in the monolayer section was even more pronounced than in standard cell culture experiments performed in chapter 1; whereas reduction in the multicellular tumor spheroid compartment was not pronounced (FIG 3-52). Killing rate in the monolayer section indicates high total concentrations of activated CPA in the joint medium by contribution of multicellular tumor spheroids to CPA conversion.

This is contradictive to the possibility of inadequate CPA conversion within the agarose wrapped spheroids due to limitations of oxygen supply as an explanation for insufficient cytotoxic effects in the spheroid compartment. In addition, limitations in oxygen supply by an agarose layer were detected to exhibit only a secondary role in the efficiency of CPA to induce cell death.

The possibility of insufficient diffusion of CPA prodrug to agarose wrapped X39 tumor cells were excluded by control experiments with prematured X39 tumor spheroids, exhibiting similar sensitivity towards CPA treatment as X39 cells grown as a monolayer (data not shown). In addition, analyses of multicellular tumor spheroids for **CYP2B1 expression** via specific antibody staining resulted in similar CYP2B1 expression for treated X39 multicellular tumor spheroids and not treated control spheroids. Hoechst33258 counterstaining in agarose wrapped X39 microspheres resulted in the detection of fragmented cell nuclei in CPA treated tumor spheroids, indicating presence of active CPA metabolites and deterioration of tumor cells (FIG 3-53). Further evaluation of resistance in the multicellular spheroid model of established wt CT26 tumor spheroids resulted in decreased sensitivity to 4-OOH-CPA compared to the monolayer systems. By the use of 4-OOH-CPA, which breaks up into phosphoramid mustard and acrolein without enzymatic conversion, effects in terms of enzymatic capability in agarose wrapped tumor microspheres were excluded. This experimental system assures that reduction in CYP2B1 dependent CPA conversion was unincisive in the case of multicellular spheroids, assuring resistance mediated effects via three dimensional conditions in the agarose wrapped microspheres (FIG 3-54).

In conclusion, these results demonstrate that resistance of CT26/X39 cells in vivo is manifested in cell culture only under three dimensional conditions in the case of multicellular tumor spheroids. Since CT26 or X39 cells were not resistant against CPA or 4-OH-CPA treatment, when grown as two dimensional monolayer cultures, (uni)cellular resistance is implausible. In several prior studies phenomena of spontaneous drug resistance in three dimensional conditions were described e.g. for vinca alkaloids and antimetabolites (180;181). Moreover, resistance towards CPA treatment, mediated by three dimensional culture conditions was described for murine mammary tumor cells (182). When treatment is performed with high molecular drugs, resistance phenomena can be explained by limited drug diffusion.

However, in the case of CPA, which is a low molecular weight drug (271 g/mol), this is unlikely to be predominant. This observation suggests that tumor tissue may be able to increase its relative resistance towards cytotoxic CPA metabolites by alterations in tissue architecture resulting in a "**group protection**" of the individual tumor cell. This point of view is assisted by the loss of resistance when treatment is performed on premature spheroid cultures. However, limited diffusion of drugs into the microspheroids seems not to be crucial, indicating other mechanisms of resistance. Usually proliferation rate is reduced in multicellular spheroids, which leads to decreased numbers of cells in the S phase of cell cycle; however, reduction in cell proliferation may play a major role in conventional spheroid culture technology and not in agarose wrapped microspheres due to constant growing over several days (183). Other mechanisms that may be involved are changes in DNA conformation or altered expression of intracellular proteins, surface proteins and cytokines. Changes in the expression of proteins mediating cell-cell or cell-ECM (extracellular matrix) contacts have to be considered. **Integrins** were shown to essentially modulate apoptotic signaling (184) and preventing CPA induced cell death in endothelial and epithelial cells (185). This might be a mechanism in epithelial CT26/X39 tumors, as alterations in cell surface integrin αv receptors of in vitro monolayers compared to subcutaneously grown tumors were observed: integrin αv cell surface receptors were only detected in CT26 tumor tissues (FIG 3-58A), whereas on CT26 tumor cells, cultured as two dimensional monolayers, a very low expression of integrin αv receptors (CD51) was observed (FIG 3-58B). Primary resistance in the context of CT26 and X39 multicellular tumor spheroids is a supposable explanation for GDEPT treatment failure in vivo.

In summary, agarose wrapped **tumor microspheres** seem to be a suitable model system for multicellular mediated drug resistance. Moreover, in contrast to establishing multicellular spheroids e.g. by the liquid overlay technique (186;187), tumor cells maintain proliferating phenotype and form spheroids via cell division over several days, which is a more natural way of generating tumor spheroids (188). Different from other techniques, agarose wrapped spheroids implies the forming of a natural extracellular matrix (189-191).

4.4.2 Secondary resistance

In contrast to primary resistance, secondary resistance is characterized by its development under ongoing therapy of tumors being sensitive prior to treatment. This

type of resistance occurred within the metronomically scheduled CPA treatment regimes of subcutaneous grown **PC3** and **HUH7**. Interestingly, therapy failure became evident around day 50 to day 70 in all both tumor models.

Despite the proposal of avoiding acquired drug resistance by metronomic CPA therapy (192;193), recent studies indicate resistance mechanisms also occurring in this treatment regimes. However, previous reimplantation studies of reisolated tumor cells presented sensitivity towards treatment again, indicating the involvement of other resistance mechanism than conventional acquired multidrug resistance (MDR), which is predominantly based on alterations of tumor cells, e.g. upregulation of DNA repair, modulation of apoptotic pathways or expression of transporter systems (20;194;195).

PC3 xenograft model

Subcutaneous human PC3 tumors in SCID mice were treated with a higher dose of CPA (120mg/kg, compared to treatment of HUH7 (75mg/kg) and Neuro2A (75mg/kg) tumor bearing mice. Tumor volume remained constant up to day 50 after tumor cell implantation, thereafter tumor volume increased despite ongoing CPA therapy. Due to initial sensitivity towards the treatment, resistance was classified as secondary resistance.

Histological analyses of collected tumor tissue, comparing relapsing CPA treated tumors and untreated control tumors resulted in similar tissue structure; however, treated tumors exhibited larger areas of condensed and fragmented cell nuclei, which probably resulted from direct cytotoxic effects of CPA or may be induced by hypoxic effects due to the antiangiogenic scheduling.

Angiogenesis was demonstrated to be associated with the aggressiveness of tumors (196). Recent studies indicate that also non-angiogenesis based mechanisms may exist in certain tumors and are predominately promoted by tumor cell plasticity (197). To give consideration to possible resistance mechanism resulting from metronomic scheduled CPA treatment, which targets predominately tumor vessel cells, immunohistochemical analysis of collected tumor tissues was performed with attention on alterations in **vascular markers**. Analysis of laminin, which is a main compound of the basal lamina of blood vessels, and staining for CD31 positive endothelial cells showed colocalisation in treated as well as in untreated tumors (FIG 4-62). Moreover, the appearance of vascular mimicry in treated PC3 tumors was not evident. Reduction in blood supply, indicated by decreased Hoechst33258 staining

levels contribute to the suggestion that regrowth of tumors are not due to malfunction of antiangiogenic scheduled CPA.

Further on, laminin and CD13, a marker expressed on angiogenic active endothelial cells, only colocalized in untreated control tumors, but not in treated tumors. Tumor angiogenesis is predominately promoted by sprouting form the existing blood vessel network which exhibits laminin as well as CD31 markers (198); therefore, organization and colocalisation of CD13 with vessel markers of already established blood vessels can be interpreted as angiogenesis. Analysis of laminin and CD13 staining indicate that ongoing metronomic CPA therapy is effective regarding antiangiogenic effects; thus the observed resistance likely results from alterations of the tumor cells themselves.

Reisolated tumor cells were characterized and identified in the context of cell **morphology** and **receptor status**; no differences in cell morphology or EGF- or transferrin receptor expression were detected by comparing reisolated tumor cells with PC3 cells from the parental cell line, indicating identity of reisolated cells (FIG 4-64). Due to the involvement of **NF-κB** on mediating resistance towards cytotoxic CPA treatment by modulating apoptotic pathways, the detected upregulation of NF-κB mediated gene expression can contribute to the resistant phenotype (199).

Reisolated tumor cells did not manifest their drug resistant phenotype in two-dimensional **monolayer**, when treatment was performed with 4-OOH-CPA (FIG 4-67). However, drug resistant phenotype of reisolated tumor cells (PC3ID3 and PC3ID4) was manifested after **reimplantation** into mice (FIG 4-68). Immunohistochemical analysis of vascular markers laminin and CD31 in the reimplanted tumors resulted in a similar distribution and colocalisation of laminin and CD31 compared to tumors of parental PC3 cells (FIG 3-68).

Multicellular spheroids were established from PC3ID3 and PC3ID4 reisolated sublines and subjected to 4-OOH-CPA treatment. Interestingly, multicellular spheroids were found to show resistance as detected by MTT assay (MTT, blue staining; FIG 4-3) when 4-OOH-CPA treatment was performed in concentrations that decreased metabolic activity levels in monolayer cultures to 15% of control values in both sublines (FIG 3-66). Comparison with parental PC3 cells failed due to it was not possible to establish agarose wrapped microspheroids of the parental PC3 cell line.

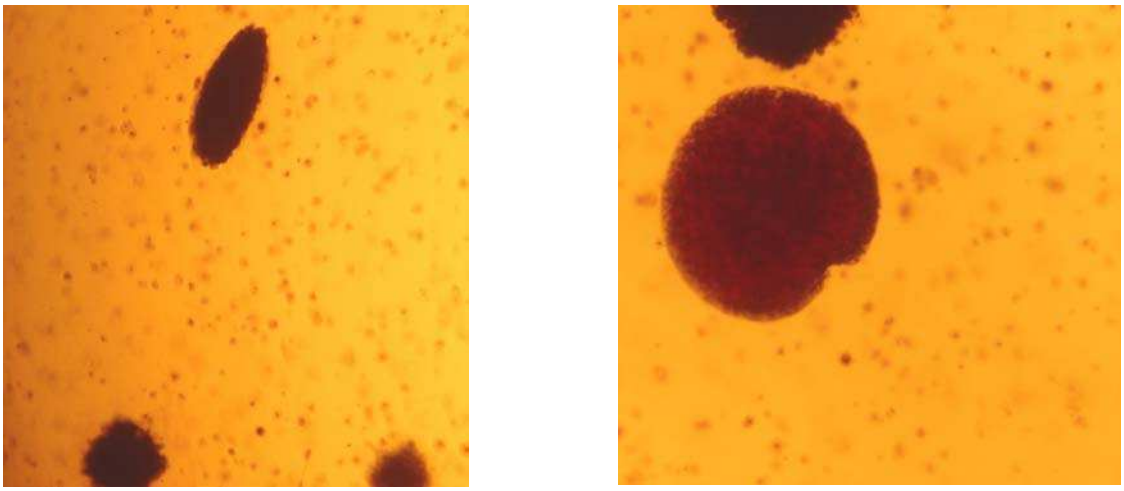

A B

Fig.: 4-3 Metabolic activity (MTT) in established PC3ID3 (A) and PC3ID4 (B) agarose wrapped multicellular spheroids after 3 days of incubation with 50.0µM 4-OH-CPA. Spheroids were incubated with MTT reagent and metabolic activity was analyzed via transmitted light microscopy after 2h of incubation. Dark or blue staining of spheroids indicates metabolic activity and cell survival.

Despite lacking comparableness to parental PC3 cells, occurring resistance in agarose wrapped spheroids indicate again possible mechanisms resulting from three dimensional growth conditions. For further clarifying possible mechanism involved in the resistant PC3 phenotype, follow up studies have to be performed.

HUH7 xenograft model

Subcutaneous human HUH7 tumors in SCID mice were treated with a low dose metronomic scheduled CPA treatment regime (75mg/kg). Tumor volume was kept constant up to day 70 after tumor cell implantation before tumor volume began to increase despite ongoing CPA therapy. Due to primary sensitivity towards the treatment, occurring resistance was likewise classified as secondary resistance.

Tumor tissue of relapsed CPA treated tumors appeared obviously different compared to untreated control tumors. Whereas, control tumors exhibited a **macroscopical** homogenous and compact tissue structure, relapsed tumors were characterized by an inhomogeneous and spongy structure and the incorporation of several blood lakes (FIG 3-70).

Further **histological analysis** via H/E stain assured the differences in tissue structure found by macroscopical analyze (FIG 3-72). Interestingly, in contrast to the increase of areas with condensed and fragmented cell nuclei in the relapsed PC3 tumors, no obvious changes in histological indicators for tumor cell death were evident in treated HUH7 tumors. Preevaluation a possible contribution of integrated

blood lakes to tumor blood supply by Hoechst33258 as a tracer, resulted in fractional staining of blood lakes, indicating connection to systemic blood circulation (FIG 3-72). The incidence of tumor cell lined blood vessels (**vascular mimicry**) (200) and **mosaic vessels** (tumor cells located in blood vessel wall) (201) was predominately described for aggressive melanomas. In the case of vascular mimicry, tumor cells acquire trans-endothelial functions and are able to participate in forming channels in order to contribute to blood supply (202). By this mechanism, tumors are less dependent on functional angiogenic processes, indicating that the appearance of vascular mimicry and mosaic vessels might be a reasonable resistance mechanism in antiangiogenic treatment strategies (203).

Again, to give consideration to possible resistance mechanism resulting from metronomic CPA treatment which targets predominately tumor vessel cells, immunohistochemical analysis of collected tumor tissues was performed with attention on alterations in **vascular markers**.

Analysis of laminin and simultaneous staining for CD31 positive endothelial cells resulted in colocalisation in treated as well as in untreated control tumors. However, a decreased rate of anatomical present tumor vessels was detected in treated tumors, likely resulting from antiangiogenic effects of metronomic CPA treatment. Moreover, tendency of functional blood flow in treated tumor was found to be reduced, indicated by decreased Hoechst33258 staining.

However, in contrast to control tumors, vessels were not continuously lined with CD31 positive endothelial cells in relapsed tumors. Hoechst33258 staining indicated that these channels within the tumor tissue are contributing to tumor blood supply and therefore provide oxygen and nutrients. By detailed fluorescence microscopical analysis of these functional channels, the presence of mosaic- as well as tumor-cell lined vessels was evident (FIG 3-73). The appearance of vascular mimicry phenomena in treated HUH7 tumors suggest a possible resistance mechanism towards antiangiogenic scheduled CPA therapy, due to the relative autonomy of tumors in the context of angiogenic processes. Analysis of laminin and CD13, resulted in colocalisation in untreated control tumors, but not in treated tumors. Moreover, organization of CD13 positive cells appeared disordered in such a manner, that sprouting of new blood vessels from existent ones was completely inhibited. Therefore, malfunction of metronomic CPA treatment regarding antiangiogenic effects was not evident, indicating sufficient conversion of CPA

prodrug and still antiangiogenic effective concentrations of active metabolites in blood stream. However, relapsing tumors achieved independence from angiogenesis and therefore were able to revoke antiangiogenic scheduled CPA treatment.

Reisolated tumor cells were characterized and identified in the context of cell **morphology** and **receptor status**; no differences in cell morphology or EGF-receptor cell surface expression were detected by comparing reisolated tumor cells with HUH7 cells from the parental cell line, indicating the identity of reisolated cells (FIG 3-74 and 3-75). Changes in endogenous CPA conversion capability may contribute to the resistant phenotype in HUH7 tumor cells due **endogenous CYP activity**. Indeed, endogenous CYP activity was significantly reduced, comparing reisolated and parental HUH7 cells (FIG 3-77). This finding suggests that decreased conversion of CPA to cytotoxic metabolites may further assist to treatment malfunction.

Involvement of **NF-κB** in resistance against cytotoxic treatment was reported in several studies. In this context, significant upregulation of NF-κB induced gene expression was detected in reisolated HUH7 cells, indicating a role in mediating CPA resistant phenotype (FIG 3-78). In addition to the modulating effects of NF-κB in apoptotic processes (161), increased NF-κB induced gene expression may also contribute to differentiation processes (204). Therefore, NF-κB might play an essential role in the case of mediating drug resistance in the HUH7 xenograft model, due to a possible involvement in structuring tumor tissue and in vascular mimicry phenomena.

Similar to PC3ID3 and PC3ID4 sublines, reisolated tumor cells did not manifest their drug resistant phenotype in a two dimensional **monolayer**, when CPA treatment was performed in a coculture system with CYP2B1 expressing X39 tumor cells (FIG 3-80). However, reisolated tumor cells manifested their drug resistant phenotype when **reimplantation** in vivo was performed. Interestingly, resistance was not absolute in this case. Reimplanted HUH7 xenografts exhibited decreased sensitivity towards CPA treatment in comparison to parental HUH7 tumors; the lag phase in tumor growth up to day 70 after cell implantation was not evident. On the other hand, tumor growth was influenced by the CPA treatment, whereby reduction in tumor growth was not significant at any time point of measurement (FIG 3-80).

Interestingly, tissue structure of reimplanted control tumors was again characterized by regions with a spongy, heterogeneous structure similar to relapsed CPA treated tumors (FIG 3-81).

Simultaneous analysis of vessel markers, laminin and CD13, resulted partly in colocalisation in reimplanted HUH7 tumors (FIG 3-81A). Interestingly, colocalisation was not evident in all tumor regions (FIG 3-81 B). Simultaneous staining of laminin and CD31 resulted in unobtrusive colocalisation of both vascular markers. However, several tumor cell lined channels were detected to be functional for tumor blood supply (FIG 3-81A and 3-81B), indicated by Hoechst33258 staining. This reaches to the conclusion that reimplanted HUH7 tumors again manifest vascular mimicry phenomena in vivo and revoke tumors, at least, partly from metronomic CPA treatment.

The ability of forming angiogenesis independent channels for tumor blood supply is therefore suggested to be “stored” in resistant HUH7 tumors and affect HUH7 phenotype in vivo even in the absence of CPA treatment.

Vascular mimicry phenomena are predominately described for aggressive melanoma tumors (205-210). However, there is growing evidence for the existence of similar phenomena in breast carcinoma (211-213), prostatic carcinoma (214;215), ovarian carcinoma (216), different sarcomas (217) and is recently detected in hepatocellular tumors (218;219). Forming angiogenesis independent channels for tumor blood supply in melanoma was linked to upregulation of the PI3K pathway and expression of several downstream controlled proteins (220;221). The “stored” significantly increased activity levels of **NF-κB** in reisolated HUH7 tumor cells (FIG 3-78) indicate possible modulation of the PI3K pathway and may be therefore involved in a HUH7 phenotype which forms a tumor cell lined channel network for blood supply.

The possibility of NF-κB/PI3K involvement in the context of the phenotype of reimplanted HUH7 tumors is further supported by differences in the regulation of NF-κB activity levels by CPA metabolites. Acrolein resulted in significantly increased NF-κB induced gene expression in reisolated HUH7 tumor cells but not on, in parental HUH7 tumors (FIG 4-4). In the cases of resistant PC3 tumors, which were unremarkable for vascular mimicry, regulation of NF-κB induced gene expression by acrolein was not evident (data not shown).

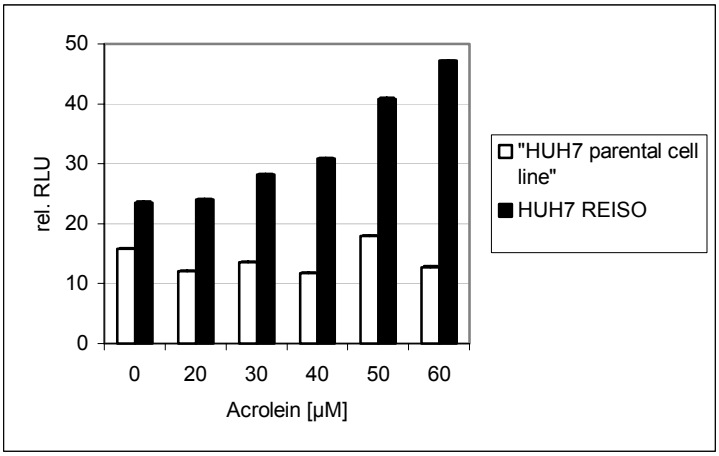

Fig.: 4-4 Induction of NF-κB induced gene expression by the metabolite acrolein in reisolated HUH7 tumor cells. Parental and reisolated HUH7 tumor cells were transfected transiently with LPEI polyplexes (N/P 6; HBS) containing luciferase encoding plasmid DNA with a NF-κB sensitive promoter/enhancer region (pNF-κB-LUC). Control experiments were performed with pTAL-LUC. 24h after the transfection cells were subjected acrolein treatment for further 24h. Luciferase measurements were performed as described in materials and methods. Values represent NF-κB activity levels in HUH7 cells. Values ±SE are means of four values.

However, a possible connection of NF-κB activity levels and phenotype of reisolated HUH7 tumor cells has to be evaluated in further studies, particularly due to the lacking knowledge about possible PI3K mediation on vascular mimicry phenomena in human hepatoma tumors.

In summary, resistance towards metronomic CPA treatment in HUH7 tumors is suggested to be based predominately on the ability of forming angiogenesis independent channels for blood supply, potentially resulting from differences in NF-κB/PIK3 modulated pathways. The spongy tissue structure, easing metabolic requirements due to lower cell count and advanced diffusion of oxygen and nutrients might contribute to this effect. Reduced endogenous CPA conversion capability of resistant tumor cells might be an additional reason for resistant HUH7 tumors in revoking CPA treatment.

4.4.3 Resistance in the syngeneic Neuro2A tumor model

Subcutaneous Neuro2A tumors were treated with a low dose metronomic scheduled CPA treatment regime (75mg/kg) in combination with CYP2B1 gene transfer via electroporation. Tumor volume was kept constant up to day 60 after tumor cell implantation before tumor volume began to increase despite ongoing treatment (FIG 3-82). Reisolated Neuro2A tumor cells from refractory tumors were characterized and identified via cell **morphology** and cell surface **receptor status**. Interestingly,

reisolated tumor cells exhibited slightly increased CD71 expression levels (FIG 3-84). Further studies, including evaluation of proliferation rate, **endogenous CYP activity** and **NF-κB** activity, showed no significant difference compared to parental Neuro2A cells.

Similar to PC3ID3, PC3ID4 and HUH7 REISO cells, reisolated Neuro2A tumor cells did not manifest their drug resistant phenotype in a two dimensional **monolayer**, when treatment was performed with 4-OOH-CPA (FIG 3-87). However, in contrast to reimplanted PC3 and HUH7 tumors, **reimplantated** Neuro2A tumors resulted in high sensitivity towards metronomic CPA treatment, indicating that reimplanted Neuro2A tumor cells are not able to manifest their drug resistant phenotype in vivo again (FIG 3-88). This suggests that in reisolated Neuro2A tumor cells the drug resistant phenotype is not a typical secondary resistance; resistance is not “stored” as in the cases of PC3 and HUH7 drug resistant tumors. This observation is conform to prior studies with experimentally PC3 and Lewis Lung carcinoma (20;222;223).

5 Summary

The development of more specific and effective anti cancer strategies is crucial in overcoming current obstacles in tumor therapy. Especially antiangiogenic approaches and gene therapy might be suitable instruments in the treatment of already metastasized cancers. Further on, the development of relevant cellular model systems, mimicking tumor environment or permitting three dimensional culture conditions, are crucial for improved assessment of therapeutic approaches.

Gene transfer with vectors coding for CYP2B1 was shown in several studies to enhance sensitivity of tumor cells towards CPA treatment. However, investigation of this concept was performed so far predominately with high dose CPA regimes. In this work, the concept was further evaluated with special attention to low dose CPA treatment regimes and in the context of tumor environmental characteristics. To provide an in vitro model system that recapitulates limited diffusion and hypoxia, an agarose overlay model was established. Evaluation of CYP2B1 enzymatic activity levels and bystander activity, which are the “supporting pillars” in the CYP/CPA concept, demonstrated great influence of the agarose overlay in terms of conversion capability and induced cytotoxicity. Restricted diffusion of activated drug metabolites was found to play a crucial role in enhancing bystander cytotoxicity.
Further on, the classical CYP/CPA GDEPT concept was extended and evaluated in terms of antiangiogenic properties. In this context, CYP2B1 expressing tumor cells were found to exert antiangiogenic bystander effects on endothelial cells in the near vicinity.

In the context of evaluation antiangiogenic properties of CYP/CPA GDEPT concept and low dose metronomic CPA treatment regimes, the 4-OH-CPA released metabolite acrolein was investigated for antiangiogenic properties. Interestingly, acrolein was detected to disturbe several crucial key steps in the angiogenic process including proliferation, migration and differentiation processes. Further on, upregulation of TSP-1, which was identified as a crucial endogenous inhibitor of angiogenesis and recently associated with metronomic scheduled CPA treatment regimes, by acrolein in primary endothelial cells, was detected. In addition, NF-κB activity levels, which were shown to exhibit important proangiogenic properties in primary endothelial cells, were reduced by acrolein treatment. Detection of acrolein-

protein adducts in CPA treated subcutaneous tumors and high levels of 4-OH-CPA (360µM) suggest a contribution of acrolein in vivo in the context of the antiangiogenic properties of metronomic CPA treatment.

Resistance towards chemotherapy is a major reason for failure of conventional chemotherapy and occurs also in metronomically scheduled treatment regimes as investigated in this thesis. Resistance can either occur as primary resistance, as detected for CT26/X39 subcutaneous tumors or secondary, acquired drug resistance occurred in experimentally PC3, HUH7 and Neuro2A tumors in a similar time period of treatment. Primary resistance phenomena result in most cases from protection of the individual tumor cell by three dimensional conditions and established cell-cell-contacts. This protection effects are supposed to play the crucial role in subcutaneous CT/X39 tumors or in established three dimensional microsphere model. In this context agarose wrapped tumor microspheres seem to be a suitable model system for multicellular mediated drug resistance.

Despite drug resistance in experimental PC3, HUH7 and Neuro2A tumor models at a similar period of CPA treatment, mechanisms resulting in drug resistance were apparently varied. While drug resistance in the experimentally PC3 xenograft model predominantly seems to be based on the protection of the individual cancer cell in a multicellular network, resistance of HUH7 xenografts was found to be a result from plasticity of tumor tissue and the ability to form angiogenesis independent structures. In contrast to reimplanted PC3 and HUH7 tumors, Neuro2A did not manifest the drug resistant phenotype in vivo again.

In summary, CPA is an anticancer drug that can be applied in conventional tumor therapy, in combination with gene transfer and in antiangiogenic approaches with low dose metronomically scheduled regimes. In the context of metronomic CPA therapy, acrolein was shown to exhibit antiangiogenic effects and therapeutic contribution has to be reconsidered. Despite improved treatment regimes, drug resistance will be still an obstacle in chemotherapeutic regimes due to different escape mechanisms; progress in the development of new strategies might be achieved by suitable in vitro models such as the agarose overlay system or agarose wrapped microspheroids.

6 Appendix

6.1 Abbreviations

4-OOH-CPA	4-hydroperoxy-cyclophosphamide
AP-1IL	activator protein 1Interleukin
ATP	adenosine triphosphate
bFGF	basic fibroblast growth factor
BPEI	branched PEI of 25 kDa
BSA	bovine serum albumine
CMV	cytomegalovirus
CPA	cyclophosphamide
CYP	cytochrom P450
DMEM	Dulbecco´s Modified Eagle´s Medium
DMSO	dimethylsulfoxide
DNA	deoxyribonucleic acid
ECM	extracellular matrix
EDTA	ethylenediaminetetraacetic acid
EGFP	enhanced green fluorescent protein
ELISA	enzyme-linked immunosorbent assay
EPR	enhanced permeability and retention effect
FCS	fetal calf serum
FITC	fluorescein
FLU	relative fluorescence units
g	relative centrifugal force
GDEPT	gene directed enzyme prodrug therapy
GSH	glutathione
HBG	HEPES-buffered glucose
HBS	HEPES buffered saline
HEPES	N-(2-hydroxyethyl)piperazine-N´-(2-ethanesulfonic acid)
HRE	hypoxia response element
huEGF	human endothelial growth factorHuman EGF
huTF	human transferrin
IFO	ifosphamide

IL	interleukin
LPEI	linear PEI of 22 kDa
LPEI polyplexes	LPEI/DNA, N/P 6
LUC	luciferase
MCR	multicellular resistance
MDR	multidrug resistance
MMP	metalloprotease
mTF	murine transferrin
MTT	methylthiazol tetrazolium salt
N/P ratio	molar ratio of PEI nitrogen to DNA phosphate
NA	numerical aperture
NF-κB	nuclear factor κB
PBS	phosphate buffered saline
PE	phycoerythrin
PEG	polyethylene glycol
PEI	polyethylenimine
PFA	paraformaldehyde
PI	propidiumiodide
PKC	protein kinase C
RLU	relative light units
RT	room temperature
SCID	severe combined immunodeficiency syndrome
SD	standard deviation
SE	standard error
SDS	sodium dodecyl sulphate
TSP-1	thrombospondin-1
V	volume
VEGF	vascular endothelial growth factor
wW	weight

6.2 Publications

6.2.1 Original papers

Gunther M, Waxman DJ, Wagner E, Ogris M.

Effects of hypoxia and limited diffusion in tumor cell microenvironment on bystander effect of P450 prodrug therapy.Cancer Gene Ther. 2006 Aug;13(8):771-9.

Gunther M, Wagner E, Ogris M.

Acrolein – unwanted side product or contribution to antiangiogenic properties of metronomic scheduled CPA therapy. *In preparation*.

Fahrmeir J, Gunther M, Wagner E, Ogris M.

An electroporetic method for purification of DNA polyplexes. *In preparation*.

Gunther M, Thoenes L, Wagner E, Ogris M.

Shielded polyplexes containing RGD or NGR peptides for vascular targeting. *In preparation*.

6.2.2 Reviews

Gunther M, Wagner E, Ogris M.

Specific targets in tumor tissue for the delivery of therapeutic genes.

Curr Med Chem Anticancer Agents. 2005 Mar;5(2):157-71. Review.

6.2.3 Poster presentation

Michael Günther, Lilja Thoenes, Ernst Wagner and Manfred Ogris

Towards an artificial virus highly specific for tumor cells and tumor vasculature. CRS world meeting, Wien, Austria (2006)

7 References

(1) Fischer C, Schneider M, Carmeliet P. Principles and therapeutic implications of angiogenesis, vasculogenesis and arteriogenesis. Handb Exp Pharmacol 2006;(176 Pt 2):157-212.

(2) Folkman J. Angiogenesis and apoptosis. Semin Cancer Biol 2003; 13(2):159-167.

(3) Folkman J. Role of angiogenesis in tumor growth and metastasis. Semin Oncol 2002; 29(6 Suppl 16):15-18.

(4) Barnhill RL, Piepkorn MW, Cochran AJ, Flynn E, Karaoli T, Folkman J. Tumor vascularity, proliferation, and apoptosis in human melanoma micrometastases and macrometastases. Arch Dermatol 1998; 134(8):991-994.

(5) Naumov GN, Akslen LA, Folkman J. Role of angiogenesis in human tumor dormancy: animal models of the angiogenic switch. Cell Cycle 2006; 5(16):1779-1787.

(6) Des GG, Uzzan B, Nicolas P, Cucherat M, Morere JF, Benamouzig R et al. Microvessel density and VEGF expression are prognostic factors in colorectal cancer. Meta-analysis of the literature. Br J Cancer 2006; 94(12):1823-1832.

(7) Schiffelers RM, Molema G, ten Hagen TL, Janssen AP, Schraa AJ, Kok RJ et al. Ligand-targeted liposomes directed against pathological vasculature. J Liposome Res 2002; 12(1-2):129-135.

(8) Marti HH. Angiogenesis--a self-adapting principle in hypoxia. EXS 2005;(94):163-180.

(9) Arvelo F, Cotte C. [Metalloproteinases in tumor progression. Review]. Invest Clin 2006; 47(2):185-205.

(10) Sato Y. Role of aminopeptidase in angiogenesis. Biol Pharm Bull 2004; 27(6):772-776.

(11) Staunton DE, Lupher ML, Liddington R, Gallatin WM. Targeting integrin structure and function in disease. Adv Immunol 2006; 91:111-157.

(12) Rice J, Courter DL, Giachelli CM, Scatena M. Molecular mediators of alphavbeta3-induced endothelial cell survival. J Vasc Res 2006; 43(5):422-436.

(13) Huang S, Chen CS, Ingber DE. Control of cyclin D1, p27(Kip1), and cell cycle progression in human capillary endothelial cells by cell shape and cytoskeletal tension. Mol Biol Cell 1998; 9(11):3179-3193.

(14) Carmeliet P, Jain RK. Angiogenesis in cancer and other diseases. Nature 2000; 407(6801):249-257.

(15) Dutour A, Rigaud M. Tumor endothelial cells are targets for selective therapies: in vitro and in vivo models to evaluate antiangiogenic strategies. Anticancer Res 2005; 25(6B):3799-3807.

(16) Milano M, Guerin O. Recent advances in targeted therapies for colorectal cancer. J Oncol Pharm Pract 2006; 12(2):69-73.

(17) Bocci G, Nicolaou KC, Kerbel RS. Protracted low-dose effects on human endothelial cell proliferation and survival in vitro reveal a selective antiangiogenic window for various chemotherapeutic drugs. Cancer Res 2002; 62(23):6938-6943.

(18) Kerbel RS, Kamen BA. The anti-angiogenic basis of metronomic chemotherapy. Nat Rev Cancer 2004; 4(6):423-436.

(19) Emmenegger U, Man S, Shaked Y, Francia G, Wong JW, Hicklin DJ et al. A comparative analysis of low-dose metronomic cyclophosphamide reveals absent or low-grade toxicity on tissues highly sensitive to the toxic effects of maximum tolerated dose regimens. Cancer Res 2004; 64(11):3994-4000.

(20) Browder T, Butterfield CE, Kraling BM, Shi B, Marshall B, O'Reilly MS et al. Antiangiogenic scheduling of chemotherapy improves efficacy against experimental drug-resistant cancer. Cancer Res 2000; 60(7):1878-1886.

(21) Ng SS, Figg WD. Upregulation of endogenous angiogenesis inhibitors: a mechanism of action of metronomic chemotherapy. Cancer Biol Ther 2004; 3(12):1212-1213.

(22) Damber JE, Vallbo C, Albertsson P, Lennernas B, Norrby K. The anti-tumour effect of low-dose continuous chemotherapy may partly be mediated by thrombospondin. Cancer Chemother Pharmacol 2006; 58(3):354-360.

(23) Folkman J. Angiogenesis. Annu Rev Med 2006; 57:1-18.

(24) Broxterman HJ, Lankelma J, Hoekman K. Resistance to cytotoxic and anti-angiogenic anticancer agents: similarities and differences. Drug Resist Updat 2003; 6(3):111-127.

(25) Edelstein ML, Abedi MR, Wixon J, Edelstein RM. Gene therapy clinical trials worldwide 1989-2004-an overview. J Gene Med 2004; 6(6):597-602.

(26) Ogris M, Wagner E. Tumor-targeted gene transfer with DNA polyplexes. Somat Cell Mol Genet 2002; 27(1-6):85-95.

(27) Haupt S, Haupt Y. Importance of p53 for cancer onset and therapy. Anticancer Drugs 2006; 17(7):725-732.

(28) Acres B, Paul S, Haegel-Kronenberger H, Calmels B, Squiban P. Therapeutic cancer vaccines. Curr Opin Mol Ther 2004; 6(1):40-47.

(29) Niculescu-Duvaz I, Springer CJ. Introduction to the background, principles, and state of the art in suicide gene therapy. Mol Biotechnol 2005; 30(1):71-88.

(30) Roy P, Waxman DJ. Activation of oxazaphosphorines by cytochrome P450: application to gene-directed enzyme prodrug therapy for cancer. Toxicol In Vitro 2006; 20(2):176-186.

(31) Salmons B, Lohr M, Gunzburg WH. Treatment of inoperable pancreatic carcinoma using a cell-based local chemotherapy: results of a phase I/II clinical trial. J Gastroenterol 2003; 38 Suppl 15:78-84.

(32) Salmons B, Lohr M, Gunzburg WH. Treatment of inoperable pancreatic carcinoma using a cell-based local chemotherapy: results of a phase I/II clinical trial. J Gastroenterol 2003; 38 Suppl 15:78-84.

(33) Elangovan N, Chiou TJ, Tzeng WF, Chu ST. Cyclophosphamide treatment causes impairment of sperm and its fertilizing ability in mice. Toxicology 2006; 222(1-2):60-70.

(34) Schimmel KJ, Richel DJ, van den Brink RB, Guchelaar HJ. Cardiotoxicity of cytotoxic drugs. Cancer Treat Rev 2004; 30(2):181-191.

(35) Zhang J, Tian Q, Yung CS, Chuen LS, Zhou S, Duan W et al. Metabolism and transport of oxazaphosphorines and the clinical implications. Drug Metab Rev 2005; 37(4):611-703.

(36) Zhang J, Tian Q, Yung CS, Chuen LS, Zhou S, Duan W et al. Metabolism and transport of oxazaphosphorines and the clinical implications. Drug Metab Rev 2005; 37(4):611-703.

(37) Dass CR, Choong PF. Targeting of small molecule anticancer drugs to the tumour and its vasculature using cationic liposomes: lessons from gene therapy. Cancer Cell Int 2006; 6:17.

(38) Eskens FA. Angiogenesis inhibitors in clinical development; where are we now and where are we going? Br J Cancer 2004; 90(1):1-7.

(39) Boussif O, Lezoualc'h F, Zanta MA, Mergny MD, Scherman D, Demeneix B et al. A versatile vector for gene and oligonucleotide transfer into cells in culture and in vivo: polyethylenimine. Proc Natl Acad Sci U S A 1995; 92(16):7297-7301.

(40) Itaka K, Harada A, Yamasaki Y, Nakamura K, Kawaguchi H, Kataoka K. In situ single cell observation by fluorescence resonance energy transfer reveals fast intra-cytoplasmic delivery and easy release of plasmid DNA complexed with linear polyethylenimine. J Gene Med 2004; 6(1):76-84.

(41) Brissault B, Leborgne C, Guis C, Danos O, Cheradame H, Kichler A. Linear topology confers in vivo gene transfer activity to polyethylenimines. Bioconjug Chem 2006; 17(3):759-765.

(42) Wightman L, Kircheis R, Rossler V, Carotta S, Ruzicka R, Kursa M et al. Different behavior of branched and linear polyethylenimine for gene delivery in vitro and in vivo. J Gene Med 2001; 3(4):362-372.

(43) Chollet P, Favrot MC, Hurbin A, Coll JL. Side-effects of a systemic injection of linear polyethylenimine-DNA complexes. J Gene Med 2002; 4(1):84-91.

(44) Ogris M, Walker G, Blessing T, Kircheis R, Wolschek M, Wagner E. Tumor-targeted gene therapy: strategies for the preparation of ligand-polyethylene glycol-polyethylenimine/DNA complexes. J Control Release 2003; 91(1-2):173-181.

(45) Gillies RJ, Schornack PA, Secomb TW, Raghunand N. Causes and effects of heterogeneous perfusion in tumors. Neoplasia 1999; 1(3):197-207.

(46) Semenza GL. HIF-1 and tumor progression: pathophysiology and therapeutics. Trends Mol Med 2002; 8(4 Suppl):S62-S67.

(47) Brahimi-Horn C, Pouyssegur J. The role of the hypoxia-inducible factor in tumor metabolism growth and invasion. Bull Cancer 2006; 93(8):E73-E80.

(48) Hussein D, Estlin EJ, Dive C, Makin GW. Chronic hypoxia promotes hypoxia-inducible factor-1alpha-dependent resistance to etoposide and vincristine in neuroblastoma cells. Mol Cancer Ther 2006; 5(9):2241-2250.

(49) Kunz M, Ibrahim SM. Molecular responses to hypoxia in tumor cells. Mol Cancer 2003; 2:23.

(50) Gunther M, Waxman DJ, Wagner E, Ogris M. Effects of hypoxia and limited diffusion in tumor cell microenvironment on bystander effect of P450 prodrug therapy. Cancer Gene Ther 2006; 13(8):771-779.

(51) Longley DB, Allen WL, Johnston PG. Drug resistance, predictive markers and pharmacogenomics in colorectal cancer. Biochim Biophys Acta 2006.

(52) Ho EA, Piquette-Miller M. Regulation of multidrug resistance by pro-inflammatory cytokines. Curr Cancer Drug Targets 2006; 6(4):295-311.

(53) Perez-Tomas R. Multidrug resistance: retrospect and prospects in anti-cancer drug treatment. Curr Med Chem 2006; 13(16):1859-1876.

(54) Hutter G, Sinha P. Proteomics for studying cancer cells and the development of chemoresistance. Proteomics 2001; 1(10):1233-1248.

(55) Desoize B, Jardillier J. Multicellular resistance: a paradigm for clinical resistance? Crit Rev Oncol Hematol 2000; 36(2-3):193-207.

(56) Elliott T, Sethi T. Integrins and extracellular matrix: a novel mechanism of multidrug resistance. Expert Rev Anticancer Ther 2002; 2(4):449-459.

(57) Croix BS, Rak JW, Kapitain S, Sheehan C, Graham CH, Kerbel RS. Reversal by hyaluronidase of adhesion-dependent multicellular drug resistance in mammary carcinoma cells. J Natl Cancer Inst 1996; 88(18):1285-1296.

(58) Abdel-Latif MM, O'Riordan JM, Ravi N, Kelleher D, Reynolds JV. Activated nuclear factor-kappa B and cytokine profiles in the esophagus parallel tumor

regression following neoadjuvant chemoradiotherapy. Dis Esophagus 2005; 18(4):246-252.

(59) Amiri KI, Richmond A. Role of nuclear factor-kappa B in melanoma. Cancer Metastasis Rev 2005; 24(2):301-313.

(60) Stavrovskaya AA. Cellular mechanisms of multidrug resistance of tumor cells. Biochemistry (Mosc) 2000; 65(1):95-106.

(61) Muerkoster S, Wegehenkel K, Arlt A, Witt M, Sipos B, Kruse ML et al. Tumor stroma interactions induce chemoresistance in pancreatic ductal carcinoma cells involving increased secretion and paracrine effects of nitric oxide and interleukin-1beta. Cancer Res 2004; 64(4):1331-1337.

(62) Vandermoere F, Yazidi-Belkoura I, Adriaenssens E, Lemoine J, Hondermarck H. The antiapoptotic effect of fibroblast growth factor-2 is mediated through nuclear factor-kappaB activation induced via interaction between Akt and IkappaB kinase-beta in breast cancer cells. Oncogene 2005; 24(35):5482-5491.

(63) Ribatti D, Vacca A, Dammacco F. New non-angiogenesis dependent pathways for tumour growth. Eur J Cancer 2003; 39(13):1835-1841.

(64) van der Schaft DW, Seftor RE, Seftor EA, Hess AR, Gruman LM, Kirschmann DA et al. Effects of angiogenesis inhibitors on vascular network formation by human endothelial and melanoma cells. J Natl Cancer Inst 2004; 96(19):1473-1477.

(65) Mueller-Klieser W. Three-dimensional cell cultures: from molecular mechanisms to clinical applications. Am J Physiol 1997; 273(4 Pt 1):C1109-C1123.

(66) An YH, Webb D, Gutowska A, Mironov VA, Friedman RJ. Regaining chondrocyte phenotype in thermosensitive gel culture. Anat Rec 2001; 263(4):336-341.

(67) Huch K, Stove J, Puhl W, Gunther KP. [Review and comparison of culture-techniques for articular chondrocytes]. Z Orthop Ihre Grenzgeb 2002; 140(2):145-152.

(68) Camp ER, Li J, Minnich DJ, Brank A, Moldawer LL, MacKay SL et al. Inducible nuclear factor-kappaB activation contributes to chemotherapy resistance in gastric cancer. J Am Coll Surg 2004; 199(2):249-258.

(69) Liu CA, Wang MJ, Chi CW, Wu CW, Chen JY. Rho/Rhotekin-mediated NF-kappaB activation confers resistance to apoptosis. Oncogene 2004; 23(54):8731-8742.

(70) Montagut C, Tusquets I, Ferrer B, Corominas JM, Bellosillo B, Campas C et al. Activation of nuclear factor-kappa B is linked to resistance to neoadjuvant chemotherapy in breast cancer patients. Endocr Relat Cancer 2006; 13(2):607-616.

(71) Salvatore C, Camarda G, Maggi CA, Goso C, Manzini S, Binaschi M. NF-kappaB activation contributes to anthracycline resistance pathway in human ovarian carcinoma cell line A2780. Int J Oncol 2005; 27(3):799-806.

(72) Karin M. Nuclear factor-kappaB in cancer development and progression. Nature 2006; 441(7092):431-436.

(73) Zhang Z, Ma J, Li N, Sun N, Wang C. Expression of nuclear factor-kappaB and its clinical significance in nonsmall-cell lung cancer. Ann Thorac Surg 2006; 82(1):243-248.

(74) Plank C, Zatloukal K, Cotten M, Mechtler K, Wagner E. Gene transfer into hepatocytes using asialoglycoprotein receptor mediated endocytosis of DNA complexed with an artificial tetra-antennary galactose ligand. Bioconjug Chem 1992; 3(6):533-539.

(75) Chen L, Waxman DJ, Chen D, Kufe DW. Sensitization of human breast cancer cells to cyclophosphamide and ifosfamide by transfer of a liver cytochrome P450 gene. Cancer Res 1996; 56(6):1331-1340.

(76) Burke B, Tang N, Corke KP, Tazzyman D, Ameri K, Wells M et al. Expression of HIF-1alpha by human macrophages: implications for the use of macrophages in hypoxia-regulated cancer gene therapy. J Pathol 2002; 196(2):204-212.

(77) Ogris M, Carlisle RC, Bettinger T, Seymour LW. Melittin enables efficient vesicular escape and enhanced nuclear access of nonviral gene delivery vectors. J Biol Chem 2001; 276(50):47550-47555.

(78) von Gersdorff K, Ogris M, Wagner E. Cryoconserved shielded and EGF receptor targeted DNA polyplexes: cellular mechanisms. Eur J Pharm Biopharm 2005; 60(2):279-285.

(79) von Gersdorff K, Ogris M, Wagner E. Cryoconserved shielded and EGF receptor targeted DNA polyplexes: cellular mechanisms. Eur J Pharm Biopharm 2005; 60(2):279-285.

(80) von Gersdorff K, Ogris M, Wagner E. Cryoconserved shielded and EGF receptor targeted DNA polyplexes: cellular mechanisms. Eur J Pharm Biopharm 2005; 60(2):279-285.

(81) Donato MT, Gomez-Lechon MJ, Castell JV. A microassay for measuring cytochrome P450IA1 and P450IIB1 activities in intact human and rat hepatocytes cultured on 96-well plates. Anal Biochem 1993; 213(1):29-33.

(82) Voelcker G, Haeglsperger R, Hohorst HJ. [Fluorometric determination of "activated" cyclophosphamide and ifosfamide in blood (author's transl)]. J Cancer Res Clin Oncol 1979; 93(3):233-240.

(83) Voelcker G, Haeglsperger R, Hohorst HJ. [Fluorometric determination of "activated" cyclophosphamide and ifosfamide in blood (author's transl)]. J Cancer Res Clin Oncol 1979; 93(3):233-240.

(84) Alarcon RA. Fluorometric determination of acrolein and related compounds with m-aminophenol. Anal Chem 1968; 40(11):1704-1708.

(85) Alarcon RA. Fluorometric determination of acrolein and related compounds with m-aminophenol. Anal Chem 1968; 40(11):1704-1708.

(86) Bosma GC, Custer RP, Bosma MJ. A severe combined immunodeficiency mutation in the mouse. Nature 1983; 301(5900):527-530.

(87) Culmsee C, Siewe J, Junker V, Retiounskaia M, Schwarz S, Camandola S et al. Reciprocal inhibition of p53 and nuclear factor-kappaB transcriptional activities determines cell survival or death in neurons. J Neurosci 2003; 23(24):8586-8595.

(88) Voll RE, Jimi E, Phillips RJ, Barber DF, Rincon M, Hayday AC et al. NF-kappa B activation by the pre-T cell receptor serves as a selective survival signal in T lymphocyte development. Immunity 2000; 13(5):677-689.

(89) Millet I, Phillips RJ, Sherwin RS, Ghosh S, Voll RE, Flavell RA et al. Inhibition of NF-kappaB activity and enhancement of apoptosis by the neuropeptide calcitonin gene-related peptide. J Biol Chem 2000; 275(20):15114-15121.

(90) Yu LJ, Matias J, Scudiero DA, Hite KM, Monks A, Sausville EA et al. P450 enzyme expression patterns in the NCI human tumor cell line panel. Drug Metab Dispos 2001; 29(3):304-312.

(91) Dutton DR, Parkinson A. Reduction of 7-alkoxyresorufins by NADPH-cytochrome P450 reductase and its differential effects on their O-dealkylation by rat liver microsomal cytochrome P450. Arch Biochem Biophys 1989; 268(2):617-629.

(92) Sladek NE. Metabolism and pharmacokinetic behavior of cyclophosphamide and related oxazophosphorines. Pergamon Press Ltd 1994; G.Powis (ed.):79-156.

(93) Hamano Y, Sugimoto H, Soubasakos MA, Kieran M, Olsen BR, Lawler J et al. Thrombospondin-1 associated with tumor microenvironment contributes to low-dose cyclophosphamide-mediated endothelial cell apoptosis and tumor growth suppression. Cancer Res 2004; 64(5):1570-1574.

(94) Hynes RO. Integrins: bidirectional, allosteric signaling machines. Cell 2002; 110(6):673-687.

(95) Kuphal S, Bauer R, Bosserhoff AK. Integrin signaling in malignant melanoma. Cancer Metastasis Rev 2005; 24(2):195-222.

(96) Tong Q, Zheng L, Lin L, Li B, Wang D, Huang C et al. Participation of the PI-3K/Akt-NF-kappaB signaling pathways in hypoxia-induced mitogenic factor-stimulated Flk-1 expression in endothelial cells. Respir Res 2006; 7:101.

(97) Uzzo RG, Crispen PL, Golovine K, Makhov P, Horwitz EM, Kolenko VM. Diverse effects of zinc on NF-kappaB and AP-1 transcription factors:

implications for prostate cancer progression. Carcinogenesis 2006; 27(10):1980-1990.

(98) Vandermoere F, Yazidi-Belkoura I, Adriaenssens E, Lemoine J, Hondermarck H. The antiapoptotic effect of fibroblast growth factor-2 is mediated through nuclear factor-kappaB activation induced via interaction between Akt and IkappaB kinase-beta in breast cancer cells. Oncogene 2005; 24(35):5482-5491.

(99) Voll RE, Jimi E, Phillips RJ, Barber DF, Rincon M, Hayday AC et al. NF-kappa B activation by the pre-T cell receptor serves as a selective survival signal in T lymphocyte development. Immunity 2000; 13(5):677-689.

(100) Millet I, Phillips RJ, Sherwin RS, Ghosh S, Voll RE, Flavell RA et al. Inhibition of NF-kappaB activity and enhancement of apoptosis by the neuropeptide calcitonin gene-related peptide. J Biol Chem 2000; 275(20):15114-15121.

(101) Elliott T, Sethi T. Integrins and extracellular matrix: a novel mechanism of multidrug resistance. Expert Rev Anticancer Ther 2002; 2(4):449-459.

(102) Shain KH, Dalton WS. Cell adhesion is a key determinant in de novo multidrug resistance (MDR): new targets for the prevention of acquired MDR. Mol Cancer Ther 2001; 1(1):69-78.

(103) Yu LJ, Drewes P, Gustafsson K, Brain EG, Hecht JE, Waxman DJ. In vivo modulation of alternative pathways of P-450-catalyzed cyclophosphamide metabolism: impact on pharmacokinetics and antitumor activity. J Pharmacol Exp Ther 1999; 288(3):928-937.

(104) Chang TK, Weber GF, Crespi CL, Waxman DJ. Differential activation of cyclophosphamide and ifosphamide by cytochromes P-450 2B and 3A in human liver microsomes. Cancer Res 1993; 53(23):5629-5637.

(105) Chang TK, Weber GF, Crespi CL, Waxman DJ. Differential activation of cyclophosphamide and ifosphamide by cytochromes P-450 2B and 3A in human liver microsomes. Cancer Res 1993; 53(23):5629-5637.

(106) Yu LJ, Drewes P, Gustafsson K, Brain EG, Hecht JE, Waxman DJ. In vivo modulation of alternative pathways of P-450-catalyzed cyclophosphamide metabolism: impact on pharmacokinetics and antitumor activity. J Pharmacol Exp Ther 1999; 288(3):928-937.

(107) Chen L, Waxman DJ. Intratumoral activation and enhanced chemotherapeutic effect of oxazaphosphorines following cytochrome P-450 gene transfer: development of a combined chemotherapy/cancer gene therapy strategy. Cancer Res 1995; 55(3):581-589.

(108) Chen L, Waxman DJ, Chen D, Kufe DW. Sensitization of human breast cancer cells to cyclophosphamide and ifosfamide by transfer of a liver cytochrome P450 gene. Cancer Res 1996; 56(6):1331-1340.

(109) Chen L, Yu LJ, Waxman DJ. Potentiation of cytochrome P450/cyclophosphamide-based cancer gene therapy by coexpression of the P450 reductase gene. Cancer Res 1997; 57(21):4830-4837.

(110) Huang Z, Waxman DJ. Modulation of cyclophosphamide-based cytochrome P450 gene therapy using liver P450 inhibitors. Cancer Gene Ther 2001; 8(6):450-458.

(111) Tzanakakis ES, Waxman DJ, Hansen LK, Remmel RP, Hu WS. Long-term enhancement of cytochrome P450 2B1/2 expression in rat hepatocyte spheroids through adenovirus-mediated gene transfer. Cell Biol Toxicol 2002; 18(1):13-27.

(112) Huang Z, Raychowdhury MK, Waxman DJ. Impact of liver P450 reductase suppression on cyclophosphamide activation, pharmacokinetics and antitumoral activity in a cytochrome P450-based cancer gene therapy model. Cancer Gene Ther 2000; 7(7):1034-1042.

(113) Jounaidi Y, Waxman DJ. Combination of the bioreductive drug tirapazamine with the chemotherapeutic prodrug cyclophosphamide for P450/P450-reductase-based cancer gene therapy. Cancer Res 2000; 60(14):3761-3769.

(114) Waxman DJ, Chen L, Hecht JE, Jounaidi Y. Cytochrome P450-based cancer gene therapy: recent advances and future prospects. Drug Metab Rev 1999; 31(2):503-522.

(115) Yu LJ, Matias J, Scudiero DA, Hite KM, Monks A, Sausville EA et al. P450 enzyme expression patterns in the NCI human tumor cell line panel. Drug Metab Dispos 2001; 29(3):304-312.

(116) Krusekopf S, Roots I, Hildebrandt AG, Kleeberg U. Time-dependent transcriptional induction of CYP1A1, CYP1A2 and CYP1B1 mRNAs by H+/K+ -ATPase inhibitors and other xenobiotics. Xenobiotica 2003; 33(2):107-118.

(117) Gilard V, Martino R, Malet-Martino M, Niemeyer U, Pohl J. Chemical stability and fate of the cytostatic drug ifosfamide and its N-dechloroethylated metabolites in acidic aqueous solutions. J Med Chem 1999; 42(14):2542-2560.

(118) Penketh PG, Shyam K, Sartorelli AC. Comparison of DNA lesions produced by tumor-inhibitory 1,2-bis(sulfonyl)hydrazines and chloroethylnitrosoureas. Biochem Pharmacol 2000; 59(3):283-291.

(119) Sanderson BJ, Shield AJ. Mutagenic damage to mammalian cells by therapeutic alkylating agents. Mutat Res 1996; 355(1-2):41-57.

(120) Schwartz PS, Waxman DJ. Cyclophosphamide induces caspase 9-dependent apoptosis in 9L tumor cells. Mol Pharmacol 2001; 60(6):1268-1279.

(121) Mirkes PE, Little SA. Cytochrome c release from mitochondria of early postimplantation murine embryos exposed to 4-

hydroperoxycyclophosphamide, heat shock, and staurosporine. Toxicol Appl Pharmacol 2000; 162(3):197-206.

(122) Jounaidi Y, Waxman DJ. Combination of the bioreductive drug tirapazamine with the chemotherapeutic prodrug cyclophosphamide for P450/P450-reductase-based cancer gene therapy. Cancer Res 2000; 60(14):3761-3769.

(123) Koebe HG, Pahernik S, Eyer P, Schildberg FW. Collagen gel immobilization: a useful cell culture technique for long-term metabolic studies on human hepatocytes. Xenobiotica 1994; 24(2):95-107.

(124) Wright JE, Tretyakov O, Ayash LJ, Elias A, Rosowsky A, Frei E, III. Analysis of 4-hydroxycyclophosphamide in human blood. Anal Biochem 1995; 224(1):154-158.

(125) Mahoney BP, Raghunand N, Baggett B, Gillies RJ. Tumor acidity, ion trapping and chemotherapeutics. I. Acid pH affects the distribution of chemotherapeutic agents in vitro. Biochem Pharmacol 2003; 66(7):1207-1218.

(126) Jahde E, Roszinski S, Volk T, Glusenkamp KH, Wiedemann G, Rajewsky MF. Metabolic response of AH13r rat tumours to cyclophosphamide as monitored by pO2 and pH semi-microelectrodes. Eur J Cancer 1992; 29A(1):116-122.

(127) Gillies RJ, Schornack PA, Secomb TW, Raghunand N. Causes and effects of heterogeneous perfusion in tumors. Neoplasia 1999; 1(3):197-207.

(128) Gillies RJ, Schornack PA, Secomb TW, Raghunand N. Causes and effects of heterogeneous perfusion in tumors. Neoplasia 1999; 1(3):197-207.

(129) Dachs GU, Tupper J, Tozer GM. From bench to bedside for gene-directed enzyme prodrug therapy of cancer. Anticancer Drugs 2005; 16(4):349-359.

(130) Braybrooke JP, Slade A, Deplanque G, Harrop R, Madhusudan S, Forster MD et al. Phase I study of MetXia-P450 gene therapy and oral cyclophosphamide for patients with advanced breast cancer or melanoma. Clin Cancer Res 2005; 11(4):1512-1520.

(131) Yuan F, Krol A, Tong S. Available space and extracellular transport of macromolecules: effects of pore size and connectedness. Ann Biomed Eng 2001; 29(12):1150-1158.

(132) Ding Q, Kestell P, Baguley BC, Palmer BD, Paxton JW, Muller G et al. Potentiation of the antitumour effect of cyclophosphamide in mice by thalidomide. Cancer Chemother Pharmacol 2002; 50(3):186-192.

(133) Schneeberger A, Wagner C, Zemann A, Luhrs P, Kutil R, Goos M et al. CpG motifs are efficient adjuvants for DNA cancer vaccines. J Invest Dermatol 2004; 123(2):371-379.

(134) Cao Z, Hardej D, Trombetta LD, Trush MA, Li Y. Induction of cellular glutathione and glutathione S-transferase by 3H-1,2-dithiole-3-thione in rat

aortic smooth muscle A10 cells: protection against acrolein-induced toxicity. Atherosclerosis 2003; 166(2):291-301.

(135) Park YS, Misonou Y, Fujiwara N, Takahashi M, Miyamoto Y, Koh YH et al. Induction of thioredoxin reductase as an adaptive response to acrolein in human umbilical vein endothelial cells. Biochem Biophys Res Commun 2005; 327(4):1058-1065.

(136) DeLeve LD. Cellular target of cyclophosphamide toxicity in the murine liver: role of glutathione and site of metabolic activation. Hepatology 1996; 24(4):830-837.

(137) Bocci G, Francia G, Man S, Lawler J, Kerbel RS. Thrombospondin 1, a mediator of the antiangiogenic effects of low-dose metronomic chemotherapy. Proc Natl Acad Sci U S A 2003; 100(22):12917-12922.

(138) Wrabetz E, Peter G, Hohorst HJ. Does acrolein contribute to the cytotoxicity of cyclophosphamide? J Cancer Res Clin Oncol 1980; 98(2):119-126.

(139) Blomgren H, Hallstrom M. Possible role of acrolein in oxazaphosphorine-induced enhancement of immunological reactivity. Cancer Immunol Immunother 1990; 31(4):221-225.

(140) Blomgren H, Hallstrom M. Possible role of acrolein in 4-hydroperoxycyclophosphamide-induced cell damage in vitro. Methods Find Exp Clin Pharmacol 1991; 13(1):11-14.

(141) Blomgren H, Hallstrom M. Release of a votile factor from solutions of oxazaphosphorines which damage normal and malignant cells. Methods Find Exp Clin Pharmacol 1989; 11(6):391-397.

(142) Kawabata TT, White KL, Jr. Enhancement of in vivo and in vitro murine immune responses by the cyclophosphamide metabolite acrolein. Cancer Res 1988; 48(1):41-45.

(143) Arikketh D, Niranjali S, Devaraj H. Detection of acrolein-lysine adducts in plasma low-density lipoprotein and in aorta of cyclophosphamide-administered rats. Arch Toxicol 2004; 78(7):397-401.

(144) Voelcker G, Haeglsperger R, Hohorst HJ. [Fluorometric determination of "activated" cyclophosphamide and ifosfamide in blood (author's transl)]. J Cancer Res Clin Oncol 1979; 93(3):233-240.

(145) Ramu K, Fraiser LH, Mamiya B, Ahmed T, Kehrer JP. Acrolein mercapturates: synthesis, characterization, and assessment of their role in the bladder toxicity of cyclophosphamide. Chem Res Toxicol 1995; 8(4):515-524.

(146) Ramu K, Perry CS, Ahmed T, Pakenham G, Kehrer JP. Studies on the basis for the toxicity of acrolein mercapturates. Toxicol Appl Pharmacol 1996; 140(2):487-498.

(147) DeLeve LD. Cellular target of cyclophosphamide toxicity in the murine liver: role of glutathione and site of metabolic activation. Hepatology 1996; 24(4):830-837.

(148) Kehrer JP, Biswal SS. The molecular effects of acrolein. Toxicol Sci 2000; 57(1):6-15.

(149) Fenteany G, Zhu S. Small-molecule inhibitors of actin dynamics and cell motility. Curr Top Med Chem 2003; 3(6):593-616.

(150) Donovan D, Brown NJ, Bishop ET, Lewis CE. Comparison of three in vitro human 'angiogenesis' assays with capillaries formed in vivo. Angiogenesis 2001; 4(2):113-121.

(151) Lawley TJ, Kubota Y. Induction of morphologic differentiation of endothelial cells in culture. J Invest Dermatol 1989; 93(2 Suppl):59S-61S.

(152) Nieuw Amerongen GP, Koolwijk P, Versteilen A, van Hinsbergh VW. Involvement of RhoA/Rho kinase signaling in VEGF-induced endothelial cell migration and angiogenesis in vitro. Arterioscler Thromb Vasc Biol 2003; 23(2):211-217.

(153) Rafiee P, Heidemann J, Ogawa H, Johnson NA, Fisher PJ, Li MS et al. Cyclosporin A differentially inhibits multiple steps in VEGF induced angiogenesis in human microvascular endothelial cells through altered intracellular signaling. Cell Commun Signal 2004; 2(1):3.

(154) Poggi P, Rota MT, Boratto R. The volatile fraction of cigarette smoke induces alterations in the human gingival fibroblast cytoskeleton. J Periodontal Res 2002; 37(3):230-235.

(155) van der FA, Sonnenberg A. Function and interactions of integrins. Cell Tissue Res 2001; 305(3):285-298.

(156) Mi J, Zhang X, Giangrande PH, McNamara JO, Nimjee SM, Sarraf-Yazdi S et al. Targeted inhibition of alphavbeta3 integrin with an RNA aptamer impairs endothelial cell growth and survival. Biochem Biophys Res Commun 2005; 338(2):956-963.

(157) Ruegg C, Mariotti A. Vascular integrins: pleiotropic adhesion and signaling molecules in vascular homeostasis and angiogenesis. Cell Mol Life Sci 2003; 60(6):1135-1157.

(158) Royds JA, Dower SK, Qwarnstrom EE, Lewis CE. Response of tumour cells to hypoxia: role of p53 and NFkB. Mol Pathol 1998; 51(2):55-61.

(159) Seo KH, Lee HS, Jung B, Ko HM, Choi JH, Park SJ et al. Estrogen enhances angiogenesis through a pathway involving platelet-activating factor-mediated nuclear factor-kappaB activation. Cancer Res 2004; 64(18):6482-6488.

(160) Zhang H, Ma G, Dong M, Zhao M, Shen X, Ma Z et al. Epidermal growth factor promotes invasiveness of pancreatic cancer cells through NF-kappaB-mediated proteinase productions. Pancreas 2006; 32(1):101-109.

(161) Piva R, Belardo G, Santoro MG. NF-kappaB: a stress-regulated switch for cell survival. Antioxid Redox Signal 2006; 8(3-4):478-486.

(162) Tergaonkar V. NFkappaB pathway: a good signaling paradigm and therapeutic target. Int J Biochem Cell Biol 2006; 38(10):1647-1653.

(163) Bhat-Nakshatri P, Newton TR, Goulet R, Jr., Nakshatri H. NF-kappaB activation and interleukin 6 production in fibroblasts by estrogen receptor-negative breast cancer cell-derived interleukin 1alpha. Proc Natl Acad Sci U S A 1998; 95(12):6971-6976.

(164) Horton ND, Biswal SS, Corrigan LL, Bratta J, Kehrer JP. Acrolein causes inhibitor kappaB-independent decreases in nuclear factor kappaB activation in human lung adenocarcinoma (A549) cells. J Biol Chem 1999; 274(14):9200-9206.

(165) Tanner JE. Nucleosomes activate NF-kappaB in endothelial cells for induction of the proangiogenic cytokine IL-8. Int J Cancer 2004; 112(1):155-160.

(166) Wrighton CJ, Hofer-Warbinek R, Moll T, Eytner R, Bach FH, de Martin R. Inhibition of endothelial cell activation by adenovirus-mediated expression of I kappa B alpha, an inhibitor of the transcription factor NF-kappa B. J Exp Med 1996; 183(3):1013-1022.

(167) Kim I, Moon SO, Kim SH, Kim HJ, Koh YS, Koh GY. Vascular endothelial growth factor expression of intercellular adhesion molecule 1 (ICAM-1), vascular cell adhesion molecule 1 (VCAM-1), and E-selectin through nuclear factor-kappa B activation in endothelial cells. J Biol Chem 2001; 276(10):7614-7620.

(168) Klein S, de Fougerolles AR, Blaikie P, Khan L, Pepe A, Green CD et al. Alpha 5 beta 1 integrin activates an NF-kappa B-dependent program of gene expression important for angiogenesis and inflammation. Mol Cell Biol 2002; 22(16):5912-5922.

(169) Shono T, Ono M, Izumi H, Jimi SI, Matsushima K, Okamoto T et al. Involvement of the transcription factor NF-kappaB in tubular morphogenesis of human microvascular endothelial cells by oxidative stress. Mol Cell Biol 1996; 16(8):4231-4239.

(170) Patel S, Leal AD, Gorski DH. The homeobox gene Gax inhibits angiogenesis through inhibition of nuclear factor-kappaB-dependent endothelial cell gene expression. Cancer Res 2005; 65(4):1414-1424.

(171) Scatena M, Almeida M, Chaisson ML, Fausto N, Nicosia RF, Giachelli CM. NF-kappaB mediates alphavbeta3 integrin-induced endothelial cell survival. J Cell Biol 1998; 141(4):1083-1093.

(172) Tong Q, Zheng L, Lin L, Li B, Wang D, Huang C et al. VEGF is upregulated by hypoxia-induced mitogenic factor via the PI-3K/Akt-NF-kappaB signaling pathway. Respir Res 2006; 7:37.

(173) Bussolati B, Assenzio B, Deregibus MC, Camussi G. The proangiogenic phenotype of human tumor-derived endothelial cells depends on thrombospondin-1 downregulation via phosphatidylinositol 3-kinase/Akt pathway. J Mol Med 2006; 84(10):852-863.

(174) Kim SA, Um SJ, Kang JH, Hong KJ. Expression of thrombospondin-1 in human hepatocarcinoma cell lines and its regulation by transcription factor Jun/AP-1. Mol Cell Biochem 2001; 216(1-2):21-29.

(175) Kim J, Kim C, Kim TS, Bang SI, Yang Y, Park H et al. IL-18 enhances thrombospondin-1 production in human gastric cancer via JNK pathway. Biochem Biophys Res Commun 2006; 344(4):1284-1289.

(176) Wu CC, Hsieh CW, Lai PH, Lin JB, Liu YC, Wung BS. Upregulation of endothelial heme oxygenase-1 expression through the activation of the JNK pathway by sublethal concentrations of acrolein. Toxicol Appl Pharmacol 2006; 214(3):244-252.

(177) Maddox JF, Roth RA, Ganey PE. Allyl alcohol activation of protein kinase C delta leads to cytotoxicity of rat hepatocytes. Chem Res Toxicol 2003; 16(5):609-615.

(178) Tada H, Kuboki K, Nomura K, Inokuchi T. High glucose levels enhance TGF-beta1-thrombospondin-1 pathway in cultured human mesangial cells via mechanisms dependent on glucose-induced PKC activation. J Diabetes Complications 2001; 15(4):193-197.

(179) Kobayashi H, Man S, Graham CH, Kapitain SJ, Teicher BA, Kerbel RS. Acquired multicellular-mediated resistance to alkylating agents in cancer. Proc Natl Acad Sci U S A 1993; 90(8):3294-3298.

(180) Sutherland RM, Eddy HA, Bareham B, Reich K, Vanantwerp D. Resistance to adriamycin in multicellular spheroids. Int J Radiat Oncol Biol Phys 1979; 5(8):1225-1230.

(181) Wibe E. Resistance to vincristine of human cells grown as multicellular spheroids. Br J Cancer 1980; 42(6):937-941.

(182) Kobayashi H, Man S, Graham CH, Kapitain SJ, Teicher BA, Kerbel RS. Acquired multicellular-mediated resistance to alkylating agents in cancer. Proc Natl Acad Sci U S A 1993; 90(8):3294-3298.

(183) Kuwashima Y, Yamada T, Saio M, Takami T. Formation and growth of multicellular spheroids in media containing low concentrations of agarose. Cancer Lett 1993; 71(1-3):31-33.

(184) Elliott T, Sethi T. Integrins and extracellular matrix: a novel mechanism of multidrug resistance. Expert Rev Anticancer Ther 2002; 2(4):449-459.

(185) Shain KH, Dalton WS. Cell adhesion is a key determinant in de novo multidrug resistance (MDR): new targets for the prevention of acquired MDR. Mol Cancer Ther 2001; 1(1):69-78.

(186) Santini MT, Rainaldi G. Three-dimensional spheroid model in tumor biology. Pathobiology 1999; 67(3):148-157.

(187) Friedman HS, Burger PC, Bigner SH, Trojanowski JQ, Wikstrand CJ, Halperin EC et al. Establishment and characterization of the human medulloblastoma cell line and transplantable xenograft D283 Med. J Neuropathol Exp Neurol 1985; 44(6):592-605.

(188) Kuwashima Y, Yamada T, Saio M, Takami T. Formation and growth of multicellular spheroids in media containing low concentrations of agarose. Cancer Lett 1993; 71(1-3):31-33.

(189) Kelly TA, Wang CC, Mauck RL, Ateshian GA, Hung CT. Role of cell-associated matrix in the development of free-swelling and dynamically loaded chondrocyte-seeded agarose gels. Biorheology 2004; 41(3-4):223-237.

(190) Quintavalla J, Kumar C, Daouti S, Slosberg E, Uziel-Fusi S. Chondrocyte cluster formation in agarose cultures as a functional assay to identify genes expressed in osteoarthritis. J Cell Physiol 2005; 204(2):560-566.

(191) Yeger H, Baumal R, Pawlin G, Tonin P, Nissen L, Kaplinsky C et al. Phenotypic and molecular characterization of inducible human neuroblastoma cell lines. Differentiation 1988; 39(3):216-227.

(192) Kerbel RS. A cancer therapy resistant to resistance. Nature 1997; 390(6658):335-336.

(193) Boehm T, Folkman J, Browder T, O'Reilly MS. Antiangiogenic therapy of experimental cancer does not induce acquired drug resistance. Nature 1997; 390(6658):404-407.

(194) Man S, Bocci G, Francia G, Green SK, Jothy S, Hanahan D et al. Antitumor effects in mice of low-dose (metronomic) cyclophosphamide administered continuously through the drinking water. Cancer Res 2002; 62(10):2731-2735.

(195) Man S, Bocci G, Francia G, Green SK, Jothy S, Hanahan D et al. Antitumor effects in mice of low-dose (metronomic) cyclophosphamide administered continuously through the drinking water. Cancer Res 2002; 62(10):2731-2735.

(196) Bremnes RM, Camps C, Sirera R. Angiogenesis in non-small cell lung cancer: the prognostic impact of neoangiogenesis and the cytokines VEGF and bFGF in tumours and blood. Lung Cancer 2006; 51(2):143-158.

(197) Hendrix MJ, Seftor EA, Hess AR, Seftor RE. Vasculogenic mimicry and tumour-cell plasticity: lessons from melanoma. Nat Rev Cancer 2003; 3(6):411-421.

(198) Quesada AR, Munoz-Chapuli R, Medina MA. Anti-angiogenic drugs: from bench to clinical trials. Med Res Rev 2006; 26(4):483-530.

(199) Piva R, Belardo G, Santoro MG. NF-kappaB: a stress-regulated switch for cell survival. Antioxid Redox Signal 2006; 8(3-4):478-486.

(200) Folberg R, Maniotis AJ. Vasculogenic mimicry. APMIS 2004; 112(7-8):508-525.

(201) di Tomaso E, Capen D, Haskell A, Hart J, Logie JJ, Jain RK et al. Mosaic tumor vessels: cellular basis and ultrastructure of focal regions lacking endothelial cell markers. Cancer Res 2005; 65(13):5740-5749.

(202) Bajcsy P, Lee SC, Lin A, Folberg R. Three-dimensional volume reconstruction of extracellular matrix proteins in uveal melanoma from fluorescent confocal laser scanning microscope images. J Microsc 2006; 221(Pt 1):30-45.

(203) van der Schaft DW, Seftor RE, Seftor EA, Hess AR, Gruman LM, Kirschmann DA et al. Effects of angiogenesis inhibitors on vascular network formation by human endothelial and melanoma cells. J Natl Cancer Inst 2004; 96(19):1473-1477.

(204) Schottelius AJ, Dinter H. Cytokines, NF-kappaB, microenvironment, intestinal inflammation and cancer. Cancer Treat Res 2006; 130:67-87.

(205) Folberg R, Hendrix MJ, Maniotis AJ. Vasculogenic mimicry and tumor angiogenesis. Am J Pathol 2000; 156(2):361-381.

(206) Maniotis AJ, Folberg R, Hess A, Seftor EA, Gardner LM, Pe'er J et al. Vascular channel formation by human melanoma cells in vivo and in vitro: vasculogenic mimicry. Am J Pathol 1999; 155(3):739-752.

(207) Mueller AJ, Maniotis AJ, Freeman WR, Bartsch DU, Schaller UC, Bergeron-Lynn G et al. An orthotopic model for human uveal melanoma in SCID mice. Microvasc Res 2002; 64(2):207-213.

(208) Seftor EA, Meltzer PS, Kirschmann DA, Pe'er J, Maniotis AJ, Trent JM et al. Molecular determinants of human uveal melanoma invasion and metastasis. Clin Exp Metastasis 2002; 19(3):233-246.

(209) Seftor RE, Seftor EA, Koshikawa N, Meltzer PS, Gardner LM, Bilban M et al. Cooperative interactions of laminin 5 gamma2 chain, matrix metalloproteinase-2, and membrane type-1-matrix/metalloproteinase are required for mimicry of embryonic vasculogenesis by aggressive melanoma. Cancer Res 2001; 61(17):6322-6327.

(210) Timar J, Toth J. Tumor sinuses- vascular channels. Pathol Oncol Res 2000; 6(2):83-86.

(211) Shirakawa K, Tsuda H, Heike Y, Kato K, Asada R, Inomata M et al. Absence of endothelial cells, central necrosis, and fibrosis are associated with aggressive inflammatory breast cancer. Cancer Res 2001; 61(2):445-451.

(212) Shirakawa K, Wakasugi H, Heike Y, Watanabe I, Yamada S, Saito K et al. Vasculogenic mimicry and pseudo-comedo formation in breast cancer. Int J Cancer 2002; 99(6):821-828.

(213) Shirakawa K, Kobayashi H, Heike Y, Kawamoto S, Brechbiel MW, Kasumi F et al. Hemodynamics in vasculogenic mimicry and angiogenesis of inflammatory breast cancer xenograft. Cancer Res 2002; 62(2):560-566.

(214) Liu C, Huang H, Donate F, Dickinson C, Santucci R, El Sheikh A et al. Prostate-specific membrane antigen directed selective thrombotic infarction of tumors. Cancer Res 2002; 62(19):5470-5475.

(215) Sharma N, Seftor RE, Seftor EA, Gruman LM, Heidger PM, Jr., Cohen MB et al. Prostatic tumor cell plasticity involves cooperative interactions of distinct phenotypic subpopulations: role in vasculogenic mimicry. Prostate 2002; 50(3):189-201.

(216) Sood AK, Seftor EA, Fletcher MS, Gardner LM, Heidger PM, Buller RE et al. Molecular determinants of ovarian cancer plasticity. Am J Pathol 2001; 158(4):1279-1288.

(217) Hao X, Sun B, Zhang S, Zhao X. [Microarray study of vasculogenic mimicry in bi-directional differentiation malignant tumor]. Zhonghua Yi Xue Za Zhi 2002; 82(19):1298-1302.

(218) Sun B, Zhang S, Zhang D, Du J, Guo H, Zhao X et al. Vasculogenic mimicry is associated with high tumor grade, invasion and metastasis, and short survival in patients with hepatocellular carcinoma. Oncol Rep 2006; 16(4):693-698.

(219) Zhao XL, Du J, Zhang SW, Liu YX, Wang X, Sun BC. [A study on vasculogenic mimicry in hepatocellular carcinoma]. Zhonghua Gan Zang Bing Za Zhi 2006; 14(1):41-44.

(220) Hess AR, Seftor EA, Seftor RE, Hendrix MJ. Phosphoinositide 3-kinase regulates membrane Type 1-matrix metalloproteinase (MMP) and MMP-2 activity during melanoma cell vasculogenic mimicry. Cancer Res 2003; 63(16):4757-4762.

(221) Khwaja A, Lehmann K, Marte BM, Downward J. Phosphoinositide 3-kinase induces scattering and tubulogenesis in epithelial cells through a novel pathway. J Biol Chem 1998; 273(30):18793-18801.

(222) Boehm T, Folkman J, Browder T, O'Reilly MS. Antiangiogenic therapy of experimental cancer does not induce acquired drug resistance. Nature 1997; 390(6658):404-407.

(223) Kerbel RS. A cancer therapy resistant to resistance. Nature 1997; 390(6658):335-336.

8 Acknowledgements

First of all I want to say a big thank you to all my colleagues; without you this thesis would not have been possible.

Foremost, I want to thank Prof. Dr. Ernst Wagner and Dr. Manfred Ogris, my supervisors and the driving forces of the project, for their overall scientific support and for always coming with competent and encouraging suggestions.

Thanks toPD Carsten Culmsee for helping me with hypoxia experiments, pathway questions and for providing NF-κB fibroblasts. Thanks to Dr. A. Kurosh for helping me also with hypoxia experiments and Dr. J. Pelisek for providing PEC cells.

A big thank to Wolfgang Roedl due to his excellent technical knowhow. I am very grateful to Dr. Martina Rüffer for her support and suggestions.

I want to thank Lilja Thoenes for a very pleasant collaboration during her master thesis in the context of delevopment tumor and tumor vasculature strategies (Spitzenforschungsgruppe). Thanks also to Dr. S. Zahler for support in endothelial cell questions and helping me with microscopy. Many thanks to Andrea Rothmeier for your time to help me with transfection experiments.

Thank you, Julia Kloeckner, my favourite lab partner, for ‘telekinetic’ experiments and our great ‘calculation collaboration’, and also to Clemens Thoma for worthy succession. Many thanks to Stefan Landshammer for “scientific” discussions and other stuff; thanks to Silke van der Piepen and Alenka Schwert for their assistance in performing in vivo experiments.

Thanks to Markus, Jaro and Greg for funny afterwork men´s nights.

But life was more than only science, and I thank you all my friends for your direct and indirect support. Especially, many thanks to Bea and Claudia for everything.

Finally, this thesis would not have been possible without the help of my family and I want to say a big thank you to my parents for so many reasons!

9 Curriculum vitae

Personal data

Date of birth: 24.12.1975

Place of birth: Buchloe, Germany

Marital status: unmarried

Education

08/2003 – to present	PhD thesis at the Department of Pharmaceutical Biology-Biotechnology, Ludwig-Maximilian-University, Munich, Germany; supervisor: Prof. Dr. Ernst Wagner
08/2003	Licensure as pharmacist
10/2002-04/2003	Internship at the Department of Pharmaceutical Biology-Biotechnology, Ludwig-Maximilian-University, Munich
05/2002-10/2002	Internship at Internationale Ludwigs Apotheke, Munich, Germany
11/1996-02/2002	Studies of pharmacy, Ludwig-Maximilian-University, Munich, Germany
08/1995-10/1996	Civilian service, Walchensee, Germany
09/1986-06/1995	Secondary school, Gymnasium Schwabmünchen, Germany

Annex

Table of contents

1 Introduction

1.1 Targeting strategies within the GDEPT concept

Tumor cells as well as tumor endothelial cells are possible targets for gene delivery within the GDEPT (gene directed enzyme prodrug therapy) concept (compare FIG 1-5 of the thesis). Therefore, development of highly specific and efficient gene delivery systems for in vivo application is necessary to achieve sufficient levels of therapeutic enzyme expression.

1.1.1 Gene delivery strategies

Current gene therapy vectors can be divided into two major groups: viral vectors which are derived form natural viruses, and nonviral, synthetic vectors (1).

Viral vectors have developed natural pathways to transfer their genetic information into cells, and offer an efficient system for introducing foreign DNA sequences into mammalian cells. Viral vectors are highly efficient in cellular uptake, intracellular delivery and therefore results in high gene transfer efficiency. Therefore viral systems were one of the first vectors used in gene delivery systems (2). Genetically engineered retroviral vectors were the first gene delivery systems used in gene therapy studies being utilized for efficient transduction of mammalian cells ex vivo and already led to therapeutic success (3;4). Good progress has been achieved in terms of modifying viral vectors in terms of removing viral genes associated with pathogenic function and in altering their natural tropism (5). In spite of recent improvements, concerns about their safety are still a strong aspect in their usage as these vectors bear the risk of random integration into the host genome followed by a possible activation of oncogenes (3;6). Moreover, inflammatory effects and host immune response are further obstacles in the application of viral vectors for gene therapy, particularly when the therapeutic concept demands multiple applications (7).

Nonviral vectors are usually based on chemically defined cationic lipids (lipoplexes) or cationic polymers (polyplexes) which condense DNA to protect it from enzymatic digestion (8-11). Polycationic carriers for gene delivery include natural DNA binding molecules like histones and protamines or chemically synthesized polycationic polymers like polylysine or polyethylenimine (PEI), which was shown to be a highly efficient carrier for the delivery of genetic information (8;12). Lipoplexes and polyplexes were already used for gene delivery in vitro and in vivo. Non viral vectors have only low immunogenicity since immunogenic proteins can be avoided in vector

design (13). This allows repeated applications of the gene delivery system. Moreover, non viral vectors offer high flexibility regarding size of the genetic material that should be delivered and exhibit a wide spectrum in surface modifications that allows a more universal usage than viral gene delivery systems. The major obstacle of non viral systems is that they are still less efficient compared to viral systems (14). For in vivo application it is necessary that the vector is small and does not exhibit unspecific interactions with biological fluids and non-target cells (15).

1.1.1.1 Targeting to tumor cells

Tumors can be targeted passively by their capacity to accumulate macromolecular components and particles due to an effect called “enhanced retention and permeability” (EPR effect) (16;17). This effect results from an abnormal leaky architecture of tumor vasculature (hyperpermeability) and inadequate lymphatic drainage. As blood flow is decelerated in tumor vessels, diffusion into the tissue is increased and accumulation of blood delivered compounds can reach 10 fold higher ranges compared to healthy tissue (18;19).

Both, tumor cells and the tumor vasculature offer specific molecular targets, which can be utilized for even more specific delivery of therapeutic genes. Various cell surface markers have been identified that are highly expressed on proliferating tumor cells. Incorporation of binding ligands against these specific surface structures into gene transfer systems has the potential to further increase selectivity and efficiency of tumor targeted vectors (20;21).

1.1.1.2 Targeting towards tumor vasculature

Due to the fact that tumor cells critically depend on a functional blood vessel network, tumor vessels seem to be an attractive target for gene therapy. Moreover drug resistance of tumors often is the reason for negative outcome of chemotherapy. Endothelial cells have a functional apoptosis system, are genetically stable and in close contact to the blood stream witch make them easily accessible for systemically applied drugs (22). The efficient, save and selective delivery of gene transfer complexes to the tumor vasculature is therefore a major goal for therapeutic approaches.

Especially the GDEPT concept seems to be useful for therapies focused to tumor vasculature and has several advantages compared to the “classical” antiangiogenic tumor therapy with low molecular drugs (1).

Tumor vasculature is characterized by mitotic activity of endothelial cells and several surface markers are highly expressed that are not present in resting blood vessels of healthy tissue. Many of these surface proteins are involved in promoting tumor angiogenesis (23;24)

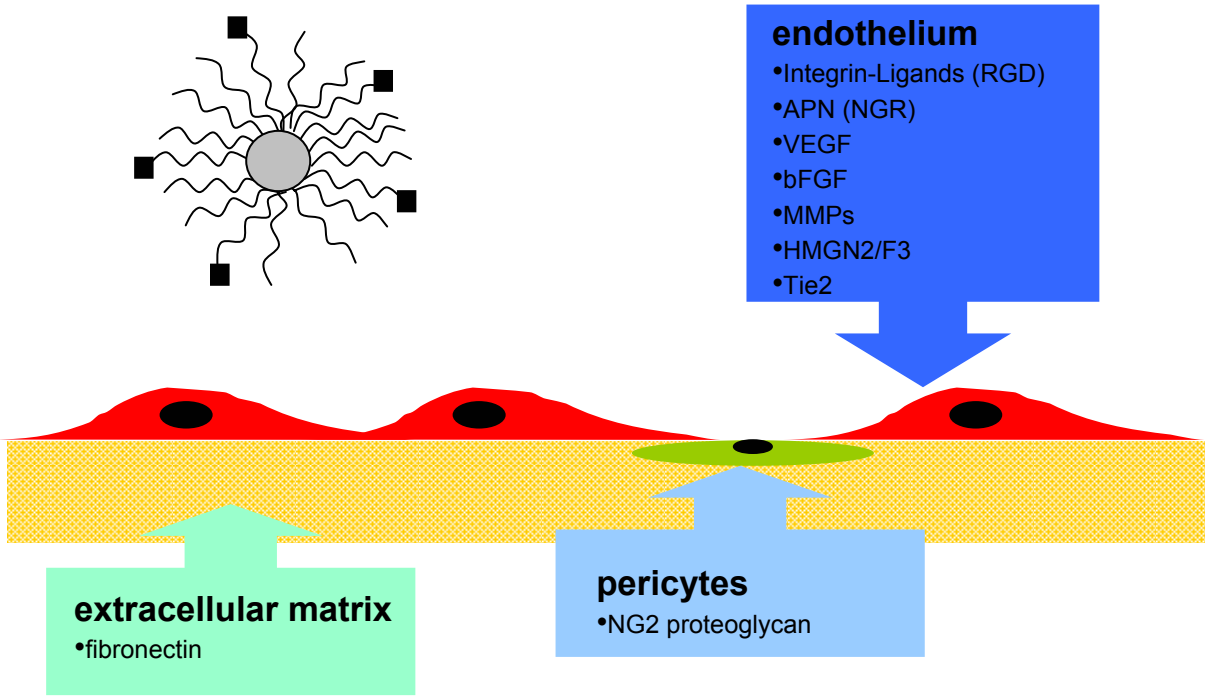

Fig.: 1-1 Tumor vessel ligands: Gene delivery vectors (top left) can be targeted to certain markers of the tumor vascular system with the help of corresponding ligands. In this work, vectors based on PEI were targeted with RGD- and NGR- peptides to achieve selectivity in gene transfer.

Targeting these specific receptors by incorporating targeting ligands into the gene delivery systems, therapeutic genes can be delivered in a selective way to tumor endothelial cells (25).

Integrins are heterodimeric cell surface receptors consisting of an α- and a β-subunit. Their function is to mediate adhesion processes, to provide for traction during cell migration and to forward mechanical and chemical signals from the surrounding matrix. Many integrin receptors are involved in cell cycle regulation, differentiation, survival and apoptosis of endothelial cells (26). Endothelial cells in angiogenic active vessels exhibit an integrin expression pattern that is different from endothelial cells in resting blood vessels. Especially the integrins αvβ5 and αvβ3 are upregulated in endothelium undergoing angiogenesis (27). Integrin antagonists are shown to induce

apoptosis and inhibit proliferation of endothelial cells, hence receptor function of αvβ3 integrins are essential for survival and maturation of newly formed blood vessels. The overexpression of these integrins in tumor vessels and integrin supported internalization of payloads (28),bound to integrin recognition sequences, makes them an attractive target for gene transfer systems.

Utilizing phage display technique, a short peptide sequence, arginine-glycine-aspartic acid (RGD) was found to be highly selective for tumor vasculature (29;30). The integrins αvβ5 and αvβ3 have been identified to be the corresponding receptors for the RGD peptide sequence. Modification of the sequence into a bicyclic version of the RGD motif showed increased binding affinity for αvβ5 and αvβ3 and decreased binding to other integrins (31).

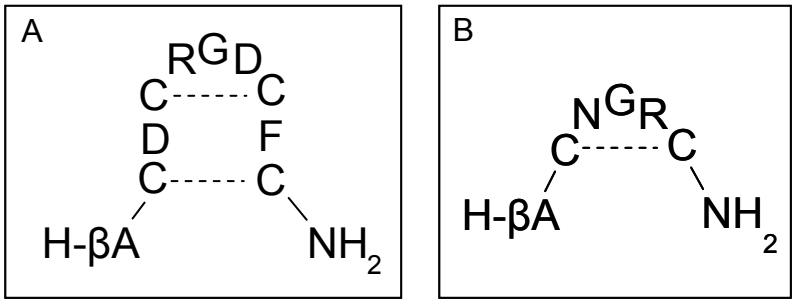

Fig.: 1-2 Targeting Peptides: A) bicyclic RGD containing peptide binding to integrins B) Cyclic NGR containing peptide binding to aminopeptidase N

Aminopeptidases are ubiquitously expressed in a wide subset of cells and have been recently identified to play an important role in angiogenesis. Aminopeptidase N (APN, also termed CD13) was shown to be expressed exclusively on newly formed blood vessels and is absent on normal vasculature (32;33). A short peptide sequence NGR has been identified to be a highly selective ligand to APN by in vivo screening of peptide libraries. Cyclic as well as linear peptides containing the NGR peptide sequence home to tumor vessels in vivo (34). Stabilizing the binding peptide through a disulfide bond (sequence CNGRC) led to conformational changes and increased targeting efficiency (35). Both, RGD and NGR-ligands were already used in tumor targeted gene delivery systems based on PEI; different efficiency in tumor targeting capability was observed (36-38).

2 Additional materials and methods

2.1 Melittin derivate (CMA-3)

The melittin analog CMA-3 was obtained from the Genzentrum (group of G.J. Arnold, Munich, Germany), or IRIS Biotech (Marktredwitz, Germany). The peptide was synthesized with a purity of > 95% and was used as acetate salt after lyophilization in 4% acetic acid. C-mel-analog (CMA-3) had the following sequence:

CMA-3: GIGA VLKV LTTG LPAL ISWI KRKR EEC

The CMA-PEI conjugate are synthesized according to (39). The molar ratio CMA-3/PEI was 9/1.

2.2 Targeting ligands and conjugates

Integrin binding sequence ACDCRGDCFC and CD13 binding sequence CNGRC were purchased from Jerini Peptide Technology.

RGD-PEG-PEI25 and NGR-PEG-PEI25 conjugates linked with a heterobifunctional 3.5kDa PEG derivate were synthesized as described in (40). The molar ratio of PEG/PEI in the resulting conjugates was approximately 0.8/1.

2.3 PEG-PEI conjugate

NHS-PEG 5kD was coupled to BPEI as described in (41). The molar ratio of PEG/PEI25 was 23/1.

2.4 Additional antibodies

Primary antibodies

Rat-anti-mouse CD13 antibody and mouse-anti-human CD13 antibody, were obtained from Dako, Copenhagen, Denmark.

Secondary antibodies

Goat-anti-mouse IgG Horseradish Peroxidase conjugate antibody was part of the Amplex Red ELISA KIT and was obtained from Invitrogen, UK.

2.5 Polyplex formulation

2.5.1 Polyplex formation for RGD/NGR targeting experiments

Plasmid DNA encoding luciferase was condensed with LPEI or peptide-PEI conjugates at an N/P ratio (PEI nitrogen to DNA phosphate ratio) of 6. DNA/PEI polyplexes were prepared at a final DNA concentration of 200µg/ml as described in Kircheis et al. 1997. Briefly, indicated amounts of plasmid DNA and PEI or peptide-

PEI conjugates were each diluted in HEPES-buffered glucose (HBG, 5% (w/w) glucose, 20mM HEPES, pH 7.1) and rapidly mixed by pipetting up and down 10-20 times. Targeted and non-targeted polyplexes were allowed to stand for at least 20min at room temperature (RT) before use.

2.5.2 Polyplex formation for in vitro transfection (GDEPT experiments)

In general, polyplexes were generated by condensing plasmid DNA encoding luciferase, EGFP-N1 or pCMV-CYP2B1 with LPEI at a molar ratio of PEI nitrogen to DNA phosphate (N/P) of 6. For this reason, plasmid DNA and PEI or PEI conjugates were each diluted in HBS (HEPES buffered saline and rapidly mixed by pipetting up and down 10 to 20 times. DNA/PEI polyplexes were prepared at a final DNA concentration of 20µg/ml. Polyplexes were allowed to stand for at least 20min at room temperature before use.

2.5.3 Measurement of particle size and zeta potential

Particle size of polyplexes was measured by laser-light scattering using a Malvern Zetasizer 3000HS (Malver Instruments, Worcestershire, UK). Polyplexes for RGD- and NGR-targeting experiments were generated in HBG at DNA concentrations of 200µg/ml and subsequently diluted in Optimem to 10µg/ml prior to size measurement. For estimation of the surface charge, polyplexes were diluted in 10mM NaCl to give a final DNA concentration of 2µg/ml and zeta potential was measured as previously described (42).

2.6 Transfection of HUVEC cells by electroporation

HUVEC cells were grown prior to the transfection up to 90% confluency in collagen G coated tissue flasks (TPP, Switzerland). Cells were harvested by treatment with Trypsin/EDTA and washed with prewarmed PBS. 10^6 cells were diluted in 100µl Nucleofector solution, followed by the administration of 1µg plasmid DNA. Afterwards, the cell suspension was transferred in the Amaxa certified cuevette and transfection was carried out according to manufactures protocol.

2.7 Covalent labelling of plasmid DNA

Plasmid pCMV-LUC was covalently labelled with the fluorophores Cy3 or Cy5 using the Label IT kits (MIRUS, Madison, WI) according to the manufacture's instructions.

20µg of DNA were diluted with 1xBuffer A to a final volume of 195µl. After addition of 5µl reconstituted Label IT reagent, the reaction mixture was incubated for 3h at 37°C.

To precipitate labelled DNA, 550µl of ice-cold 100% ethanol and 22µl of 3M sodium acetate were added. The solution was then mixed and placed at -20°C overnight. Subsequent centrifugation at 16000g for 60min (4C) allowed removal of unreacted label in the supernatant. The pellet was gently washed with ice-cold 70% ethanol, centrifuged again and all traces of ethanol were removed. Labelled DNA was allowed to dry for 5min and finally resuspended in sterile HBG.

Cy3 (ε550nm=150,00lxmol-1xcm-1) and CY5 (ε650nm=250,00lxmol-1xcm-1) content was measured by absorption at 550nm and 650nm, respectively. DNA was quantified by measuring the absorbance at 260nm with the ratio of 260nm/280nm serving as an index for DNA purity (≥1.8 ≤1.9). On average, one dye molecule was bound per 50bp to 100bp, approximately.

2.8 Hypoxia induced regulation of integrin and aminopeptidase N expression

Cells were seeded in collagen G (Biochrome AG, Germany) coated 24 well plates (TPP, Switzerland) at a density of 15000 cells per well. About 20h after the seeding, standard medium M199 containing 10% FBS and 20ng/ml bFGF was replaced by a M199 medium, containing 2% FBS and 20ng/ml bFGF. Cells were cultured for further 24h at 37ºC in humified atmosphere containing either air (20.9% oxygen; normoxia) or air sufficient to give 1% oxygen. 5% CO_2 was used in all normoxic and hypoxic incubators, with the balance being nitrogen in the hypoxic incubation. Oxygen partial pressure was measured with a digital oxymeter (GMH 3690, Greisinger Electronic, Germany). The treatment was followed by a washing step with prewarmed PBS and fixing the cells with paraformaldehyde (4% in PBS) for 5min.

After removing surplus fixing solution, cells were washed repeatedly with MACS buffer (PBS containing 2.5% FBS). For receptor status detection, cells were exposed to the mouse-anti-human CD51/CD61 (Dako) antibody and the mouse-anti-human CD13 antibody (Dako) for 2h at room temperature. Both antibodies were dissolved in MACS buffer (PBS containing 2.5% FBS) at a dilution of 1:200. Background staining was determined by exposing the cells to the mouse IgG control antibody (Dako), likewise. The incubation was followed by a repeatedly washing procedure with MACS buffer (PBS containing 2.5% FBS) whereas the last washing step was performed with PBS containing 0.05% Tween 20. Afterwards cells were exposed to the goat-anti-mouse IgG Horseradish Peroxidase Conjugate (Invitrogen) for 1h at room temperature. The secondary antibody was used at a dilution of 1:500 in MACS buffer

(PBS containing 2.5% FBS).The incubation was again followed by a repeated washing procedure with MACS buffer (PBS containing 2.5% FBS) to remove unbound secondary antibody, whereas the last washing step was performed with PBS. Following HRP detection was performed according to manufactures protocol, using the Amplex® Red ELISA KIT #1 (Invitrogen).

Fluorescence signal of in situ converted resorufin was measured using a Cary Eclipse fluorimeter (Cary, Mulgrave, Australia) with excitation and emission wavelengths set to 562 and 585 nm, respectively. Measurements were performed in triplicate and receptor status was expressed as relative fluorescence units (RFU) after normalizing on DNA content via the Hoechst33258 based DNA content assay.

2.9 Flow cytometric analysis of integrin receptor and aminopeptidase N on MDA-435 and CT26 tumor cells

MDA-MB435 and CT26 tumor cells were seeded in collagen G (Biochrome AG, Germany) coated 24 well plates (TPP, Switzerland) at a density of 30000 cells per well, 24h prior receptor status detection. Cells were washed with prewarmed PBS and harvested by treatment with collagenase (Biochrome AG) (625 U/ml). The obtained cell suspensions were pooled and adjusted to 10^6 cells/ml with MACS buffer (PBS containing 2.5% FBS) after centrifugation for 5min at 150g (Haereus, Megafuge 1.0 R). The cell suspension was divided up and exposed separately to the following antibodies at 4°C for 1h; mouse-anti-human CD51/61 antibody (Dako), mouse-anti-human aminopeptidase N (CD13) (Dako), rat-anti-mouse CD51 (Dako) and rat-anti-mouse CD13 (Biolegend). All antibodies were applied at a total dilution of 1:200.

Afterwards, cells were washed repeatedly with prewarmed MACS buffer (PBS containing 2.5% FBS) to remove unbound antibody. Secondary antibody staining was performed by exposing the cell suspension to ALEXA488 labelled anti-mouse- or anti-rat-antibody (Invitrogen), respectively for 1h at 4°C. The secondary antibody was applied at a total dilution of 1:400.

Samples were kept on ice until analysis. Receptor status was assayed by flow cytometry using a Cyan™ MLE flow cytometer (Dako). The fluorophore was excited at 488nm and emission was detected by using a 530/40nm bandpass filter. To discriminate between viable and dead cells and to exclude doublets, cells were appropriately gated by forward/side scatter and pulse width. Antibody staining was evaluated via electronically analysis by using the WINMDI software.

2.10 Flow cytometric analysis of cellular polyplex association after inhibition with antibody and free peptide ligands

Cells were seeded in a collagen G (Biochrome AG, Germany) coated 24 well plate (TPP, Switzerland) at a density of 30000 cells per well 24h prior the inhibition experiment. About 30min prior to administration of indicated polyplexes, containing Cy5-labelled DNA (20% Cy5 DNA), anti-human CD51/61 antibody (1:100) (Dako), free peptide ligands RGD or NGR (1000-fold excess, compared to polyplex incorporated ligands), respectively were added to the cells in 300µl of serum free Optimem I medium at 4°C. Indicated polyplexes were added (350ng/well, N/P 6, HBG) and cells were further incubated for 30min at 4°C. After total incubation time of 1h, supernatant was removed and cells were washed with cold PBS to remove unbound polyplexes. Cells were harvested by treatment with collagenase (625 U/ml) (Biochrome) and kept on ice until analysis. Cell association of polyplexes was assayed by flow cytometry using a Cyan^{TM} MLE flow cytometer (Dako). The fluorophore Cy5 was excited at 635nm and emission was detected at 665/20nm. To discriminate between viable and dead cells and to exclude doublets, cells were appropriately gated by forward/side scatter and pulse width. Polyplex association was evaluated via electronically analysis by using the WINMDI software.

2.11 In vivo application of polyplexes

For the intravenous application of polyplex formulations mice were fixed in a modified 50 ml Falcon tube, whereas supply of air was enabled by a hole in the bottom of the tube. Another hole near the closure head of the tube provided accession to the tail of the mice. Shortly before the injection, the tail was heated with warm water (about 38-39ºC) in order to reach a dilatation of the tail veins. Polyplex formulations were administered into the tail vein (applied volume was about 250µl) with an insulin needle (30 G needle, U40, Becton Dickinson) within about 20 seconds.

2.12 In vivo application of Cy3-labeled polyplexes

At a tumor volume of approximately 400mm^3, NGR- peptide ligand containing polyplexes (LPEI-NGR30) and control polyplexes containing BPEI instead of NGR-PEG-conjugate were injected into the tail vein of CT26 tumor bearing mice at a dose of 50µg DNA/20g body weight 2h before mice were sacrified.

2.13 In vivo application of FITC-dextran

For systemic application of FITC-dextran (42kDa) (10mg/ml in PBS, 200µl), as a marker for vessel leakiness, procedure of injection was similar to the application of the polyplex formulations described above. After the injection mice were removed from the tube. At 0.5h after the application of the FITC-dextran mice were sacrified.

2.14 Luciferase reporter gene expression, in vivo experiments

Animals were sacrified 48h after the application of polyplex formulations with CO_2. Before organs were removed the vein to the liver was cut in order to reduce rest blood. Removed organs were immediately frozen in liquid nitrogen and kept at -80C.

For luciferase assay, organs were thawed on ice followed by lyses with 1ml of 250mM TRIS buffer pH 7.5. For homogenisation of tissue samples an IKA-tissue homogenizer (IKA, Staufen) was used. The homogenisation process was performed on ice to avoid heating of the samples. Homogenisized samples were centrifuged for 10min at 4C and 2800g (Haereus, Megafuge 1.0 R). For measurement of luciferase activity 25µl of the clear supernatant was submitted to luciferase measurement in a luminometer (Berthold, Bad Wildbad, Austria) as described previously (42). Background signal (about 200RLU) was substracted; reporter gene expression was calculated in RLU for each organ.

2.15 GFP reporter gene expression, in vivo experiments

Animals were sacrified 48h after the application of polyplex formulations with CO_2. Before organs were removed the vein to the liver was cut in order to reduce rest blood. Collected organs were fixed with 4% PFA in PBS for 24h before embedding in OTC and freezing. Analysis was performed by fluorescence microscopy.

3 Results

3.1 Evaluation of endothelial cells as producer cells in the antiangiogenic GDEPT concept

In situ activated CPA influences primary endothelial cells in terms of proliferation, migration and differentiation processes. CPA activation in the context of the CYP/CPA GDEPT concept can be mediated either by CYP2B1 expressing tumor cells via bystander activity or directly by CYP2B1 expression in tumor endothelial cells. In following studies the suitability of primary endothelial cells to act as producer cells was investigated.

3.1.1 Transient transfection of HUVEC cells with polyplexes based on PEI

3.1.1.1 Evaluation of optimized transfection conditions for HUVEC cells with PEI22lin polyplexes

For evaluation of optimal in vitro transfection conditions, HUVEC cells were transfected with increasing amounts of LPEI polyplexes, containing plasmid DNA encoding luciferase as a reporter gene. Transfection efficiency was investigated by determination of luciferase activity 24h after the transfection as described in materials and methods.

In a parallel performed experiment, transfected cells were analyzed for their viability. Therefore the MTT assay was performed 24h after the transfection with the LPEI polyplexes.

Up to 300ng of plasmid DNA per 15000 cells, HUVEC cells did not show significant reduction in metabolic activity determined by the MTT assay. When the transfection was performed with 400ng of plasmid DNA or more, decrease in metabolic activity was more distinctive (FIG 3-1).

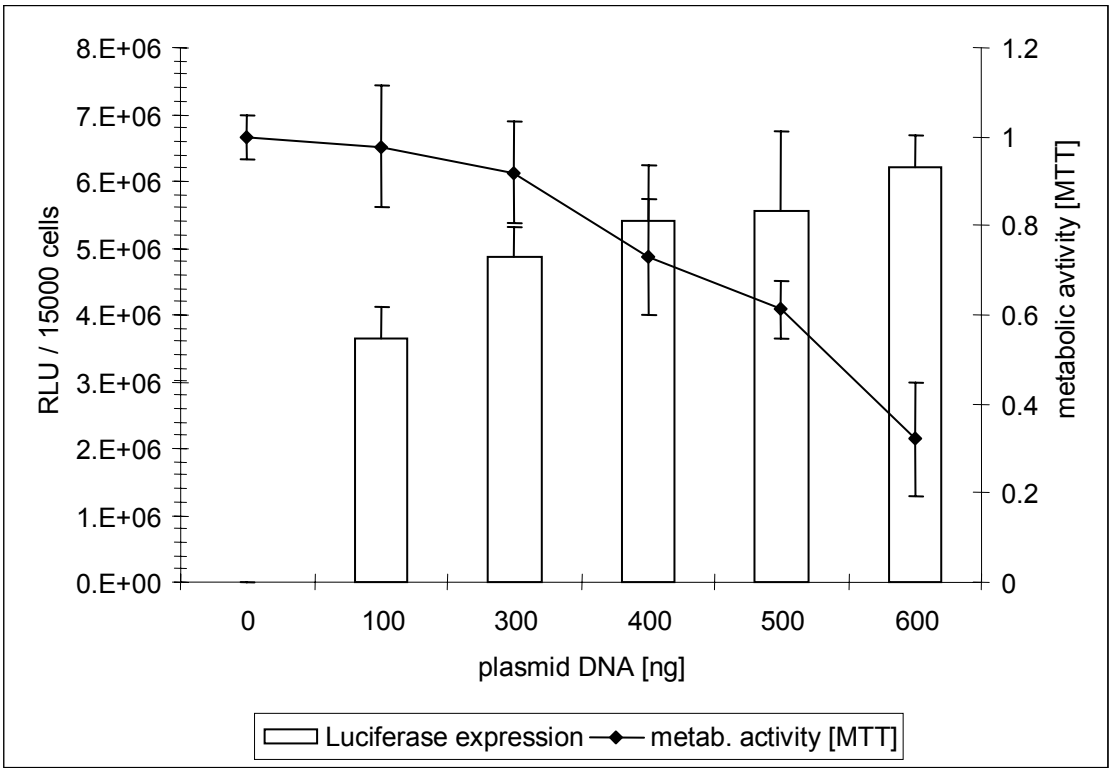

Fig.: 3-1 Luciferase expression and metabolic activity of transfected HUVEC cells. HUVEC cells were transfected with LPEI (N/P=6, HBS) polyplexes and indicated amounts of transfection complexes. Luciferase and metabolic activity was determined 24h after the transfection as described in materials and methods. Values are means ± SE of triplicates.

In summary, transfection efficiency and cell viability LPEI polyplexes at a dose of 300ng of plasmid DNA was chosen for further experiments.

3.1.1.2 Evaluation of CYP expression of transient transfected HUVEC cells

3.1.1.2.1 Detection of CYP2B1 expression in HUVEC cells

HUVEC cells were transfected with LPEI (N/P=6, HBS) polyplexes containing pCMV-CYP2B1 plasmid DNA and 48h after transfection antibody-staining against rat CYP2B1 protein was performed as described in materials and methods. Control-experiments were performed with plasmid DNA encoding for luciferase and additionally, staining was performed with the negative control antibody (Dako).
Expressed CYP2B1 protein was detected in several HUVEC cells.

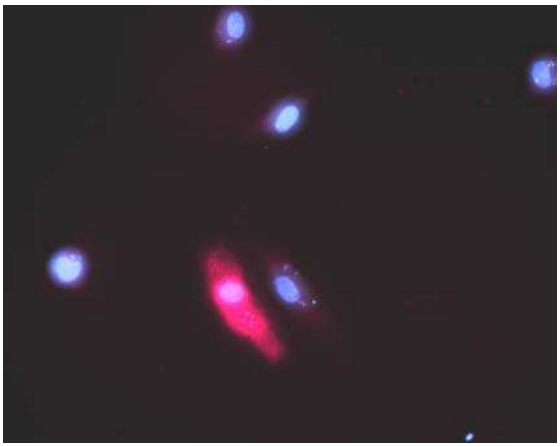

Fig.: 3-2 Antibody-staining of expressed rat CYP2B1 protein in HUVEC cells. Expression of CYP2B1 protein was detectable in HUVEC cells 48h after the transfection with pCMV-CYP containing LPEI polyplexes. Samples were visualized by epifluorescence microscopy. Blue: Hoechst 33258 stained nuclei. Red: antibody stained CYP2B1 protein.

3.1.1.2.2 Transfection efficiency with pCMV-CYP2B1

HUVEC cells were transfected under optimized conditions (300ng plasmid DNA, LPEI N/P=6, HBS) with pCMV-CYP2B1 plasmid DNA containing polyplexes. 48h after the transfection antibody-staining against ratCYP2B1 protein was performed and transfection efficiency was quantified by epifluorescence microscopy. The detected rate of ratCYP2B1 expressing HUVEC cells was 6.7%.

3.1.1.2.3 Detection of CYP2B1 enzymatic activity by the resorufin assay

HUVEC cells were transfected under optimized transfection conditions (300ng plasmid DNA, LPEI N/P=6, HBS) with pCMV-CYP2B1 plasmid DNA containing polyplexes. Control experiment was performed with LPEI polyplexes containing plasmid DNA encoding for luciferase. Forty eight hours after transfection CYP2B1 enzymatic activity was evaluated by performing the resorufin assay. Fluorescence levels of the CYP2B1 transfected cells were at the same level of pCMV-LUC transfected cells. Specific CYP2B1 enzymatic activity was not detectable by the resorufin assay (data not shown).

This might be due to rather low transfection efficiency of LPEI polyplexes on HUVEC cells and/or insufficient enzymatic activity of expressed ratCYP2B1 in HUVEC cells.

3.1.1.3 Evaluation of biological activity of transient CYP2B1 expression

3.1.1.3.1 Proliferation

HUVEC cells were transfected under optimized conditions with pCMV-CYP2B1 and pCMV-LUC as a control (300ng plasmid DNA, LPEI N/P=6, HBS). Thirty six hours after the transfection cells were incubated with different concentrations of CPA (0mM, 0.05mM, 0.5mM and 1mM) in the medium. After culturing the transfected cells for 3

days in the absence or in the presence of CPA, respectively, proliferation rate was determined by Hoechst DNA content assay. Additionally metabolic activity of the cells was measured by MTT assay. Proliferation rate of HUVEC cells transfected with pCMV-CYP and with pCMV-LUC was decreased in the same manner when cells were cultivated with 1.0mM CPA, indicating the occurrence of unspecific toxicity (data not shown). When transfected cells were cultured for 3 days with 0.05 and 0.5mM CPA in the medium no anti-proliferative effects of CPA treatment were detectable (data not shown). Additionally performed MTT assay resulted in similar decrease in metabolic activity of CYP2B1 transfected HUVECs and reporter gene transfected HUVEC cells when incubation was performed for 3 days with 1.0 mM CPA in the medium (data not shown). Similar to the result of the DNA content assay, CPA concentrations of 0.05mM and 0.5mM CPA did not influence metabolic activity of the cells (data not shown).

3.1.1.3.2 Migration

HUVEC cells were transfected under optimized conditions with pCMV-CYP2B1 and pCMV-LUC as a control (300ng plasmid DNA, LPEI N/P=6, HBS). 24h after the transfection the medium was removed and cells were washed 2 times with warm (37°C) PBS. Cells were harvested with trypsin/EDTA (Promega) and seeded on collagen coated glass dishes. When the cell layer was confluent after 12h the scratch wound assay was performed in the absence or in the presence of 0.5mM or 1.0mM CPA. Migration was visualized by transmitted light microscopy and quantification was performed by picture analysis using Axio Vision LE.

No antimigrative effects in CYP2B1 transfected cells were detectable in comparison to the reporter gene transfected HUVEC cells (data not shown).

3.1.1.3.3 Tube forming

HUVEC cells were transfected under optimized conditions with pCMV-CYP2B1 and pCMV-LUC as a control (300ng plasmid DNA, LPEI N/P=6, HBS). 36h after the transfection the medium was removed and cells were washed 2 times with warm (37°C) PBS. Cells were harvested with trypsin/EDTA (Promega) and the matrigel tube forming assay was performed in the absence or in the presence of 0.5mM or 1.0mM CPA. Tube forming was visualized by transmitted light microscopy.

There was no difference detectable in the ability of the cells in forming tube like structures between pCMV-CYP and pCMV-LUC transfected cells (data not shown).

3.1.1.4 Transient transfection of HUVEC cells by electroporation

3.1.1.4.1 Transfection efficiency and detection of the CYP2B1 protein by antibody staining

HUVEC cells were transfected with pCMV-CYP by electroporation as described in materials and methods (Amaxa). Transfection efficiency was quantified 48h after the transfection by antibody staining against rat CYP2B1 protein. Control experiment was performed with luciferase encoding plasmid (pCMV-LUC). Following the antibody staining, cell nuclei were counter stained with Hoechst 33258 and quantification was performed by epifluorescence microscopy. The detected rate of ratCYP2B1 expressing cells was 38%.

3.1.1.4.2 Detection of CYP2B1 enzymatic activity by the resorufin assay

HUVEC cells were transfected with pCMV-CYP by electroporation as described in materials and methods (Amaxa). Enzymatic activity of expressed CYP2B1 protein was measured by resorufin-assay 48h after the transfection. Control experiments were performed with Luciferase encoding plasmid (pCMV-LUC).

Enzymatic activity of expressed CYP2B1 was detectable in HUVEC cells transfected with CYP2B1 encoding plasmid. Fluorescence levels in control plasmid (pCMV-LUC) transfected cells were not clearly distinguishable from signal to noise ratio.

Yet detected fluorescence signal in pCMV-CYP transfected HUVEC cells was low compared to X39 cells.

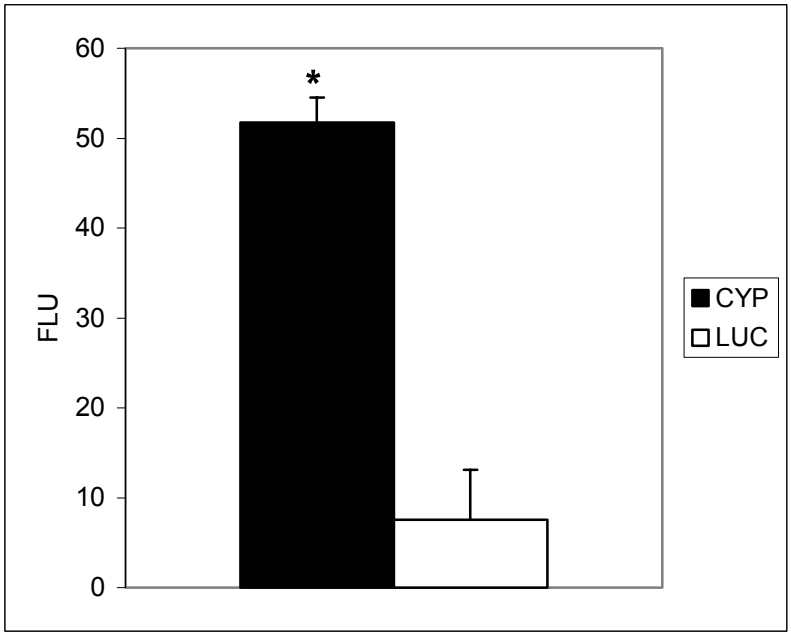

*Fig.: 3-3 Enzymatic activity of transiently CYP2B1 expressing HUVEC cells. HUVEC cells were transfected by electroporation (Amaxa, standard protocol for HUVEC cells) with either pCMV-LUC or pCMV-CYP2B1 plasmid DNA. CYP2B1 enzymatic activity was measured 48h after the transfection by resorufin-assay. Values are means ±SE of triplicates. *p<0.05 compared to control plasmid DNA (Mann-Whitney U-test).*

3.1.1.5 Evaluation of biological activity of transient CYP2B1 expression

3.1.1.5.1 Antiproliferative effects

HUVEC cells were transfected with pCMV-CYP2B1 by electroporation as described in materials and methods (Amaxa). Control transfections were performed with Luciferase encoding plasmid (pCMV-LUC). Thirty six hours after transfection HUVEC cells were cultured for 3 days in the absence or in the presence of indicated concentrations of CPA, followed by determination of cell proliferation by Hoechst DNA content assay. Additionally metabolic activity of treated cells was measured by MTT assay.

The proliferation rate of transfected HUVEC cells was not decreased in pCMV-CYP2B1 and in control plasmid (pCMV-LUC) transfected cells when cultivation was performed in the presence of up to 0.5 mM CPA. Culturing CYP2B1 transfected HUVEC cells in the presence of 1.0mM CPA resulted in a reduction in proliferation rate by 50%, whereas control plasmid expressing cells did not exhibit a significant decrease in proliferation rate.

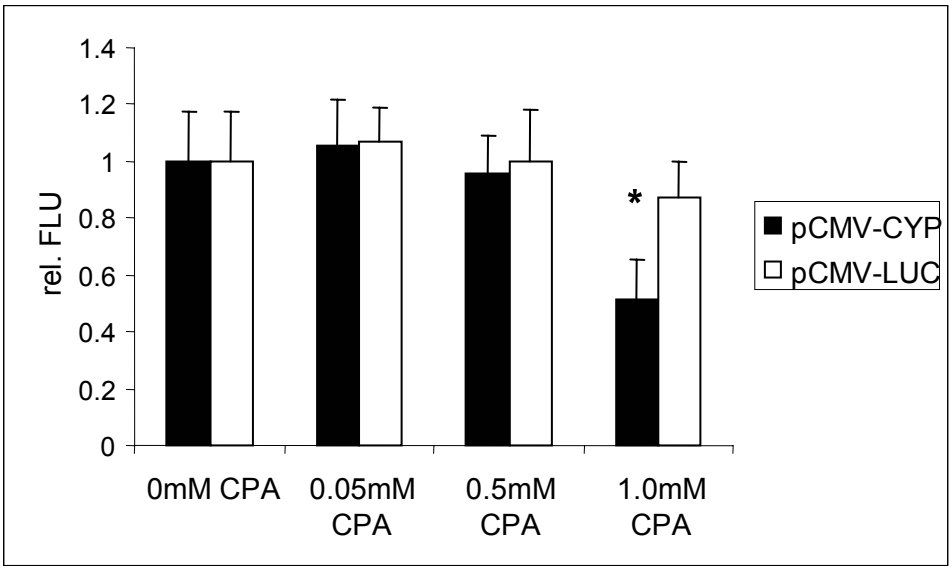

*Fig.: 3-4 Proliferation of pCMV-CYP transfected HUVEC cells (by electroporation) treated with different concentrations of CPA.HUVEC cells were transfected by electroporation as described in materials and methods (Amaxa) with either pCMV-LUC or pCMV-CYP2B1 plasmid DNA. 36h after the transfection cells were treated for 3 days with different concentrations of CPA (0mM, 0.05mM, 0.5mM and 1.0mM). Cell proliferation was determined by the Hoechst DNA content assay. Measurements were normalized on DNA content of CPA untreated cells. Values are means ±SE of triplicates. *p<0.05 compared to control plasmid DNA (Mann-Whitney U-test).*

Similar to DNA content, metabolic activity of CYP transfected HUVEC cells was not significantly decreased in pCMV-CYP and in control plasmid (pCMV-LUC) transfected cells when culture was performed up to 0.5 mM CPA. However, treatment of pCMV-CYP transfected cells with 1.0 mM CPA resulted in a reduction of metabolic activity by 53%, whereas control plasmid expressing HUVEC cells did not exhibit significant decrease in metabolic activity (data not shown).

3.1.1.5.2 Antimigrative effects of transient expressed CYP2B1 in HUVEC cells

HUVEC cells were transiently transfected with pCMV-CYP or pCMV-LUC plasmid DNA by electroporation as described in materials and methods. 24h after the transfection cells were seeded on collagen coated glass dishes and cultivated in the absence of CPA for further 12h, followed by the scratch wound assay in the presence of indicated concentrations of CPA.

Migration capability of HUVEC cells transfected with the pCMV-CYP was decreased in the presence of CPA. However also control cells transfected with pCMV-LUC exhibited reduced migration rate when the scratch wound assay was performed in the presence of CPA. Inhibition of migration was not significantly different comparing pCMV-CYP and pCMV-LUC when the scratch wound assay was performed in the presence of 0.5mM CPA. A more pronounced decrease in migration rate occurred

when pCMV-CYP transfected HUVEC cells were incubated with 1mM CPA whereas migration rate of pCMV-LUC transfected cells was not further decreased.

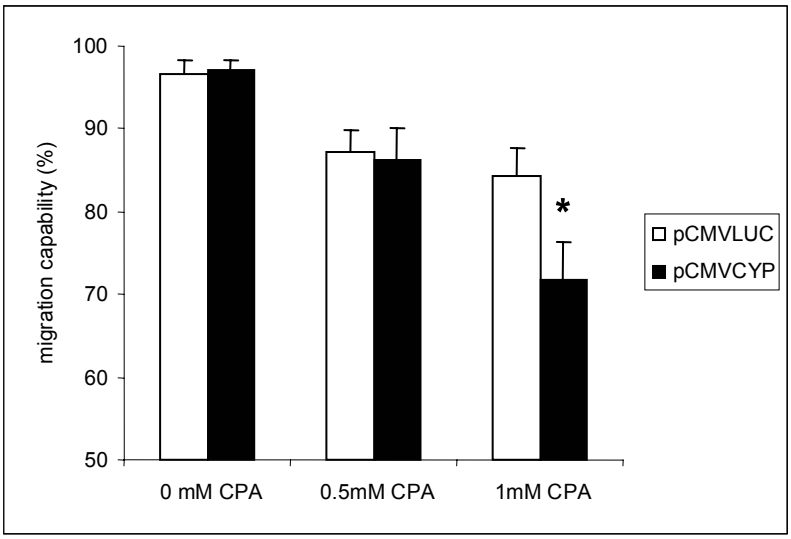

*Fig.: 3-5 Inhibition of migration after transient transfection of HUVECs with pCMV-CYP in the presence of CPA. HUVEC cells were transfected by electroporation (Amaxa) with either pCMV-LUC or pCMV-CYP plasmid DNA. Scratch wound assay was performed 36h after transient transfection for 12h at CPA concentrations 0.0mM, 0.5mM and 1.0mM. Measurements were normalized on migration capability of untreated cells. Values are means ±SE of four measurements. *p<0.05 compared to control plasmid DNA (Mann-Whitney U-test).*

3.1.1.5.3 Transient expressed CYP2B1 inhibits tube forming in the presence of CPA

HUVEC cells were transiently transfected with pCMV-CYP or pCMV-LUC by electroporation (Amaxa). 24h after the transfection a matrigel tube forming assay was performed in the presence of indicated concentrations of CPA. After an incubation time of 4h, tube forming was analyzed by transmitted light microscopy.

Forming of tube like structures was similar in pCMV-CYP and pCMV-LUC transfected HUVEC cells. The count rate of tube like structures was reduced in the presence of CPA in pCMV-CYP and pCMV-LUC transfected cells in a similar manner, indicating unspecific toxic effects of the prodrug CPA (data not shown).

3.2 Tumor and tumor vasculature targeting

Gene therapy is a promising strategy to treat tumors due to the potential of higher specificity and lower side effects in comparison to established therapies with cytotoxic chemotherapeutics. In the in vitro evaluated GDEPT concept it was shown that tumor cells as well as endothelial cells can act as producer cells for in situ activated cyclophosphamide. CYP2B1 metabolic activity in the tumor/tumor vessels would cause higher, therapeutic relevant concentrations of activated

cyclophosphamide in the tumor area leading to more effective treatment and lower side effects.

Insufficient transfection efficiency of target cells in vivo is one main obstacle in current gene therapy approaches with polyplexes based on PEI. Therefore it is necessary to improve gene delivery vectors to enhance their specificity and transfection efficiency. Tumor cells and tumor vasculature can both act as promising targets for the delivery of therapeutic genes. Microenvironmental conditions in the tumor (hypoxia) can be utilized for further increasing transfection specificity of vectors by choosing ligands, targeted to receptors, upregulated by hypoxia. As hypoxia sensitive targeting ligands the RGD-peptide and the NGR-peptide were chosen. The receptors for these ligands are present on tumor and/or tumor vessel cells and are upregulated on endothelial cells in hypoxic environment (43-45).

3.2.1 Biophysical Characterisation of Targeted PEI Polyplexes

3.2.1.1 Size and stability in salt containing media

Different polyplex formulations for tumor and tumor vasculature targeting with defined amounts of PEG-PEI and Peptide ligand (Tab 3-1) were analyzed in terms of particle size and stability in salt containing medium (Optimem I).

Polyplex	LPEI	BPEI-PEG	BPEI	BPEI-PEG-ligand
Plain LPEI	100%			
LPEI-BPEI-PEG50	50%	50%		
LPEI-BPEI-PEG20-BPEI30	50%	30%	20%	
LPEI-RGD50	50%			50% RGD-
LPEI-RGD45	50%	5%		45% RGD-
LPEI-RGD40	50%	10%		40% RGD-
LPEI-RGD35	50%	15%		35% RGD-
LPEI-RGD30	50%	20%		30% RGD-
LPEI-RGD25	50%	25%		25% RGD-
LPEI-RGD20	50%	30%		20% RGD-
LPEI-RGD15	50%	35%		15% RGD-
LPEI-RGD10	50%	40%		10% RGD-
LPEI-NGR50	50%			50% NGR-
LPEI-NGR45	50%	5%		45% NGR-
LPEI-NGR40	50%	10%		40% NGR-
LPEI-NGR35	50%	15%		35% NGR-
LPEI-NGR30	50%	20%		30% NGR-
LPEI-NGR25	50%	25%		25% NGR-
LPEI-NGR20	50%	30%		20% NGR-
LPEI-NGR15	50%	35%		15% NGR-
LPEI-NGR10	50%	40%		10% NGR-
LPEI-NGR5	50%	45%		5% NGR-

Tab 3-1: Polyplex formulations for control and targeted PEI-Polyplexes

Incorporation of at least 15 to 20% of the PEG-PEI25br compound leads to the formation of polyplexes that did not aggregate in salt containing medium. PEG-containing polyplexes (LPEI-RGD30 to LPEI-RGD5 and LPEI-NGR30 to LPEI-NGR30 to LPEI-NGR5, LPE-BPEI-PEG50 and LPEI-BPEI-PEG20-BPEI30) had a size around 250nm.

Above mentioned polyplex formulations remained stable for 16h, whereas unshielded or insufficient shielded polyplexes formed aggregates.

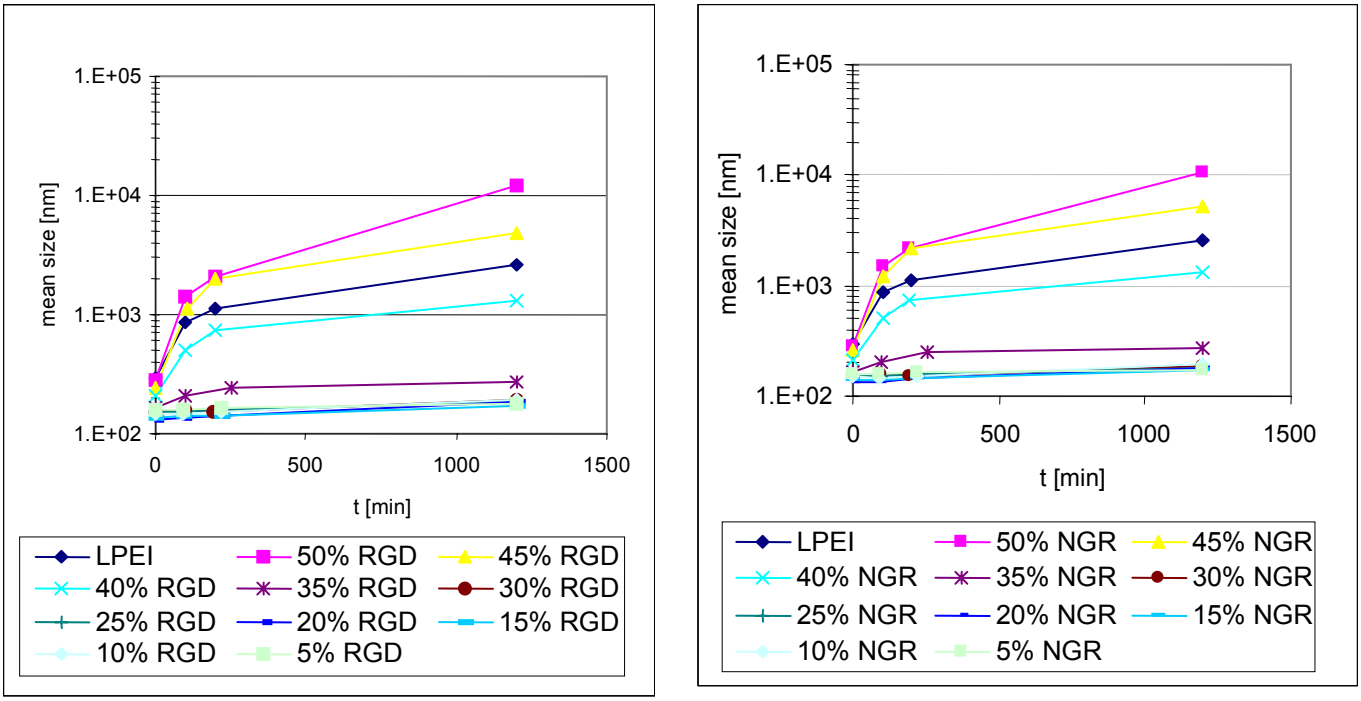

A B

Fig.: 3-6 Evaluation of stability of A) RGD-targeted polyplex formulations and B) NGR targeted polyplex formulations over the time in a salt containing medium.

Additionally, stability of size over the time was confirmed by fluorescence microscopy. Therefore, the different polyplex formulations used for the transfection experiments were labelled with sytox green. Polyplex formulations were analyzed after 30min of polyplex formation time in HBG and again after 16h incubation in Optimem. Particles LPEI-RGD20 and LPEI-NGR30 as well as LPEI-BPEI-PEG50 and LPEI-BPEI-PEG20-BPEI30 did not form aggregates whereas unshielded LPEI particles formed large aggregates (data not shown).

3.2.1.2 Zetapotential measurements of polyplexes

Measurements for Zeta potential was performed as described in materials and methods. Shielded polyplexes without peptide ligand incorporation exhibited a Zeta potential of 4.0±0.2 mV for LPEI-BPEI-PEG50 and 3.0±0.9mV for LPEI-BPEI-PEG20-BPEI30. Unshielded PEI polyplexes (plain LPEI22) had a Zetapotential of 21.0±1.6mV. The replacement of BPEI-PEG by BPEI-PEG-Ligand of up to 30% of peptide ligand in the polyplex did not change the zeta potential of the PEG-shielded polyplexes.

Polyplex	Particle Size [nm]	Zeta Potential [mV]
Plain LPEI	>1000 (aggregates)	21.0 ± 1.6
LPE-BPEI-PEG50	170 ± 22	4.0 ± 0.2
LPEI-BPEI-PEG20-BPEI30	141± 4	3.0 ± 0.9
LPEI-RGD20	199± 15	3.8 ± 0.5
LPEI-NGR30	176 ± 18	4.1 ± 0.4

Table 3-2: Particle size and Zeta potential of Targeted PEI-Polyplexes

3.2.1.3 Freeze/Thaw stability

Storage capability of ligand-containing polyplex formulations in the context of particle size was evaluated. Therefore particle size of freshly prepared polyplex formulations was determined. Afterwards polyplexes were subjected a freeze/thaw cycle followed by particle size measurements at 3 different time points.

The unshielded PEI-polyplexes (plain LPEI) initially of a medium size (400nm) formed aggregates within 30min after thawing. PEG-shielded polyplexes (LPE-BPEI-PEG50 and LPEI-BPEI-PEG20-BPEI30) initially of a medium size (150nm) were stable in size during the freeze/thaw cycle and maintained their particle size for at least 60min after thawing. The incorporation of 20% or 30% peptide ligand, respectively, did not decrease freeze/thaw stability. LPEI-RGD20 and LPEI-NGR30 did not form aggregates for at least 60min after thawing (data not shown).

3.2.2 Biological activity/Targeting

3.2.2.1 Receptor status

Receptor status for integrin αvβ3 (CD51/61) and aminopeptidase N (CD13) was determined on the human tumor cell line MDA-MB435 and the mouse tumor cell line CT26 by antibody-staining followed by FACS analysis. For detection of the receptor-

status for integrin αvβ3 and aminopeptidase N on primary endothelial cells, antibody staining was performed on HUVEC cells and analyzed also by FACS.

Cellular binding of MDA-MB-435 cells with a CD51/61 mouse-anti-human antibody clearly increased fluorescence, whereas preparations with control antibody against murine CD51/61 and with the unspecific IgG1 isotype control did not.

Antibody-staining of MDA-MB-435 cells for aminopeptidase N did not increase the fluorescence signal compared to isotype control or rat-anti-mouse CD13 antibody.

Incubation of CT26 cells with a CD13 anti-mouse antibody resulted in significantly increased fluorescence compared to the preparations with mouse-anti-human CD13 and unspecific IgG control antibody. Quantitative evaluation of the FACS data demonstrated that about 58% of the CT26 showed positive reaction for aminopeptidase N on the cell surface.

Staining of CT26 cells for integrin αv receptor did not increase fluorescence signal compared to the isotype control or anti-human integrin αvβ3 control antibody.

Incubating HUVEC cells with a CD51/61 mouse-anti-human antibody resulted in clearly increased fluorescence signal compared to the preparations with control antibody against murine CD51 and compared to the unspecific IgG isotype control. Also antibody-staining for the aminopeptidase N on HUVEC cells significantly increased the fluorescence signal compared to isotype control or rat-anti-mouse CD13 antibody.

Cell line	**Integrin αv**	**aminopeptidase N**
MDA-MB435	100%	-
CT26	-	58%
HUVEC	100%	100%

TAB.: 3-3. Receptor status of MDA-MB435, CT26 and HUVEC cells in terms of integrin αvβ3 and aminopeptidase N. Antibody-staining was performed as described in materials and methods, followed by FACS analysis. Measurements represent % positively stained cells.

3.2.2.2 Cell association

In order to evaluate differences in cell association of RGD-targeted polyplex formulations (LPEI-RGD20) versus not targeted control formulations (plain LPEI and LPE-BPEI-PEG50), integrin αvβ3 expressing MDA-MB435 cells were incubated with Cy5-labelled, indicated polyplex formulations for 1h at 4°C. Afterwards, cell association was analyzed by FACS as described in materials and methods.

Association of polyplexes occurred within 1h in all cases. Unshielded plain LPEI were detected to exhibit a broad distribution in cell association, whereas shielded

polyplexes LPEI-BPEI-PEG50 and LPEI-RGD20 resulted in narrower distributions. Association of targeted LPEI-RGD20 polyplexes resulted in increased fluorescence signal compared to the shielded control polyplex LPE50-BPEI-PEG50, despite similar biophysical properties (compare TAB 3-2).

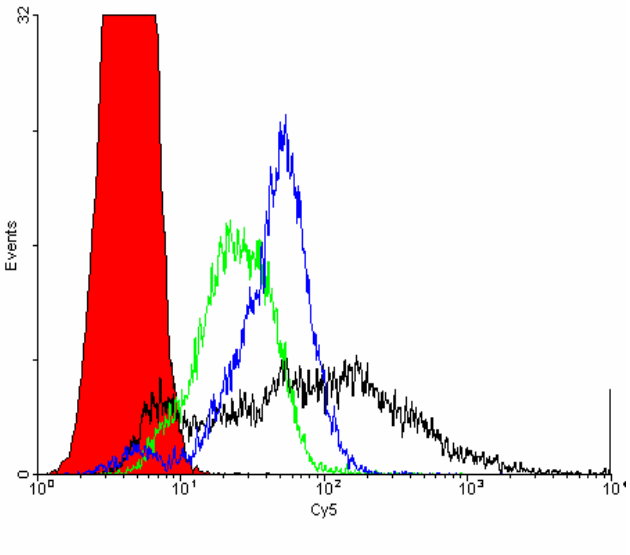

Fig.: 3-7 Total cellular association after transfection with polyplexes at 4°C. MDA-MB435 cells were transfected with plain LPEI (black), shielded LPE50-BPEI-PEG50 (green) and RGD-targeted LPEI-RGD20 (blue) polyplexes. (HBG, N/P 6) containing Cy5-labeled plasmid DNA. Total cellular association was determined by flow cytometry after 1h.

3.2.2.3 Inhibition of cell association by competition

In order to further evaluate specific binding of the peptide ligand containing polyplexes to the target cells, competition experiments with an excess of free peptide or antibody were performed on the integrin αvβ3 positive MDA-MB435 cell line.

Competition of RGD-containing polyplexes (LPEI-RGD20) with the antibody against integrin αvβ3 did not show an inhibition of cell association indicating a different binding location than the RGD binding site. Competition of LPEI-RGD20 with free RGD peptide (1000-fold molar excess) decreased clearly cell association. Interestingly, competition of K7 with free NGR peptide (1000-fold molar excess) resulted also in a similar decrease of cell association (FIG 3-8B).

The preincubation of the MDA-MB435 cells with antibody, free RGD- and free NGR-peptide (1000-fold molar excess) did not influence cell association of control polyplexes LPE50-BPEI-PEG50 (FIG 3-8A).

However, preincubation of MDA-MB435 cells with antibody resulted in decreased cellular association of plain LPEI polyplexes, whereas preincubation with free RGD- and NGR- peptide exhibited no influence on total cell association (FIG 3-8C and D).

Interestingly, no decreased fluorescence signal was detected when NGR-targeted polyplexes LPEI-NGR30 were inhibited by an excess of free NGR-peptide, whereas

an excess of free RGD-peptide influenced total association of LPEI-NGR30 polyplexes (FIG 3-8D).

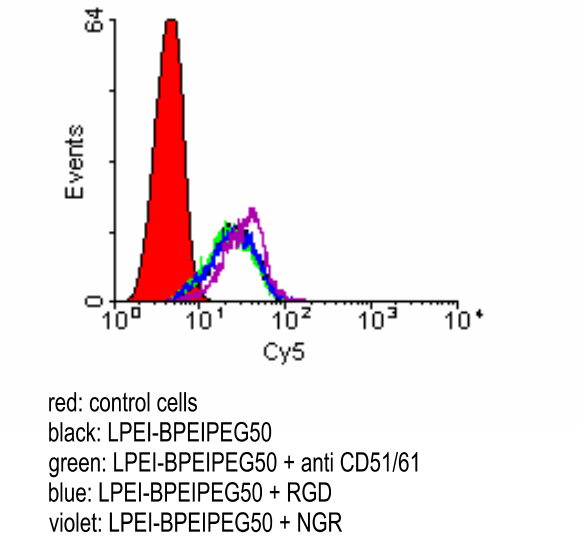

A

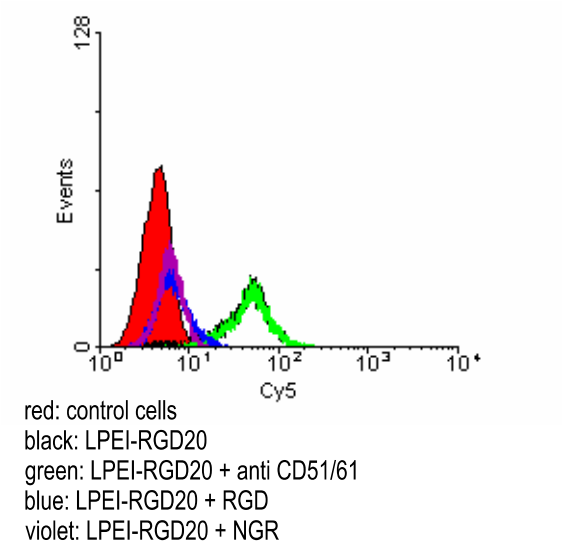

B

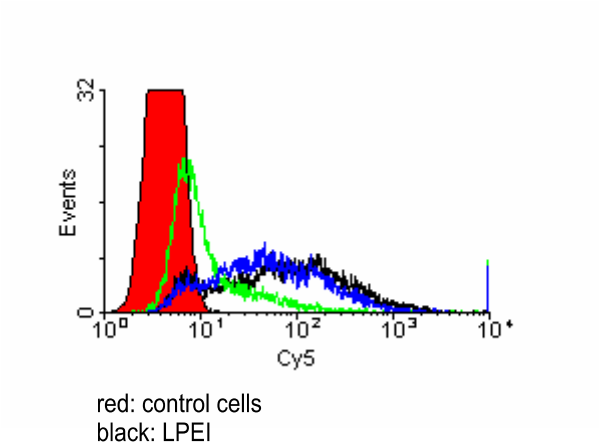

C

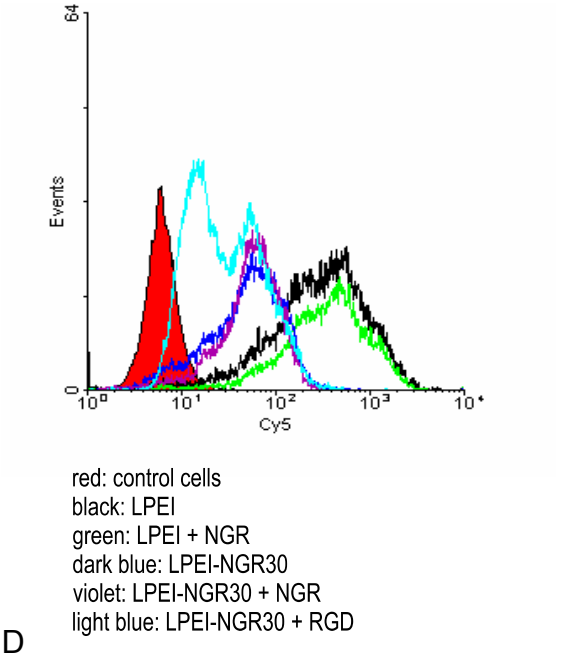

D

Fig.: 3-8 Total cellular association of indicated polyplexes formulations after preincubation of MDA-MB435 tumor cells with anti-human CD51/61 antibody or an excess of free RGD- or NGR-peptide. Cells were transfected with (A) LPE50-BPEI-PEG50 polyplexes, (B) LPEI-RGD20 polyplexes, (C) plain LPEI polyplexes and (D) plain LPEI or LPEI-NGR30 polyplexes, containing Cy5 labelled plasmid DNA. Total cellular association was analyzed by flow cytometry.

3.2.2.4 Increase in transfection efficiency by stepwise increasing ligand in shielded polyplexes on HUVECs

Reporter gene expression (luciferase activity) was evaluated on primary endothelial cells (HUVECs). HUVEC cells were transfected with pegylated polyplexes containing increasing amounts of incorporated peptide ligand. Control transfection was performed with the unshielded LPEI polyplexes.

The luciferase expression was significantly increased by incorporating peptide ligand in the PEG-shielded polyplexes. Incorporation of RGD-PEG-PEI and NGR-PEG-PEI resulted in an increase in luciferase activity in a targeting-peptide rate dependent manner.

PEG-shielded, peptide ligand containing polyplexes reached a similar luciferase expression level as the unshielded plain LPEI22 control when the transfection was performed in the presence of serum.

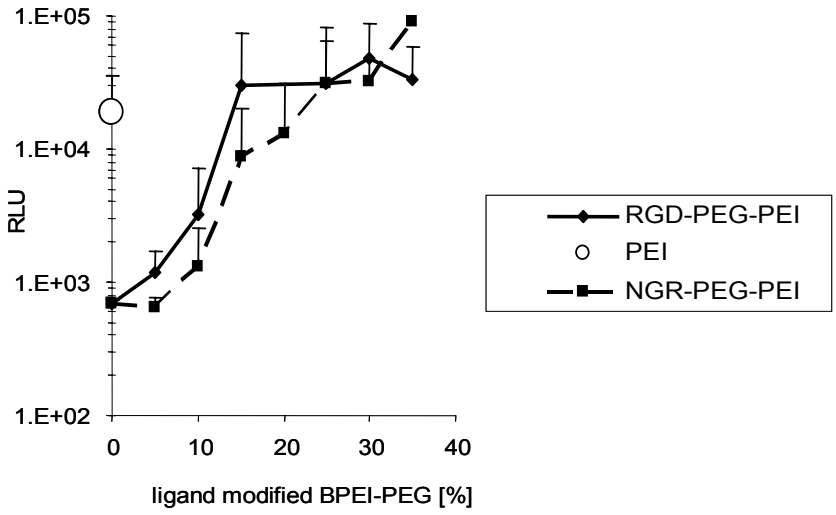

Fig.: 3-9 Increase in luciferase expression levels by equipping shielded polyplex formulations with increasing amounts of RGD- or NGR- peptide ligands. HUVEC cells were transfected with polyplex formulations incorporated indicated amounts of targeting ligand in the polyplexes. Control transfection was performed with plain LPEI polyplexes. Luciferase activity was measured 24h after the transfection as described in materials and methods. Values are means ± SE of triplicates.

3.2.2.5 In vitro transfection efficiency of LPEI-RGD20 and LPEI-NGR30

Reporter gene expression (luciferase activity) was evaluated in the tumor cell lines MDA-MB435 and CT26 and in primary endothelial cells (HUVECs). Cells were transfected with different polyplex formulations and luciferase assay was carried out 24h after the transfection as described in materials and methods. For the transfection experiments all polyplexes were generated at an N/P ratio of 6 in HBG.

Polyplex formulations included the biophysically characterized polyplexes with RGD- and NGR-peptides (LPEI-RGD20 and LPEI-NGR30). Cells were also transfected with plain LPEI polyplexes as a control for unshielded polyplexes; LPEI-BPEI-PEG50 and LPEI-BPEI-PEG20-BPEI30 were used as a control for ligand free shielded polyplexes in the transfection experiments.

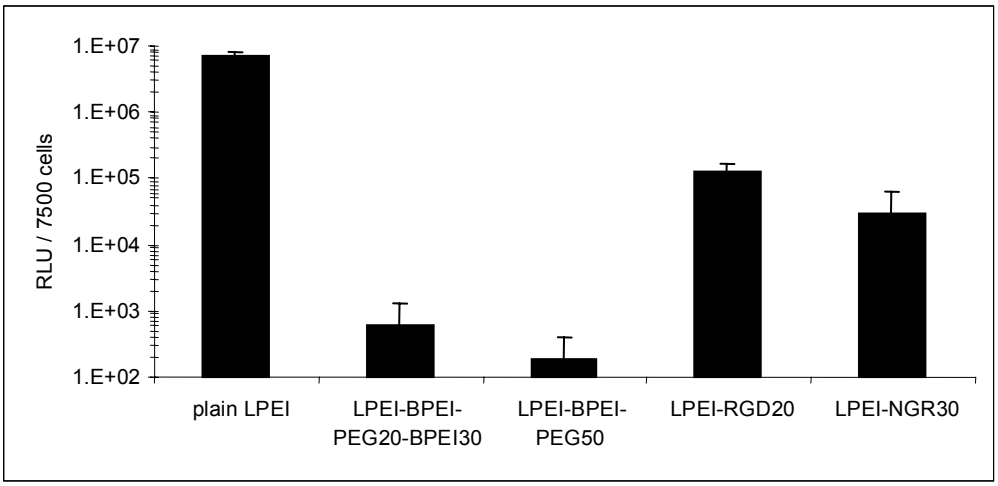

A

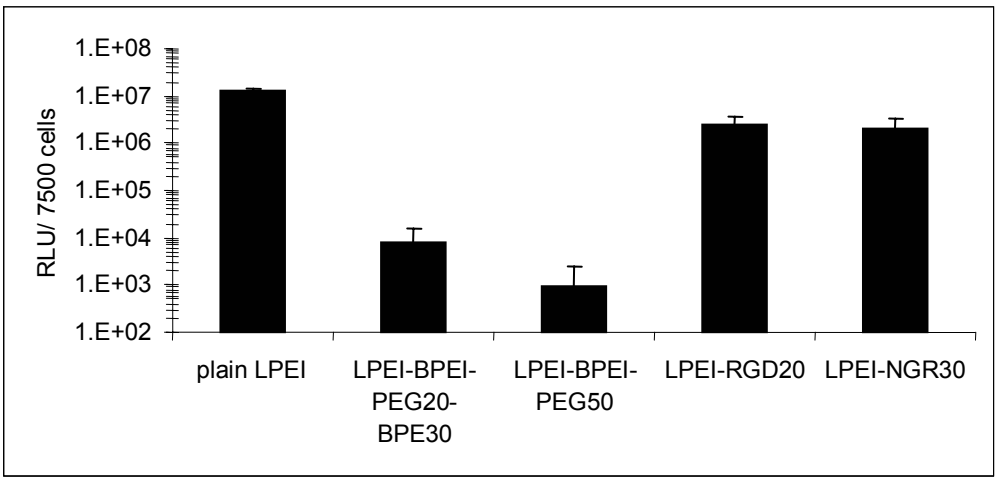

B

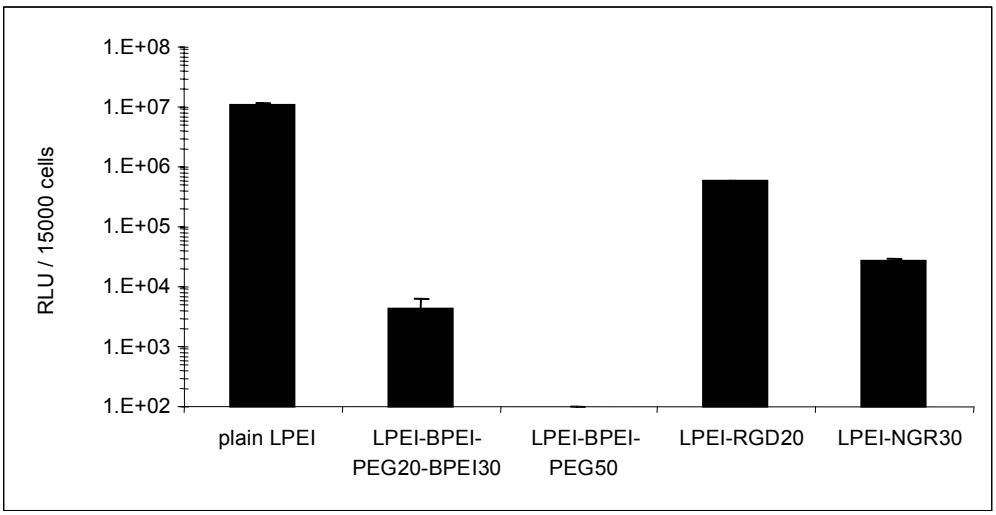

C

Fig.: 3-10 Transfection efficiency of RGD- and NGR-peptide ligands containing polyplexes. (A) MDA-MB435, (B) CT26 and (C) HUVEC cells were transfected with plain LPEI22, LPEI-BPEI-PEG20-BPEI30, LPEI-BPEI-PEG50 or targeted polyplexes LPEI-RGD20 and LPEINGR30. Polyplexes were prepared in HBG at N/P 6. Luciferase assay was performed 24h after transfection as described in materials and methods. Mean values ± SE of triplicates are shown.

3.3 Hypoxia increases selectivity of RGD- and NGR- peptide ligands containing polyplexes

Hypoxia is a common phenomenon in solid tumors. Hypoxia triggers several adjustment processes as well in tumor cells and in tumor stroma cells. Endothelial cells are able to adjust to hypoxic environment, among other mechanism, by increasing several types of receptors on the cell surface.

3.3.1 Receptor regulation in primary endothelial cells by hypoxia in terms of integrin αvβ3 and aminopeptidase N

Primary endothelial cells (HUVECs) were grown in normoxic and hypoxic environment for 24h (21% Oxygen or 1% Oxygen). To evaluate regulations in integrin αvβ3 and aminopeptidase expression on the cell surface antibody staining was performed followed by the Amplex® red assay. Simultaneous cell number was evaluated by Hoechst 33258 based DNA content assay as described in materials and methods. HUVEC cells showed upregulation of the integrin αvβ3 and the aminopeptidase receptor indicated by higher enzymatic activity when cells were grown for 24h in the hypoxic environment. Fluorescence signal was normalized on cell count in order to avoid falsification by unequal proliferation rate in different environments.

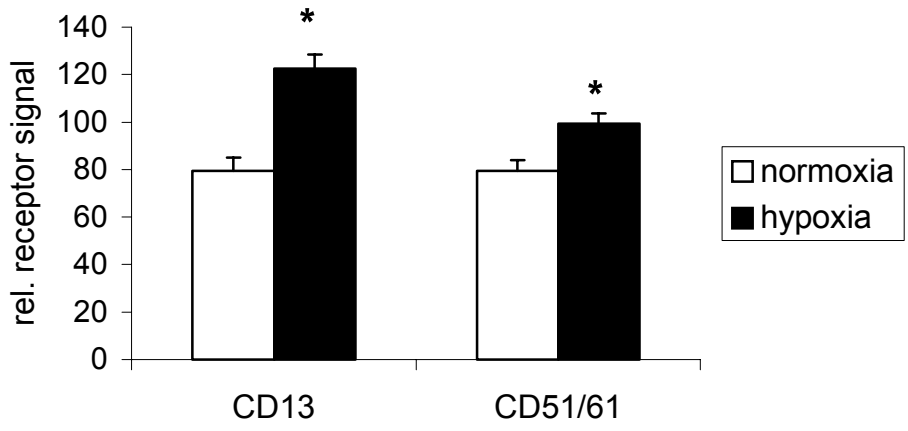

*Fig.: 3-11 Receptor status CD13 and CD51/61 of HUVEC cells; normoxic versus hypoxic conditions. HUVEC cells were cultured for 24h either in a normoxic (21% O2) or in hypoxic atmosphere (1%) in the presence of 2% serum. Receptor status was determined by incubating the pretreated cells with antibodies against integrin avb3 or aminopeptidase followed by incubation with a second antibody with enzymatic activity. Conversion of a non-fluorescent compound to resorufin by the enzymatic activity of the second antibody is therefore representative for the amount of receptors on the cell surface. Receptor signal was normalized on DNA content measured by Hoechst 33258 based DNA content assay. Mean values ± SE of triplicates are shown. *p<0.05, compared to normoxic receptor expression levels (Mann-Whitney U-test).*

3.3.1.1 Enhancement of transfection efficiency by hypoxic pre-treatment

Primary endothelial cells (HUVECs) were grown in normoxic and hypoxic environment for 24h before transfection with peptide ligand containing polyplexes. In order to investigate a targeting specific enhancement of receptor regulation HUVEC cells were parallel transfected with the unshielded plain LPEI22 and the pegylated LPEI-BPEI-PEG50 polyplex. Transfection efficiency of the untargeted polyplexes remained at a similar level when cells were pretreated in a hypoxic environment. In contrast, targeted polyplexes reached higher levels of transfection efficiency when cells were pretreated in hypoxic environment before the transfection.

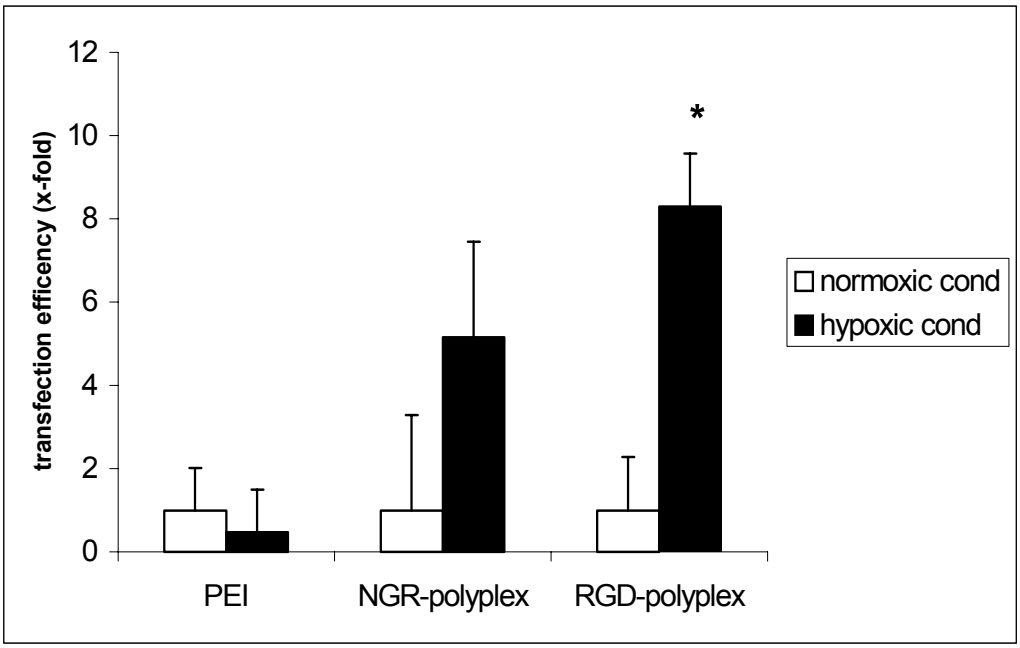

*Fig.: 3-12 Transfection efficiency of targeted polyplexes on HUVEC cells after hypoxic pre-treatment. HUVEC cells were cultured for 24 in a normoxic (21% oxygen) or hypoxic (1% oxygen) containing atmosphere with 2% serum. Afterwards transfection was performed as described in materials and methods with indicated polyplex formulations in a normoxic atmosphere and in the presence of 10% serum. Luciferase expression levels were determined 24h after the transfection. Values were normalized on expression levels of cells grown under normoxic conditions. Values are means ± SE of four measurements. *p<0.05, compared to reporter gene expression levels at normoxic conditions (Mann-Whitney U-test).*

3.3.2 Enhancement of transfection efficiency by incorporation of the endosomolytic compound CMA-3

Endosomal release of internalized polyplexes is an important step in achieving efficient gene expression with non viral gene vectors. Coupling an analog of the membrane active peptide melittin (CMA-3) to PEI25 and incorporation into the targeted polyplex should improve endosomal release and therefore enhance gene expression of the targeted polyplexes (39;46). To evaluate effects on transfection

efficiency in terms of improved endosomal release of the targeted polyplexes CMA-3-PEI25br was incorporated instead of LPEI into the polyplexes. MDA-MB435 cells were transfected with different targeted and non targeted, plain and pegylated polyplexes. CMA-3 could enhance luciferase expression to the level of the unshielded plain LPEI control polyplex for shielded RGD-targeted polyplex. Incorporation of CMA-3-PEI25br instead of LPEI resulted in a 120- to 320-fold increase in luciferase activity.

The incorporation of CMA-3 into the untargeted pegylated control polyplexes LPEI-BPEI-PEG50 did not enhance transfection efficiency significantly.

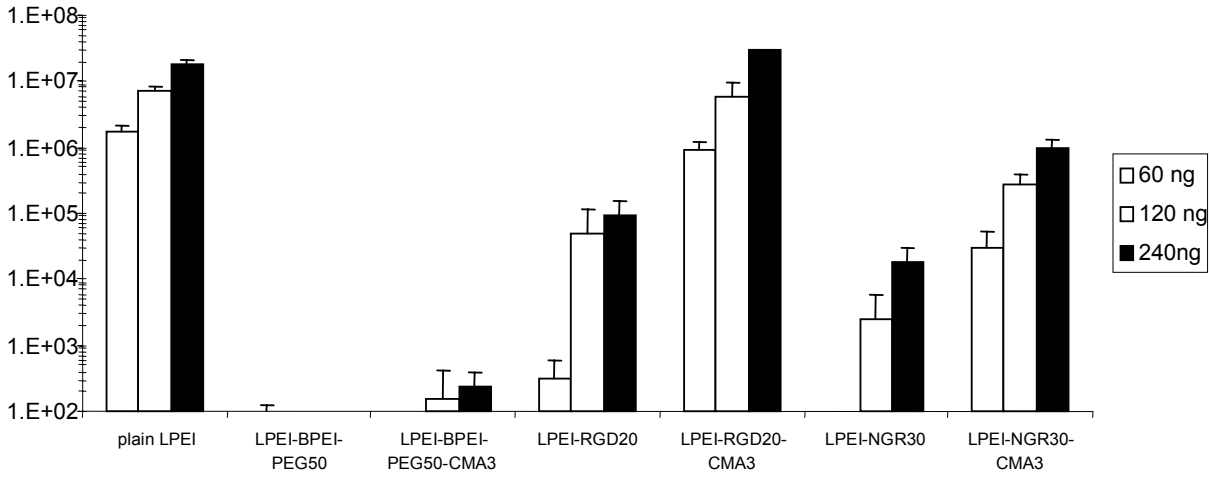

Fig.: 3-13 Effect of the melittin analog CMA-3 on transfection efficiency of targeted PEI polyplexes. 7500 cells were seeded in 48-well plates 24h prior to transfection. Cells were transfected with either plain LPEI22, LPEI-BPEI-PEG50, LPEI-RGD20 or LPEI-NGR30 and compared to cells transfected with CMA-3 containing formulations of these polyplexes (-CMA3) (formulations see Tab. 4-4). Polyplexes were prepared in HBG at N/P 6. Polyplexes in a total volume of 300µl with serum containing medium were kept on cells for 4h, thereafter the solution was replaced by fresh medium. Luciferase assay was performed 24h after transfection. Mean values + SD from n=3 are shown.

In order to verify that increased transfection efficiency is not based on altered biophysical properties of the polyplexes, particle size and zeta potential measurements were performed (TAB 3-5).

The size of the polyplexes was not altered significantly when PEI22 was exchanged by CMA3-PEI25br; polyplexes maintained their small size of <250nm for at least 60min. Furthermore incorporation of CMA-3 into the polyplexes did not result in changes in the surface charge of the indicated polyplexes.

Polyplex	CMA-3-PEI25	PEG-PEI25	Ligand-PEG-PEI25
LPEI-PEG50-CMA-3	50%	50%	
LPEI-RGD20-CMA-3	50%	30%	20% RGD-
LPEI-NGR30-CMA-3	50%	20%	30% NGR-

Tab.: 3-4: CMA-3 containing polyplex formulations

Polyplex	Particle size	Zeta potential
LPEI-PEG50-CMA3	192 ± 15	4.0 ± 1.2
LPEI-RGD20-CMA3	213 ± 8	7.1 ± 2.6
LPEI-NGR30-CMA-3	210 ± 15	4.2 ± 0.3

Tab.: 3-5: Particle size and Zeta potential of CMA-3 containing Polyplexes

3.4 In vivo evaluation

In order to evaluate characteristics of RGD- and NGR- peptide containing polyplexes in vivo, experiments were performed with subcutaneous CT26 tumor bearing SCID mice. Prior to polyplex administration morphology, blood supply and properties of tumor vesselas were analyzed.

3.4.1 Morphology of subcutaneous CT26 tumors in SCID mice

Morphology of subcutaneous CT26 tumors was evaluated by Haematoxilin/Eosin stain and is described in the thesis, chapter 1.

3.4.2 Blood supply, distribution of endothelial cells and aminopeptidase N expression

Areas of high level of CD31 staining (rat anti mouse antibody, which can specifically identify endothelial cells) correlates well with Hoechst stain, indicating sufficient blood supply in these parts of the tumor. The well vascularized regions were detected in most cases in the peripheral of the subcutaneous tumors. Regions in the core showed less CD31 staining and also less Hoechst stained nuclei.

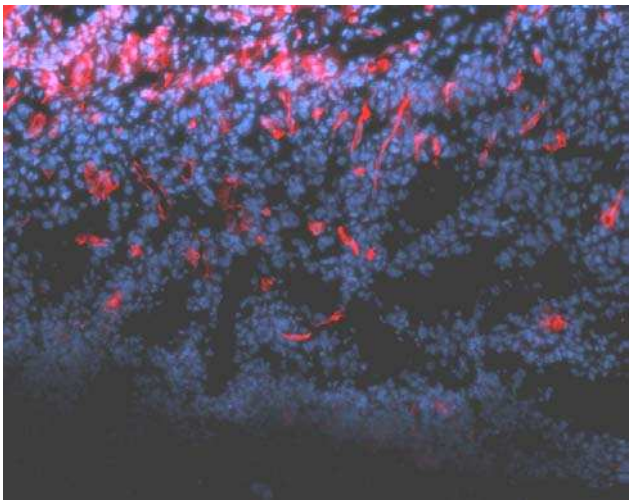

Fig.: 3-14 Distribution of endothelial cells (CD31+ cells) and functional blood vessels in subcutaneous CT26 Xenografts in SCID mice. Cryo-sections (5µm) were fixed with 4% paraformaldehyde and stained with the specific antibody rat-anti-mouse CD31 (red). The second antibody was labelled with Alexa 488. The intravenously injected Hoechst 33258 stain was visualized as well (blue). Analysis was performed with 20x 0.4 Zeiss objective with a Zeiss Axiovert 200 fluorescence microscope equipped with a Zeiss Axiocam.

Cryosections were further investigated for CD13 staining. In contrast to the CD31 staining, positive immunoreactions was detected for CD13 all over the tumor tissue. This indicates an expression of aminopeptidase N on the CT26 tumor cells themselves. Control staining was performed with the unspecific control IgG.

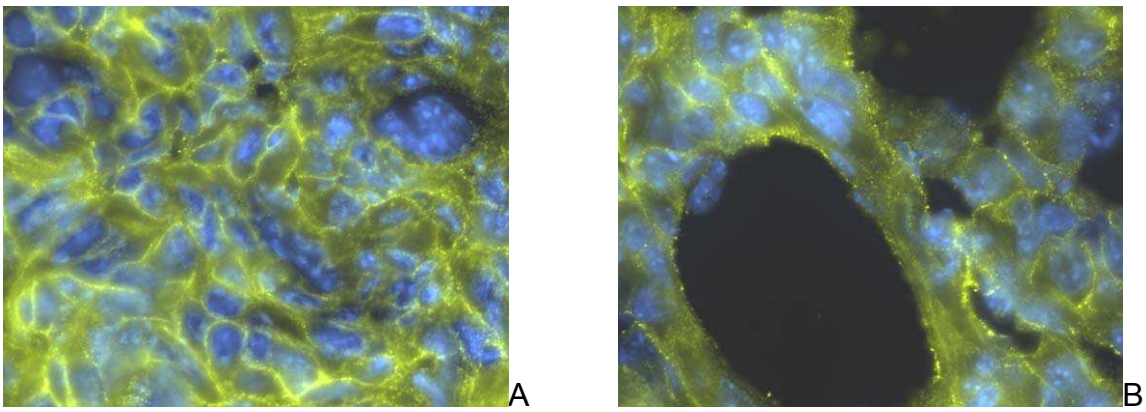

Fig.: 3-15 Cryo sections (5µm) were fixed with 4% paraformaldehyde and stained with specific antibodies for A,B rat-anti-mouse CD13 (yellow). Secondary antibodies were labelled with Alexa 488. The intravenously injected Hoechst 33258 stain was visualized as well (blue). Analysis was performed either with 63x1.4 Zeiss oil immersion objective with a Zeiss Axiovert 200 fluorescence microscope, equipped with a Zeiss Axiocam.

3.4.2.1 Blood supply and vessel leakiness in the CT26 tumor model

Gene vector systems depend highly on vascular escape to achieve efficient delivery; leakiness of tumor vessels enhances uptake of polyplex formulations within the tumor tissue and increases transfection efficiency. Therefore, to investigate the tumor vessels in the subcutaneous CT26 tumor model in terms of leakiness, experiments with high molecular fluorescent marked dextrane (FITC-dextrane, 42 kDa) were performed. 200 µl of FITC-dextran, solved in PBS (10mg/ml) were administered intravenously to CT26 bearing SCID mice. One h after the FITC-dextran application, mice were subjected to a second intravenous injection with Hoechst33258 in PBS

(2.5mg/ml). The Hoechst 33258 staining was detected in all organs and the tumor (blue staining). The staining of the FITC-dextran was located all over the tumor tissue (green staining) (FIG 3-16), whereas FITC-dextran was distributed in healthy tissue only in a small degree (data not shown). In brain tissue FITC-dextran staining was only detectable in the cavity of blood vessels (data not shown). The localisation of FITC staining within the tumor tissue indicates leakiness of vessels.

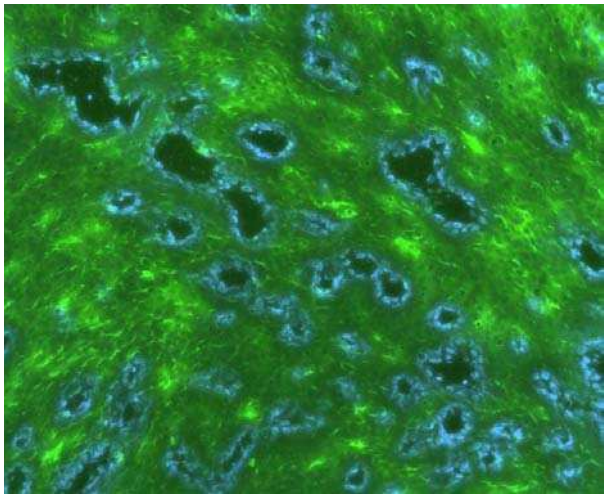

Fig.: 3-16 Cryo sections (8µm) were visualised unfixed immediately after preparation. Distribution of FITC-dextran in the tissue was visualized by fluorescence microscopy. The intravenously injected Hoechst 33258 stain was visualized as well (blue).Analysis was performed with 20x 0.4 Zeiss objective with a Zeiss Axiovert 200 fluorescence microscope equipped with a Zeiss Axiocam.

3.4.2.2 Distribution of polyplexes

Evaluation of polyplex distribution of the untargeted polyplex LPEI-BPEI-PEG50 and NGR- peptide containing polyplex LPEI-NGR30 was performed by fluorescence microscopy. Therefore Cy3 labelled DNA was incorporated into the polyplexes and the polyplexes were administered intravenously. At 2h after the application mice were sacrified and organs were collected. Both polyplex formulations were found in the tumor tissue. No obvious difference in tissue distribution could be found by fluorescence microscopic analysis. 2h after application, polyplexes were not distributed within the tumor tissue but associated to vessel like structures in the tumor tissue.

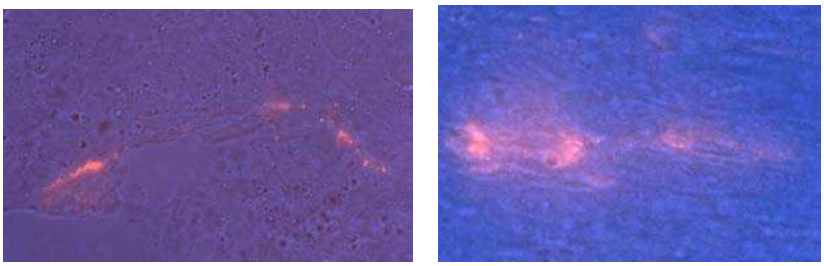

A B

Fig.: 3-17 Cryo sections (8µm) were fixed with 4% paraformaldehyde and visualized with Zeiss 64x1.4 immersion oil objective and a Zeiss Axiovert 200 fluorescence microscope equipped with a Zeiss Axiocam. Localisation of polyplex formulations in the tumor tissue is indicated by the fluorescence signal of the incorporated Cy3 labelled plasmid DNA (red) A) control polyplexes and B) NGR targeted polyplexes.

3.4.2.3 In vivo transfection efficiency

In order to investigate targeting effects in subcutaneous CT26 bearing mice, polyplex formulations LPEI-BPEI-PEG20-BPEI30 and LPEI-NGR30 with incorporated CMV-LUC plasmid DNA were administered intravenously. Mice were sacrified 48h after the application; tumor and organs were collected and analyzed for luciferase activity. No significant difference in the luciferase expression in the tumors could be found. Only a slight enhancement in luciferase activity was found in tumors when LPEI-NGR30 was administered compared to the control polyplex LPEI-BPEI-PEG20-BPEI30. Transgene expression levels were low in control tumors and as well in tumors targeted with LPEI-NGR20. Yet, administration of NGR- peptide containing polyplexes tended to result in decreased transfection rate of non targeted organs.

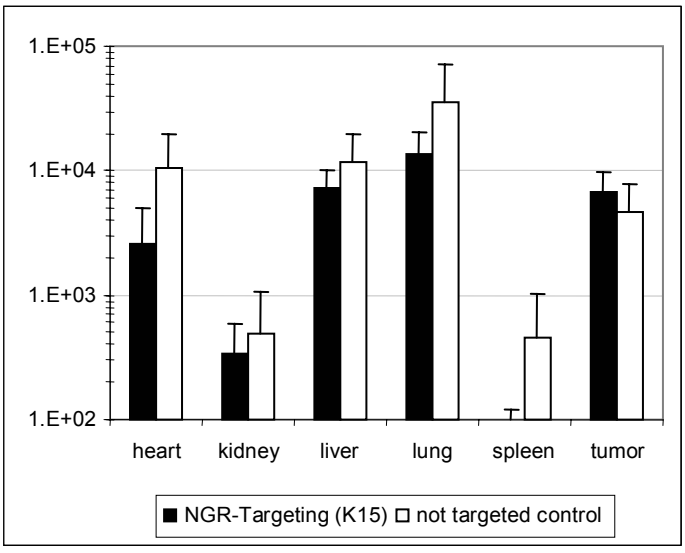

Fig.: 3-18 Reporter gene expression (luciferase) 48h after systemic application of polyplex formulations LPEI-BPEI-PEG20-BPEI30 (untargeted control polyplex) and LPEI-NGR30 (NGR-targeted polyplex) in HBG, N/P 6 in CT26 tumor bearing SCID mice. 250 µl of the polyplex formulations (total amount of plasmid DNA: 50µg) were injected into the tail vene of the mice. Luciferase activity was determined by performing the luciferase assay as described in materials and methods. Luciferase activity is visualized as total luciferase activity per organ. Values are means ± SE of four animals per groups.

3.4.2.4 Transfection GFP

Localisation of transfected cells in the tumor tissue after the administration of the NGR- peptide containing polyplex LPEI-NGR30 was performed by fluorescence microscopy. Therefore p-CMV-EGFP containing LPEI-NGR30 polyplexes were administered intravenously. 48h after the administration mice were sacrified and tumor tissue was fixed with 4% PFA in PBS before embedding in OTC and freezing.

Clusters of GFP fluorescent cells were detectable in the tumor tissue. Also GFP positive endothelial cells were detected by fluorescent microscopy in the tumor tissue.

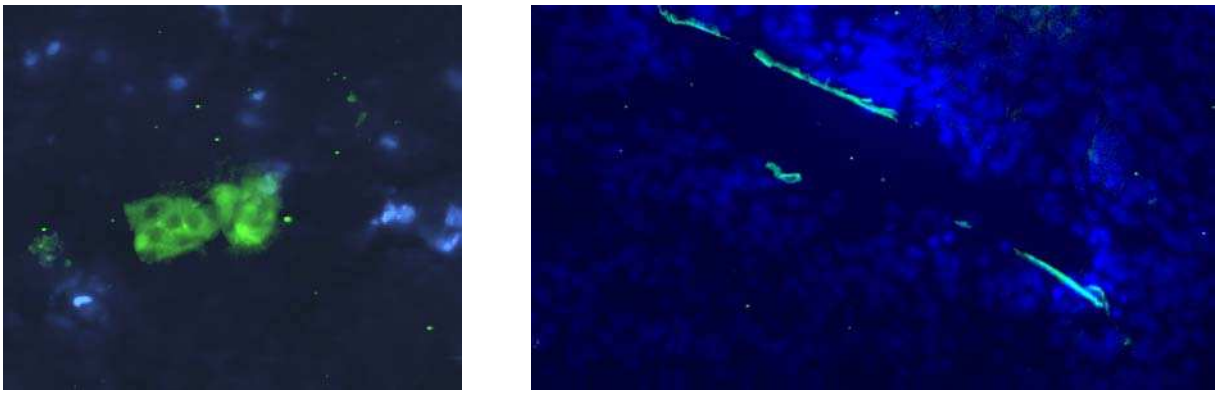

A B

Fig.: 3-19 Cryo sections (8µm) were fixed with 4% paraformaldehyde and analyzed for GFP positive cells by fluorescence microscopy. The intravenously injected Hoechst 33258 stain was visualized as well (blue). Slide A shows clustered GFP positive cells in distant to areas with blood supply (blue stain). In slide B GFP fluorescence is located directly in an area of blood supply (blue stain), indicating endothelial cells of a tumor blood vessel. Analysis was performed with 20x 0.4 Zeiss objective with a Zeiss Axiovert 200 fluorescence microscope equipped with a Zeiss Axiocam.

4 Discussion

4.1 Evaluation of endothelial cells as producer cells in the antiangiogenic GDEPT approach

In the following, the suitability of primary endothelial cells as **producer cells** is discussed in terms of an antiangiogenic CYP-CPA-GDEPT approach. Therefore, HUVEC cells were transiently transfected with the therapeutic plasmid, followed by CPA treatment. Gene transfer was performed with LPEI polyplexes (N/P 6; HBS) containing pCMV-CYP2B1 plasmid DNA or by in vitro electroporation (Amaxa).

Both transfection methods resulted in ratCYP2B1 gene expression in HUVEC cells; protein expression was detected by specific antibody staining, indicating that in principle HUVEC cells are suitable for therapeutic CYP2B1 gene expression. However, CYP2B1 enzymatic activity was only detectable when gene transfer was performed via electroporation. This difference in conversion capability in the resorufin assay is probably due to the difference in transfection efficiency: ratCYP2B1 protein was detected in only 6.7% of HUVEC cells after **LPEI** transfection versus 38% in the case of gene transfer via electroporation. Compared to enzymatic activity of transiently expressed CYP2B1 in tumor cells, HUVEC cells exhibited only moderate conversion capability. This might be provoked by an unincisive endoplasmatic reticulum, low activity of P450 reductase or the low total metabolic activity of this cells type. However, HUVEC cells are an artificial model and do not reflect specific characteristic of tumor derived endothelial cells; discrepancies can occur in several aspects e.g. expansion of the endoplasmatic reticulum (47).

Due to the insufficient CYP2B1 enzymatic activity in LPEI transfected HUVEC cells, specific effects in terms of preventing proliferation, migration and differentiation were not detected.

In the case of gene transfer via **electroporation**, specific effects of the transgene were detected in the context of proliferation and survival (FIG 3-4).

Inhibition of migration capability after gene transfer via electroporation and following CPA treatment was measured at concentrations of 1.0mM. Decrease in migration capability of endothelial cells was not pronounced and resulting partly from unspecific toxic effects of the treatment (FIG 3-5). Unspecific effects were even more distinctive in the matrigel tube forming assay, resulting a non detectable specific effect of the therapeutic gene.

In summary, CYP2B1 expression in primary endothelial cells is a possible concept in an antiangiogenic GDEPT approach. However, gene transfer via plain LPEI polyplexes to primary endothelial cells suffer from low transfection efficiency. Moreover, endothelial cells exhibit only low conversion capability, when transfection is performed with pCMV-CYP2B1 plasmid DNA via electroporation. These limitations seem to be due to characteristic properties of primary endothelial cells, at least in the HUVEC model system, and resulted only in weak specific antiangiogenic effects. Tumor derived endothelial cells might be therefore a better model in evaluation of CYP2B1 based antiangiogenic strategies and indicates that improvement of the gene delivery system is necessary.

4.2 Targeted gene transfer to tumor cells and tumor vasculature

Gene therapy is a promising approach in tumor therapy due to the potential of higher specificity in comparison to established cytotoxic treatment wit low molecular drugs. In the in vitro evaluated GDEPT concept it was found that tumor as well as endothelial cells might be in principal adequate target cells for expressing therapeutic genes in the context of GDEPT. Polyethylenimine (PEI) is one of the most efficient nonviral gene delivery systems in vitro and in vivo. However, to achieve specificity in transfer of therapeutic genes, several modifications of PEI are necessary. Unmodified, plain PEI polyplexes bind, due to their positive surface charge, to any cell membrane via unspecific electrostatic interactions. Therefore, systemic administration of plain PEI polyplexes is associated with high lung gene expression (48) and pronounced toxicity (49). Moreover, positively charged polyplexes were detected to be not suitable for tumor targeted gene transfer in vivo due to interactions with erythrocytes, resulting again in toxic effects and fast clearing from the blood stream. Incorporation of the hydrophilic 5kDa PEG-PEI25 conjugates were resulted in low surface charge (41). On the other hand, pegylation of polyplexes resulted in strong decrease of gene transfer efficiency also in target cells. Gene transfer efficiency was restored partly by incorporation of RGD- and NGR- peptide ligands into the vector system.

Biophysical Characterization of targeted PEI-polyplexes

Due to the fact that **biophysical characteristics** of polyplexes (Zeta Potential and particle size) play a crucial role for transfection efficiency (50) and their applicability for systemic administration, polyplexes were analyzed for these parameters.

Measurements showed that a minimum amount (at least 15-20% (w/w)) of pegylated conjugate is necessarily incorporated into the PEI polyplexes to generate small sized and stable vector systems. Incorporation of lower ratios of pegylated compounds resulted in aggregation of polyplexes in the presence of salt containing medium, indicating insufficient shielding (FIG 3-6). Small polyplexes have been shown to internalize more efficiently by receptor-mediated uptake than larger polyplexes (51). In addition, extravasation into tumor tissue as well as tissue diffusion is proposed to be dependent on a small particle size. This turns up the achieved particle size of about 150 to 250nm to be optimal for in vivo application and receptor-mediated uptake and tissue diffusion.

Another aspect in developing polyplexes for in vivo applications is their **storage capability**. Therefore polyplexes were analyzed for their stability in terms of particle size during a freeze/thaw cycle. Previous experiments demonstrated that pegylation effectively stabilizes PEI-polyplexes during a freeze/thaw cycle (41). This could be confirmed for peptide targeted polyplex formulations LPEI-RGD20 and LPEI-NGR30, which were further analyzed in transfection and targeting experiments.

Targeting to tumor- and endothelial cells

Main part of this section was the analysis of targeting capabilities and specificity of RGD- and NGR-peptide containing polyplexes in vitro. Therefore, cell association and transfection efficiency has been investigated on **MDA-MB-435** and **CT26** tumor cells as well as **primary endothelial (HUVECs)** cells. It was described previously that human MDA-MB-435 breast carcinoma cells highly express integrins on their cell surface (52). Antibody staining followed by cell flow cytometric analysis could confirm integrin αvβ3 expression on MDA-MB-435 cells, whereas expression of aminopeptidase N on the cell surface was not detected.

Antibody staining followed by cell flow cytometric analysis resulted in the detection of aminopeptidase N expression on approx. 58% of CT26 tumor cells, whereas expression of αv integrins was not evident.

In contrast to above mentioned tumor cells, which express either integrin receptors of αv family or aminopeptidase N, both receptors were detected on HUVEC cells.

In order to evaluate for targeting specificity of peptide ligand modified vector systems, **inhibition studies** with polyplex formulations were performed by incorporation of fluorescence labeled plasmid DNA and an excess of free peptide ligand or an specific antibody, respectively. Attention was directed towards RDG-peptide ligand containing

polyplexes, due to pronounced targeting effects in terms of transfection efficiency, compared to NGR (FIG 3-10). Increased targeting effects may be based on an effect called “integrin supported internalization”, which increases the uptake of payloads bound to integrin recognition sequences (53). Inhibition studies were therefore performed on the MDA-MB-435 cell line, due to expression of integrin αvβ3 receptors, but not aminopeptidase N. Cell association of plain LPEI polyplexes as well as shielded, untargeted LPEI-BPEI-PEG50 polyplexes was, as expected, not inhibited by an excess of free RGD- and NGR-peptides. Interestingly, cell association was disturbed when binding of plain LPEI polyplexes was inhibited with the integrin specific antibody; presumably, antibody and plain LPEI polyplexes form complexes. This effect might be triggered by high positive surface charge of plain LPEI polyplexes and therefore resulting in adhesiveness. Thus, this effect was not evident in the inhibition studies with the shielded control polyplex formulation LPEI-BPEI-PEG50, whereas cell association was not altered due to administration of the integrin specific antibody (FIG 3-8A and B). Further on, cell association was not altered when inhibition studies were performed with the specific anti-integrin antibody and the PEI-RGD20 polyplex formulation. This indicates that antibody binding location and RGD recognition region are different; further on, in contrast to plain LPEI polyplexes which associate assumedly with the integrin antibody, PEI-RGD20 polyplexes exhibit sufficient shielding to avoid interaction. However, cell association was diminished when binding of the PEI-RGD-20 polyplex formulation was inhibited with an excess of free RGD peptide, indicating targeting specificity. Interestingly, cell association was reduced in the same degree when inhibition was performed with an excess of free NGR-peptide even though MDA-MB-435 tumor cells were negative for aminopeptidase N on the cell surface (FIG 3-8B). This finding, however, is consistent with previously performed studies, where cross reactivity between RGD- and NGR-recognition sequences were already described. The NGR binding motif resembles RGD, consequently NGR peptides can bind to integrin receptors; however binding affinity of the NGR peptides is lower (54). Consequently, cell association with integrin expressing MDA-MB-435 tumor cells was not altered when the NGR-peptide ligand containing polyplex formulation (PEI-NGR30) competed with an excess of free NGR-peptide for recognition sequences, though an excess of free RGD peptide leaded to reduced cell association of PEI-NGR30 (FIG 3-8D).

In summary, the LPEI-RGD20 polyplex formulation exhibited high specificity in cell association. The described cross reactivity is a plausible explanation for the increased transfection efficiency by NGR-peptide containing polyplexes on aminopeptidase N negative MDA-MB435 cells and of RGD-peptide containing peptides on integrin αv negative CT26 tumor cells. The developed polyplex formulations PEI-RGD20 and PEI-NGR30 exhibited similar binding attitudes as phages, displaying the conformable binding sequence (34).

In the context of developing gene delivery systems specific for tumor cells and, to a greater extent, for angiogenic active endothelial cells, polyplex formulations were optimized in terms of **transfection efficiency** on primary **endothelial cells**. Therefore, reporter gene expression was evaluated on integrin αvβ3 and aminopeptidase N expressing HUVEC cells with different peptide targeted polyplex formulations delivering plasmid DNA encoding for luciferase. Control transfection experiments were performed with plain LPEI polyplexes and the shielded untargeted polyplex formulation LPEI-BPEI-PEG50. Luciferase expression levels were significantly increased by incorporating peptide ligand into PEG-shielded polyplexes; increase in transfection efficiency was dependent on the ratio of RGD-PEG-PEI or NGR-PEG-PEI, respectively. The influence of incorporating peptide ligands into the shielded polyplex formulations in terms of transfection efficiency was further evaluated on integrin αvβ3 expressing **MDA-MB-435** and aminopeptidase N positive **CT26** tumor cells. The incorporation of targeting ligands into the shielded polyplex formulations resulted in increased transfection efficiency of MDA-MB-435 and CT26 tumor cells, compared to both untargeted, shielded polyplex formulations. Transfection efficiency was significantly increased for the NGR-targeted polyplex formulation LPEI-NGR30 on aminopeptidase N negative MDA-MB435 cells; transfection with LPEI-RGD20 resulted on CT26 tumor cells in similar expression levels as with the NGR-peptide containing formulation, even though integrin αv-receptors were not detected on the cell surface. This finding, however, can be explained by a cross reactivity of RGD- and NGR- recognition sequences.

Comparing targeting capability in the context of transfection efficiency, higher reporter gene expression levels were detected for the LPEI-RGD20 polyplexes compared to the LPEI-NGR20 polyplex formulation on MDA-MB435 tumor cells and on primary endothelial cells. The increased transfection efficiency is probably based on “integrin supported internalization”, which increases the uptake of payloads bound

to integrin recognition sequences (55). Transfection of integrin αv negative CT26 tumor cells with RGD-targeted polyplex formulations is presumably driven by binding to aminopeptidase N receptors due to cross reactivity, which exhibit, in contrast to integrin receptors, no supported internalization. Alternatively, internalization of RGD-peptide ligand containing polyplexes may be supported by integrin receptors of other families, which exhibit as well RGD-recognition sequences.

Receptor regulation by hypoxia influences targeting properties

Hypoxia is a common phenomenon in solid tumors. **Hypoxia** triggers several processes in tumor cells as well as in tumor stroma cells. Endothelial cells adapt to hypoxic environment by, amongst other mechanisms, increasing several cell surface molecules relevant for angiogenic processes. Among these angiogenesis promoting receptors, **integrin αvβ3** and **aminopeptidase N** were found to be upregulated by hypoxic stimuli in prior studies (32;56). Modulation of integrin αvβ3 and aminopeptidase N cell surface expression by hypoxia was further on confirmed by specific antibody staining followed by quantification with the Amplex-Red kit within this work (FIG 3-11). In order to evaluate if hypoxia therefore enhances **transfection efficiency** by upregulation of hypoxia responsible integrin αvβ3 and aminopeptidase N receptors on the cell surface of primary endothelial cells transfection experiments were performed after preincubation of HUVEC cells in a hypoxic environment. Indeed, transfection efficiency was increased when the transfection was carried out with the targeted polyplex formulations LPEI-RGD20 and LPEI-NGR30, whereas transfection efficiency with plain LPEI polyplexes remained unchanged. This supposes increased transfection efficiency due to upregulation of cell surface receptors by the hypoxic treatment (FIG 3-12). Increase in transfection efficiency of LPEI-RGD20 was even more pronounced compared to the LPEI-NGR-30 polyplex formulation, though, integrin αvβ3 receptor was lower than aminopeptidase N upregulation (FIG 3-11). This effect might be triggered by “integrin supported internalization”, which increases the uptake of payloads bound to integrin recognition sequences (57) and indicates integrin αvβ3 receptor mediated gene transfer with RGD-peptide containing polyplexes as highly effective to primary endothelial cells, especially in hypoxic environments.

Incorporation of endosomolytic escape domains in targeted polyplexes

After cellular association of polyplexes, particles are internalized by receptor-mediated endocytosis, macropinocytosis, phagocytosis or related processes (58-60).

Internalized particles are captured in intracellular vesicles such as endosomes. For efficient transgene expression, polyplexes need to **escape from the endosomes** by endosomal release. Incorporation of the **melittin analog CMA-3** into the polyplex formulations indicated an effective approach towards enhanced transfection efficiency of targeted polyplexes. The membrane active peptide melittin was able to enhance endosomal release of internalized polyplexes. However, effective cellular uptake is necessary and can be accomplished by receptor mediated internalization. Therefore, transfection efficiency of RGD-peptide containing polyplexes can be enhanced up to levels of plain LPEI polyplexes. Targeted polyplexes profit from effective endocytosis via integrins, whereas the incorporated CMA-3 enhances intracellular endosomal release of the polyplexes. Importantly, transfection efficiency of shielded, but untargeted control polyplex formulation LPEI-BPEI-PEG50 was not enhanced by the incorporation of CMA-3, indicating that internalization of polyplexes play a crucial role for their intracellular trafficking. The internalization of LPEI-BPEI-PEG50 is less efficient on MDA-MB-435 cells and/or may be accomplished by a pathway leading directly to degradation of the polyplexes. Targeted polyplexes with NGR-peptide were shown to exhibit lower total transfection efficiency compared to RGD-peptide containing polyplexes, however, enhancement in transfection efficiency by the incorporation of the endosomolytic compound CMA-3 was similar.

In vivo evaluation of targeted polyplex formulations

Receptor expression strongly depends on cellular microenvironment. Moreover in vivo transfection efficiency is influenced by several tissue specific parameters as e.g. total tumor **blood supply**, vessel diameter and **vessel leakiness**. Further on distribution of polyplex formulations in vivo depend on diffusion capability in the indicated tissue. CT26 tumors are well vascularized especially in the peripheral regions, whereas less blood supply was detected in the central areas (FIG 3-14). However, reasoning view of a therapeutic approach, gene delivery to the angiogenic active peripheral regions is supposed to be sufficient. Antibody staining of CD31 positive endothelial cells in combination with systemically Hoechst33258 staining indicated that functional blood supply and the existence of endothelial cell lined blood vessels correlated in this tumor model. Antibody staining against mouse aminopeptidase N (CD13) indicated that aminopeptidase N is distributed over the whole tumor tissue, including vessel like structures (FIG 3-15A and B). Subcutaneous CT26 were evaluated for vessel leakiness by systemic administration of FITC-dextran

(42kDa) in combination with likewise systemically applied Hoechst33258 dye. Accumulation of FITC-dextran was evident within the tumor tissue (FIG 3-16), whereas FITC-dextran was distributed in healthy control tissue only in a small degree. Despite the difference in molecular weight of the FITC-dextran used as a marker in comparison to the indicated polyplex formulations, its accumulation in the tumor tissue indicates enhanced vessel leakiness compared to healthy tissue. Leakiness of vessels has great impact on passive tumor targeting effects (EPR effect), allows escape of gene vector systems from the blood stream and is therefore crucial for uptake within the tumor tissue.

For evaluation of delivery and subsequent **distribution of polyplexes** in the tumor tissue, targeted LPEI-NGR30 and control polyplexes LPEI-BPEI-PEG20-BPEI30, containing Cy3-labeled plasmid DNA, were administered into the tail vain of CT26 bearing SCID mice. Both, targeted as well as shielded, untargeted control polyplexes were detected in the tumor indicating that both polyplex formulations reach the tumor via blood stream (FIG 3-17). Nevertheless, 2h after polyplex administration, labeled polyplexes were still found in close vicinity to vessel like structures. This indicates limited diffusion within the tumor tissue and may result from the compact structure of subcutaneous CT26 tumors (compare thesis, chapter 1). Differences in the distribution of targeted and untargeted control polyplexes were not detectable by microscopic analysis. However, in order to investigate if the incorporation of peptide ligands enhances **transfection efficiency**, the polyplex formulation LPEI-NGR30 and shielded control polyplexes LPEI-BPEI-PEG20-BPEI30 were utilized for systemic delivery of plasmid DNA encoding for **luciferase** in the subcutaneous CT26 tumor model. In contrast to in vitro experiments, enhanced tumor transfection efficiency by incorporation of NGR-peptide into the polyplex formulation for was not significant. Notably, transgene expression in not targeted organs, however, tended to result in lower levels, when the application was performed with the LPEI-NGR30 polyplex in comparison to the shielded, untargeted control (FIG 3-18). Indistinctive enhancement in tumor transfection efficiency by the incorporation of the NGR-peptide may be on one hand explained by rather low transfection rates in total. On the other hand, low tumor transfection efficiency might result form insufficient diffusion processes within the tumor tissue. Incorporation of the endosomolytic compound CMA-3 can be utilized in further experiments to overcome these limitations and may lead to more distinctive targeting characteristics of NGR-peptide containing polyplex formulations,

due to the enhancement of transfection efficiency only for receptor mediated uptake (FIG 3-13).

Aminopeptidase N, which is the receptor targeted by LPEI-NGR30 polyplexes is expressed on CT26 tumor as well as on tumor vessel endothelial cells. For evaluation of transfected cell type in vivo, delivery of plasmid DNA encoding for **EGFP** was performed by systemic application of LPEI-NGR30 polyplex formulation. Prior to sacrifying, Tumor tissue was collected and analyzed via fluorescence microscopy for EGFP positive cells, resulting in the detection of EGFP expressing tumor as well as endothelial cells in the direct vicinity of functional blood flow (FIG 3-19). Recently, transfection of tumor vessel endothelial cells with NGR-targeted PEI polyplex formulations was described (37).

In summary, pegylated LPEI polyplexes containing RGD- and NGR-peptide ligands are small and stable particles (<200nm). RGD- and NGR- ligands are able to enhance transfection efficiency significantly on target cells, moreover, tumor specific environmental properties, like hypoxia further enhance selectivity. Transfection efficiency of peptide ligand containing polyplex formulations on target cells can be further enhanced by the incorporation of endosomolytic compounds.

Reasons for indistinctive enhancement of tumor transfection efficiency in vivo have to be further investigated by establishment of in vitro spheroid tumor models and further transfection experiments.

Incorporation of CMA-3, as a compound enhancing endosomal release, might be performed in further in vivo studies to overcome limitations and may further adjust tumor selectivity and transgene expression levels.

5 Additional References

(1) Gunther M, Wagner E, Ogris M. Specific targets in tumor tissue for the delivery of therapeutic genes. Curr Med Chem Anticancer Agents 2005; 5(2):157-171.

(2) Blaese M, Blankenstein T, Brenner M, Cohen-Haguenauer O, Gansbacher B, Russell S et al. Vectors in cancer therapy: how will they deliver? Cancer Gene Ther 1995; 2(4):291-297.

(3) Hacein-Bey-Abina S, Von Kalle C, Schmidt M, McCormack MP, Wulffraat N, Leboulch P et al. LMO2-associated clonal T cell proliferation in two patients after gene therapy for SCID-X1. Science 2003; 302(5644):415-419.

(4) Markert ML, Hershfield MS, Schiff RI, Buckley RH. Adenosine deaminase and purine nucleoside phosphorylase deficiencies: evaluation of therapeutic interventions in eight patients. J Clin Immunol 1987; 7(5):389-399.

(5) Ghosh SS, Gopinath P, Ramesh A. Adenoviral vectors: a promising tool for gene therapy. Appl Biochem Biotechnol 2006; 133(1):9-29.

(6) Amstad P, Reddel RR, Pfeifer A, Malan-Shibley L, Mark GE, III, Harris CC. Neoplastic transformation of a human bronchial epithelial cell line by a recombinant retrovirus encoding viral Harvey ras. Mol Carcinog 1988; 1(3):151-160.

(7) Cantore M, Fiorentini G, Zamagni D, Muttini MP, Mambrini A, Rabbi C. Molecular therapy: clinical applications. intra-arterial adenoviruses administration. J Exp Clin Cancer Res 2003; 22(4 Suppl):47-49.

(8) De Smedt SC, Demeester J, Hennink WE. Cationic polymer based gene delivery systems. Pharm Res 2000; 17(2):113-126.

(9) Haag R, Kratz F. Polymer therapeutics: concepts and applications. Angew Chem Int Ed Engl 2006; 45(8):1198-1215.

(10) Li SD, Huang L. Gene therapy progress and prospects: non-viral gene therapy by systemic delivery. Gene Ther 2006; 13(18):1313-1319.

(11) Wasungu L, Hoekstra D. Cationic lipids, lipoplexes and intracellular delivery of genes. J Control Release 2006.

(12) Zuber G, Dauty E, Nothisen M, Belguise P, Behr JP. Towards synthetic viruses. Adv Drug Deliv Rev 2001; 52(3):245-253.

(13) Wagner E, Culmsee C, Boeckle S. Targeting of polyplexes: toward synthetic virus vector systems. Adv Genet 2005; 53:333-354.

(14) Wagner E. Strategies to improve DNA polyplexes for in vivo gene transfer: will "artificial viruses" be the answer? Pharm Res 2004; 21(1):8-14.

(15) Ogris M, Walker G, Blessing T, Kircheis R, Wolschek M, Wagner E. Tumor-targeted gene therapy: strategies for the preparation of ligand-polyethylene

glycol-polyethylenimine/DNA complexes. J Control Release 2003; 91(1-2):173-181.

(16) Greish K, Fang J, Inutsuka T, Nagamitsu A, Maeda H. Macromolecular therapeutics: advantages and prospects with special emphasis on solid tumour targeting. Clin Pharmacokinet 2003; 42(13):1089-1105.

(17) Maeda H, Fang J, Inutsuka T, Kitamoto Y. Vascular permeability enhancement in solid tumor: various factors, mechanisms involved and its implications. Int Immunopharmacol 2003; 3(3):319-328.

(18) Kopecek J, Kopeckova P, Minko T, Lu ZR, Peterson CM. Water soluble polymers in tumor targeted delivery. J Control Release 2001; 74(1-3):147-158.

(19) Satchi-Fainaro R, Puder M, Davies JW, Tran HT, Sampson DA, Greene AK et al. Targeting angiogenesis with a conjugate of HPMA copolymer and TNP-470. Nat Med 2004; 10(3):255-261.

(20) Ogris M, Wagner E. Tumor-targeted gene transfer with DNA polyplexes. Somat Cell Mol Genet 2002; 27(1-6):85-95.

(21) Ruoslahti E, Rajotte D. An address system in the vasculature of normal tissues and tumors. Annu Rev Immunol 2000; 18:813-827.

(22) Boehm T, Folkman J, Browder T, O'Reilly MS. Antiangiogenic therapy of experimental cancer does not induce acquired drug resistance. Nature 1997; 390(6658):404-407.

(23) Alessi P, Ebbinghaus C, Neri D. Molecular targeting of angiogenesis. Biochim Biophys Acta 2004; 1654(1):39-49.

(24) Nanda A, St Croix B. Tumor endothelial markers: new targets for cancer therapy. Curr Opin Oncol 2004; 16(1):44-49.

(25) Ruoslahti E. Targeting tumor vasculature with homing peptides from phage display. Semin Cancer Biol 2000; 10(6):435-442.

(26) Kuphal S, Bauer R, Bosserhoff AK. Integrin signaling in malignant melanoma. Cancer Metastasis Rev 2005; 24(2):195-222.

(27) Erdreich-Epstein A, Shimada H, Groshen S, Liu M, Metelitsa LS, Kim KS et al. Integrins alpha(v)beta3 and alpha(v)beta5 are expressed by endothelium of high-risk neuroblastoma and their inhibition is associated with increased endogenous ceramide. Cancer Res 2000; 60(3):712-721.

(28) Isberg RR, Hamburger Z, Dersch P. Signaling and invasin-promoted uptake via integrin receptors. Microbes Infect 2000; 2(7):793-801.

(29) Brown CK, Modzelewski RA, Johnson CS, Wong MK. A novel approach for the identification of unique tumor vasculature binding peptides using an E. coli peptide display library. Ann Surg Oncol 2000; 7(10):743-749.

(30) Pasqualini R, Koivunen E, Ruoslahti E. Alpha v integrins as receptors for tumor targeting by circulating ligands. Nat Biotechnol 1997; 15(6):542-546.

(31) Arap W, Pasqualini R, Ruoslahti E. Cancer treatment by targeted drug delivery to tumor vasculature in a mouse model. Science 1998; 279(5349):377-380.

(32) Fukasawa K, Fujii H, Saitoh Y, Koizumi K, Aozuka Y, Sekine K et al. Aminopeptidase N (APN/CD13) is selectively expressed in vascular endothelial cells and plays multiple roles in angiogenesis. Cancer Lett 2006.

(33) Pastorino F, Brignole C, Marimpietri D, Sapra P, Moase EH, Allen TM et al. Doxorubicin-loaded Fab' fragments of anti-disialoganglioside immunoliposomes selectively inhibit the growth and dissemination of human neuroblastoma in nude mice. Cancer Res 2003; 63(1):86-92.

(34) Pasqualini R, Koivunen E, Kain R, Lahdenranta J, Sakamoto M, Stryhn A et al. Aminopeptidase N is a receptor for tumor-homing peptides and a target for inhibiting angiogenesis. Cancer Res 2000; 60(3):722-727.

(35) Colombo G, Curnis F, De Mori GM, Gasparri A, Longoni C, Sacchi A et al. Structure-activity relationships of linear and cyclic peptides containing the NGR tumor-homing motif. J Biol Chem 2002; 277(49):47891-47897.

(36) Kunath K, Merdan T, Hegener O, Haberlein H, Kissel T. Integrin targeting using RGD-PEI conjugates for in vitro gene transfer. J Gene Med 2003; 5(7):588-599.

(37) Moffatt S, Wiehle S, Cristiano RJ. Tumor-specific gene delivery mediated by a novel peptide-polyethylenimine-DNA polyplex targeting aminopeptidase N/CD13. Hum Gene Ther 2005; 16(1):57-67.

(38) Suh W, Han SO, Yu L, Kim SW. An angiogenic, endothelial-cell-targeted polymeric gene carrier. Mol Ther 2002; 6(5):664-672.

(39) Boeckle S, Wagner E, Ogris M. C- versus N-terminally linked melittin-polyethylenimine conjugates: the site of linkage strongly influences activity of DNA polyplexes. J Gene Med 2005; 7(10):1335-1347.

(40) Suh W, Han SO, Yu L, Kim SW. An angiogenic, endothelial-cell-targeted polymeric gene carrier. Mol Ther 2002; 6(5):664-672.

(41) Kursa M, Walker GF, Roessler V, Ogris M, Roedl W, Kircheis R et al. Novel shielded transferrin-polyethylene glycol-polyethylenimine/DNA complexes for systemic tumor-targeted gene transfer. Bioconjug Chem 2003; 14(1):222-231.

(42) Wightman L, Kircheis R, Rossler V, Carotta S, Ruzicka R, Kursa M et al. Different behavior of branched and linear polyethylenimine for gene delivery in vitro and in vivo. J Gene Med 2001; 3(4):362-372.

(43) Bhagwat SV, Lahdenranta J, Giordano R, Arap W, Pasqualini R, Shapiro LH. CD13/APN is activated by angiogenic signals and is essential for capillary tube formation. Blood 2001; 97(3):652-659.

(44) Koike T, Kimura N, Miyazaki K, Yabuta T, Kumamoto K, Takenoshita S et al. Hypoxia induces adhesion molecules on cancer cells: A missing link between Warburg effect and induction of selectin-ligand carbohydrates. Proc Natl Acad Sci U S A 2004; 101(21):8132-8137.

(45) Walton HL, Corjay MH, Mohamed SN, Mousa SA, Santomenna LD, Reilly TM. Hypoxia induces differential expression of the integrin receptors alpha(vbeta3) and alpha(vbeta5) in cultured human endothelial cells. J Cell Biochem 2000; 78(4):674-680.

(46) Boeckle S, Fahrmeir J, Roedl W, Ogris M, Wagner E. Melittin analogs with high lytic activity at endosomal pH enhance transfection with purified targeted PEI polyplexes. J Control Release 2006; 112(2):240-248.

(47) Zhang WJ, Ye LY, Wu LQ, Xin YL, Gu F, Niu JX et al. Morphologic, Phenotypic and Functional Characteristics of Endothelial Cells Derived from Human Hepatic Cavernous Hemangioma. J Vasc Res 2006; 43(6):522-532.

(48) Goula D, Benoist C, Mantero S, Merlo G, Levi G, Demeneix BA. Polyethylenimine-based intravenous delivery of transgenes to mouse lung. Gene Ther 1998; 5(9):1291-1295.

(49) Chollet P, Favrot MC, Hurbin A, Coll JL. Side-effects of a systemic injection of linear polyethylenimine-DNA complexes. J Gene Med 2002; 4(1):84-91.

(50) Ogris M, Steinlein P, Kursa M, Mechtler K, Kircheis R, Wagner E. The size of DNA/transferrin-PEI complexes is an important factor for gene expression in cultured cells. Gene Ther 1998; 5(10):1425-1433.

(51) Ogris M, Carlisle RC, Bettinger T, Seymour LW. Melittin enables efficient vesicular escape and enhanced nuclear access of nonviral gene delivery vectors. J Biol Chem 2001; 276(50):47550-47555.

(52) Wong NC, Mueller BM, Barbas CF, Ruminski P, Quaranta V, Lin EC et al. Alphav integrins mediate adhesion and migration of breast carcinoma cell lines. Clin Exp Metastasis 1998; 16(1):50-61.

(53) Isberg RR, Hamburger Z, Dersch P. Signaling and invasin-promoted uptake via integrin receptors. Microbes Infect 2000; 2(7):793-801.

(54) Pasqualini R, Koivunen E, Kain R, Lahdenranta J, Sakamoto M, Stryhn A et al. Aminopeptidase N is a receptor for tumor-homing peptides and a target for inhibiting angiogenesis. Cancer Res 2000; 60(3):722-727.

(55) Isberg RR, Hamburger Z, Dersch P. Signaling and invasin-promoted uptake via integrin receptors. Microbes Infect 2000; 2(7):793-801.

(56) Walton HL, Corjay MH, Mohamed SN, Mousa SA, Santomenna LD, Reilly TM. Hypoxia induces differential expression of the integrin receptors alpha(vbeta3) and alpha(vbeta5) in cultured human endothelial cells. J Cell Biochem 2000; 78(4):674-680.

(57) Isberg RR, Hamburger Z, Dersch P. Signaling and invasin-promoted uptake via integrin receptors. Microbes Infect 2000; 2(7):793-801.

(58) Rejman J, Oberle V, Zuhorn IS, Hoekstra D. Size-dependent internalization of particles via the pathways of clathrin- and caveolae-mediated endocytosis. Biochem J 2004; 377(Pt 1):159-169.

(59) Goncalves C, Mennesson E, Fuchs R, Gorvel JP, Midoux P, Pichon C. Macropinocytosis of polyplexes and recycling of plasmid via the clathrin-dependent pathway impair the transfection efficiency of human hepatocarcinoma cells. Mol Ther 2004; 10(2):373-385.

(60) Kopatz I, Remy JS, Behr JP. A model for non-viral gene delivery: through syndecan adhesion molecules and powered by actin. J Gene Med 2004; 6(7):769-776.